



Development of EV Charging Protocol Using
AI for Fast Charging Under Dynamic
Environment: Towards Vehicle to Grid
Integration

By

Peter Makeen Toghyan Besada (BEng, MSc)

<https://orcid.org/0000-0003-2907-9800>

A Doctoral Thesis

submitted in partial fulfilment of the requirements of the

London South Bank University

for the award of the degree of Doctor of Philosophy

August 2023

Abstract

This thesis focuses on the development of electric vehicle (EV) charging protocols under a dynamic environment using artificial intelligence (AI), to achieve Vehicle-to-Grid (V2G) integration and promote automobile electrification. The proposed framework comprises three major complementary steps. Firstly, the DC fast charging scheme is developed under different ambient conditions such as temperature and relative humidity. Subsequently, the transient performance of the controller is improved while implementing the proposed DC fast charging scheme. Finally, various novel techno-economic scenarios and case studies are proposed to integrate EVs with the utility grid.

The proposed novel scheme is composed of hierarchical stages; In the first stage, an investigation of the temperature or/and relative humidity impact on the charging process is implemented using the constant current-constant voltage (CC-CV) protocol. Where the relative humidity impact on the charging process was not investigated or mentioned in the literature survey. This was followed by the feedforward backpropagation neural network (FFBP-NN) classification algorithm supported by the statistical analysis of an instant charging current sample of only 10 seconds at any ambient condition. Then the FFBP-NN perfectly estimated the EV's battery terminal voltage, charging current, and charging interval time with an error of 1% at the corresponding temperature and relative humidity. Then, a nonlinear identification model of the lithium-polymer ion battery dynamic behaviour is introduced based on the Hammerstein-Wiener (HW) model with an experimental error of 1.1876%.

Compared with the CC-CV fast charging protocol, intelligent novel techniques based on the multistage charging current protocol (MSCC) are proposed using the Cuckoo optimization algorithm (COA). COA is applied to the Hierarchical technique (HT) and the Conditional random technique (CRT). Compared with the CC-CV charging protocol, an improvement in the charging efficiency of 8% and 14.1% was obtained by the HT and the CRT, respectively, in addition to a reduction in energy losses of 7.783% and 10.408% and a reduction in charging interval time of 18.1% and 22.45%, respectively. The stated charging protocols have been implemented throughout a smart charger. The charger comprises a DC-DC buck converter controlled by an artificial neural network predictive controller (NNPC), trained and supported by the long short-term memory neural network (LSTM). The LSTM network model was utilized in the offline forecasting of the PV output power, which was fed to the NNPC as the training data. The NNPC–LSTM controller was compared with the fuzzy logic (FL) and the conventional PID controllers and perfectly ensured that the optimum transient performance with a minimum battery terminal voltage ripple reached 1 mV with a very high-speed response of 1 ms in reaching the predetermined charging current stages.

Finally, to alleviate the power demand pressure of the proposed EV charging framework on the utility grid, a novel smart techno-economic operation of an electric vehicle charging station (EVCS) in Egypt controlled by the aggregator is suggested based on a hierarchical model of multiple scenarios. The deterministic charging scheduling of the EVs is the upper stage of the model to balance the generated and consumed power of the station. Mixed-integer linear programming (MILP) is used to solve the first stage, where the EV charging peak demand

value is reduced by 3.31% (4.5 kW). The second challenging stage is to maximize the EVCS profit whilst minimizing the EV charging tariff. In this stage, MILP and Markov Decision Process Reinforcement Learning (MDP-RL) resulted in an increase in EVCS revenue by 28.88% and 20.10%, respectively. Furthermore, the grid-to-vehicle (G2V) and vehicle-to-grid (V2G) technologies are applied to the stochastic EV parking across the day, controlled by the aggregator to alleviate the utility grid load demand. The aggregator determined the number of EVs that would participate in the electric power trade and sets the charging/discharging capacity level for each EV. The proposed model minimized the battery degradation cost while maximizing the revenue of the EV owner and minimizing the utility grid load demand based on the genetic algorithm (GA). The implemented procedure reduced the degradation cost by an average of 40.9256%, increased the EV SOC by 27%, and ensured an effective grid stabilization service by shaving the load demand to reach a predetermined grid average power across the day where the grid load demand decreased by 26.5% (371 kW).

Keywords: Electric vehicles (EVs), Fast charging protocols, Lithium-ion battery, Constant current-constant voltage (CC-CV), Multi-stage charging current (MSCC), EV recognition, EV aggregators, Degradation Cost, Grid-to-Vehicle (G2V), Vehicle-to-Grid (V2G).

Acknowledgement

Words cannot express my gratitude to my supervisors **Professor Saim Memon**, **Professor Hani Ghali**, and **Associate Professor Fang Duan** for their invaluable patience, guidance and feedback. I also could not have undertaken this journey without them, who generously provided knowledge and expertise. Additionally, this endeavour would not have been possible without the generous support from the Electrical Department, Faculty of Engineering, the British University in Egypt (BUE) and the Electrical and Electronic Division, School of Engineering, London South Bank University (LSBU), who financed my research and output publications and supported me with the required research equipment and environment.

I'd like to express my gratitude to **Professor Saim Memon**, my esteemed exemplary advisor and mentor, for all the guidance, support, advice and instruction he provided me throughout my doctoral studies as he has a pioneer vision in the academics and research field. Also, he delivered me generously his pure knowledge and years of experience. Also, I'd like to express my gratitude to **Professor Hani Ghali** my respectable mentor for his always guidance, support, and motivation for hard work. He taught me the dedication to the research and provided me with the perfect practical experience and built up my mental thinking. He did not hesitate to guide me through the journey and support me with all the facilities. Also, I'd like to express my gratitude to **Associate Professor Fang Duan** for her always support and guidance. She did not hesitate to support me and provided me with all the required facilities to accomplish my PhD. In addition, she supported me with the experience of communications with researchers from all over the world.

I am also grateful to my colleagues and cohort members, especially for their editing help, insightful discussions and moral support (**Dr. Anwar Magdy**, and **Dr. Nathalie Nazih**). Thanks should also go to the research assistants, and study participants from the university, who impacted and inspired me (**Dr. Ahmed Helmy**, and **Eng. Ola Hassan**).

Lastly, I would be remiss in not mentioning my family, especially my spouse (**Mira Magdy Fakhoury**), children (**Holly** and **Kevin**), and parents (**Makeen Toghyan**, **Hayah Mikaeel**, and **Samer Makeen**). They withstand the hard circumstances of my study in the United Kingdom. Their belief in me has kept my spirits and motivation high during this process.

Table of Contents

ABSTRACT	I
ACKNOWLEDGEMENT	III
LIST OF PUBLICATIONS	VII
LIST OF FIGURES	IX
LIST OF TABLES	XIII
ABBREVIATIONS	XIV
NOMENCLATURE	XVII
1 CHAPTER 1 INTRODUCTION	1
1.1 Introduction	1
1.2 Research problem statement	2
1.3 Research aim and objectives	3
1.4 Research Methodology	6
1.5 Significant Contribution to Knowledge	7
1.6 Structure of thesis	8
2 CHAPTER 2 LITERATURE REVIEW	10
2.1 Introduction	10
2.2 Electric Vehicle Batteries	12
2.3 Lithium-Ion Battery Fast Charging Protocols	14
2.3.1 Constant Current Constant Voltage (CC-CV) Protocol.....	15
2.3.2 Multi-Stage Charging Currents (MSCC) Protocol	16
2.3.3 Thermal Management Protocols	22
2.3.4 Pulse Charging Current (PCC) Protocol	25
2.3.5 Material Aspects Charging Protocol.....	30
2.4 EV Battery Dynamic Behaviour, Classification, and Recognition	31

2.5	Charge Controller for Off-Board Electric Vehicles	33
2.6	Electric Vehicles Smart Connectivity to the Utility Grid.....	38
2.6.1	Grid-to-Vehicle (G2V) Technology	38
2.6.2	Vehicle-to-Grid (V2G) Technology	40
2.7	Chapter Summary	44
3	CHAPTER 3 PROPOSED EV CHARGING PROTOCOL USING AI FOR FAST CHARGING UNDER DYNAMIC ENVIRONMENT	45
3.1	Introduction.....	45
3.2	Temperature and Relative Humidity Investigation.....	46
3.2.1	Experimental Setup	46
3.2.2	Temperature Impact on the Charging Process	48
3.2.3	Relative Humidity Impact on the Charging Process.....	49
3.3	EV Classification and Recognition Process based on the Feed-forward Backpropagation Artificial Neural Network (FFBP-NN).....	51
3.4	Constant Current-Constant Voltage (CC-CV) Charging Protocol Under Dynamic Temperature and Relative Humidity	54
3.4.1	EV fast-charging parameters estimation by the CC-CV protocol	54
3.4.2	Hammerstein-Wiener (HW) modelling of the EV battery dynamic behaviour.....	57
3.5	Chapter Summary	60
4	CHAPTER 4 CAD, DESIGN, AND DEVELOPMENT OF EV CHARGING PROTOCOL USING AI FOR FAST CHARGING UNDER DYNAMIC ENVIRONMENT.....	61
4.1	Introduction.....	61
4.2	Multi-stage Charging Current (MSCC) Charging Protocol based on Cuckoo Optimization Algorithm (COA) at Constant Ambient Conditions.....	61
4.2.1	Estimation and calculation of the internal parameters of the proposed lithium-ion polymer battery model	61
4.2.2	Derivation of the Fast-Charging Fitness Function.....	68
4.2.3	Limitations of Fast Charging Algorithms	69
4.2.4	Fast Charging Implementation Algorithms	70
4.2.5	Analysis of the Weighting Factors.....	77
4.3	Off-Board Charging Implementation using the Neural Network Predictive Controller (NNPC).....	78
4.3.1	Parasitic Buck Converter Model.....	78

4.3.2	Charging Controllers Under Study	80
4.3.3	Simulated Results and Experimental Analysis	85
4.4	Chapter Summary	89
5	CHAPTER 5 SYSTEM INTEGRATION, TESTING, VALIDATION, AND VERIFICATION.....	91
5.1	Introduction.....	91
5.2	Electric Vehicle Charging Station (EVCS) based on the Grid-to-Vehicle (G2V) Technology.....	91
5.2.1	Elements of the System Under Study	92
5.2.2	Proposed hierarchal roles of the aggregator (operator).....	96
5.2.3	The implemented programming methodologies	100
5.2.4	The Proposed Operation of the EVCS	102
5.3	Stochastic EVs Parking Operations based on the Vehicle-to-Grid (V2G) and Grid-to-Vehicle (G2V) Technologies	107
5.3.1	Operating Framework	107
5.3.2	Battery Degradation Cost Model	108
5.3.3	Proposed V2G Scheduling Modelling and Constraints	109
5.3.4	Solving Based on the Genetic Algorithm (GA).....	110
5.3.5	Charging/Discharging System Understudy.....	112
5.4	Chapter Summary	119
6	CHAPTER 6 CONCLUSIONS, MAJOR FINDINGS, RECOMMENDATIONS, AND FUTURE WORK	122
5.1.	Conclusion	122
5.2.	Recommendations and future work	124
	REFERENCES.....	125
	APPENDIX A SOURCE CODE LISTINGS.....	155
	APPENDIX B COMPLEMENTARY DATA.....	176

List of Publications

- [1] **Makeen, Peter**, Hani A. Ghali, and Saim Memon. "A Review of Various Fast Charging Power and Thermal Protocols for Electric Vehicles Represented by Lithium-Ion Battery Systems." *Future Transportation* 2, no. 1 (2022): 15.
<https://doi.org/10.3390/futuretransp2010015>
<https://www.mdpi.com/2673-7590/2/1/15>
- [2] **Makeen, Peter**, Hani A. Ghali, and Saim Memon. "Investigating an influence of temperature and relative humidity on the electrical performance of lithium polymer ion battery using constant-current and constant voltage protocol at small scale for electric vehicles." 11th International Conference on Power Electronics, Machines and Drives (PEMD 2022), 2022 p. 126 – 130.
[DOI: 10.1049/icp.2022.1030](https://doi.org/10.1049/icp.2022.1030)
<https://digital-library.theiet.org/content/conferences/10.1049/icp.2022.1030>
- [3] **Makeen, Peter**, Hani A. Ghali, Saim Memon, and Fang Duan. "Impacts of electric vehicle fast charging under dynamic temperature and humidity: Experimental and theoretically validated model analyses." *Energy* 261 (2022): 125335.
<https://doi.org/10.1016/j.energy.2022.125335>
<https://www.sciencedirect.com/science/article/abs/pii/S0360544222022198>
- [4] **Makeen, Peter**, Hani Ghali, and Saim Memon. "Controllable electric vehicle fast charging approach based on multi-stage charging current methodology." In 2020 IEEE International Conference on Power and Energy (PECon), pp. 398-403. IEEE, 2020.
[DOI: 10.1109/PECon48942.2020.9314471](https://doi.org/10.1109/PECon48942.2020.9314471)
<https://ieeexplore.ieee.org/stamp/stamp.jsp?tp=&arnumber=9314471>
- [5] **Makeen, Peter**, Hani A. Ghali, and Saim Memon. "Experimental and theoretical analysis of the fast charging polymer lithium-ion battery based on Cuckoo Optimization Algorithm (COA)." *IEEE Access* 8 (2020): 140486-140496.
[DOI: 10.1109/ACCESS.2020.3012913](https://doi.org/10.1109/ACCESS.2020.3012913)
<https://ieeexplore.ieee.org/abstract/document/9152007>
- [6] **Makeen, Peter**, Hani A. Ghali, and Saim Memon. "Theoretical and Experimental Analysis of a New Intelligent Charging Controller for Off-Board Electric Vehicles Using PV Standalone System Represented by a Small-Scale Lithium-Ion Battery." *Sustainability* 14, no. 12 (2022): 7396.
<https://doi.org/10.3390/su14127396>
<https://www.mdpi.com/2071-1050/14/12/7396>

- [7] **Makeen, Peter**, Hani A. Ghali, Saim Memon, and Fang Duan. "Smart techno-economic operation of electric vehicle charging station in Egypt." *Energy* (2022): 126151.
<https://doi.org/10.1016/j.energy.2022.126151>
[Smart techno-economic operation of electric vehicle charging station in Egypt - ScienceDirect](#)
- [8] **Makeen, Peter**, Hani A. Ghali, Saim Memon, and Fang Duan. "Insightful Electric Vehicle Utility Grid Aggregator Methodology Based on the G2V and V2G Technologies in Egypt" *Sustainability* 15, no. 2: 1283.
<https://doi.org/10.3390/su15021283>
[Sustainability | Free Full-Text | Insightful Electric Vehicle Utility Grid Aggregator Methodology Based on the G2V and V2G Technologies in Egypt \(mdpi.com\)](#).

All the mentioned papers have been presented on the following platforms

Scopus: [Makeen, Peter - Author details - Scopus](#)
Google Scholar: <https://scholar.google.com/citations?user=a2raLPgAAAAJ&hl=en>
Researchgate: <https://www.researchgate.net/profile/Peter-Makeen>
Linkedin: <https://eg.linkedin.com/in/peter-makeen-7346a788>
ORCID: [Peter Makeen Toghyan Besada \(0000-0003-2907-9800\) \(orcid.org\)](https://orcid.org/0000-0003-2907-9800)
SCIprofile: [Peter Makeen \(sciprofiles.com\)](https://sciprofiles.com/Peter-Makeen)
BUE: https://www.bue.edu.eg/bue_person/peter_makeen/

List of Figures

Figure 1-1 Schematic diagram of the main research gaps.	3
Figure 1-2 Schematic diagram of the main stages of this thesis.	5
Figure 2-1 Overview of the electric vehicle (EV) research tracks.	10
Figure 2-2 Main fast-charging protocols of the Lithium-ion battery.	15
Figure 2-3 Schematic diagram of the Constant Current-Constant Voltage (CC-CV) Protocol.	16
Figure 2-4 Schematic diagram of the Multi-Stage Charging Current (MSCC) Protocol.	18
Figure 2-5 Schematic diagram of the Constant Temperature Constant Voltage (CT-CV) Protocol.	23
Figure 2-6 Overall schematic diagram of the Pulse Charging Current (PCC) Protocol.	25
Figure 2-7 Types of the Standard Positive Pulsed Charging Current (PPCC) Protocol; (a) standard protocol with equal duty cycle, (b) standard protocol with various duty cycles, (c) standard protocol with decaying current, (d) standard protocol with upper and lower current limit, and (e) different pulse charge voltages.	27
Figure 2-8 (a) Pulse Charging Current-Constant Voltage (PCC-CV) protocol, and (b) Constant Current-Pulse Charging Current (CC-PCC) protocol.	28
Figure 2-9 Different types of the ideal bidirectional pulsed current.	29
Figure 2-10 The pros and cons of the power management protocol with all its categories.	30
Figure 3-1 Schematic diagram of the proposed EV charging process starting from plugging it into the charging point until it is fully charged using the CC-CV and MSCC charging protocols.	46
Figure 3-2 Climatic chamber to control temperature and humidity.	47
Figure 3-3 Batteries charging topology (a), (b) charging current and terminal voltage of the 1000 mAh polymer lithium-ion battery at two various temperatures (30°C and 40°C) and the same relative humidity (52%), (c) and (d) charging current and terminal voltage of the 2200 mAh polymer lithium-ion battery pack at two various temperatures (30°C and 40°C) and same relative humidity (50%).	49
Figure 3-4 The charging topology of the polymer lithium-ion batteries at the same temperature (40°C) and various RH (35%, 52%, and 70%) and (30%, and 50%) for 1000 mAh and 2200 mAh, respectively.	50
Figure 3-5 Schematic overview of the proposed classification and recognition process of various electric vehicles with different temperatures and relative humidity.	52
Figure 3-6 (a) The charging current of different operating conditions, and (b) The confusion matrix of the overall recognition and classification process.	53

Figure 3-7 Schematic overview of the estimation stage of the fast-charging process using the CC-CV protocol.....	56
Figure 3-8 Extracted output results from the FFBP-NN (a) the training regression results, (b) validation regression results, (c) test regression results, (d) overall system regression plots, (e) the measured and simulated charging current, and (f) the percentage of error between the measured and simulated terminal voltage of the lithium-ion battery.	57
Figure 3-9 Schematic diagram of Hammerstein-Wiener model block diagram.	58
Figure 3-10 Output from the HW model (a) Measured and simulated model output, and (b) Difference between the measured data and simulated HW model output.	58
Figure 3-11 Flowchart of the overall proposed system starting from EV connected to the charging pile till the battery is fully charged.	59
Figure 4-1 The proposed RC second-order transient equivalent model of a lithium-polymer battery.	62
Figure 4-2 Illustrates (a) the procedures of the OCV-SOC test method and (b) the relation between OCV-SOC of the lithium-polymer battery cell at room temperature 25°C.....	64
Figure 4-3 Discharging current pulse sample graph measured by NI myRIO during the interval time 20 s at room temperature 25°C.	65
Figure 4-4 The relationship between the internal parameters of the proposed battery model (a) The ohmic internal resistance R_i , (b) The electrochemical polarization internal resistance R_α , (c) The concentration polarization internal resistance R_β , (d) The electrochemical polarization capacitance C_α and (e) The concentration polarization capacitance C_β corresponding to SOC during an interval discharging pulse 20s at room temperature 25°C.....	68
Figure 4-5 (a) The proposed scenarios of charging the lithium-polymer battery, and (b)The procedures performed to implement the proposed multi-stage charging current methodologies.	71
Figure 4-6 The flowchart of the Cuckoo Optimization Algorithm (COA).....	72
Figure 4-7 Relationship between different charging methodologies for polymer lithium-ion battery at room temperature 25°C (a) The standard CC-CV protocol, (b) Multi-stage charging current method based on HT and (c) Multi-stage charging current method based on CRT....	75
Figure 4-8 The maximum error declaration between experimental and simulated voltage results for both HT and CRT at room temperature 25°C, respectively.	76
Figure 4-9 (a) The proposed construction of the charging control system, and (b) Graphical s-plane model of the DC-DC buck converter.	80
Figure 4-10 A schematic diagram of the proposed charging process using different controllers.	81
Figure 4-11 Graphical illustrative schematic of the PID, FLC, and NNPC controllers, respectively.	83
Figure 4-12 The LSTM-specific dissemination as illustrated in [317].....	85

Figure 4-13 The experimental setup used in the charging process.	86
Figure 4-14 Simulated results for NNPC-LSTM and PID controllers where (a) reference voltage changes 7.7V, 5.6V, and 8V; (b) the input voltage changes from 25V to 12V.	87
Figure 4-15 (a) The daily average amount of the total solar radiation incident the horizontal surface at the surface at El-Sherouk City, Cairo, Egypt; (b) the PV output power readings for 34 minutes; (c) the relation between the PV output voltage and current of the solar panel under study; and (d) Predicted and measured PV output voltage from the LSTM method.	88
Figure 4-16 (a) Experimental results of the NNPC-LSTM, FL, and PID controllers with the reference voltage changes 7.7V, 5.6V, and 8V; (b) Experimental results for NNPC-LSTM, FL, and PID controllers with an input voltage change from 25V to 12V, and (c) The Dynamic behaviour of the lithium-ion battery during the charging process.	89
Figure 5-1 The system under study is (a) a real place at the Cairo-Alexandria desert road, Egypt, and (b) Implemented schematic diagram of the proposed system.	92
Figure 5-2 Overall RESs and EVCS characteristics (a) Solar irradiance all over the year (W/m^2), (b) PV output power on the 15 th of May 2017, (c) Wind speed over the year (m/s), (d) wind energy system output power on the 15 th of May 2017, (e) Distribution of the EVs entering the EVCS daily, and (f) DC fast charging curve of the 2015 Chevrolet Spark EV battery.	95
Figure 5-3 Schematic diagram of the probability of the upper stage hierarchal model.	97
Figure 5-4 Schematic diagram of EVs fast charging optimum track based on a sequence of the decision on the selection of supplying source to reach full capacity 94% using the Markov Decision Process Reinforcement Learning (MDP-RL).	101
Figure 5-5 Results from the upper stage of the hierarchal model (a) EVCS active power difference between the generated power from RESs and the consumed power from the EVCS, (b) Declaration of the measurement method between the two peaks, and (c) peak to peak percentage of the surplus power from charging the EVs from the RESs between the MILP and traditional operation.	103
Figure 5-6 Results from the upper stage of the hierarchal model (a) EV charging demand using MILP and compared with traditional operation at 19:00, (b) EV charging demand using MILP and compared with traditional operation at 23:00, (c) EVs' charging demand peak-to-average change of the MILP and traditional operation, and (d) Load factor of the proposed model concerning the traditional operation.	105
Figure 5-7 Results from the second stage of the hierarchal model compared to the standard operation (a) EVs charging tariff percentage of change, (b) EVCS revenue percentage of change, and (c) Total EVs charging tariff and EVCS revenue obtained by the main equation represented by the two objective functions.	106
Figure 5-8 Operational V2G/G2V time across the day.	107
Figure 5-9 Relationship between the charging/discharging cycles and the battery degradation depths (BDDs) during their life span [246].	109
Figure 5-10 Flowchart for Genetic Algorithm (GA).	111

Figure 5-11 Complete flowchart architecture of the proposed aggregator methodology. 112

Figure 5-12 Load active power demand across the day without EV penetration. 113

Figure 5-13 Framework outputs while continuously parking for a 2 h interval time for both scenarios (a) state of charge levels of all EV categories, (b) total degradation cost, (c) EV owner revenue from the V2G technology and (d) resultant load profile. 115

Figure 5-14 Framework outputs while stochastic parking for a 2 h interval time for both scenarios (a) state of charge levels of all EV categories, (b) total degradation cost, (c) EV owner revenue from the V2G technology and (d) resultant load profile. 117

Figure 5-15 Framework outputs while parking for 1 h interval time for both scenarios (a) state of charge levels of all EV categories, (b) total degradation cost, (c) EV owner revenue from the V2G technology and (d) resultant load profile. 119

List of Tables

Table 2-1 Charging rates of IEC standards, SAE standards, and CHAdeMO.....	12
Table 2-2 Comparison between algorithms presented in the literature survey using the multi-stage charging current (MSCC) protocol, and Thermal Management Protocol.	19
Table 2-3 Comparison between different types of Positive Pulsed Charging Current (PPCC) Protocol.	28
Table 2-4 A Comparison between the negative pulsed charging current and CC-CV protocol.	30
Table 2-5 Comparison between various controllers from the literature survey concluding the proposed controller.	37
Table 2-6 A glancing overview of the literature survey.....	42
Table 3-1 Specifications of the selected Lithium-ion Polymer batteries [252].....	48
Table 3-2 Testing the proposed classification and recognition process.....	54
Table 4-1 A detailed comparison between the CC-CV method and the proposed scenarios based on COA at room temperature 25°C.	77
Table 4-2 The results of changing the weights of energy loss and charging interval time.	78
Table 4-3 The rule table of the fuzzy logic controller (FLC).....	81
Table 5-1 Statistics of 2015 Chevrolet Spark EV battery	94
Table 5-2 Analysis summary of the proposed microgrid.....	102
Table 5-3 The utilized EVs' categories, rated battery capacity, and battery cost as extracted from the EV's model specification [244, 246].....	108
Table 5-4 The V2G/G2V output summary of the 1 st case study.	114
Table 5-5 The V2G/G2V output summary of the 2 nd case study.....	116
Table 5-6 The V2G/G2V output summary of the 3 rd case study.	118
Table B-1 Switching manoeuvring status of sources	176

Abbreviations

Abbreviations	Explanation
ANFIS	Adaptive Neuro-Fuzzy Inference System
ACE	Annual Carbon Emission
ATC	Annual Total Cost
AI	Artificial Intelligent
AILMS	Artificial Intelligent Learning Methods
ANN	Artificial Neural Network
ATM	Asymmetric Temperature Modulation
BEVs	Battery Electric Vehicles
BESS	Battery Energy Storage System
BMS	Battery Management System
BSS	Battery Swapping Station
BPCC	Bidirectional Pulsed Charging Current
CO ₂	Carbon Dioxide
CSP	Concentrating Solar Power
CRT	Conditional Random Technique
CC-CV	Constant Current Constant Voltage
CC-PCC	Constant Current Pulse Charging Current
CPCV	Constant Power Constant Voltage
CPLs	Constant Power Loads
CT-CV	Constant Temperature Constant Voltage
CNN	Convolutional Neural Network
COA	Cuckoo Optimization Algorithm
CMC	Current Mode Controller
DCFC	DC Fast Charging
D-EVSE	Decentralized Electric Vehicle Supply Equipment
DPMA	Decentralized Profit Maximization Algorithm
DR	Demand Response
DOD	Depth of Discharge
DGs	Distributed Generators
DFR	Distribution Feeder Recognition
DP	Dual Polarization Model
DPM	Dynamic Programming Method
EEUN	Egyptian Electrical Unified Network
LE	Egyptian Pound
EVCS	Electric Vehicle Charging Station
EVs	Electric Vehicles
ECM	Equivalent Circuit Model
XFC	Extreme Fast Charging
FFBP-NN	Feed-forward Backpropagation Artificial Neural Network

FCEVs	Fuel Cell Electric Vehicles
FLC	Fuzzy Logic Controller
FC-ASCC	Fuzzy Controlled Active State-of-Charge Controller
GA	Genetic Algorithm
GHG	Greenhouse Gas
GWOA	Grey Wolf Optimization Algorithm
GP-LBCS	Grey Predicted Lithium-ion Battery Charge System
G2V	Grid-to-Vehicle
HW	Hammerstein-Wiener
HT	Hierarchical Technique
HEMS	Home Energy Management Systems
HEVs	Hybrid Electric Vehicles
IES	Integrated Energy System
ICEVs	Internal Conventional Engine Vehicles
IRR	Internal Rate of Return
IEC	International Electrotechnical Commission
JoAP	Joint Admission and Pricing
LM	Levenberg Marquardt
LP	Linear Programming
LF	Load Factor
LSTM	Long Short-Term Memory
MDP-RL	Markov Decision Process Reinforcement Learning
MAPE	Mean Absolute Percentage Error
MOERE	Ministry of Electricity and Renewable Energy
MILP	Mixed Integer Linear Programming
MPC	Model Predictive Controllers
ML MCC-CV	Multilevel Multistage Constant Current-Constant Voltage
MOPSO	Multi-Objective Particle Swarm Optimization
MSCC	Multi-Stage Charging Currents
MCCCV	Multistage Constant Current-Constant Voltage
NPCC	Negative Pulsed Charging Current
NNPC	Neural Network Predictive Controller
NPC	Neutral Point Clamped
OCV	Open Circuit Voltage
OCP	Optimal Charge Pattern
OAs	Optimization Algorithms
PSO	Particle Swarm Optimization
PCM	Phase Change Material
PV	Photovoltaic
PEV	Plug-in Electric Vehicle
PHEB	Plug-in Hybrid Electric Bus
PHEVs	Plug-in Hybrid Electric Vehicles
PMP	Pontryagin's Minimum Principle

PED	Positive Energy Districts
PPCC	Positive Pulsed Charging Current
PID	Proportional-Integral-Derivative
P2D	Pseudo-Two-Dimensional
PCC	Pulse Charging Current
PCC-CV	Pulse Charging Current-Constant Voltage
PWM	Pulse Width Modulated
ROM	Reduced-Order Electrochemical Model
RL	Reinforcement-Learning
RH	Relative Humidity
RESs	Renewable Energy Sources
ROI	Return of Investment
RMSE	Root Mean Square Error
SPM	Single Particle Model
SMC	Sliding Mode Control
SAE	Society of Automotive Engineers
SEI	Solid Electrolyte Interphase
STC	Standard Test Condition
SOC	State of Charge
SVM	Support Vector Machine
TPSO	Taguchi-Orthogonal-Based Particle Swarm Optimization
ToU	Time-of-Use
VLR	Vehicle Logo-Recognition
VMR	Vehicle Manufacturer Recognition
V2B	Vehicle-to-Building
V2X	Vehicle-to-Everything
V2G	Vehicle-to-Grid
V2H	Vehicle-to-Home
vTOU-DP	Virtual Time of Use Rate Dynamic Programming
VMC	Voltage Mode Controller
WT	Wavelet Transform
WTG	Wind Turbine Generators
WC	Wireless Charging

Nomenclature

Symbol	Description
A_{pv}	Installed PV module surface (m^2).
a_0	Polynomial Coefficient of the Cycle Depth Degradation Function.
$b_{(f,i,g,o)}$	The bias vectors of the long-short-term memory model.
$C_{chproposed}$	The charging capacity of the proposed technique.
$C_{disproposed}$	The discharging capacity of the proposed technique.
C_{Rate}	The rated capacity of the battery (Ah).
c_T	The temperature coefficient of the PV module ($^{\circ}C^{-1}$).
c_t	The memory cell of the LSTM model.
C_{α}	Electrochemical polarization capacitance.
C_{β}	Concentration polarization capacitance.
d	Depth of Discharge.
DOD	Maximum Depth of the Discharge in each segment.
d_{pj}	Measured output of the Feedforward backpropagation neural network (FFBP-NN).
$E(\omega)$	The objective function of the FFBP-NN.
$E_p(\omega)$	Output error for each p .
E_{Saved}	The saved energy.
E_c^{max}	Maximum Battery Capacity (kWh).
f_t	The output values of the forget gate.
G_i	Global solar irradiance (W/m^2).
g_t	The output values of the update gate.
h_{t-1}	The LSTM output value at time step $t - 1$.
i_t	The output values of the input gate.
$I_{C_{\alpha\lambda}}$	The stage current passes through the electrochemical polarization capacitance (C_{α}).
$I_{C_{\beta\lambda}}$	The current passes through the concentration polarization capacitance (C_{β}).
$I_{\xi\lambda}$	The maximum permitted charging current for each stage.
I_{λ}	The current of the present stage λ .
$I_{\lambda-1}$	The current of the battery at stage $(\lambda - 1)$.
N	The number of observations of the sample.
N_{cl}	EV Battery Life Span Charging/Discharging Cycles.
o_t	The output values of the output gate.
$P(u)$	The linear variable region between the cut-in and cut-out speed (kW).
$P_{\alpha}(u)$	Wind turbine generator output power (kW).
$P_{EV_{m,h}}$	Active power is required for EV fast charging at a specific minute and hour (kW).
P_{pv}	PV output power (W).

$P_{PV_{m,h}}$	Generated active power from the PV system at a specific minute and hour (kW).
P_r	The rated output power of the wind turbine (kW).
$P_{W_{m,h}}$	Generated active power from the wind energy system at a specific minute and hour (kW).
P_{tc}^{G2V}	EV Charging Power (kW).
P_{tc}^{V2G}	Discharging Power (kW).
R_C	capacitor internal resistances.
R_i	Ohmic internal resistance.
R_L	Inductor internal resistance.
R_α	Electrochemical polarization internal resistance.
R_β	Concentration polarization internal resistance.
SOC_f	Final State of Charge.
SOC_i	Initial State of Charge.
SOC_λ	The state of the present charging stage λ .
T_{P-set}	Set of Parking Time Slots (h).
T_{PV}	PV cell temperature ($^{\circ}C$).
$T_{reduced}$	The reduced charging interval time.
T_{STC}	Standard test condition temperature ($^{\circ}C$).
T_λ	The total time of current charging at the stage λ .
V	Wind speed (m/s).
V_A	The average voltage on the diode.
V_{c-i}	Cut-in wind speed (m/s).
V_{c-o}	Cut-out wind speed (m/s).
V_m	The measured voltage on the resistance R_m .
V_r	Rated wind speed (m/s).
V_{RES}	The renewable energy source's voltage.
$W_{(f,i,g,o)}$	The weight matrices.
\bar{x}	Distribution mean.
X_t	The input data.
y_{pj}	Predicted output.
α, β	Coefficients of Battery Specifications.
Δt	The change in interval time.
ε	Switching Binary Number 1 or 0.
η	The Coulomb coefficient is constant =1 for discharging and constant =0.98 for charging.
$\eta_{charging}$	The improved efficiency of the proposed technique.
$\eta_{C,EV-FC}$	The efficiency of the DC/DC EV fast-charging converter (%).
$\eta_{C,PV}$	The efficiency of the DC/DC PV converter (%).
η_{C-W}	The efficiency of the AC/DC wind converter (%).
η_D	Discharging Efficiency (%).
η_{pv}	The reference module efficiency (%).

$\eta_{R,Grid-DC}$	The efficiency of the grid rectifier (%).
$\rho_{B,EV-G}$	EV charging tariff using the utility grid in (LE).
$\rho_{B,EV-PV}$	EV charging tariff using the PV system in (LE).
$\rho_{B,EV-W}$	EV charging tariff using the wind turbine generator in (LE).
$\rho_{S,PV}$	Price of selling the power to the utility grid from the PV system (LE).
$\rho_{S,W}$	Price of selling the power to the utility grid from the wind energy turbine generator (LE).
σ	Standard deviation.
Ψ	A scenario of supplying the EVCS from PV, Wind, Grid or any combination of them.
Ψ_c^{BC}	Price of the Battery (LE).
Ψ_{tc}^{RC-V2G}	EV Owner Discharging Revenue Cost (LE/kWh).
Ψ_{tc}^{TC-G2V}	EV Charging Tariff Cost (LE/kWh).
ω	Weight matrix.
ω_1, ω_2	The weighting factor of the total energy loss and it could be adjusted from 0 to 1 where $\omega_2 = 1 - \omega_1$.
3	The percentage of error.

Chapter 1

Introduction

1.1 Introduction

The world is facing problems of ecological deterioration represented by greenhouse gas emissions and energy shortages. Meanwhile, conventional vehicles consume a large amount of fossil fuels and cause environmental pollution due to carbon emissions. According to the report of the European Union, 28% of the total carbon dioxide (CO₂) is produced from the transport sector, while road transport is considered over 70% of the transport sector emissions [1]. The electrification of conventional vehicles has become one of the most promising measures to solve these problems. Over the 2011–2021 decade, the projected size of the global electric vehicles (EVs) fleet is showing a booming trend, seeking a green sustainable eco-environment. EVs have been rapidly developed due to the need for automobile electrification, minimizing fuel consumption, and grid integration with their advantages of energy saving, environmental protection, and automation improvement capability, which leads to widespread attention by governments, automakers, and energy companies. The major two main problems that hinder the widespread of EVs are certainly the battery charging process which can be split into conventional charging protocols, identification of the battery dynamic behaviour, and the transient performance while implementing the charging schemes and their integration with the utility grid throughout the charging and discharging processes which influence on the grid peak demand. Typical concerns of potential customers are usually classified as the ‘driving range anxiety’: will they be able to find charging stations along their way, and the charging process takes too long? These two concerns come from the experience with internal combustion engine vehicles, where the re-fuelling process finishes in minutes and fuel stations are standardised and therefore widely spread. This created a direct need for EV DC fast charging protocols that aim for a minimal charging time requirement, optimum efficiency, effective cycle life, minimal battery degradation, and minimum charging loss. Several batteries manufacturing technologies are widely approved by companies at the manufacturing level such as Lead acid (Pb-acid), Nickel Cadmium (NiCd), Nickel-Metal-Hydride (NiMH), Sodium Nickel Chloride (NaNiCl), and Lithium-ion (Li-ion) batteries. However, lithium-ion polymer batteries have the advantages of high energy density (Wh/kg), high energy/volume coefficient (Wh/L), and high power/weight coefficient (W/kg) concerning the other batteries. The DC fast charging protocols under dynamic ambient conditions could be implemented through an effective identification of the battery dynamic behaviour supported by a smart controller.

While there is an increased use of fossil fuels accompanied by subsequent negative environmental impacts and supply decline, Renewable Energy Sources (RESs) such as photovoltaic (PV) and wind turbines (WTs) are pressed to be utilized for electric power generation and integration to supply electric vehicles. Furthermore, electric vehicles can be used as distributed storage resources to contribute to ancillary services for the system, such as peak-shaving power, or help integrate fluctuating renewable resources. The management of electric vehicles as distributed resources fits well in the paradigm of smart grids, where an advanced use of communication technologies and metering infrastructure, increased

Chapter 1

controllability, load flexibility, and a larger share of fluctuating and distributed resources are foreseen. Hence, researchers are tending to implement fast-charging centralized stations supplied by the utility grid and renewable energy resources to DC fast charge the EVs as will be scrutinized in the literature. The EV charging process places an excessive overload on the power grid and can cause fluctuations in the voltage and shortages in the supply. The mentioned issues were revealed during the peak demand period across the day. In the peak demand period, the ancillary power generators enter the network to avoid fluctuations that increase the operational and maintenance costs. In the off-demand period, unused and extra-generated power is wasted. Hence, vehicle-to-grid (V2G) and grid-to-vehicle (G2V) technologies which represent the EV discharging and charging processes, respectively should be utilized and improved to fill the research gap as will be mentioned in the literature.

1.2 Research problem statement

The regional climate can vary from coast to coast and the battery management system can be triggered by a variety of internal and external factors, thus fast charger deployment requires careful consideration regarding the impact of the regional ambient conditions (temperature accompanied by the relative humidity) [2]. The impact of the relative humidity factor on the charging process wasn't investigated or mentioned in the literature survey. However, the implementation of a lithium-ion battery fast charging protocol is depending on the current state of the battery at the specific ambient conditions. The identification model of the EVs represented in the lithium-ion battery while entering the charging station, connecting to the charging pile, and during the charging process is considered a challenging problem from many perspectives. The main problem is ensuring high charging efficiency accompanied by full recognition of the EV under different ambient circumstances (temperature and relative humidity). The authors in the literature, proposed recognition and classification methodologies that depend on the light intensity and vehicle logo recognition however, the dynamic electrical behaviour of EV batteries while charging under different circumstances is not investigated yet. Besides, there is a significant research gap in identifying a model that can describe the dynamic behaviour of the battery with the minimum percentage of error at the corresponding temperature and relative humidity. In addition, the conventional charging protocols are familiarised with slow charging time, high energy loss, and battery degradation.

Furthermore, the implementation of the charging protocols requires a smart power conversion controllable charger for regulating the voltage levels of the battery and enhancing the transient performance of the charging process while using renewable energy sources (RESs). Where the output voltage ripples and charging current ripples overheat the battery, accelerate side reactions and shorten its lifespan due to electrode degradation [3, 4].

Consequently, the EV charging process places an excessive overload on the power grid and can cause fluctuations in the voltage and shortages in the supply. The mentioned issues were revealed during the peak demand period. In the peak-demand period, the ancillary power generators have to enter the network to avoid fluctuations which increase the operational and maintenance costs. On the other hand in the off-demand period, the unused and extra-generated power will be wasted in vain due to the lack of flexible storage systems [5, 6]. Generally, the

Chapter 1

distribution of the utility grid is designed with a limited margin and overloading capacity due to the dynamic behaviour of the EV charging process. Additional loads would increase the risk of overloads for power lines and transformers, which can lead to extra energy losses and power quality degradation. Therefore, the vehicle-to-grid (V2G) concept has been introduced to solve the mentioned obstacles and issues based on smart charging and discharging schedules to reduce the peak load and shape the load profile in the power grid. However, the uncertainty and random behaviour during the charging and discharging operations, EVs may negatively affect the system efficiency and reliability where the uncoordinated EV charging could significantly change the shape of the aggregate residential demand. Hence, EV charging and discharging operations need to be aggregated by an EV aggregator to qualify the market entrance criteria, actively participate in the demand response (DR) balancing between the supply and demand sides, ensure minimum EV charging tariff while increasing the revenue, and minimize the battery degradation cost. Hence, aggregators are considered the interface between the distribution network and electric vehicle charging station (EVCS) which combine multiple EVs and coordinate and schedule the charging of the plug-in electric vehicle (PEV).

A summary of the main research gaps that have been mentioned above is presented in Figure 1-1.

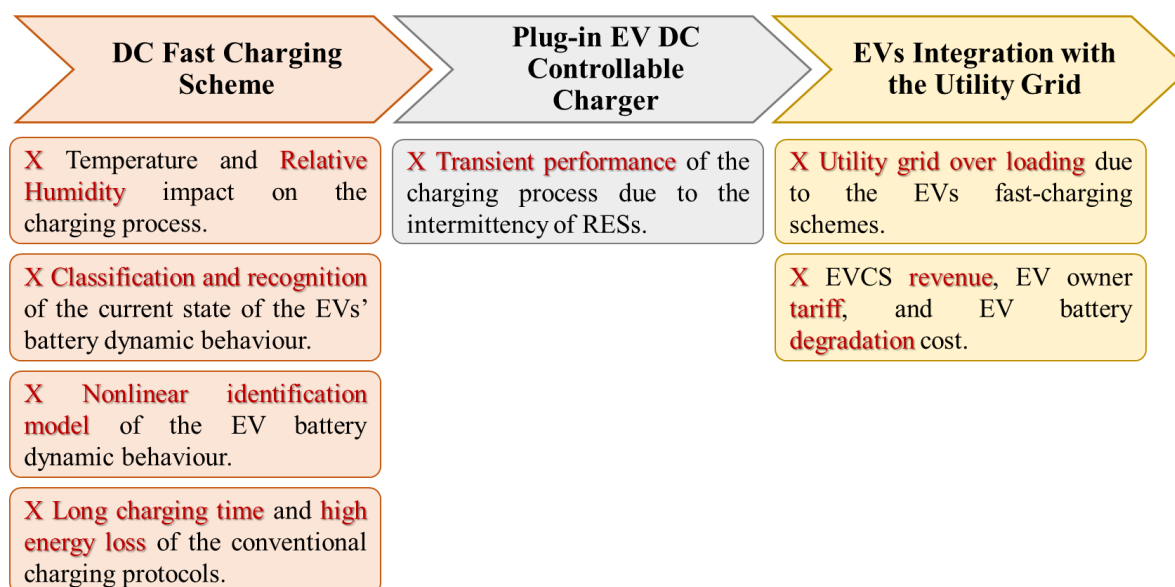


Figure 1-1 Schematic diagram of the main research gaps.

1.3 Research aim and objectives

The research aim is the development of an EV charging protocol using AI for fast charging under dynamic environment: towards Vehicle-to-Grid (V2G) Integration.

The objectives of this thesis could be represented by multiple stages as shown briefly in Figure 1-2 and could be summarised into three substantial points preceded by a detailed literature survey of the EVs' fast charging protocols, classification and recognition, battery identification models, and the integration scenarios and methodologies with the utility grid. The major points are:

Chapter 1

- Proposing a novel fast-charging framework that started from entering the EV to the charging station and connecting to the charging pile till leaving the station/parking point fully charged. This framework is based on a full investigation of the temperature and relative humidity impact on the charging process of plug-in electric vehicles (PEVs) represented by lithium-polymer ion batteries. This was followed by a novel EV classification and recognition model under the impacts of various ambient circumstances. Then intelligent fast charging techniques based on the multi-stage charging current (MSCC) charging protocol are proposed to improve the existing approaches in order to speed up the charging process whilst reducing energy consumption concerning the conventional charging protocol represented by the CC-CV charging protocol. The proposed framework is simulated and experimentally tested, validated, and verified.
- In the next stage, a smart plug-in EVs off-board controllable charger is implemented on a small-scale lithium-polymer ion battery of 1000 mAh. The controllable charger is simulated and experimentally tested, validated, and verified. The transient performance represented by the settling time and steady-state error is enhanced during the charging process throughout the conventional and proposed charging protocols.
- In the last stage, insightful controllable techno-economic scenarios and case studies of the charging/discharging process between the EVs and the utility grid are introduced using the grid-to-vehicle and vehicle-to-grid technologies. These scenarios are simulated and verified to fast charge the EV while minimizing the peak load demand, charging tariff, and battery degradation cost and maximizing the EV owner revenue.

Chapter 1

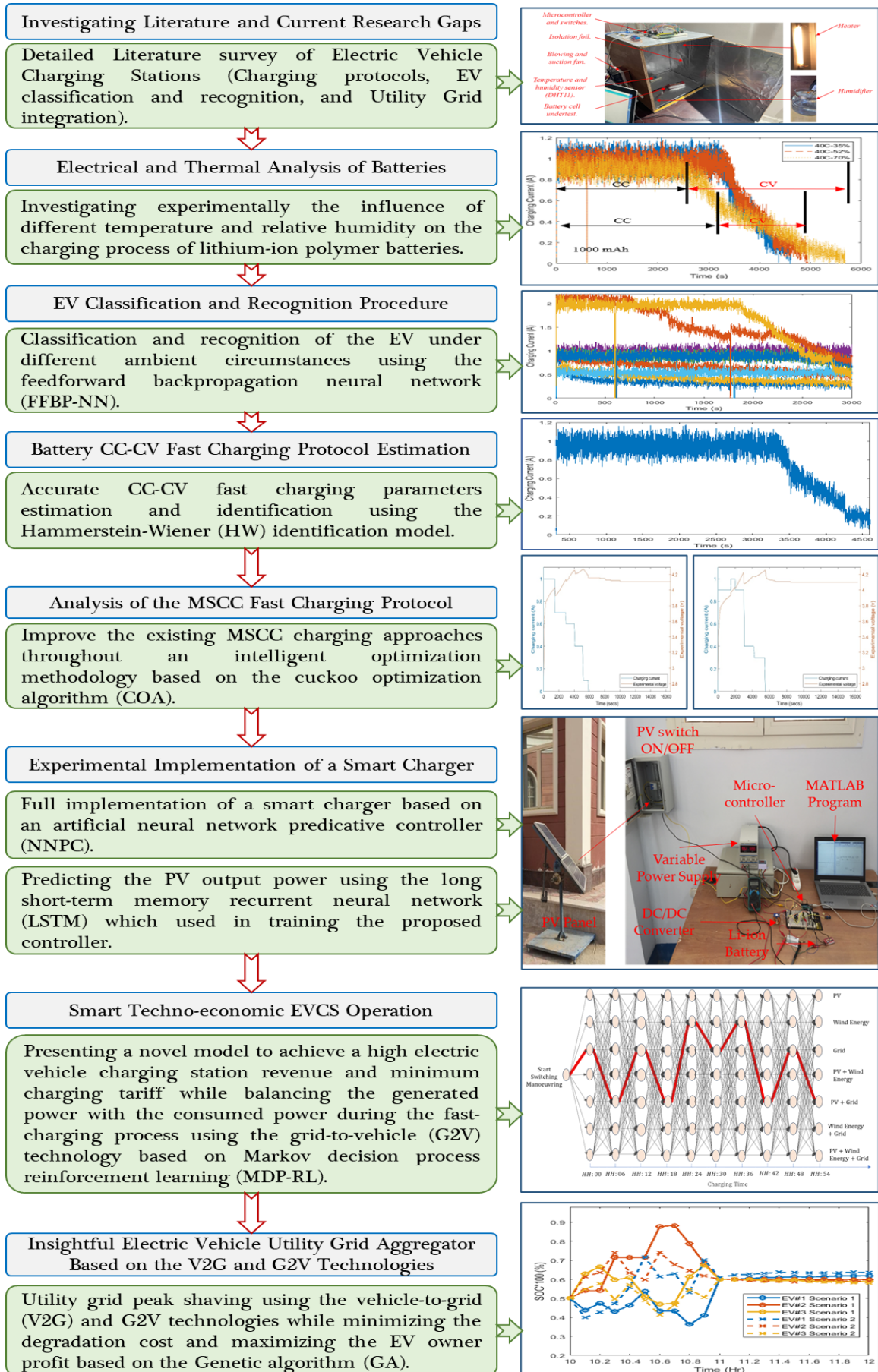


Figure 1-2 Schematic diagram of the main stages of this thesis.

Chapter 1

1.4 Research Methodology

The research methodology could be categorized into three substantial points with the corresponding specific procedures and techniques used to process, test, validate and verify the obtained results and findings as follows:

- The off-board charging scheme: a novel DC fast-charging framework started by connecting the EV to the charging pile till fully charged and leaving the charging point. This stage is implemented using the MATLAB/Simulink simulation program and validated experimentally as follows:
 - a) Full experimental investigation of the temperature and relative humidity impact on the charging process while charging the lithium-polymer ion batteries by the conventional Constant Current-Constant Voltage (CC-CV) charging protocol.
 - b) Classification and recognition of the EV at the charging operating temperature and relative humidity using the feedforward backpropagation neural network (FFBP-NN).
 - c) An artificial estimation of the CC-CV charging protocol parameters represented by the total charging interval time, charging current and battery terminal voltage using the FFBP-NN.
 - d) Effective identification and recognition of the battery dynamic behaviour using the Hammerstein-Wiener (HW) identification model.
 - e) Suggesting new intelligent charging techniques based on the multi-stage charging current (MSCC) charging protocol to improve the existing approaches in order to speed up the charging process whilst reducing energy consumption without degradation in the light of the outrageous demand for lithium-ion polymer battery in EVs using the Cuckoo optimization algorithm (COA).
- The plug-in EV off-board controllable charger: simulation and experimental implementation of the CC-CV and MSCC charging protocols on a smart charger controlled by an artificial neural network predictive controller (NNPC), trained, and supported by the long short-term memory recurrent neural network (LSTM). The proposed controller is compared with the conventional PID controller and the advanced fuzzy logic controller (FLC). This stage is implemented using the MATLAB/Simulink simulation program, tested, verified, and validated experimentally.
- EVs integration with the utility grid: novel techno-economic scenarios and case studies have been implemented and investigated using the integration between the EVs and the utility grid to optimise the EVs charging demand and the utility grid load demand as follows:
 - a) A novel hierarchal framework model for electric vehicle charging station (EVCS) aggregators is proposed to achieve a high EVCS revenue and minimum charging tariff using the mixed integer linear programming (MILP) and Markov decision process reinforcement learning technique (MDP-RL). Besides organizing and scheduling the EVs while entering the station during the day

Chapter 1

using MILP to satisfy the balance between the generated and consumed powers and minimizing the peak load charging demand.

- b) A vital development of a central aggregator to utilise the EVs stochastic parking across the day throughout the vehicle-to-grid (V2G) and grid-to-vehicle (G2V) technologies. The proposed model minimized the battery degradation cost while maximizing the revenue of the EV owner using the V2G technology and ensuring a sufficient grid peak load demand shaving using the genetic algorithm (GA).

1.5 Significant Contribution to Knowledge

The major contributions of this research have been published in 8 top-tier journals and conference papers in the publications listed above and represented briefly in the following main bullets:

- The Off-Board Charging Scheme:
 - a) The experimental influence of different ambient temperatures and relative humidity on the charging process is investigated through the charging interval time, current, and terminal voltage while charging by the CC-CV protocol. Where the relative humidity impact on the charging process wasn't concluded in the literature survey however the total charging interval time was reduced by 23.54% while fixing the temperature and increasing the relative humidity.
 - b) Classification and recognition of the EV battery at the corresponding operating temperature and relative humidity are implemented using the FFBP-NN. The accuracy for the overall network reached 83.2%.
 - c) A full charging estimation of the CC-CV fast charging protocol represented in the total charging interval time, charging current and battery terminal voltage is obtained using the FFBP-NN. The error between the simulated and measured terminal voltage reached 1%.
 - d) Effective identification of the battery dynamic behaviour is obtained using the HW non-linear identification model. The maximum error between the measured experimental data and the simulated model of the battery terminal voltage reached 0.05V.
 - e) Novel techniques based on the MSCC charging protocol using the COA are proposed and compared with the conventional CC-CV charging protocol. The charging interval time was reduced by 22.45% and the energy loss is reduced by 10.408% concerning the CC-CV charging protocol.
- The plug-in EV off-board controllable charger:
 - a) The NNPC supported by the LSTM model is implemented to enhance the transient performance of the charger and compared with the PID and FLC controllers. The battery charging settling time reached 1 ms and the terminal voltage ripples reached 1 mV using the NNPC-LSTM controller.

Chapter 1

- EVs integration with the utility grid: the EVs are represented by the electric vehicle charging station and stochastic parking during the day. The aggregator has substantial roles to optimize the integration between the EVs and the utility grid could be represented as follows.
 - a) Organizing and scheduling the EVs while entering the EVCS during the day using MILP to satisfy the balance between the generated and consumed powers. The proposed methodology is based on selecting an appropriate and accurate time to plug in the electric vehicle to be fully charged (94% SOC) according to the specification of the EV battery to ensure the satisfaction of the driver.
 - b) Minimizing the peak load demand occurred due to the DC fast charging and consequently flattening the difference between the power generated from the RESs and power consumed by the EVCS. As the peak demand is reduced, the generation capacity of the RESs and utility grid will not be overstretched, and system stability would be improved. The EV charging peak load demand was reduced by 3.31% (4.5 kW) and the load factor increased by 3.1276%.
 - c) Maximizing the profit of the EVCS while minimizing the EVs' charging tariff which is considered a conflicting objective function using the manoeuvring capability of the switches between the renewable energy sources and the utility grid. The status of each switch is perfectly predetermined using the MDP-RL and compared with MILP and traditional operation. The revenue using the MDP-RL reached 20.10% however the EV charging tariff increased by 15.03%.
 - d) Utilizing the EVs stochastic parking during the day in order to minimize the utility grid load demand while minimizing the EV battery degradation cost and EV owner tariff using the G2V and V2G technologies based on the GA. The degradation cost was reduced by 40.9256% while increasing the SOC by 27.77% and the utility load demand decreased by 26.5% (371 kW)

1.6 Structure of thesis

The work chapters of the thesis are structured as follows:

Chapter 2: an in-depth investigation of the current literature on EV's fast charging protocols represented by small-scale lithium-ion batteries, control systems used in the chargers, and the methodologies used in the integration between the EVCS or any parking pile and utility grid. The gap in the literature is supported by tables to emphasize the main parameters that will be improved and investigated in this thesis.

Chapter 3: presented a novel EV fast charging protocol using AI: towards Vehicle-to-Grid integration through a full investigation of the ambient conditions (temperature and relative humidity) in the charging process accompanied by classification, recognition, identification, modelling and estimation of the battery's dynamic behaviour.

Chapter 4: proposed CAD, design, and development of EV charging protocol using AI for fast charging under dynamic environment. New techniques based on the multi-stage charging current (MSCC) charging protocol are proposed and compared with the conventional constant

Chapter 1

current-constant voltage (CC-CV). In addition, an off-board smart charger is controlled using the neural network predictive controller to have the optimum charging transient performance.

Chapter 5: included the system integration, testing, validation, and verification. Various insightful integration scenarios and case studies between the EVs and utility grid are proposed throughout the charging and discharging processes using the grid-to-vehicle (G2V) and vehicle-to-grid (V2G) technologies.

Chapter 6: declared the conclusions, major findings, recommendations, and future work.

Appendix A: stated the MATLAB source code of the proposed fast charging techniques using the multi-stage charging current (MSCC) protocol based on the cuckoo optimization algorithm.

Appendix B: introduced the complementary tables to the methodologies used in the thesis.

Chapter 2

Literature Review

2.1 Introduction

Electric Vehicles (EVs) are gaining strong momentum in the vehicle market due to their low price compared with conventional vehicles, low greenhouse gas (GHG), low emissions, low dependency on fossil fuels, low noise, and increasing climate and environmental awareness [1, 7]. According to the report in [8], there were 10 million electric vehicles in the world at the end of 2020. In the first quarter of 2021, EV sales rose by 140% compared to the same period in 2020, despite the global pandemic (COVID-19).

In this chapter, an overview of different research tracks concerning EVs is presented; see Figure 2-1. We will review the state of the art of the EV connection to energy source categories, charging standards, charging methodologies, modelling of the lithium-ion battery, scrutinizing the various fast-charging protocols, implementation of the corresponding charging protocol, and the aggregator roles in connecting the EVs to the utility grid.

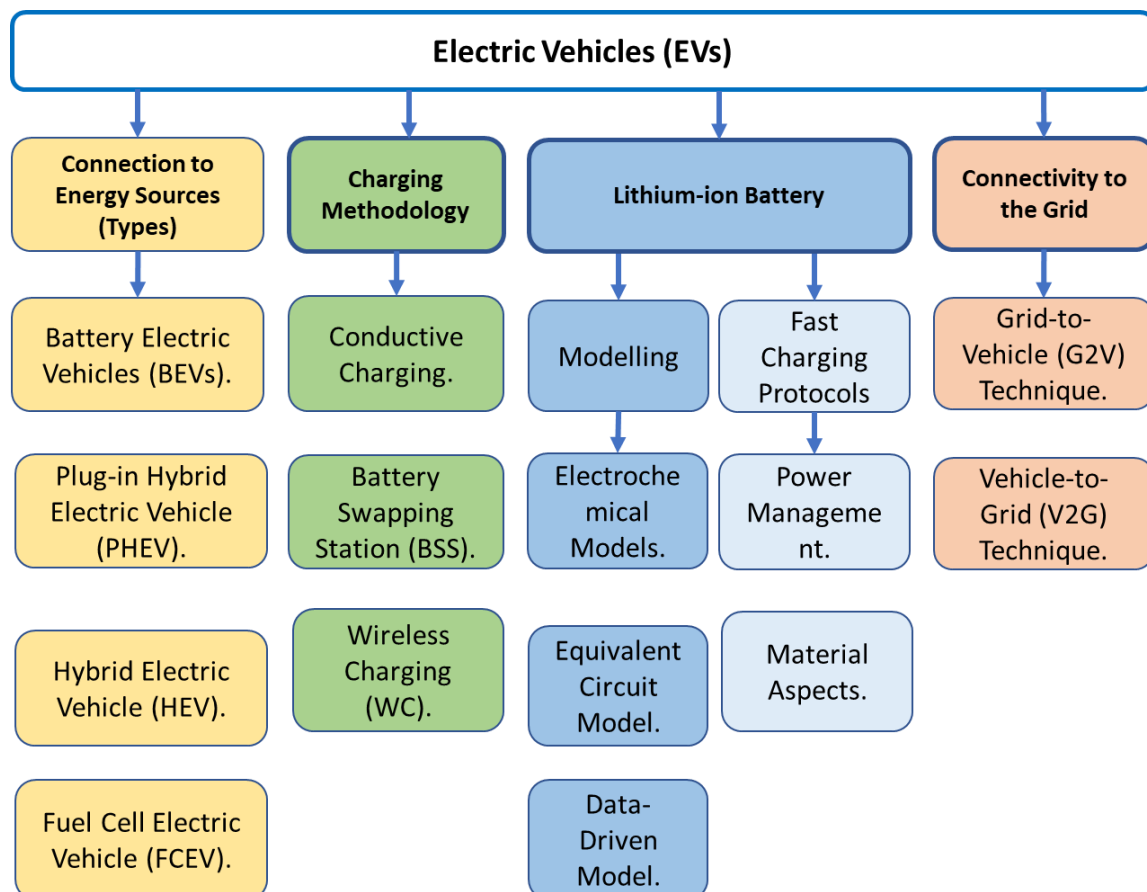


Figure 2-1 Overview of the electric vehicle (EV) research tracks.

EVs are divided into four main categories based on their connection to energy sources, namely plug-in hybrid electric vehicles (PHEVs), hybrid electric vehicles (HEVs), battery electric

Chapter 2

vehicles (BEVs), and fuel cell electric vehicles (FCEVs) [9, 10]. PHEVs and HEVs depend on both electrical and internal combustion engines; BEVs require EVs that only run with electrical energy; and FCEVs use the onboard generation of hydrogen to reduce hydrogen storage and handling issues [11-13].

The authors in [14] predicted that around 130 million private chargers and 13 million public chargers will be needed by 2030 to fulfil the energy demand of different types of EVs. To facilitate this advancement, there is a direct need to invest in charging infrastructure. Chargers must be structured to charge EVs according to the standard set by international institutions such as the International Electrotechnical Commission (IEC), the Society of Automotive Engineers (SAE), and CHAdeMO [1, 15]. EV standards, according to IEC-62196, SAE-J1772 and CHAdeMO, are provided in [1, 16-19]. Those standards are proposed in Table 2-1, and categorized based on the available maximum power rating, voltage, maximum rating current, and charging time.

Charging methodologies are classified into three main categories, namely conductive charging, wireless charging (WC), and a battery-swapping station (BSS) [13]. The battery can be charged anywhere, from an electric vehicle charging station (EVCS) to separate street chargers, workplace chargers, and private in-home chargers. The conductive charging technique depends on the advancement of the EV, which can have on-board and off-board properties. On-board chargers are widely known as AC chargers, which can be single-phase Level 1 and Level 2, as defined in SAE-J1772, and three-phase AC charging, as defined in SAE-J3068. Off-board chargers are referred to as DC chargers, which ensure higher charging current rates, as defined in SAE-J1772-Combo/CHAdeMO standards [20-22]. Wireless charging (WC) allows EVs to charge without any physical contact or cable connection between the supply and the battery [23, 24]. Battery-swapping stations (BSS) are stations where an empty battery can be replaced with a fully charged battery within a few minutes [25, 26].

Chapter 2

Table 2-1 Charging rates of IEC standards, SAE standards, and CHAdeMO.

Charging Levels	Maximum Power Rating (kW)	Voltage (V)	Maximum Current Rating (A)	Charging Time
IEC-62196 Standard [1]				
AC Level 1	3.8	230–240 V AC	16	NA
	7.6	480 V AC		
AC Level 2	7.6	230–240 V AC	32	
	15.3	480 V AC		
AC Level 3	60	230–240 V AC	32–250	
	120	480 V AC		
DC	400	600–1000 V DC	250–400	
SAE-J1772 Standards [27]				
AC Level 1	1.9	120 V AC	16	PHEV: 7 h BEV: 17 h
	3.3			PHEV: 3 h BEV: 7 h
AC Level 2	7	240 V AC	80	PHEV: 1.5 h BEV: 3.5 h
	20			PHEV: 22 min BEV: 1.2 h
DC Level 1	40	200 to 500 V DC	80	PHEV: 22 min BEV: 1.2 h
DC Level 2	Up to 100	200 to 500 V DC	200	PHEV: 10 min BEV: 20 min
CHAdeMO [1, 28]				
DC Fast Charging	400	400 DC	200	20 min

2.2 Electric Vehicle Batteries

Several batteries manufacturing technologies are widely approved by companies at the manufacturing level such as Lead acid (Pb-acid), Nickel Cadmium (NiCd), Nickel-Metal-Hydride (NiMH), Sodium Nickel Chloride (NaNiCl), and Lithium-ion (Li-ion) batteries [29, 30]. Pb-acid batteries are considered the oldest type of batteries and have low energy/weight and energy/volume ratios, which is a disadvantage due to the presence of lead in their construction. NiCd batteries have the highest number of cycles, but the use of cadmium in their construction is considered harmful to the environment, animals, and human health. NiMH batteries have a lack of memory effect, which affects the maximum load capacity of the battery, but they have low energy storage capacity and a high self-discharge coefficient. NaNiCl

Chapter 2

batteries have the advantage of working at high temperatures of 270-350°C; however, they have issues related to safety during operation and storage for long periods. Li-ion batteries have the advantages of high-power storage capacity, low self-discharge rate, thermal stability, high nominal voltage, and good energy density/weight ratio. However, they have a very low overcharge tolerance and high cost. The main source of lithium-ions in Li-ion batteries is the positive electrode material or the cathode. The types of cathode materials include lithium cobalt oxide (LiCoO_2), lithium manganese oxide (LiMn_2O_4), lithium iron phosphate (LiFePO_4), lithium nickel manganese-cobalt oxide (LiNiMnCoO_2), lithium nickel cobalt aluminium oxide (LiNiCoAlO_2) and lithium titanate ($\text{Li}_4\text{Ti}_5\text{O}_{12}$). Li-ion batteries can be packed in two major formations, which are metal cans in cylindrical or prismatic shapes or laminate films (stacked cells) that are called Lithium-ion polymer batteries, where a gel or polymer is often used to prevent the electrolyte from leaking. Lithium-ion polymer batteries have the advantages of high energy density (Wh/kg), high energy/volume coefficient (Wh/L), and high power/weight coefficient (W/kg) compared to other types of Li-ion batteries; however, they become unstable when overloaded or discharged below a certain limit [29].

In this thesis, all the algorithms and methodologies are implemented using Lithium-polymer ion batteries while avoiding heating and degradation, which can result from exceeding the limits of charging and discharging processes [29, 30]. In addition, the charging and discharging procedures are implemented within the acceptable temperature range of 25°C to 70°C, where high temperature accelerates side reactions and electrode degradation [3, 31], and low temperatures make a drop in active material, increase internal resistance, reduce energy and power capacity, and leads to lithium plating [32, 33], as will be explained in the following sections. Overcharging and over-discharging are also considered to avoid heating inside the battery, cracking the solid electrolyte interface (SEI), and loss of active area inside the battery [34, 35]. Increasing the charging current accelerates battery ageing disproportionately, leading to capacity and power fade while posing an unacceptable safety hazard during operation [36]. Several protocols have been developed to solve the dilemma between charging speed, battery surface temperature, and battery ageing. In addition, car manufacturers have targeted faster charging times by calculating the charging time in km/min to achieve a more user-oriented and comparative figure over different vehicle sizes [36]. Unfortunately, these ideas usually pose several trade-offs, in reality, especially the slow charging rate which is considered one of the major limitations [36-38].

Hence, the lithium-ion batteries from the electrical perspective (modelling, fast charging protocols, and temperature and relative humidity impact on the charging process) are investigated to reveal the research gap and focus on our contribution in the corresponding area. The trailing section scrutinizes the comparison between the methodologies used for each protocol in a fair comparison where the main contributions of this review are as follows:

- a) Clearly and systematically presents and classifies various charging protocols and the main controllable input and output parameters for each.
- b) Reveals a full comparison between the sub-charging methodologies of each charging protocol and the impact on the charging time, efficiency, and energy loss.

Chapter 2

- c) Define new up-to-date strategies depending on the power management, thermal management, and material aspects. In addition, full identification of the pros and cons of each protocol is stated clearly which may lead the researchers to improve the existing protocols.

2.3 Lithium-Ion Battery Fast Charging Protocols

Rechargeable Lithium-ion batteries are the intrinsic technology of EVs and they are commercialized for energy storage devices due to their high energy density, low self-discharge rate, high efficiency, fast charging capability, and longer lifespan [39-41]. However, Li-ion batteries are sensitive to fast charging which accelerates the ageing effect and capacity loss [20, 42]. The charging processes can be influenced substantially by the manufacturers throughout realizing and implementing a specific charging protocol, that combines the charging time, capacity, and cycle life [43, 44]. The following subsections will provide an overview of the various categories of charging protocols and their characteristics, pros, and cons. However, the experimental procedures for each protocol vary among the publications, which impedes a direct comparison. Due to the different cell types that have been used in the experiments, no dependencies are revealed between the charging protocol and cell type. After an extensive literature review of different charging protocols, it is observed that no detailed fair comparison of the various types of charging protocols because of the various lithium-ion batteries capacity used in each research.

Before discussing the different categories of the charging protocols, the dynamic behaviour of the Lithium-ion battery has to be established throughout various models based on mathematical equations and/or collected data [45]. The most common models used are the electrochemical mechanism model which describes the internal chemical process of the battery, the equivalent circuit model which represents the chemical nature as electrical components, and the data-driven model which includes artificial neural network, support vector machine, black box, etc. [45-48]. Electrochemical models can describe the battery chemistry through the reactions that take place in the electrodes and the electrolyte deployed and they can be categorized as Single Particle Model (SPM) [49, 50], Pseudo-two-Dimensional (P2D) model [51, 52], comprehensive capacity degradation model [53]. Equivalent Circuit models such as the Rint model, Partnership for a New Generation of Vehicles (PNGV) model, Thevenin model, modified Thevenin model, RC first-order transient, RC second-order transient model, and RC cascaded transient model [37, 54-56]. Finally, the Data-driven model consists of the black-box model that is considered as a linear and nonlinear mapping function of the terminal voltage instead of the description of the electrochemical physics process of the battery, machine learning techniques with pattern recognition, clustering, and classification, and artificial neural network which employed to predict the charging and discharging behaviour of the battery, etc. as stated in [45].

Fast charging protocols are targeting minimum charging time, optimum efficiency, effective cycle life, and minimum charging loss. Researchers are seeking to eliminate the high C-rate charging and high depth of discharge (DOD) range which increase the loss of active material and reform the solid electrolyte interphase (SEI) at the surface of the electrode, hence resulting

Chapter 2

in increasing the internal impedance and minimizing the capacity of the battery [57-59]. In addition, researchers recommended avoiding overcharge and over-discharge of the battery which cause unwanted heating inside the battery, therefore cracking the SEI and loss of active area inside the lithium-ion battery, and minimizing the number of ions participating in electrochemical reaction respectively [34, 35]. The efficiently designed and high-quality charging protocol not only reduces the charging time but will also improve the performance of the battery, energy conversion efficiency, and lifespan, and reduce energy loss.

The main lithium-ion battery fast charging protocols could be expressed in Figure 2-2. The protocols can be split into power management which depends on the topology of applying the voltage and current during the charging process, thermal management which manipulates the temperature of the lithium-ion battery while charging, and the material aspects which pertain to the electrolyte modifications (concentrated electrolyte and low viscosity additives). The most up-to-date articles in each category will be discussed in the following subsections.

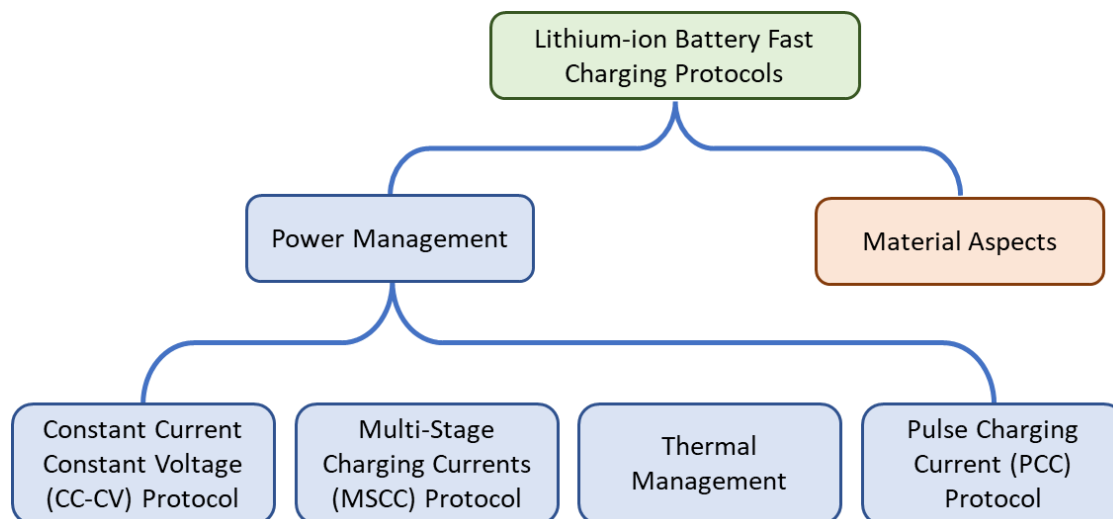


Figure 2-2 Main fast-charging protocols of the Lithium-ion battery.

2.3.1 Constant Current Constant Voltage (CC-CV) Protocol

The power management charging protocol is depending on charging the lithium-ion battery with various current and voltage topologies to ensure fast charging, minimum charging loss, high efficiency, and lifespan. An investigation for each protocol will be introduced in this chapter starting from the CC-CV protocol.

CC-CV is considered the traditional charging protocol for lithium-ion batteries. CC-CV method is based on charging the battery with a constant charging current until the voltage reaches the cut-off value and then the voltage is held constant while the current decays to the minimum value as expressed in Figure 2-3. This protocol is efficient with a battery management system (BMS) [60], easy to implement, needs simple requirements, and avoids overcharging due to the constant voltage mode. However, it is so conservative due to the long charging time while gradually reducing the current density to 0.1C [61], low efficiency, and

Chapter 2

short battery runtime [62, 63]. The authors in [64] revealed that the CV charging stage can cause degradation whenever the voltage exceeds the cut-off voltage.

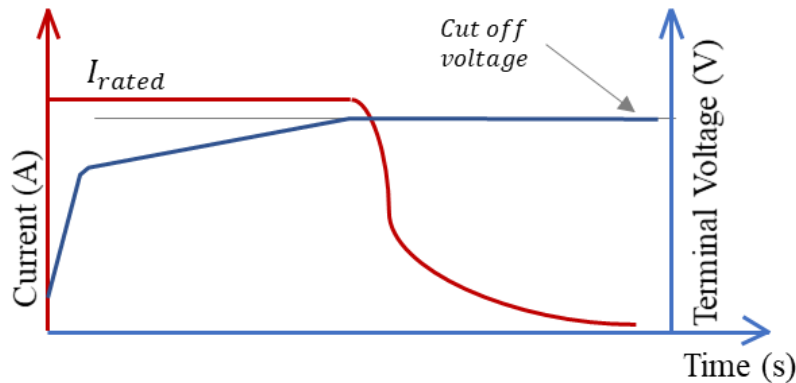


Figure 2-3 Schematic diagram of the Constant Current-Constant Voltage (CC-CV) Protocol.

2.3.2 Multi-Stage Charging Currents (MSCC) Protocol

Researchers are seeking protocols to reduce the charging time and the degradation compared to the CC-CV method. In the multi-stage charging currents protocol, the battery is charged by a multi-stage of different currents and the lifetime extends without a degradation impact. Many algorithms and techniques have been implemented for multi-stage constant current charging of the lithium-ion battery to reduce the charging time, reduce the energy loss and improve the charging efficiency. However, it is time-consuming to find the optimal charging strategy throughout charging and discharging experiments. Recently, lithium-ion batteries dominate all modern technologies according to their high voltage variety, low charging rate, low self-discharging rate, long life cycle, and high energy efficiency [65-67]. Due to the dynamic characteristics and complex behaviour of the lithium-ion battery, knowledge of its various equivalent circuit models is an essential step to understand its performance [68-72].

The charging process in [73] is split into n stages of constant current (CC) [I_1, I_2, \dots, I_n], which are combined with n voltage thresholds [V_1, V_2, \dots, V_n], which control the end of each CC stage. An optimization algorithm is formulated by the `fmincon` MATLAB function to estimate the parameters of MSCC protocol where the number of stages is set to $n=10$. MSCC is investigated and compared with the CC-CV charging protocol at different chosen temperatures of 5°C, 25°C, and 45°C representing a cold, mild, and hot climate, respectively. An optimal charging pattern is implemented in [74] of 5 MSCC and the Grey Wolf Optimization algorithm (GWOA) is used to find the optimal charging current for each stage. An improvement in the charging time, maximum temperature rise, and charging efficiency is ensured in this article. The advantages of the GWOA are including a few parameters, easy implementation, and a special capability to strike the balance between exploration and exploitation during the searching process. The charging current stage using GWOA is changed whenever the battery voltage reaches the cut-off voltage, and these procedures are repeatable till the change in voltage is minimized as shown in Figure 2-4-a.

Multistage constant current-constant voltage protocol (MCCCV) based on particle swarm optimization algorithm is proposed in [75] where three strategies are proposed: a fast charging

Chapter 2

for motorway driving (ageing loss of the battery is not considered $\beta=1$), minimum ageing charging for family use ($\beta=0$), and a balanced charging for daily use which expressed by Pareto frontier boundaries plot. MCCC method are the battery is first charged at constant current till the voltage reaches cut-off voltage then a new set of charging currents is applied accordingly, till the SOC of the battery reaches $\geq 90\%$ then finally the constant voltage stage is implemented. Also, the authors in [76] used the Particle Swarm Optimisation (PSO) algorithm with the strategies in [75]. The Taguchi-orthogonal method has been employed in [77] to search for an optimal fast-charging 5-stage pattern. The Taguchi method is based on experimental analysis to avoid complicated modelling of the lithium-ion battery. In [78] the Taguchi-orthogonal-based particle swarm optimization (TPSO) algorithm has been utilized using four MSCC protocols and the results were compared with five MSCC protocols. It is concluded that 4 or 5 MSCCs do not have a significant impact on the charging time and efficiency. The multi-objective particle swarm optimization (MOPSO) method based on the Pareto front has been used in [79]. The optimum solution is selected using the technique for order of preferences by similarity to the ideal solution (TOPSIS).

To prevent the voltage from rising to the cut-off voltage level during the charging process, multilevel multistage constant current-constant voltage superfast charging (ML MCC-CV) method has been implemented in [80]. The initial charge mode is set to trickle mode to avoid battery damage. When the voltage of the battery is within the normal operating range ($\geq 3V$) ML MCC-CV charging starts as shown in Figure 2-4-b where the charging voltage and current are set to be 4.1V and 10C, respectively. Whenever the battery voltage reached $\geq 4.1V$ a charge voltage of 4.15V and CC of 5C are applied. Finally, when the voltage reached $\geq 4.15V$ a charging voltage of 4.2V and CC of 2C is implemented till the end of charging.

In [81] large-scale EV battery with a capacity of 50kW has been charged from 20% to 90% SOC using the constant power constant voltage (CPCV) method and the results are compared with the conventional CC-CV charging protocol. It is concluded that optimal power charging can reduce energy loss and 9% of the cost compared to the existing fast-charging conventional mode. Such power management approaches based on MSCC are often motivated by reducing heat generation, avoiding lithium plating, avoiding overcharging, and reducing mechanical stresses when the diffusion of Li^+ ions is constrained[82]. However, the MSCC protocol requires a full estimation of all the internal equivalent parameters of the electric circuit used in modelling [67].

Chapter 2

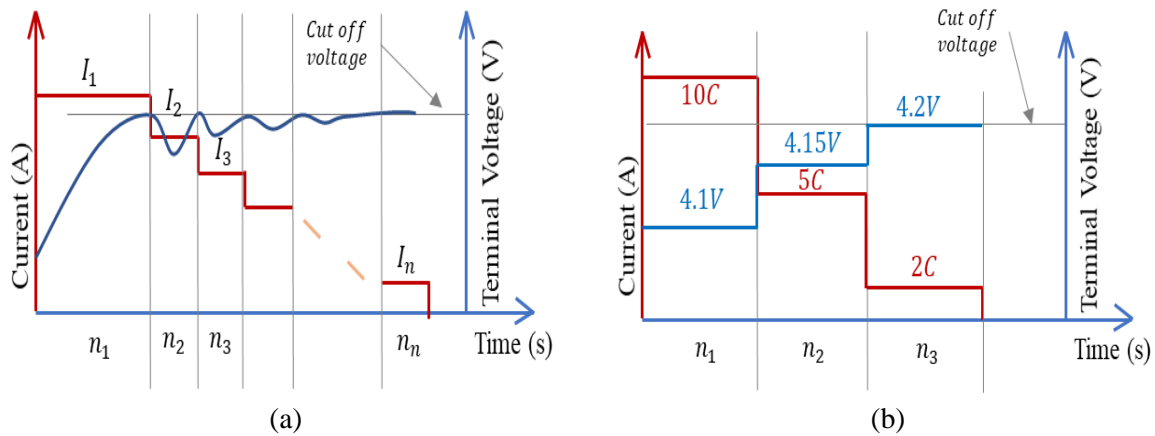


Figure 2-4 Schematic diagram of the Multi-Stage Charging Current (MSCC) Protocol.

In the multi-stage charging current technique, the battery is charged by a multi-stage of different currents. Many algorithms and techniques have been implemented for multi-stage constant current charging of the lithium-ion battery in Table 2-2 such as Particle Swarm Optimization (PSO) based Fuzzy Logic, Consecutive Orthogonal Arrays, Correcting Slope Iteratively, Taguchi Approach, Ant Colony algorithm, Optimal charge pattern (OCP), Balance of Internal Consumption and Charging Speed, PSO, Negative pulse, Boost-charging, and Dynamic programming algorithm. Previous researchers used various methodologies to study the charging process, such as the type of model used, the charging time or/and energy consumption, charging efficiency performance, charging capacity, and several tests and stages, which are summarized in Table 2-2.

Chapter 2

Table 2-2 Comparison between algorithms presented in the literature survey using the multi-stage charging current (MSCC) protocol, and Thermal Management Protocol.

Type	Battery	Circuit	Charging Time (min)	Maximum charging current (A)	No of stages	SO C _f (%)	Charging Efficiency (%)	Charging loss (J)	Cycling	Temperature Rise (°C)					
Numerical optimization [73]	INR18650HG2 from LG, 3Ah	Coupled Electro-thermal model	Case A 25°C	CC-CV	61	1.33C	---	96.2	N/A	N/A	330	N/A			
			Case B 25°C	MSCC	65	1.917C	10	96.8	N/A	N/A	700-800	N/A			
			Case C 25°C	CC-CV	43	1.66C	---	96.2	N/A	N/A	N/A	330	N/A		
				MSCC	52	3C	10	93.5	N/A	N/A	N/A	450	N/A		
			Case D 5°C	CC-CV	46	1.67C	---	83.3	N/A	N/A	N/A	600	N/A		
				MSCC	37	3C	5	78.4	N/A	N/A	N/A	1200	N/A		
			Case E 45°C	CC-CV	66	1.33C	---	91.4	N/A	N/A	N/A	100	N/A		
				MSCC	91	1.167C	10	90.4	N/A	N/A	N/A	400	N/A		
			Grey Wolf optimization algorithm [74]	SAMSUNG INR18650-25R Li-Ion Battery	Thevenin equivalent circuit	Case-1	2C-CC-CV	66	2C	---	98.43	98.31	N/A	N/A	~ +2 K
						Case-2	1C-CC-CV	97	1C	---	100	98.4	1363.04	167	~ +1.75 K
Case-3	Case-1	92				0.8292C	5	98.45	98.87	1133.91	300	~ +1.75K			
Case-4	Case-2	93				0.832C	5	98.46	98.82	1142.4	N/A	~ +1.75K			
Case-5	Case-3	85				1C	5	98.79	98.69	1334.99	N/A	~ +2.1K			
Case-6	Case-4	89				0.9092C	5	98.48	98.7	1239.26	N/A	~ +2K			
Case-7	Case-5	91				0.8692C	5	98.01	98.79	1175.86	N/A	~ +1.9K			

Chapter 2

	Case-6		93	0.822C	5	98.4 6	98.81	1132.1	N/A	~ +1.75K
Adaptive MSCC [75]	Fast Charging ($\beta=1$)	CC-CV	52.7	1C	---	N/A	N/A	N/A	N/A	+5.1°C
	Minimum aging ($\beta=0$)	CC-CV	68.383	0.75C	---	N/A	N/A	N/A	N/A	+3°C
		MCCCV	NCR18650B battery	52.7	1C	N/A	N/A	N/A	N/A	N/A
	Balanced charging ($\beta=0.014$)	MCCCV	200	0.25C	N/A	N/A	N/A	N/A	N/A	+0.35°C
	MCCCV	NCR18650B battery	58	0.7836 C	N/A	99.0 13	N/A	N/A	N/A	+3.5°C
	CC-CV		102.77	0.5C	---	N/A	N/A	N/A	N/A	+1.5°C
Taguchi-orthogonal based Particle Swarm Optimisation (TPSO) [78]	CC-CV		119	0.7C	---	99.5	99.10	N/A	280	~ +2.75°C
	ECCCV		114	0.8036 C	---	98.7	98.93	N/A	N/A	~ +1.5°C
	MSCC	Sanyo UR14500P 840 mAh	67	1.262C	4	94.7	98.97	N/A	190	~ +3.5°C
	MSCC	Sanyo UR14500P 2200 mAh	51	1.44C	5	N/A	98.91	N/A	N/A	N/A
	CC-CV		118	1.44C	---	N/A	98.54	N/A	N/A	N/A
Multi-objective particle swarm optimisation (MOPSO) [79]	MSCC	LiFePO ₄ battery 8Ah and 3.2V	25.567	4.925C	8	N/A	N/A	N/A	N/A	+4.1°C

Chapter 2

Taguchi-orthogonal method [77]	CC-CV_0.1C	3150 mAh	1 Resistor + 1 Impedance	59.4	1.55C	---	94.1	93.3	N/A	N/A	+20.3°C
	CC-CV_0.2C			49.37	1.55C	---	92.3	93	N/A	N/A	N/A
	MSCC_1			54.22	1.55C	5	93	93.9	N/A	N/A	+19.2°C
	MSCC_2			55.47	2C	5	93.1	91.1	N/A	N/A	+28.5°C
Particle Swarm Optimisation (PSO) [76]	1C-CC-CV	Panasonic 18650 LI-ION CELLS	IRC transient	50	1C	---	N/A	N/A	N/A	N/A	~ +6°C
	2C-CC-CV			~ 29.2	2C	---	N/A	N/A	N/A	N/A	~ +18°C
	Minimum charging time ($\beta=1$)			27.43	2C	---	N/A	N/A	N/A	Decays 0.8%	~ +18°C
	Minimum Aging charging ($\beta=0$)			~ 60	0.077C	---	N/A	N/A	N/A	Decays 0.557 6%	~ +0.04°C
	Balanced charging ($\beta=0.0113$)			51.832	0.89C	---	N/A	N/A	N/A	Decays 0.627 6%	~ +4°C
Constant Temperature Constant Voltage (CT-CV) protocol [83]	CC-CV	Samsung INR18650-25R cylindrical cell	Thevenin model + Second-order thermal model	85	1C	---	100	N/A	N/A	N/A	+7.5°C
	CT-CV			69.5	2C	---	100	N/A	N/A	N/A	+7.5°C

Chapter 2

Pontryagin's Minimum Principle (PMP) [84]	Real-time PMP	Panasonic NCR18650PF	Thermal Dynamics	18	5C	---	20 to 70	N/A	N/A	N/A	~ +6°C
	CC-CV			16	1.61C	---	20 to 70	N/A	N/A	N/A	~ +5.5°C
Genetic Algorithm (GA) optimal charging strategy [85]	CC	LiNMC, 5Ah, 3.6V	IRC transient	40.05	0.5C	---	95.34	N/A	0.77	N/A	+2.13°C
	Optimal Improvement			36.1	0.5C	---	95.34	N/A	0.7	N/A	+1.91°C
Two Stage Constant Current (2SCC) [86]	High-low profile	A123 26650 LiFePO4 graphite cylindrical battery	N/A	30	2.6C to 0.6C	2	80	98.1	6.62	N/A	~ +8°C
	Low high profile			30	0.6C to 2.6C	2	80	95.1	6.83	N/A	~ +8.5°C

2.3.3 Thermal Management Protocols

Thermal management charging protocol is depending on the control of the ambient and cell (battery) temperatures while the charging process. Due to battery temperature being considered a key degradation metric, a new fast-charging constant temperature constant voltage (CT-CV) protocol has been presented in [83] and represented in Figure 2-5. The CT-CV protocol is based on applying an initial current reached 2C of the battery and then an exponentially decaying current profile till 1C, whenever the battery voltage reaches 4.2V, the current starts decaying till 0.1C as shown in Figure 2-5. Where t_{pk} is the time for which the initial charging current is held at its peak value (2C) and t_{cv} is the time at which the CV mode is reached. To maintain a constant temperature, the Proportional-Integral-Derivative (PID) conventional controller is utilized with the aid of a feed-forward term.

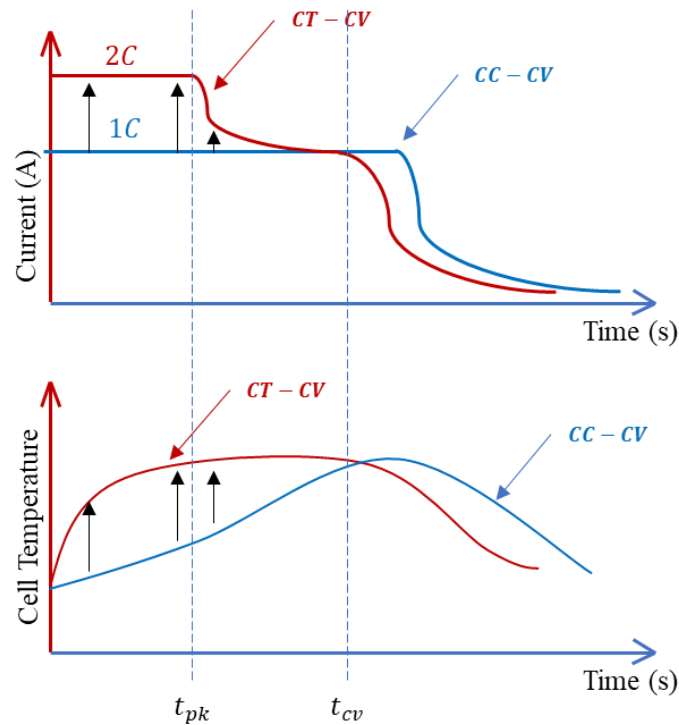


Figure 2-5 Schematic diagram of the Constant Temperature Constant Voltage (CT-CV) Protocol.

Due to the complexity of the working environment and the sensitivity of lithium-ion batteries specifically in EVs where temperatures vary according to the ambient conditions, researchers investigated the impact of variable ambient temperature on the optimal cycle rate of the lithium-ion batteries in [31, 87-89]. It is concluded that the performance of the batteries is depending on the surrounding temperature and to gain maximum efficiency, the battery must be charged within an acceptable temperature range [90, 91].

In [84] Pontryagin's Minimum Principle (PMP) is implemented in fast charging to solve the optimal control framework to minimize the charging time and ohmic heat generation. In [85] 1RC transient equivalent circuit, power loss model, and thermal model have been built. The integrated fitness function is formulated to minimize the energy loss and temperature increment during the charging process where the parameters have been estimated by the genetic algorithm (GA). In [86] two-stage constant current (2SCC) charging protocol without constant voltage (CV) charge has been introduced. The 2SCC is based on applying different levels of currents and combinations to a pseudo-two-dimensional (P2D) electro-chemical-thermal coupled model. The proposed protocol studied the thermal behaviour and energy efficiency of a lithium-ion battery for 30-minute charging with an 80% rated capacity. To limit the degradation of the battery, it is recommended in [73] to limit the temperature not exceeding 50°C, the surface temperature not rising more than 15°C, and the current charging level not exceeding 3C capacity of the battery.

Ultrafast charging is proposed on 209Wh/kg pouch cells lithium-ion battery in [92] using the asymmetric temperature modulation (ATM) method. The battery is charged with an initial 5% SOC to 88% SOC in almost 5 mins retaining 97.7% capacity after 1,000 cycles. In addition, the ATM method is preventing lithium plating within the range of 30-90% SOC and slows

Chapter 2

down capacity fade by raising the usable capacity by 10%. The ageing behaviour of cycled Li-ion batteries within a wide temperature range -20°C to 70°C is investigated in [31]. In this temperature range of -20°C to 25°C , the ageing rate increases with a decrease in temperature from its nominal value. In the other range of 25°C to 70°C , the ageing rate increases with an increase in temperature from its nominal operable value. The influence of low ambient temperatures on lithium-ion battery performance was examined in [32, 33], where a drop in activity and amount of useable active material, as well as an increase in resistance, resulted in a decrease in operating voltage and energy supplied.

It is concluded that temperature is a main critical barrier in the fast-charging process where Li-ion batteries are strongly impacted by temperature change. The acceptable temperature range of thermal management, performance, and safety of the li-ion batteries is from 20°C to 60°C [93]. Battery Kinetics is sluggish at low temperatures while ageing accelerates at high temperatures [94]. Charging at low ambient temperatures leads to lithium plating [95, 96]. So it is recommended to enhance the cold-climate charging ability by pre-heating the batteries such as in [94]. In addition, a multilayer nickel foil is embedded into the battery and used as a heater and sensor where the SOC reached 80% within 15 mins at a -50°C and the preheating process derived the 9.5Ah pouch cell from -50°C to room temperature 25°C within 1 min. In contrast, high temperatures accelerate side reactions and electrode degradation [3]. Hence, the thermal management system is mandatory during charging, else the battery could reach abuse conditions and trigger the uncontrollable release of heat due to exothermic reactions and catastrophic hazards [97, 98].

The performance of batteries at higher temperatures of 26°C and 70°C has been investigated in [87] and it is observed that the charging capability of the batteries at 70°C is relatively higher than that of the 26°C . Moreover, it is noticed that with an increase in cycle rate, the degradation behaviour is worsened. In [88] the effect of electrode porosity on lithium plating and the performance of the battery while charging and discharging protocol at the range from 20°C to 50°C temperature have been scrutinized. The performance of the lithium-ion battery at elevated ambient temperatures of 50°C , 60°C , and 70°C was investigated by [89]. In addition, the application of phase change material (PCM) under these conditions was studied in the thermal management of the battery. It is observed that heat generation of the battery decreases with the increase of ambient temperatures and the decay rates of batteries under high-temperature circumstances accelerated greatly.

One of the hypotheses of this research is that any change in ambient temperature is accompanied by a variation in relative humidity (RH) which affects the electrical and thermal behaviour of lithium-ion batteries. Very few researchers investigated the humidity effect on lithium-ion batteries such as Guo *et al.* [99] investigated the performance of Li-O₂ batteries in pure/dry O₂. The humidity effect on the reactions inside the battery has been analysed in two conditions, Pure O₂ with an RH of 15% and ambient air with an RH of 50%. In [100] the high temperature and high humidity storage behaviours of LiNi_{0.6}CO_{0.2}O₂ cathode material were scrutinized where a great degradation in electrochemical performance after being stored at 55°C and RH of 80%.

Chapter 2

The articles that used thermal management protocol and MSCC protocol have been summarized in Table 2-2 from the perspective of the charging time, energy consumption, charging efficiency performance, maximum applied current, cycling, and temperature rise.

2.3.4 Pulse Charging Current (PCC) Protocol

As an alternative to the CC-CV and MSCC protocols, periodically changed current protocols which are called pulse charging current (PCC) protocols have been utilized in the charging process of lithium-ion batteries. PCC depends on the control parameters of the duty cycle, frequency, and peak amplitude of the charging current pulses. PCC is implemented in the charging process of lithium-ion to speed up the charging rate, heating the battery at low-temperature conditions, and inhibiting the growth of lithium dendrites [61]. The reason is eliminating concentration polarization, increasing the power transfer rate, and removing the constant voltage mode [101].

PCC can be categorized into positive pulsed charging current protocol (PPCC), negative pulsed charging current protocol (NPCC), and bidirectional pulsed charging current protocol (BPCC) as described in Figure 2-6.

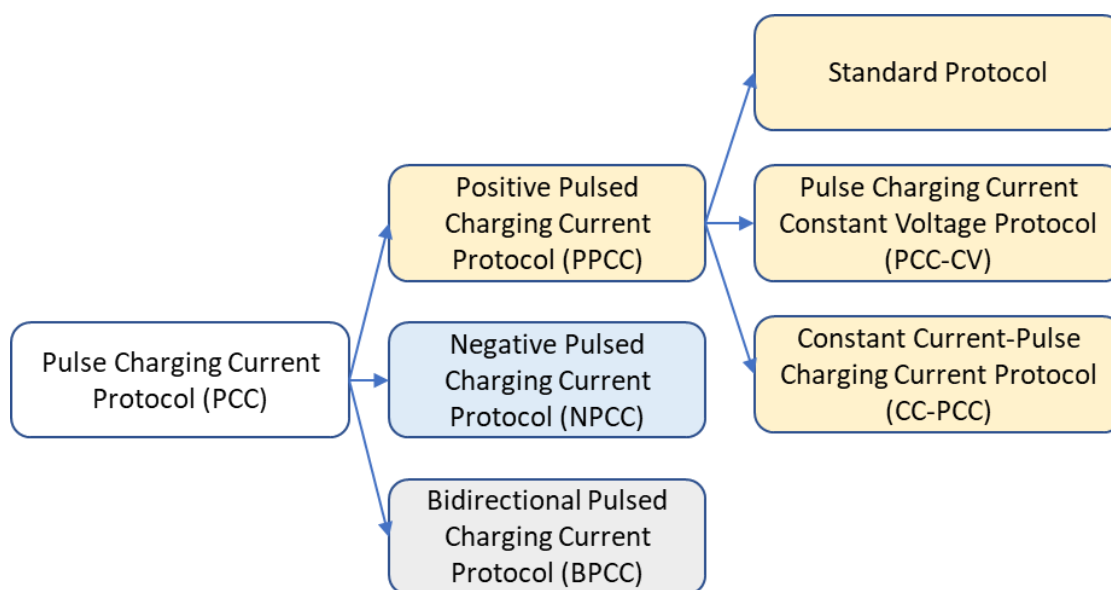


Figure 2-6 Overall schematic diagram of the Pulse Charging Current (PCC) Protocol.

2.3.4.1 The Positive Pulsed Charging Current (PPCC) Protocol

Standard PCC protocol is depending on the charging current pulses alternating with high and low current values, frequency, and duty cycle. The impact of charging using this protocol is a reduction in diffusion resistance, better active material utilization, improved cycle life, and reduced charging time as the constant voltage phase becomes redundant [101, 102]. Standard PCC is categorized into constant rest periods with constant amplitude current pulses where $I_{Low} = 0A$ as expressed in Figure 2-7-a, constant current pulses with different rest periods as in Figure 2-7-b, decaying current pulses with constant rest periods as in Figure 2-7-c, current pulses consisting of two different charge steps vary between predetermined currents I_{High} and

Chapter 2

I_{Low} as in Figure 2-7-d where I_{Low} is 20% of I_{High} , and different pulse charge voltages [102, 103] as shown in Figure 2-7-e. The mentioned methodologies of the standard PCC protocol allow the lithium surface concentration to reach a high level early in the charging cycle [102].

It is stated that the capacity and power density decreases simultaneously while energy efficiency drops as overpotential is increased[103]. Consequently, the decrease in the capacity of the cell leads to performance degradation. In [62] the performance of the lithium-ion battery has been investigated throughout various duty cycles of 20%, 50%, and 80%, at different frequencies 0.1 kHz, 1 kHz, 6 kHz, 12 kHz, 50 kHz, and 100 kHz. The orthogonal arrays (OA) method is used to solve the big experimental domain to find the optimal parameters combination. The remaining battery capacity after 400 full cycles (charge/discharge) at room temperature is almost 81%, and 75% for both pulsed charging current and CC-CV protocols, respectively.

It is concluded that at 50% duty cycle a better energy efficiency is obtained and a 25% less efficiency is obtained at 20% duty cycle. In addition, frequencies less than 6 kHz and greater than 50 kHz produced longer charge times, and energy losses were minimized especially at 12 kHz, thereby resulting in improved performance with an increase in the cycle life compared to the CC-CV protocol. Also, it is observed that the higher the peak current, the faster the charging time obtained, safety circuits implemented to prevent overcharging and overvoltage conditions, and a good cooling system should be applied due to the increase in battery surface temperature.

Chapter 2

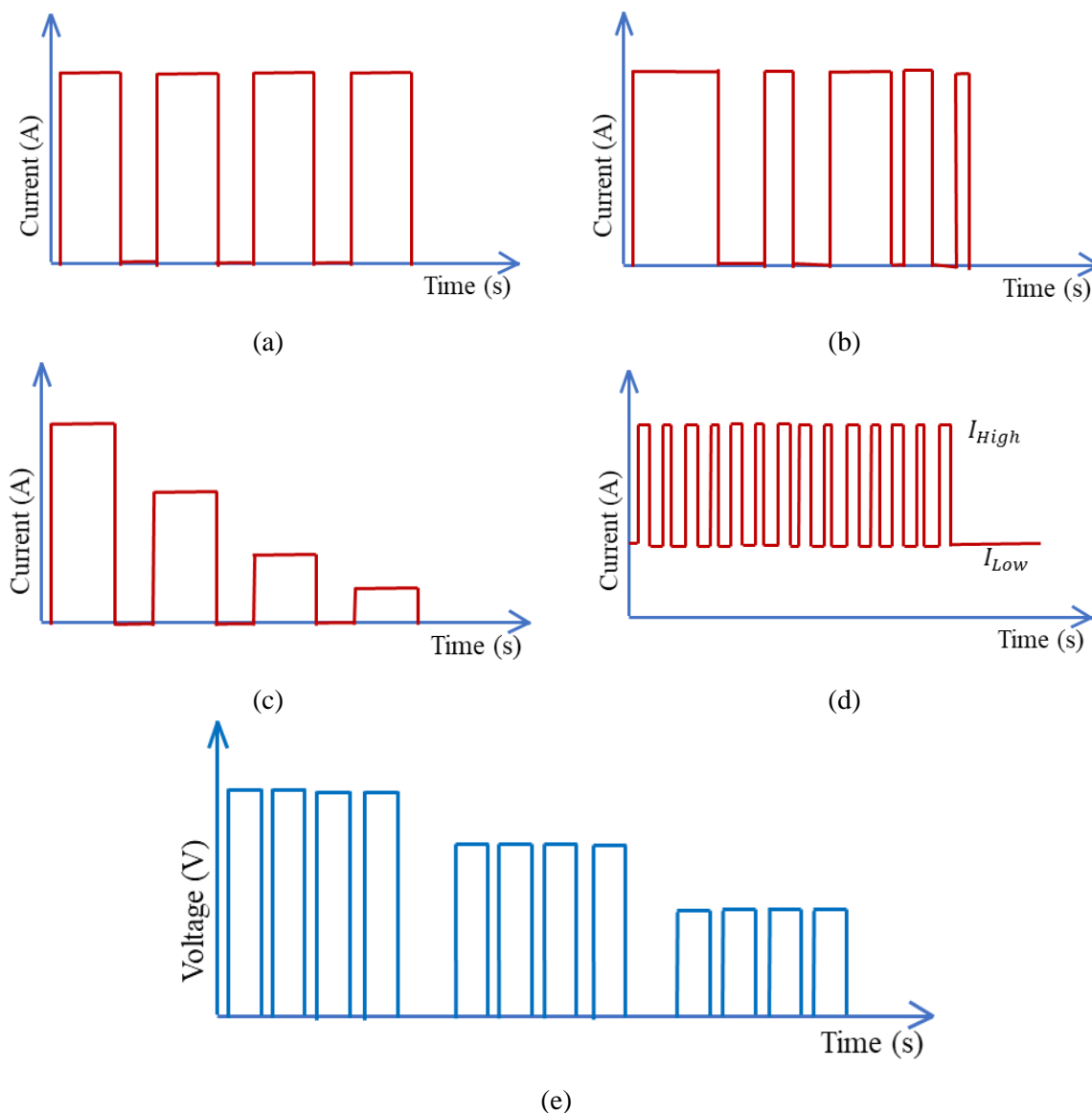


Figure 2-7 Types of the Standard Positive Pulsed Charging Current (PPCC) Protocol; (a) standard protocol with equal duty cycle, (b) standard protocol with various duty cycles, (c) standard protocol with decaying current, (d) standard protocol with upper and lower current limit, and (e) different pulse charge voltages.

The Pulse Charging Current-Constant Voltage (PCC-CV) protocol is depending on a sequence of pulse charging currents for a specific interval time then followed by a constant voltage stage till full charging capacity is reached as shown in Figure 2-8-a. The PCC-CV has been proposed in [104] to study the capacity fading and service life of lithium-ion batteries under different charging-discharging strategies which reflects on the growth of solid electrolyte interphase (SEI). Compared with the CC-CV protocol, the PCC-CV revealed better cyclic performances because of the smaller average currents.

In the Constant Current-Pulse Charging Current (CC-PCC) protocol, the lithium-ion battery is charged with a constant current (CC) mode till reaching a predetermined voltage level then the CC mode is switched to pulsating charging current mode as shown in Figure 2-8-b. In [43] the Constant Current-Pulse Charging Current (CC-PCC) protocol has been proposed. Rectangular

Chapter 2

current pulses with a constant duty cycle of 50% were specified and utilized to avoid distortions due to different mean charging currents reflected by reducing the charging current or increasing the pause lengths. However, it is concluded that the CC-PCC protocol leads to a longer charging time than the CC-CV protocol.

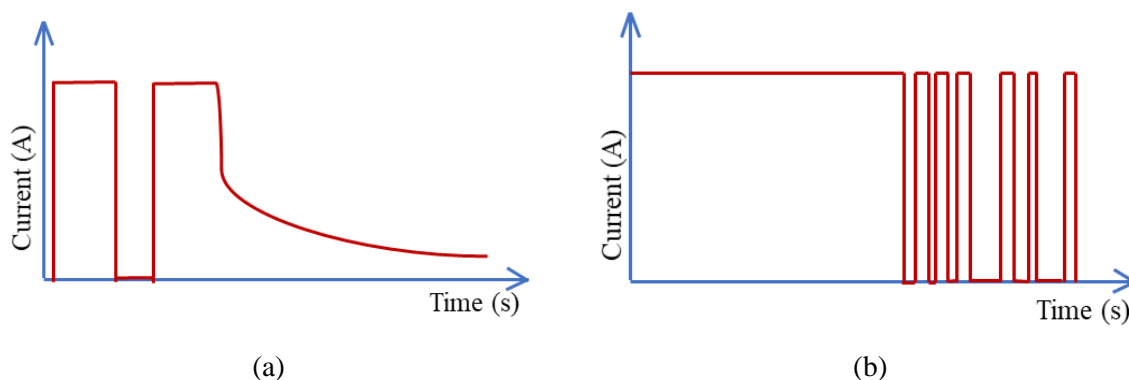


Figure 2-8 (a) Pulse Charging Current-Constant Voltage (PCC-CV) protocol, and (b) Constant Current-Pulse Charging Current (CC-PCC) protocol.

A comparison between the different categories of the positive pulsed charging current (PPCC) protocol is presented in Table 2-3. Herein, it is concluded that all the proposed methodologies of the PPCC protocol almost have the same effect on the cycle life while used in the charging process.

Table 2-3 Comparison between different types of Positive Pulsed Charging Current (PPCC) Protocol.

Protocol Type	Duty Cycle	Frequency	Compared with	Impact
Standard PCC based on Orthogonal arrays [43]	50%	12 kHz	CC-CV	+ 100 cycle life
Standard PCC [105]	50%	25 Hz	CC-CV	Same cycle life
	50%	1 Hz		Same cycle life, only a somewhat faster capacity fade can be observed
Pulse charging current constant voltage (PCC-CV)[104]	50%	0.02 Hz	CC-CV	Same cycle life
Constant Current-Pulse Charging Current (CC-PCC)[43]	50%	2.5 Hz	CC-CV	Same cycle life

2.3.4.2 Bidirectional Pulsed Charging Current (BPCC) Protocol

Low-temperature charging is considered a major challenge for lithium-ion batteries due to their degradation and cycle lifespan [101]. Charging at low temperatures is increasing polarization,

Chapter 2

affecting capacity, causing an internal short circuit, and the possibility of lithium plating. Herein Joule heat is used to generate self-heat by the internal resistance of the battery and eliminate heat loss from any external heating equipment [101]. PCC protocol is used to warm up the battery from -10°C to 3°C firstly and then the charging is switched to the CC-CV protocol [101]. Herein bidirectional pulsed current is proposed to obtain the main data of the thermal action for comprehensively analysing heat generation characteristics and thermoelectric coupling model based on the second-order RC circuit to verify the basic principle [106]. The bidirectional pulsed current increases heating speed, consequently decreasing the risk of lithium plating and ensuring safety. It is concluded that whenever the bidirectional pulsed current method is implemented, at low temperatures, a high current rate, and overcharge or discharge will not significantly affect the life span or increase the safety risk of lithium-ion batteries. BPCC protocol has different implementation types as shown in Figure 2-9 based on the existing interval time between the positive and negative pulses [106]. Normally the negative current helps in reducing the polarization voltage caused by the positive pulses and makes it polarized in the opposite direction as stated in [107].

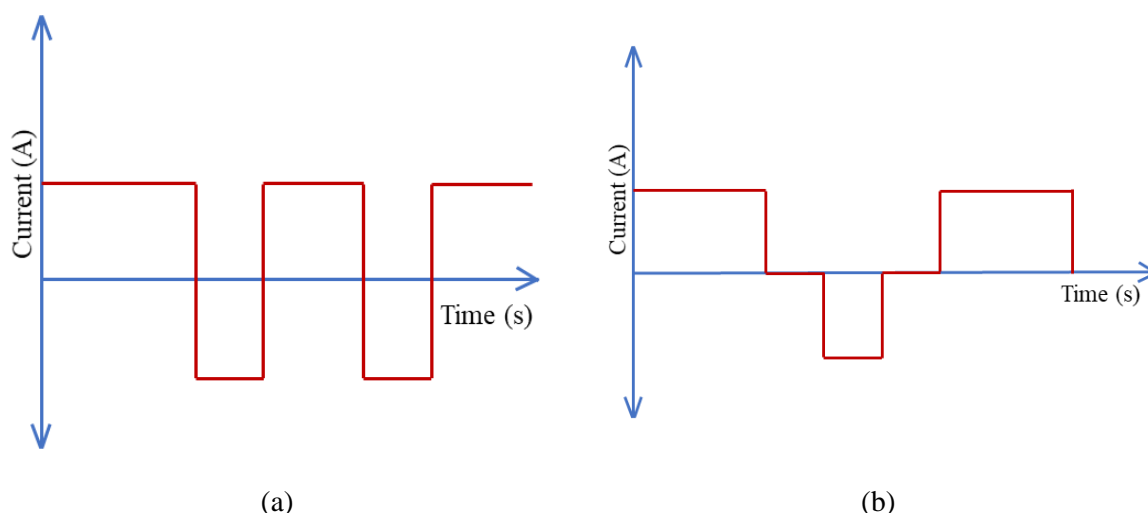


Figure 2-9 Different types of the ideal bidirectional pulsed current.

2.3.4.3 Negative Pulsed Charging Current (FCNP) Protocol

The negative pulse fast charging method (FCNP) is analysed in [108] and ensured ion recovery from metallic lithium, hence the capacity loss is minimized however same charging speed is obtained compared with the CC charging protocol. In addition, FCNP limits side reaction throughout anode potential, terminal cut-off voltage, and side reaction rate by incorporating it into a reduced-order electrochemical model (ROM) with an extended Kalman filter. A full comparison between the CC-CV at different capacities and FCNP is implemented on a pouch type of lithium-ion battery cell freshly charged and after various cycles and expressed in Table 2-4. The charging time up to 100% SOC by FCNP is longer than that by 3C CC-CV charging protocol, however, it becomes shorter as degradation is in progress, particularly after 40 cycles. On the other hand, the capacity loss by FCNP is comparable with that by the 2C CC-CV charging protocol, which is approximately 23% less than that by the 3C CC-CV charging protocol after 60 cycles.

Chapter 2

Table 2-4 A Comparison between the negative pulsed charging current and CC-CV protocol.

	Up to 80% SOC fresh cell	Up to 100% SOC fresh cell	Up to 100% SOC after 20 cycles	Up to 100% SOC after 60 cycles
3C CC-CV	15.7 min	44 min	47.3 min	55.2 min
2C CC-CV	22.8 min	56 min	56.1 min	59.2 min
FCNP	16.6 min	49 min	51.1 min	52 min

Pulse Charging Current Protocol with all its proposed categories reduces the risk of lithium plating, reduces the charging time, increases charging efficiency and battery lifespan[109], and reduces heating and degradation [20]. In addition, the risk that occurs due to the charging of batteries at low temperatures can be alleviated throughout this protocol. However, the main drawback is the complexity of the controller.

The previous findings and the current challenges of the power management protocol with all its methodologies could be summarized by stating the advantages and disadvantages of each as introduced in Figure 2-10.

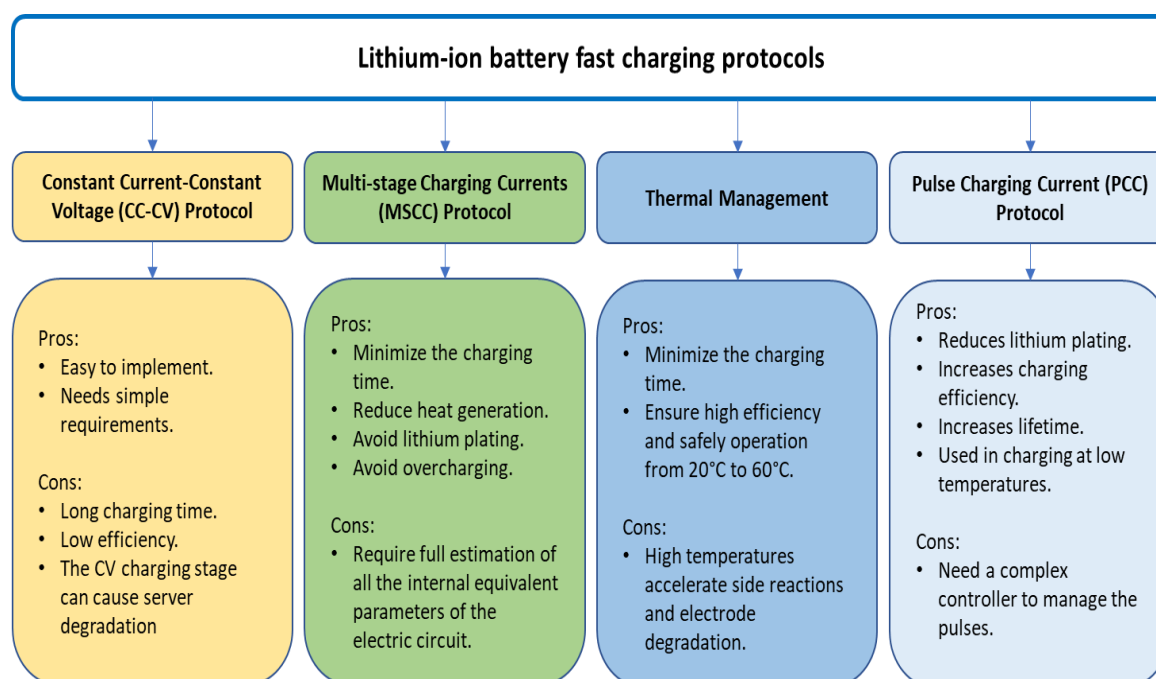


Figure 2-10 The pros and cons of the power management protocol with all its categories.

2.3.5 Material Aspects Charging Protocol

An increased number of researchers are directed to Extreme Fast Charging (XFC) which mandates a charging rate equal to or greater than 6C [110]. XFC leads to cathode particle cracking, low active material utilization, electrolyte-electrode side reactions, and lithium plating at the anode. The mentioned cons can be summarized in electrode variability [110, 111]. In [110] the cathode particle cracking and electrolyte modifications (concentrated electrolyte and low viscosity additives) limitations have been identified to ensure safety and stability

Chapter 2

problems. In [112] an electrolyte additive trimethylsilyl isothiocyanate (TMSNCS) based on amino silane with a high electron-donating ability that can scavenge HF and PF₅ has been proposed to solve the detrimental effects of LiPF₆. Authors in [113] investigated the XFC performance for a cell with a low loading of 1.5 mAh.cm⁻² and moderate loading of 2.5 mAh.cm⁻². It is concluded that the combination of increasing the battery temperature, reduction in the electrode tortuosity, and enhancement of the ion transport in the electrolyte are required to facilitate the CFC for high-energy lithium-ion batteries. Lithium bis (fluor sulfonyl) imide (LFDI) has been utilized in [114] to enable fast charging capability of high energy density because of its high conductivity and high lithium ion transference number compared to LiPF₆ salt. In addition, a physical-chemical model is introduced in [115] which improved the discharge rate capability of the lithium-ion cells throughout laser-structured graphite anodes.

Fast charging protocols based on the changing in the material aspects and physical or/and chemical structures are interesting and require a detailed description and comparison to test, validate, verify, and evaluate the effectiveness of the corresponding charging protocol on the proposed Li-ion battery as mentioned in the review papers [110, 111, 116, 117]. However, it will not be mentioned in this thesis as we are focusing on the CC-CV and MSCC fast-charging protocols due to their easy implementation with simple requirements and fast-charging effectiveness.

2.4 EV Battery Dynamic Behaviour, Classification, and Recognition

Due to the high automobile electrification, network integration, and minimizing fuel consumption, EVs have been rapidly developed with their advantages of energy saving and environmental protection and automation improvement capability [118]. Battery packs, which are composed of hundreds of lithium-ion batteries, can provide enough energy for the regular work of EVs [119, 120]. However, there are still some challenges in the safety, cost, and charging operation at different temperatures [119]. In some countries such as Russia, Canada, China, and the USA, winter-driven EVs face a low charge and discharge capacity, lower voltage, and shorter cycle life [121, 122]. Fundamentally, at low temperatures, the rate of chemical reaction in lithium batteries will be slowed down, thus affecting the overall performance of batteries. In addition, lithium-ion batteries face lithium plating at low temperatures, which reduces the energy and power capacity and leads to battery degradation [123]. Temperature variation in the battery module occurred primarily due to the temperature rise of coolant along the flow path [124]. It is stated that the well-designed battery module should be capable of confining the battery temperatures between +15°C to +35°C in different regions, climates, and seasons [124]. It is perceived that the temperature is a main critical barrier in the fast-charging process where lithium-ion batteries are strongly impacted by the temperature change (caused by engines, environment and power electronic drive systems and the battery itself). Temperature change is reflected in the equivalent circuit model (ECM) parameters which depend on the pulse discharging signals and are composed of internal parameters such as the internal ohmic resistance, the electrochemical polarization internal parameters, and the concentration polarization internal parameters [75, 125, 126]. It is stated that the acceptable temperature range for thermal management, performance, and safety of

Chapter 2

lithium-ion batteries is from 20°C to 60°C [93]. Very few researchers investigated the relative humidity (RH) effect on lithium-ion batteries, such as Guo *et al.* [99] investigated the performance of Li-O₂ batteries in pure/dry O₂. The RH affects the performance of the battery where the reactions inside the battery have been analysed in two conditions, Pure O₂ with an RH of 15% and ambient air with an RH of 50%. The water can deteriorate the cyclic ability of the battery. In [100] the high temperature and high humidity storage behaviours of LiNi_{0.6}Co_{0.2}O₂ cathode material were scrutinized where a great degradation in electrochemical performance after being stored at 55°C and RH of 80% is observed.

The implementation of a lithium-ion battery fast charging protocol in different ambient temperatures requires an accurate representation and modelling of the EV battery dynamic behaviour. There is a significant research gap in identifying a model that can describe the dynamic behaviour of the battery with the minimum percentage of error in determining the battery terminal voltage to ensure high charging efficiency under different ambient conditions (temperature and relative humidity). In [46, 127-129], the authors modelled the lithium-ion battery storage systems using the white-box, black-box and grey-box models with certain ambient conditions. In [130] Adaptive Neuro-Fuzzy Inference System (ANFIS) model has been used as a black box to model the lithium-ion battery. In [131], continuous-time and discrete-time system identification methods represented the internal parameters of the 2RC equivalent circuit model. In [132] Least squares algorithm has been utilized to obtain the unknown coefficients for the normalized battery model. It is observed that no model for the dynamic behaviour of the battery can be utilized under different ambient circumstances (temperatures and relative humidity) and only a few articles proposed models that represent the battery at various temperatures; however, multiple tests and measurements of the internal parameters at all the operating conditions are required.

The identification and modelling of the EVs represented in the lithium-ion battery while entering the charging station and during the charging process are considered challenging problems from many perspectives. Non-linearities, multiple-input variable parameters (charging current, temperature and relative humidity), and high system order are all issues that gather to the complexity of the problem in the charging stations and the home energy management systems (HEMS) [65]. The starting state of charge (SOC), specification of the battery, and the charging interval time are vital prerequisites to design a plug-in electric vehicle (PEV) charging model [133-136]. Several works have focused on indirect methods for calculating the home charging SOC and charging time, by using the patterns of people's driving behaviours of daily trip distance, length and time at the end of the trip [137-139]. In Winnipeg, Canada, 76 GPS devices are installed in representative vehicles to predict the electric load profiles as a time function for future plug-in electric vehicles [140]. However, the issues related to GPS communication access and post-processing can jeopardize the process of gathering vehicle data [133]. The communication between the charging piles with the onboard charger of the existing PEVs to access the information on the battery temperature, relative humidity, and SOC is missing [133, 141]. In [142], a driving pattern recognition using Pongtryagin's Minimum Principle (PMP) based energy management has been applied to the plug-in hybrid electric bus (PHEB). The authors investigated the impact of stochastic vehicles on energy

Chapter 2

management, which reflects on the recognition of the co-state. In [143], a recognition method has been used based on monocular vision and non-feature identification where the recognition process combined the Hough circle and Hough line to get the position information of the charging port. The average success rate achieved is 94.8% without considering the different light intensities. An automatic recognition and location system of the electric vehicle charging port has been introduced in [118] using the convolutional neural network (CNN) in different illumination environments. The recognition has been implemented through image processing and a robot arm that is used to complete the charging gun insertion of the automatic charging link. However, the range of the light intensity used was from 500 lux to 10,000 lux. It is concluded that the highest recognition success rate of 98.9% is achieved at a light intensity of 4,000 lux and the lowest success rate of 84.4% at 500 lux. Herein, Vehicle Logo Recognition (VLR) method provided a critical supplement to the manufacturing version evaluation of the car. In [144], Vehicle Manufacturer Recognition (VMR) eliminated the requirements for identification and analysis of the CNN system. The authors proposed recognition and classification methodologies that depend on the light intensity and vehicle logo recognition however, the dynamic electrical behaviour of EV batteries while charging under different circumstances is not investigated yet.

In summary, fast-charging an EV is susceptible to different environmental conditions. Therefore, in large countries, the regional climate can vary from coast to coast, so fast charger deployment requires careful consideration regarding the impact of the regional ambient temperature and relative humidity. Consequently, the rate of charge is variable as it is controlled by the vehicle's onboard battery management system which can be triggered by a variety of internal and external factors[2]. Hence, EV category recognition and identification at various operating ambient conditions is a substantial process to fast charge the EV precisely.

2.5 Charge Controller for Off-Board Electric Vehicles

Technological advancement reveals the EV as a revolutionary technology for minimizing greenhouse gas emissions and contributing to power grid electricity compensation [145]. Over the ten years, EVs were increasing exponentially and have been proposed as an alternative direction for freedom from dependence on oil, and air pollution, and to be used in advanced energy storage systems [146-148]. The rechargeable battery employed in EVs is often characterized as having a long-term lifetime where current ripple and low coulomb charge-discharge cycles at high frequencies affect the battery performance degradation and lifespan [149, 150]. EVs' battery chargers are broadly classified as on-board and off-board chargers [151]. The onboard chargers are widely known as AC chargers, which can be single-phase Level-1 and Level-2, as defined in SAE-J1772, and three-phase AC charging, as defined in SAE-J3068. The off-board chargers are referred to the DC chargers, which ensure higher charging current rates, as defined in SAE-J1772-Combo/CHAdeMO standards [20, 21]. The off-board charger ensures safe and fast charging capability [152]. Its charging protocols are the constant current constant voltage (CC-CV), multistage charging current (MSCC) and pulsating charging current (PCC) protocols [153]. The constant voltage (CV) stage is replaced by the fuzzy-controlled active state-of-charge controller (FC-ASCC) and grey-predicted lithium-ion

Chapter 2

battery charge system (GP-LBCS) to speed up the charging process based on the sense and charge modes in [154, 155]. However, integrating those techniques into a commercial battery charger is not available due to the complicated control algorithm [153]. In [4, 156], the design of different battery chargers for EVs has been introduced with some particular aspects of power electronics in the EV battery charger design. It is stated that one of the main challenges in the design is limiting the current ripple to not exceed 10% according to the standards. Hence, the MSCC protocol has been used due to the high charge/discharge energy efficiency and short charging time [65, 75]. In [157], a control strategy for EV charging has been proposed based on a three-phase three-level neutral point clamped (NPC) rectifier. The controller is optimized using the genetic algorithm (GA) to reduce the DC-bus current fluctuation in the level-1, level-2, and DC modes. However, the input voltage is constant, and a DC mutation period reached 15ms in the single-phase charging mode is observed. In [153], the off-board charger has been used based on four-stage constant current stages where the Taguchi method is employed to determine the charging current of the Sanyo 840 mAh, 3.6V lithium-ion battery. However, it is observed a fluctuation in the output voltage during the PWM waveform of the inverter without any further investigation.

As a result, industries are focusing on EV battery chargers, which are considered the main interface between the electric power supply and vehicles [151]. Renewable energy sources (RESs) such as photovoltaic (PV) and wind turbine generators (WTG) are utilized for charging the EVs (PV-EV, and WTG-EV, respectively) to reduce the utility grid overload [151]. PV stand-alone system is one of the on-board and off-board chargers used for charging the EV solely without support from the utility grid. It is more beneficial in remote areas and more efficient because of the fewer conversion stages [158, 159]. The main disadvantage of the PV systems is the irregular stochastic voltage level. Hence, this challenge is requiring power conversion for regulation and matching the voltage levels for the battery chargers. Where the output voltage, and charging current ripples are overheating the battery and shortening its lifespan [160]. With the blossoming development of EVs, DC-DC converters have been utilized to regulate the output voltage and alleviate the battery current ripples [147, 150, 161]. However, converters are still facing challenges to reach rapidly the desired output voltage with minimum error, such as load variation, disturbances in the input voltage, parameter deviation, and pulse width modulated (PWM) saturation constraints of the converters [148, 162].

Toward the confrontation of challenges stated above, three main categories of control methods, conventional, advanced, and artificial intelligent (AI) control techniques are used for the control of the DC-DC converters. The conventional control methods can be classified as voltage mode controller (VMC), and current mode controller (CMC). The VMC uses PI, Type II, or Type III compensators with a single closed loop voltage feedback [163, 164]. The CMC uses dual voltage and current loops to improve the performance of the converter but it depends on a current sensor and a latching circuit based on a clocking signal and also the output voltage control could be affected by the two controlled loops [147, 165]. In recent years, diversified advanced control techniques have been investigated such as sliding mode control (SMC), fuzzy logic controller (FLC), and model predictive controllers (MPC). SMC method improved the performance of measuring the transient response. However, the need for an extra capacitive

Chapter 2

current sensor and high switching frequency, to ensure a good dynamic response which causes losses, and a complicated filter design as it is not suitable for high-power converters [147, 166, 167]. FLC responds quickly to changing environmental conditions with the knowledge of the system parameters and deals only with the error and change of error of the predetermined reference [168]. MPC is a method of designing and implementing a feedback control system that performed better results than conventional methods [169, 170]. In [170] the output voltage has been controlled based on MPC under variable load conditions. An offset-free MPC for a DC-DC buck converter has been proposed in [171] for optimal voltage tracking and optimizing transient dynamics. However, this controller is used to feed only constant power loads (CPLs). AI is a prevailing control technique to develop efficient methodologies to deal with a huge amount of data by investigating patterns and underlying structures in various scientific fields where heterogeneous data are available [172]. Some of the most widely used AI techniques are: heuristic techniques, expert systems and machine learning with its categories and sub-categories are unsupervised learning (clustering, metric learning, and anomaly detection), supervised learning (decision trees, support vector machines, and neural networks) and reinforcement learning (Markov decision processes, deep Q networks, and Q-learning) [173, 174].

AI has been exploited in the fields of vehicular environments like charging management, transmission scheduling, and control [172, 174, 175]. The Q-learning technique which is a kind of reinforcement learning has been used in [176] to forecast the plug-in hybrid EV charging loads. In [133] online plug-in electric vehicles (PEV) recognition has been provided with statistical modelling of the charging habits through a supervised classification method. The Q learning was used in the interaction between the electric vehicle and grid in [177] by investigating the grid-to-vehicle (G2V) charging and vehicle-to-grid (V2G) discharging approaches. Machine learning has been developed in [178] to optimize a parameter space specifying the charging voltage and current profiles for batteries. Planning of the PEV load modelling has been verified by fuzzy method, artificial neural network, Markov chain, and pdf fitting method as stated in [179]. The driver's perception has been expanded to enhance the comfort, safety, and efficiency of driving based on a vehicle-to-everything (V2X) system with AI [173]. Energy storage management systems between the lithium-ion battery and the supercapacitors have been utilized to feed the vehicle's traction electric motor [180]. Optimal scheduling of networked microgrids considering the penetration of EVs has been proposed efficiently based on support vector machine (SVM) in [181]. A boost converter based on an artificial neural network (ANN) has been used in the battery charger [160]. However, the mean absolute percentage error (MAPE) reached 0.282% and 0.307% in the training and testing, respectively.

In addition to the penetration of AI in the EV market, to be more precise DC-DC converter controllers based on NN supervised/unsupervised learning and reinforcement learning techniques are powerful tools concerning noise and uncertainties [182-185]. AI networks have been used to identify a black-box converter model in [186]. The neural network predictive controller (NNPC) that combines the advantages of both the NN and MPC has been applied to the buck converter in [182] which investigated the accuracy in the start-up and during the

Chapter 2

reference voltage variation. Also in [184] NNPC improved the transient characteristics of the digitally controlled buck converter. NNPC proved its efficiency, accuracy, and speed response concerning other advanced controllers in [147, 187].

We can conclude that researchers used various methodologies to control the buck converter under various input and load conditions. Some of the papers presented in the literature are summarized in Table 2-5 where the performance and efficiency of the controller can be investigated by substantial effective parameters such as steady-state error, peak voltage, output ripple voltage, and settling time.

Chapter 2

Table 2-5 Comparison between various controllers from the literature survey concluding the proposed controller.

Type of controller	Steady-State error (V)	Peak Overshoot (V)	Output ripple voltage (V)	Settling time (ms)	Input Voltage (V)	Load
MNSGA-II-based PID [188]	0	0	0.06	1.34	Variable 25V-18V	Resistive
NSGA-II-based PID [188]	1.2	5	0.8	5.32	Variable 25V-18V	Resistive
Offset-free model predictive controller [171]	0	2	NA	2	Variable 200V - 400V	Resistive
Model Predictive Controller [189]	NA	0	NA	1.4	Variable 26.04V - 30.38V	Battery
Second-Order Sliding-Mode [190]	NA	NA	0.1	~10	Variable 30V - 20V	Resistive
Sliding mode-based control [191]	0	0.1	NA	0.15	Constant 10V	Resistive
Artificial neural network (ANN) based approximate dynamic programming (ADP) [147]	0	2	NA	3	Variable 42V - 47V	Resistive
PSO-optimized fuzzy PI controller [192]	NA	NA	2.5	~5	Constant 24V	PMSM motor
Tuned Fuzzy Logic controller (TFLC) [193]	0.01	0	NA	7	Constant 15V	Resistive
Fractional-order PID controller[194]	0	0.6	NA	0.02	Constant 100V	Resistive

Chapter 2

2.6 Electric Vehicles Smart Connectivity to the Utility Grid

2.6.1 Grid-to-Vehicle (G2V) Technology

The electric vehicle revolution has enabled complicated security and economic challenges to the distribution power network by a substantial drive towards electrification of transportation, spurred not only by growing carbon emissions but also by rising fossil fuel prices [195, 196]. EVs are replacing internal conventional engine vehicles (ICEVs) using the state of art power electronics, motor drives, energy storage technologies, renewable energy power generation, and smart grids [197]. However, ensuring this transition required addressing several grid integration challenges supported by distributed generators (DGs) [198]. DGs, especially renewable energy sources (RESs) are providing higher efficiency and ensuring green electricity with low environmental pollution. However, the fluctuation of RESs made challenges to the operation of the distribution network [199]. Demand response (DR) is considered the key to improve system flexibility, maintaining the balance between the generated and demand power, and enhancing system reliability [199, 200]. One of the substantial participants in DR is the EVs which are considered a viable solution for resolving microgrid distribution networks [201]. However, due to the uncertainty and random behaviour during the charging and discharging operations, EVs may negatively affect the system efficiency and reliability [199] where the uncoordinated EV charging could significantly change the shape of the aggregate residential demand [202]. Hence, EV charging and discharging operations need to be aggregated by an EV aggregator to qualify the market entrance criteria [203] and actively participate in the DR balancing between the supply and demand sides [199].

Aggregators are considered the interface between the distribution network and electric vehicle charging station (EVCS) which combine multiple EVs [199] and coordinate and schedule the charging of the plug-in electric vehicle (PEV) [204]. So, the EVCS represented and controlled by the aggregator (operator) has main challenges concerning the balance of generated and consumed power, minimizing EVs' charging tariff, and maximizing the EVCS's revenue by electricity trading. Recent studies, in the field of charge scheduling of EVs, reported the minimization of the charging time and maximization of the charging State-Of-Charge (SOC) capacity by changing the charging rates (AC Level 1, AC Level 2, AC Level 3, and DC fast charging) [22]. However, the technical impact represented in the required charging power demand of the different charging methodologies and rates on the utility grid has not been considered. The EV charging process presents a major challenge to utility grid security, particularly at the local distribution network level which is represented in peak load [205]. A conventional approach involving capacity addition is widely used to supply the peak load. However, this approach is insufficient and not economically concerning generator usage since the utilities need to maintain the generation capacity that will be used a few hours per day [206]. This approach revealed several disadvantages, such as high fuel consumption and carbon dioxide (CO₂) emission, increase in transportation and maintenance costs and faster deterioration of equipment [206, 207]. Thus, the peak load shaving methodology is becoming a vital area of active research which is targeting to flatten the load curve by reducing the peak load power and shifting it to times of lower load [206]. This methodology has benefits for the

Chapter 2

grid operator and End-User and carbon emission reduction. The virtual time of use rate dynamic programming (vTOU-DP) approach has been used to flatten the load profile of the transformer and reduce the peak power demand based on utilizing the advantage of the vehicle to grid (V2G) property, however, this property requires a proper infrastructure and control systems for EVs integration with the utility grid which considered as a great challenge, especially in the developing countries where EVs are initiating in the transportation market. The time of rising pricing method has been used to minimize the peak load charging, whereas the pricing incentive method based on the energy price during the day is implemented in New South Wales, Denmark, Finland, Norway, and Sweden [195, 196]. Time-of-Use (ToU) tariff pricing motivation is used in charging EVs across the day [208]; however, additional control is required to minimize the effect of sudden load ramping up at the same time instance [208]. In [209] a virtual battery pool is proposed to charge and discharge the EVs based on a genetic algorithm to control the demand and supply processes. Peak-shifting and peak-cutting are achieved by using the charging (G2V) and discharging (V2G) capability of the EVs in [199, 210-212]. In [213], the peak demand for the week charging period has been reduced to 45% using RESs supplied from PV panels installed on a roof parking area and wind turbines supported by a battery energy storage system (BESS) of the Nissan-Leaf model EV with 24kWh lithium-ion battery capacity. EVs have been charged during the off-peak to reduce the peak demand without being tied to renewable generation. In [214] different charging strategies have been proposed to improve the system load factor (the ratio between the average load to the peak load of the system) by shifting the charging process out of peak hours where all EVs are not allowed to charge between the time 17:00 and 19:00 which considered as a drawback for EVs' fast charging.

Hence, the aggregator has another vital role represented in maximizing the profit of the station [215, 216]. Private aggregators are directed to maximize their profit by including additional services and selling secondary reserves in the electricity market [217]. The charging and discharging operations capability of EVs in the parking lots was investigated in [218] to maximize the profit of vehicles and parking. A reinforcement-learning (RL) approach was used in [219] for the EVCS pricing and scheduling strategies. However, some EVs may be parked at the station for a very long time till the electricity price is very low where the charging and pricing decisions are made each time. A decentralized profit maximization algorithm (DPMA) was introduced in [220] in the city of Ottawa, Canada to help a decentralized electric vehicle supply equipment (D-EVSE) supported with a solar energy system of 11.5 to 19 MW and equipped with a BESS of 30 MW to fast charge the EVs with 180 kWh as a charging rate. However, the operation time of the station was set from 06:00 am to 12:00 am and based on the ToU pricing without considering the stochastic behaviour of the PV system. A marginal price-based coordination optimization model has been proposed in [221] to coordinate electric vehicle charging stations and electric vehicles using mixed-integer linear programming (MILP). MILP has been widely adopted to model the number of charging and discharging EVs, the charging and discharging status of EVS, and the charging interval time [222]. An islanded microgrid scheduling policy of RESs represented by a solar system of 100 kW and BESS of 319 kWh with the minimal operational cost of a diesel generator of 100 kW has been provided in [223] using the dynamic programming method (DPM). However, the minimum allowable

Chapter 2

state of charge was set at 40% for each EV. The joint admission and pricing (JoAP) operation mechanism has been proposed in [224] to maximize the charging station's profit where the profit is defined as the difference between the revenue and penalty corresponding to the average charging waiting time. An optimization algorithm for commercial sectors has been proposed in [225] to find the optimum EV charging/discharging profile considering the maximum demand tariff. A case study of DC fast charging (DCFC) stations at the highway service centres in Ontario and Alberta (Canada) has been declared in [226]. The station economy has been improved by reducing utility charges and maximizing the utilization of PV systems in the presence of the BESS. However, the capital cost of the PV and battery cannot be recovered within a reasonable period where the BESS has longer payback periods than those of the PV systems only [226]. The profit of the distribution system operator has been maximized in [227] using the Markov decision process reinforcement learning technique (MDP-RL) while guaranteeing only the voltage security.

2.6.2 Vehicle-to-Grid (V2G) Technology

The fast development of EVs brings a significant load on the power system which requires efficient control frameworks [228]. The EV charging process makes an excessive overload on the power grid and can cause fluctuation in the voltage and shortage in the supply [5]. The mentioned problems have been revealed during the peak demand period. In the peak-demand period, the ancillary power generators have to enter the network to avoid fluctuations which increase the operational and maintenance costs. On the other hand in the off-demand period, the unused and extra-generated power will be wasted in vain [5, 6]. Generally, the distribution utility grid is designed with a limited margin and overloading capacity due to the dynamic behaviour of the EV charging process [229]. Additional loads would increase the risk of power lines and transformers overload which will be followed by extra energy losses and power quality degradation [229]. Hence vehicle-to-grid (V2G), vehicle-to-building (V2B) and vehicle-to-vehicle (V2V) concepts have been introduced to solve the mentioned obstacles and problems based on the smart charging and discharging scheduling to reduce the peak load and shape the load profile in the power grid [230].

According to a study in the USA, 90-95% of EVs' daily time is idle and parked in parking lots [231]. In the V2G and V2V processes, the coordinated EVs need to be charged and discharged frequently to receive power and send extra power to the grid and other EVs. These processes increase the internal residence and consequently decrease the battery's usable capacity. Hence the battery degradation costs have a significant influential effect on the feasibility of the V2G and V2V technologies [5].

Researchers were targeting the minimum cost of recharging [232, 233], minimum waiting time based on the final SOC, charging protocol, charging time, and maximum profit [234]. In [235], a comprehensive analysis of the impact of e-mobility in Positive Energy Districts (PED) has been analysed. Where millions of green kilometres have been provided and a potential 71% saving in carbon emissions has been saved using EVs alone compared to the use of fossil-fuel vehicles. In [236], the total cost of building a battery energy management system (BEMS) in the presence of a PV system has been minimized using the plug-in electric vehicles (PEVs)

Chapter 2

charging/discharging schedule. The actual payment of the PEV owners has decreased by 17.6% and 52.3% while the degradation effect of the battery and the charging/discharging aspects have not been investigated. A general framework has been proposed in [237] to formulate a day-ahead EVs recharging scheduling problem. EVs are considered to arrive between 6:00 am and 8:00 am with a state of charge (SOC) that varies from 10% to 50% and leaves uniformly at random between 4:00 pm and 8:00 pm with a SOC from 70% to 100%. However, the impact on the grid and the degradation effect have not been mentioned. In [238] V2G coupled with an integrated energy system (IES) has been investigated to minimize the annual total cost (ATC) and annual carbon emission (ACE). However, the benefits gained from growing the EV penetration would gradually decrease when the number of EVs reaches 300 and the impact on the grid is missing. In [239], an optimization problem of electricity prices and the battery degradation cost has been proposed. However, this study did not consider the EV charging/discharging levels.

Two stochastic linear programming models for scheduling EV charging processes have been discussed in [240]. Three applications have been investigated consisting of load flattening, load peak shaving, and demand response where EV charging behaviours respond to the volatile output of wind energy. However, the battery degradation effect is ignored. In [241], an approach has been introduced to reduce the peak demand by 7.8%. However, the charging and discharging levels and limits have been ignored. In [242, 243], the authors emphasized factoring the battery degradation cost in the bids to ensure that the revenue will at least covers the true cost of operation. In [230] a flexible power transfer based on the V2V concept has been investigated to reduce energy consumption. However, the initial and targeted SOC and the battery degradation factor have not been mentioned. A brief of the literature survey concerning the same research field is presented in Table 2-6. The findings of the stated articles declare the ability to minimize the battery degradation cost and maximize the V2G revenue, utilising various optimization algorithms (OAs), battery degradation cost with and without using the corresponding OA, initial and final SOC, number of participated EVs and a summarized conclusion. Our proposed methodology dealt with various EV categories and specifications as will be investigated in the trailing chapters.

Chapter 2

Table 2-6 A glancing overview of the literature survey.

Ref s.	Battery Degradation Cost	V2G Revenue	Optimization Algorithm (OA)	Battery Degradation Cost without Using the OA	Battery Degradation Cost Using the OA	SOC_i	SOC_f	Number of EVs	Findings Brief
[24 4]	√	√	Nonlinear Programming (NLP)	0.4970 \$/day	0.4347 \$/day	≈40 %	80%	1050	<ul style="list-style-type: none"> The system either uses EV in the V2G mode to regulate the grid or charges it according to the owner's request. The optimization is proposed across the day (24 h).
[24 5]	√	X	Mixed-Integer Linear Problem (MILP)	135.02 \$/day	6.36 \$/day	≈25 %	≈35 %	400	<ul style="list-style-type: none"> The proposed system is supported by a battery energy storage system (BESS). The linearized BESS degradation cost is presented in this row. The optimization is proposed across the day (24 h).
[24 3]	√	√	Mixed-Integer Linear Problem (MILP)	N/A	0.834, 1.119, 2.477 and 2.146 \$/kWh	70%	100 %	N/A	<ul style="list-style-type: none"> The degradation cost varies based on the charging time across the day at 10:00, 14:00, 18:00 and 22:00. The charging period is assumed to be 14 h.

Chapter 2

				N/A	0.834, 0.834, 1.119 and 1.811 \$/kWh	70%	100 %	N/A	<ul style="list-style-type: none"> The degradation cost varies based on the charging duration of 6, 8, 10 and 12 h. The charging period is assumed to be 14 h. This approach can reduce the peak demand by 7.8%.
[24 1]	√	√	CVX	39 \$/day	23 \$/day	N/A	N/A	100	<ul style="list-style-type: none"> However, the degradation cost increased from 28 \$ to 86 \$ based on the scenario used.
[24 6]	√	√	Nonlinear or Programming (NLP)	0.4969 \$/day	0.4348 \$/day	≈40 %	80%	1000	<ul style="list-style-type: none"> The system introduced day-ahead scheduling for EVs. The system's objectives have been verified on real-time UK National Grid regulation data.
[24 7]	√	√	Generalized Reduced Gradient (GRG)	N/A	168.18 \$/day	20% - 50%	80%	1000	<ul style="list-style-type: none"> EV aggregators can charge the EVs during the valley periods and discharge during peak periods. The New York market has been taken as the case study for the economic evaluation.

Chapter 2

2.7 Chapter Summary

This chapter discussed the main aspects of electric vehicle charging stations (EVCSs) and parking lots, based on recent publications in high-ranked journals and conferences. It started by describing the types of electric vehicles (EVs), standards for charging rates, and brief differences between EV batteries. This was followed by a discussion of the types of EV charging protocols, supported by schematic diagrams, and a summary of comparisons between them in tables. Recent articles concerning EV battery dynamic behaviour identification, classification, and recognition processes are scrutinized in detail. Advanced charge controllers used to implement the charging protocols are discussed, and a comparison table is provided to reveal the controllers proposed in the following chapters. Finally, the chapter investigated the smart connectivity of EVs to the utility grid, which is expressed through EVCSs and stochastic parking throughout the day. The scenarios and case studies utilized in recent articles are summarized in tables to reveal the novelty of this thesis, as will be explained and substantiated in the following chapters.

Chapter 3

Proposed EV Charging Protocol using AI for Fast Charging Under Dynamic Environment

3.1 Introduction

This chapter proposes a novel approach for electric vehicles' fast charging with lithium-polymer ion batteries based on a sufficient database of different EV categories at different ambient conditions. This approach starts when the EV is entering the electric vehicle charging station and plugging it into the charging point until it is fully charged. The schematic diagram of this approach was introduced in Figure 3-1. The system should have a sufficient database of various categories of EVs with the DC charging electrical characteristics (voltage and current with respect to the charging interval time) for each category at different ambient conditions (temperature and relative humidity). Once connecting the EV to the charging pile, a 10 secs sample of the charging current will be implemented then the system will be able to classify the category of the EV. In addition, the system will classify the EV category and recognise the corresponding temperature and relative humidity. Classification and recognition will be followed by a full estimation of the charging time, charging current topology and the battery terminal voltage of the corresponding EV. Then, two new techniques based on the multistage charging current (MSCC) protocol are compared with the traditional constant current constant voltage (CC-CV). The dynamic behaviour of the lithium-polymer ion battery using the mentioned protocols is modelled, identified, and scrutinized in the next chapter. In the final stage, an off-board charging pile controller has been simulated and practically implemented to serve the fast-charging process with minimum error.

Chapter 3

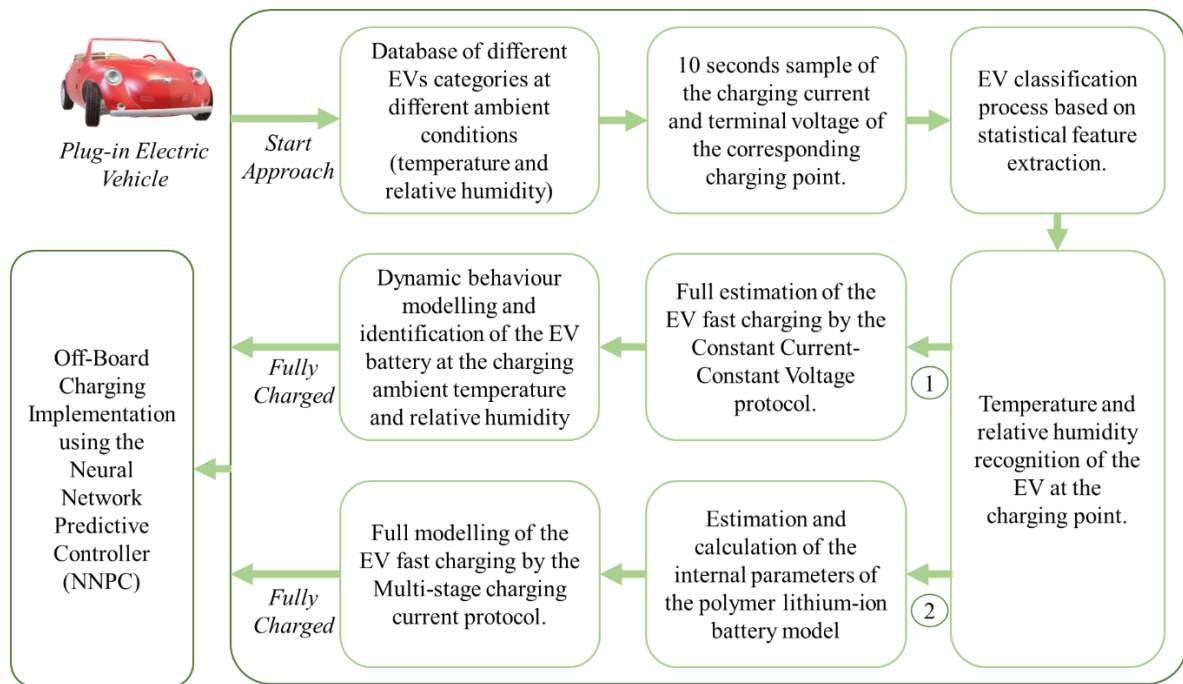


Figure 3-1 Schematic diagram of the proposed EV charging process starting from plugging it into the charging point until it is fully charged using the CC-CV and MSCC charging protocols.

In the following section, the first stage has been investigated by collecting the database of various electric vehicles represented by lithium-ion polymer batteries at different ambient conditions (temperature and relative humidity).

3.2 Temperature and Relative Humidity Investigation

3.2.1 Experimental Setup

The battery packs in electric vehicles were built from thousands of cells connected in series and parallel and vary according to the battery type and EV model [60, 248, 249]. Hence, a full investigation of the temperature and relative humidity impact on the lithium-ion battery while charging has been implemented to collect the required data. The constant current-constant voltage (CC-CV) protocol has been implemented in charging the EVs as it is simple and commonly used in DC fast-charging stations where is utilized to minimize the queuing delay per EV [250]. A fully controlled temperature and relative humidity chamber have been fabricated as shown in Figure 3-2 and is composed of a heater, humidifier, microcontroller, switches to ON/Off the sources, blowing and suction fan, and a DHT11 temperature/humidity sensor. The sensor was fixed just beside the lithium-ion polymer battery under test. The operating switches (relays) have been controlled by an Arduino-Uno microcontroller board to set the temperature and relative humidity inside the chamber effectively throughout a closed-loop system. The chamber was coated with an aluminium foil laminated paper to minimize heat dissipation. The goal of the proposed chamber is to limit the temperature and relative humidity to the predetermined values which are obtained throughout this design. The system measured the temperature/humidity in a 1 ms sample and feedbacks the relays for further action. The charge/discharge process has been implemented using the IMAX-B6 80W battery

Chapter 3

charger. The batteries were discharged at $0.9C$ (A) until the voltage reaches $2.8N$ (V). C is the rate at which a battery is charged/discharged relative to its maximum capacity; N is the number of packed batteries used in the test. After 10 mins of relaxation, the battery is discharged by $0.1C$ (A) until the voltage reaches $2.8N$ (V). After relaxing for 12 hrs, the batteries under test are placed in the Temperature/Humidity chamber for 10 mins at a specific ambient temperature and then charged at different values of temperature and humidity with the CC-CV protocol. This protocol is started with a CC charging process of $0.9C$ (A) until the voltage reaches $4.2N$ (V) followed by a CV process of $4.2N$ (V) until the current decays to $0.1C$ (A) and then relaxing the battery for 12 hrs. This stage is considered the database collection for the next stages.



Figure 3-2 Climatic chamber to control temperature and humidity.

EVs' battery pack consists of hundreds of cells connected in series and in parallel such as the 2015 Chevrolet Spark EV where the LG Chem lithium-ion battery with a nominal cell voltage of $3.7V$, and a nominal system voltage of $355.2V$ consists of 192 cells of 6 modules. The battery module is composed of 16 cells in series and parallels with another 16 series cells. This category has 6 modules in a series connection to form the battery pack [251]. In this chapter, two different lithium-polymer ion batteries of a single cell and battery pack have been used to represent the EVs and are presented in Table 3-1. The utilized batteries have a nominal capacity of 1000 mAh and 2200 mAh and with recommended working temperature within the range from $0^{\circ}C$ to $40^{\circ}C$. However, no data concerning the working or charging relative humidity has been mentioned except for the recommended storage humidity.

Chapter 3

Table 3-1 Specifications of the selected Lithium-ion Polymer batteries [252].

Item	Specifications	
Type	Polymer lithium-ion single-cell battery	Polymer lithium-ion battery Pack
Nominal Capacity	1000 mAh	2200 mAh
Maximum charging current	1C Amp	1C Amp
Maximum discharging current	2C Amp	2C Amp
Charging cut-off voltage	4.2 ± 0.05 V	12.9 V
Discharging cut-off voltage	2.75 V	8.4 V
Working temperature	0-40°C	0-45°C
Storage humidity	65% ± 20% RH	65% ± 20% RH

3.2.2 Temperature Impact on the Charging Process

The electro-thermal charging behaviour of the proposed batteries of 1000 mAh and 2200 mAh is investigated at 40°C and 30°C with the same relative humidity of 52%. It is observed from Figure 3-3 that at 30°C the battery reached full capacity faster than 40°C. At 30°C the battery with a capacity of 1000 mAh is fully charged in 4,742 sec (79.0333 min), and at 40°C the battery reaches full capacity in 4,919 sec (81.9833 min). The battery, with a capacity of 2200 mAh, has been fully charged in 3,784 sec (63.0667 min) and 3,845 (64.08333 min) at 30°C and 40°C, respectively. It is concluded that the variation in temperature leads to a change in the total charging interval time process but with a small variation based on the manufacturer's charging specifications reaching around ≈ 1 to 3 mins.

Chapter 3

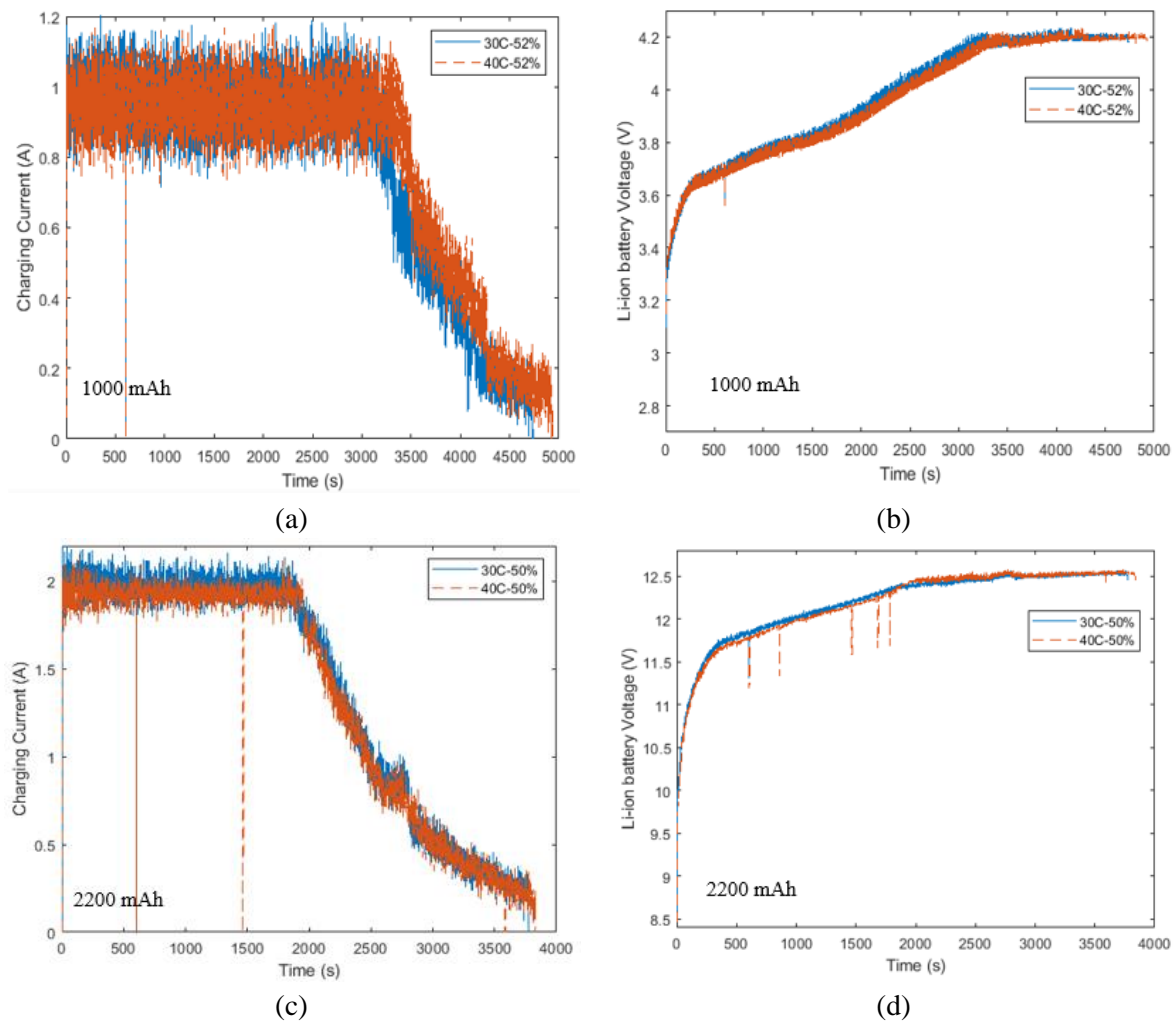


Figure 3-3 Batteries charging topology (a), (b) charging current and terminal voltage of the 1000 mAh polymer lithium-ion battery at two various temperatures (30°C and 40°C) and the same relative humidity (52%), (c) and (d) charging current and terminal voltage of the 2200 mAh polymer lithium-ion battery pack at two various temperatures (30°C and 40°C) and same relative humidity (50%).

3.2.3 Relative Humidity Impact on the Charging Process

In this subsection, the electro-thermal charging behaviour is cycled by 0.9C (A) using the CC-CV protocol at the same ambient temperature of 40°C but with different RH (35%, 52%, and 70%). As shown in Figure 3-4, there is a significant impact of RH on the terminal voltage and charging current. While increasing the humidity, the charging interval time becomes slower than the low humidity. The total charging time for the battery with 1000 mAh at RH-35%, RH-52%, and RH-70% is 4,606 sec (76.7667 min), 4,938 sec (82.3 min), and 5,690 sec (94.8333), respectively and for the other battery with a capacity 2200 mAh at RH-30%, and RH-50% are 3,700 sec (61.6667 min), and 3,845 sec (64.0833 min), respectively.

In the 1000 mAh lithium-ion battery, a significant slow variation in the total interval charging time at both RH-52% and RH-70% with respect to RH-35% reached 7.2% and 23.53%, respectively. And corresponding to a 2200 mAh lithium-ion battery, the slow variation reached

Chapter 3

4% between RH-30% and RH-50%. It is observed that whenever the RH increases, the moisture effect reveals the chemical reactions of the battery, where the terminal voltage reaches the cut-off value faster than in low RH conditions. In addition, the CC charging stage takes a small interval time and the CV stage takes much more time to reach the battery's full capacity.

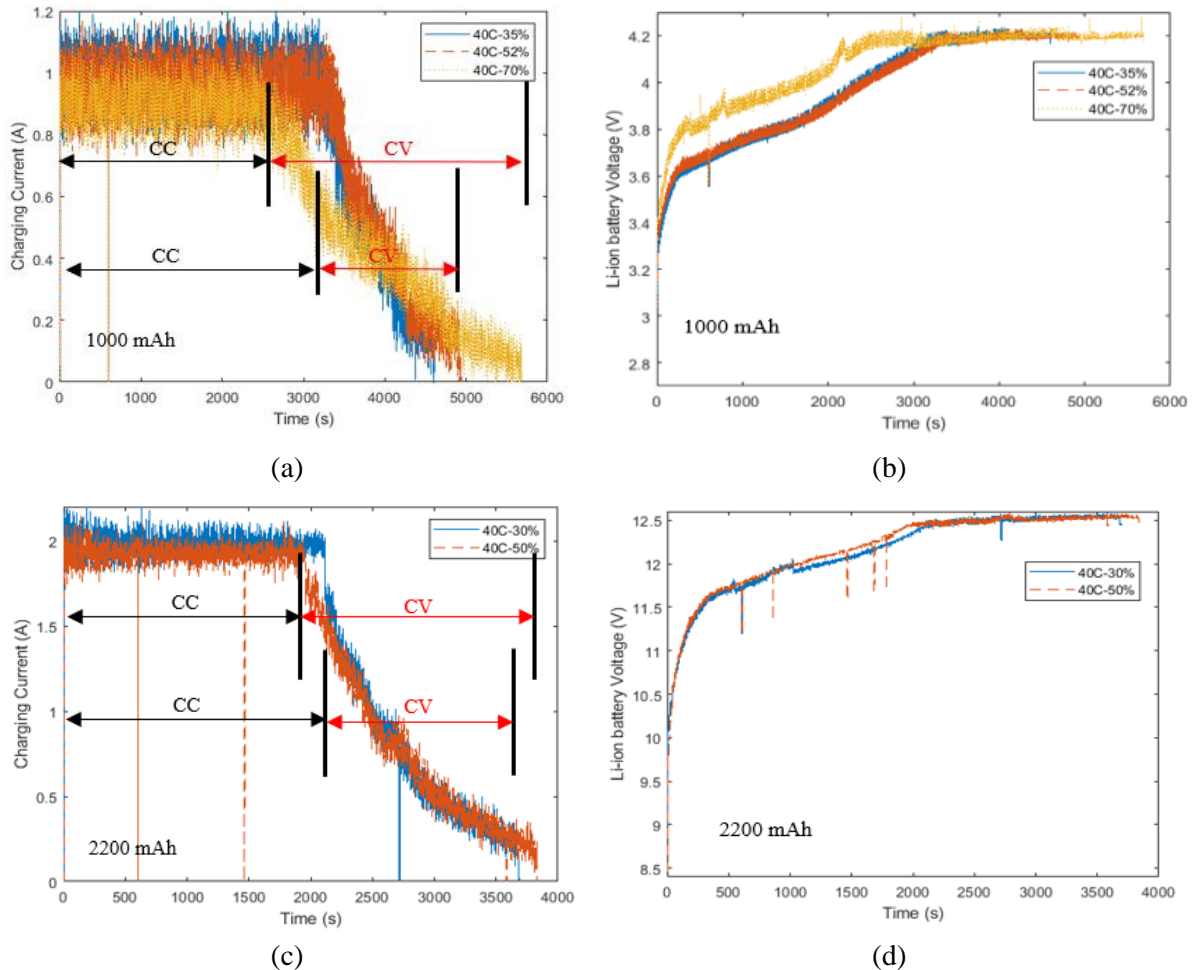


Figure 3-4 The charging topology of the polymer lithium-ion batteries at the same temperature (40°C) and various RH (35%, 52%, and 70%) and (30%, and 50%) for 1000 mAh and 2200 mAh, respectively.

It is obvious that any change in the temperature or/and relative humidity directly reflects on the charging performance of the EV, which straightly impacts the overall performance of the charging process. Thus, full recognition, modelling and fast charging of the plug-in electric vehicles have been presented, starting from connecting the EV to the charging pile till the battery is fully charged.

In the following section, the EV classification and recognition process is proposed to identify the category, the operational ambient conditions, and the EV lithium-ion battery dynamic behaviour to be used in the modelling and estimating of the charging parameters of its corresponding charging protocol.

3.3 EV Classification and Recognition Process based on the Feed-forward Backpropagation Artificial Neural Network (FFBP-NN)

The proposed approach starts since the plug-in Electric Vehicle (PEV) is connected to the charging pile in the charging stations, private homes, or any parking lot equipped with EV chargers. The classification and recognition processes are mandatory to avoid confusion between the different EV categories and different operational temperatures and relative humidity for each EV category connected to any charging pile. Various features have been used to efficiently classify the charging signal's physical nature. Those features have been proposed in various recognition applications concerning speech recognition [253], natural language processing [254], and other pattern recognition introduced in [255-257]. The feature extraction parameters used in this thesis have been implemented throughout probability and statistical analysis composed of Skewness, Kurtosis, Variance, Maximum Value, and Arithmetic Mean. The main equations of the feature extraction parameters are

$$Skewness = \frac{\sum_{i=1}^N (x_i - \bar{x})^3}{(N - 1)\sigma^3} \quad 3-1$$

$$Kurtosis = \frac{\sum_{i=1}^N (x_i - \bar{x})^4}{(N - 1)\sigma^4} \quad 3-2$$

$$Variance = \frac{\sum_{i=1}^N (x_i - \bar{x})^2}{(N - 1)} \quad 3-3$$

$$Maximum\ Value = \sqrt{2} \times x_{rms} \quad 3-4$$

$$Arithmetic\ Mean = \frac{\sum_{i=1}^N x_i}{N} \quad 3-5$$

Where σ is the standard deviation, \bar{x} is the distribution mean, and N is the number of sample observations.

A charging current sample of 0.9C (A) was used for a 10 sec interval time to perfectly recognize and classify the type of the battery, its temperature, and relative humidity based on the probability and statistical analysis represented in Equations 3-1 to 3-5. The main schematic diagram that declares the main recognition process of the EVs is presented in Figure 3-5. In the proposed recognition model, a two-layer feedforward backpropagation neural network (FFBP-NN) has been used to recognize the EV by a sample charging in a very short time interval. The FFBP-NN is trained with a scaled conjugate gradient backpropagation algorithm. Different EVs with different temperatures and relative humidity have been expressed in the first part of Figure 3-5 and used to train the network with 43,009 samples: 70% for training, 15% for validation, and 15% for testing the network in recognition.

Chapter 3

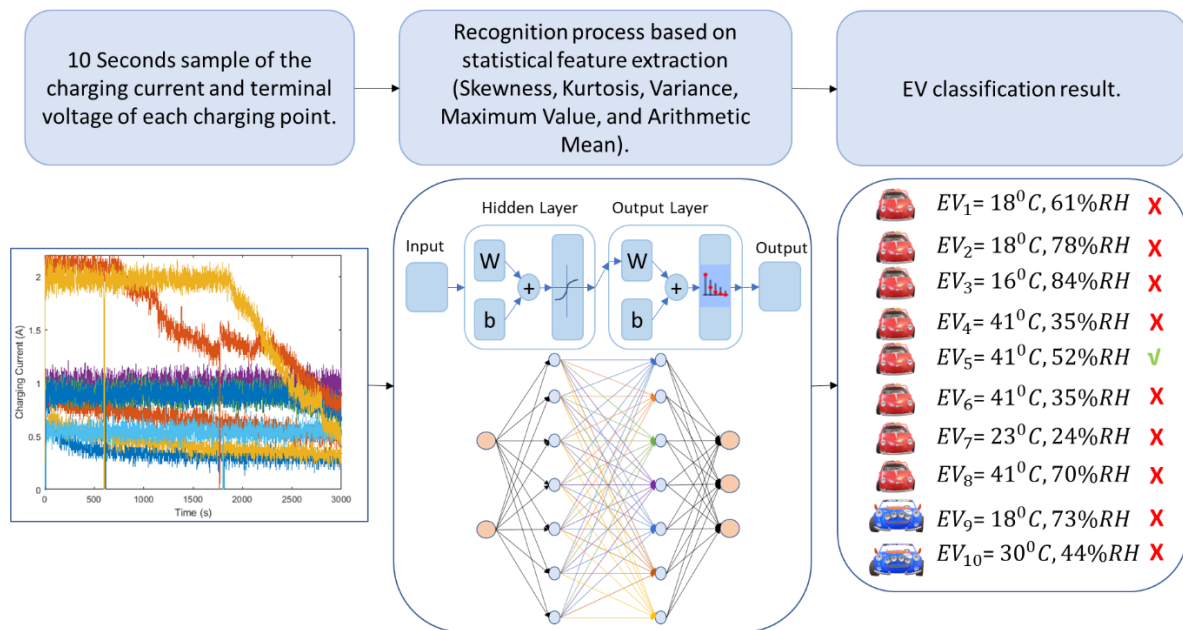


Figure 3-5 Schematic overview of the proposed classification and recognition process of various electric vehicles with different temperatures and relative humidity.

A lot of data on two lithium-ion batteries at different ambient conditions (temperature and relative humidity) has been collected from the previous section. A charging current sample of 0.9C (A) was used for a 10 sec interval time to recognize the type of battery, its temperature, and relative humidity. Figure 3-6-a presents a short charging sample of the proposed classification and recognition model. As concluded from the figure, the challenge is represented in the instant recognition and the tiny variations between the charging current characteristic of the different categories, charging temperatures and relative humidity. The results of the online recognition are presented in the Confusion matrix in Figure 3-6-b. The proposed classification ensured a perfect performance of the training, validation, and test samples. However, the complexity of the classification as the amplitude of the charging current is the same as 0.9C (A) for the two types of EVs with different temperatures and relative humidity. The accuracy of the training, validation and testing are 83.2%, 82.9%, and 83.1%, respectively. As shown in Figure 3-6-b, the accuracy for the overall network is 83.2% which is acceptable compared to the literature. The increase in the size of the online training database could improve the recognition and classification process. In addition, the statistical analysis of charging current signals at all the charging points daily is explored to detect a new class to be fed to the database.

Chapter 3

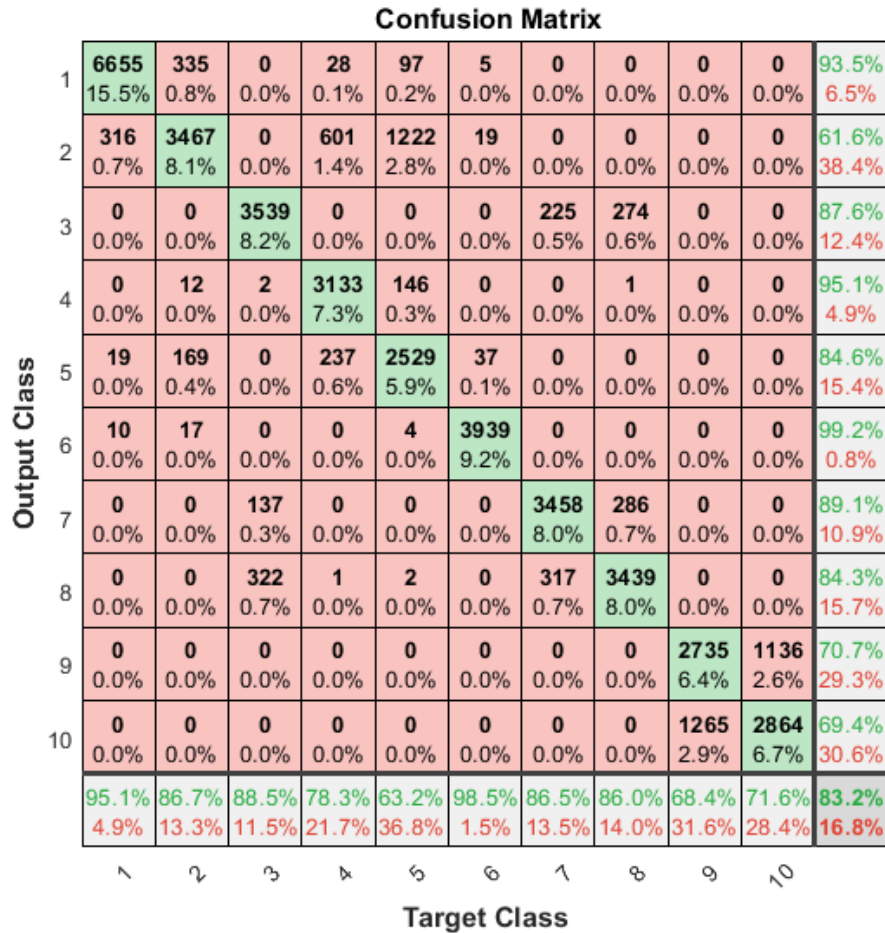
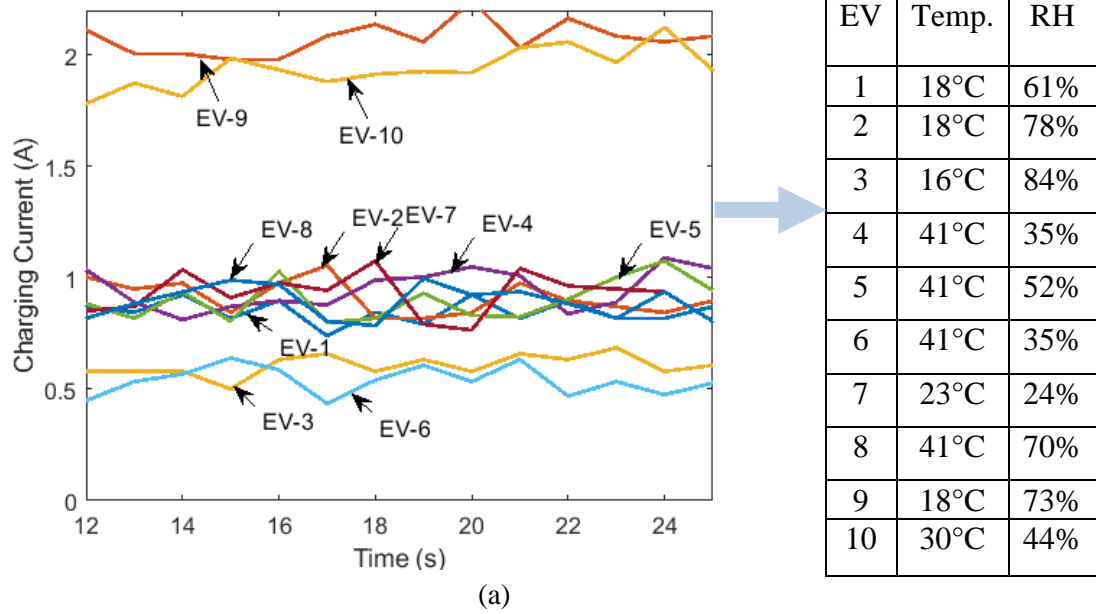


Figure 3-6 (a) The charging current of different operating conditions, and (b) The confusion matrix of the overall recognition and classification process.

Chapter 3

Despite the different EV types and battery surrounding temperature and relative humidity, the proposed recognition system based on the FFBP-NN has been implemented on an extra percentage of the initial terminal voltage. Therefore, each terminal voltage is directly reflected on a specific state of charge (SOC) which is considered a practical implementation of the electric vehicle charging station, and the results are expressed in Table 3-2. As shown, the system can perfectly recognize the type of EV, its temperature, and relative humidity. The numbers represent the probability of each recognition, and the shaded cells express the selection of the classifier to its corresponding EV. It is observed that in Test_6 however, the values are very close, the proposed neural network recognized the status of the corresponding EV precisely. For future work, it is recommended that for the same test, we can test the network with multiple samples to increase the decision probability.

Table 3-2 Testing the proposed classification and recognition process.

	Initial Voltage (V)	EV_1	EV_2	EV_3	EV_4	EV_5	EV_6	EV_7	EV_8	EV_9	EV_10
Test_1	4.19	0.9705	0.0176	0	0.0049	0.0055	0.0015	0	0	0	0
Test_2	4.23	0	0.4561	0	0.1411	0.3905	0.0002	0	0	0.0064	0.0056
Test_3	4.19	0	0	0.7049	0	0.0005	0	0.1732	0.1214	0	0
Test_4	3.376	0	0	0	0.9657	0.0336	0	0	0.0006	0	0
Test_5	3.19	0.0001	0	0	0	0	0.9999	0	0	0	0
Test_6	11.55	0	0	0	0	0	0	0	0	0.4955	0.5045

3.4 Constant Current-Constant Voltage (CC-CV) Charging Protocol Under Dynamic Temperature and Relative Humidity

This section proposes fast charging parameters estimation of the lithium-ion battery under the dynamic temperature and relative humidity using the CC-CV charging protocol based on the EV recognition and classification in the previous section.

3.4.1 EV fast-charging parameters estimation by the CC-CV protocol

The classification and recognition results will be followed by a full estimation of the CC-CV protocol parameters. In the proposed charging estimation stage, the feedforward backpropagation neural networks (FFBP-NN) have been used to represent the non-linear system by mapping the observables to the desired output. In [258, 259], the feedforward neural

Chapter 3

networks offered fast computational speeds online since, it is composed of a series of matrix multiplications, and other algorithms that contain computational intensive calculations like partial differential equations.

During the training, the inputs received are multiplied by randomly corresponding weights. The product is summed up and the error is determined and compared with the measured value. The error is backpropagated as an input to the network, with the weights readjusted. The process is repeated till the least error margin has been obtained. The main target of the FFBP-NN is to determine the optimal weights that can predict output proximity to the measured as given in the following equations [260].

$$W^* = \operatorname{argmin} E_p(\omega) \quad 3-6$$

$$E(\omega) = \sum_p E_p(\omega) \quad 3-7$$

$$E_p = \frac{1}{2} \sum_p (d_{pj} - y_{pj}(\omega))^2 \quad 3-8$$

$$E(\omega) = \frac{1}{2} \sum_{p=1} \sum_{j=1} (d_{pj} - y_{pj}(\omega))^2 \quad 3-9$$

Where ω is the weight matrix, $E(\omega)$ is an objective function on ω . $E(\omega)$ is to be minimized and calculated at any point of ω , p is the number of examples in the training set, $E_p(\omega)$ is the output error for each p , y_{pj} , and d_{pj} are the predicted output and measured output, respectively.

This study is based on the premise of the data-driven method, where the FFBP-NN is used based on the Levenberg-Marquardt algorithm as the learning algorithm to model the battery dynamic charging process at different temperatures and relative humidity by a dataset used for learning. The dynamic dataset utilized in this study consists of battery parameters (terminal voltage, charging current, temperature, and relative humidity) which have been measured during the charging process. The parameters have been carefully extracted from the battery under a controlled Temperature/Humidity chamber using precisely calibrated sensors, as presented in Figure 3-2. The output results from this stage are a full estimation of the EV charging current and terminal voltage at the operating ambient corresponding to the EV category.

Chapter 3

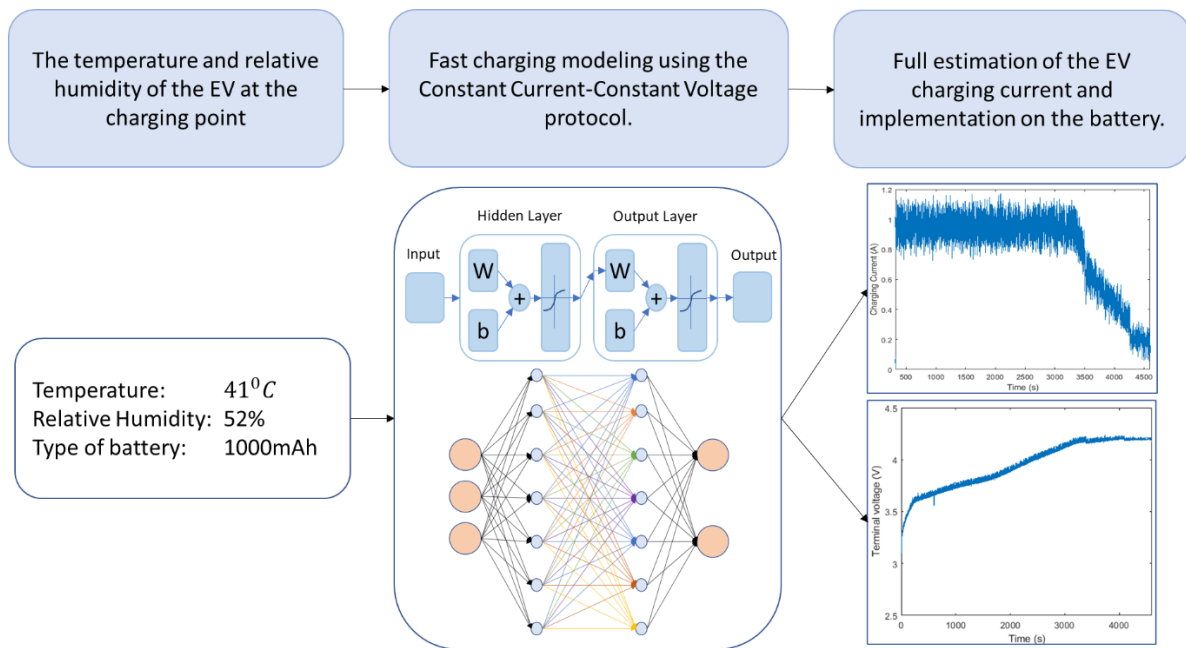


Figure 3-7 Schematic overview of the estimation stage of the fast-charging process using the CC-CV protocol.

After the classification of the electric vehicle described in the previous section, the recognition has been fed to the FFBP-NN as three inputs temperature, relative humidity, and the type of EV represented by the lithium-ion polymer battery. The training, validation, test, and overall regressions plots are proposed in Figures 3-8-a to 3-8-d. The plots show that the regression coefficients (R) of the training, validation, test, and overall system are 0.99953, 0.99948, 0.99951, and 0.99952, respectively. It is observed that the regression coefficients are in close agreement with unity which validates the accuracy of the FFBP-NN model.

Two graphs for both the proposed charging current and the predicted terminal voltage of the lithium-ion battery will be extracted from the FFBP-NN. As shown in Figure 3-8-e, the actual measured charging current agrees with the simulated current extracted from the NN. The error between the simulated and measured terminal voltage is expressed in Figure 3-8-f. It varies between -1% to 1% due to the variation in the applied current, which is considered an acceptable range.

Chapter 3

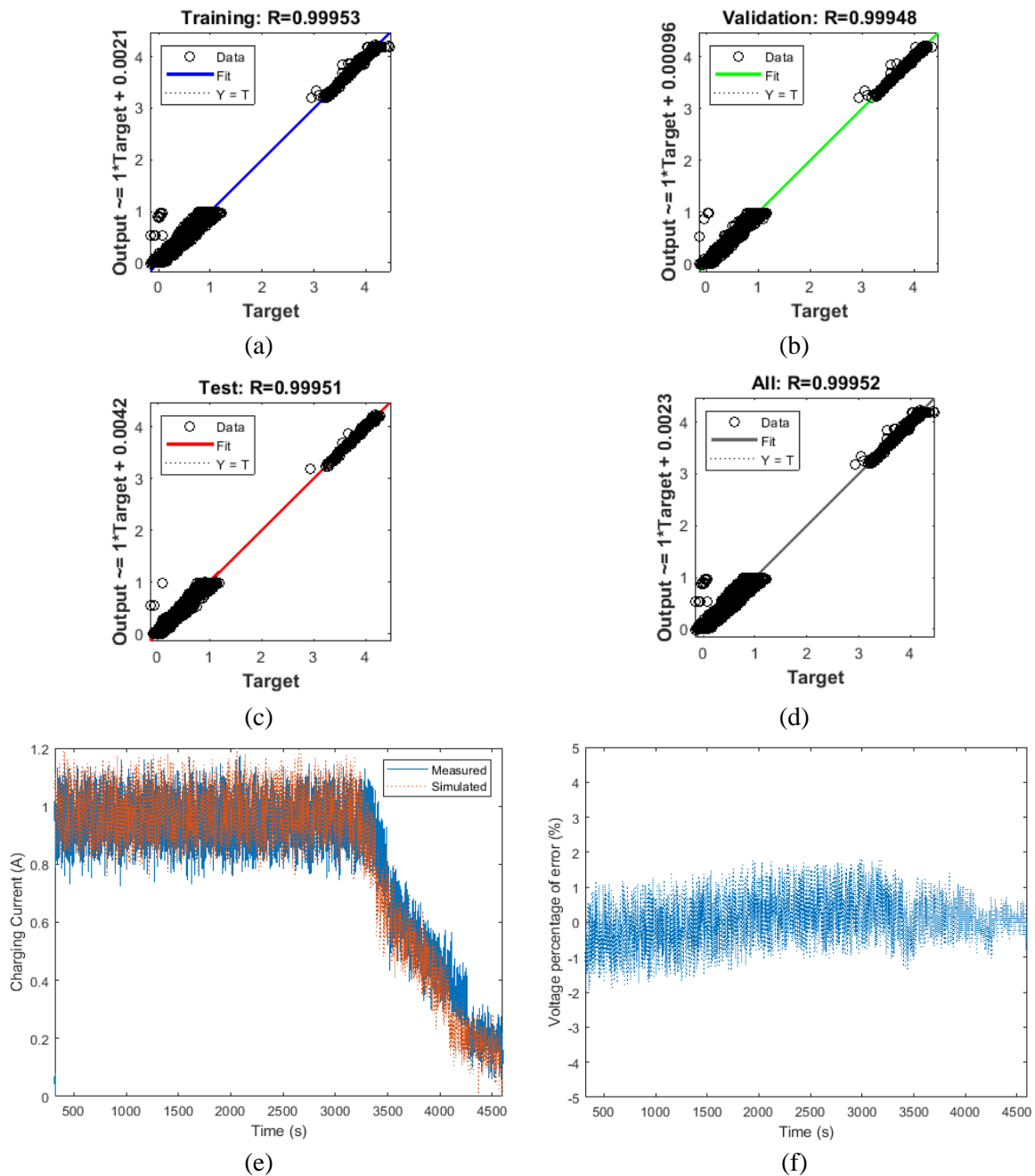


Figure 3-8 Extracted output results from the FFBP-NN (a) the training regression results, (b) validation regression results, (c) test regression results, (d) overall system regression plots, (e) the measured and simulated charging current, and (f) the percentage of error between the measured and simulated terminal voltage of the lithium-ion battery.

3.4.2 Hammerstein-Wiener (HW) modelling of the EV battery dynamic behaviour

The last stage is the sufficient and accurate modelling of the EV battery dynamic behaviour. Instead of the conventional electrical representation of the lithium-ion battery as mentioned in the literature, Hammerstein-Wiener (HW) identification model is utilized to present the nonlinear output dependency of the system on its input. HW model has been widely used for

Chapter 3

nonlinear industrial systems [261]. This model is cascaded with a nonlinear block either preceding (Hammerstein model) or following (Wiener model) the linear block as expressed in Figure 3-9 [262]. HW is composed of up to three steps: calculating the linear block input $w(t)$ from the input experimental data using nonlinear equation of $w(t) = f(u(t))$, then calculating the output of the dynamic linear box by $x(t) = \frac{B}{F}w(t)$ then finally the output of the HW model by $y(t) = h(x(t))$ has been calculated as expressed in [46, 262, 263].

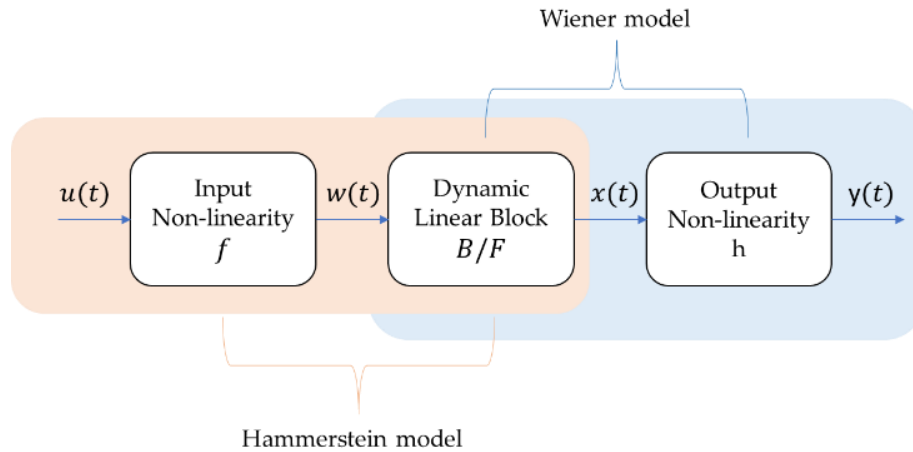


Figure 3-9 Schematic diagram of Hammerstein-Wiener model block diagram.

The modelling and identification of the battery cell dynamic behaviour are obtained using the nonlinear Hammerstein-Wiener (HW) model. HW is used based on the Levenberg-Marquardt (lm) search method with one numerator order and three denominator orders. The measured and simulated model output is expressed in Figure 3-10-a. As shown, the HW model perfectly predicted the behaviour of the battery using the CC-CV charging protocol parameters with the best fit of 89.62%, which is acceptable as stated in [46]. In addition, the difference between the measured experimental data and the simulated model of the battery terminal voltage is presented in Figure 3-10-b. The maximum error observed is 0.05 V, representing 1.19%.

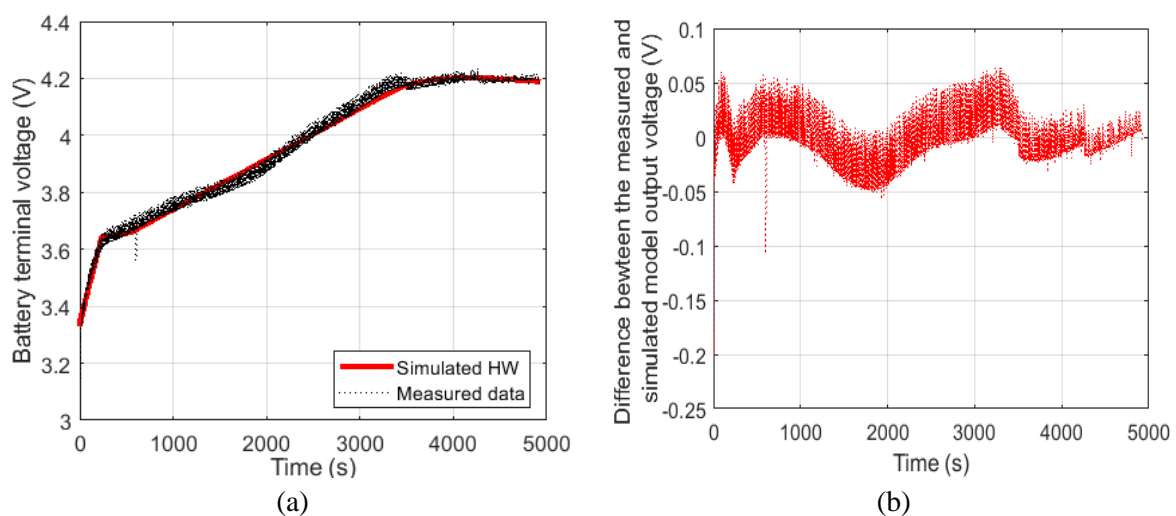


Figure 3-10 Output from the HW model (a) Measured and simulated model output, and (b) Difference between the measured data and simulated HW model output.

Chapter 3

The overall novel approach of this charging process is summarized in Figure 3-11. Where all the above-mentioned stages are presented in a flowchart with the ascending flow starting from collecting data, classification, and recognition, estimating the CC-CV protocol parameters, and finally modelling and identification of the EV battery dynamic behaviour.

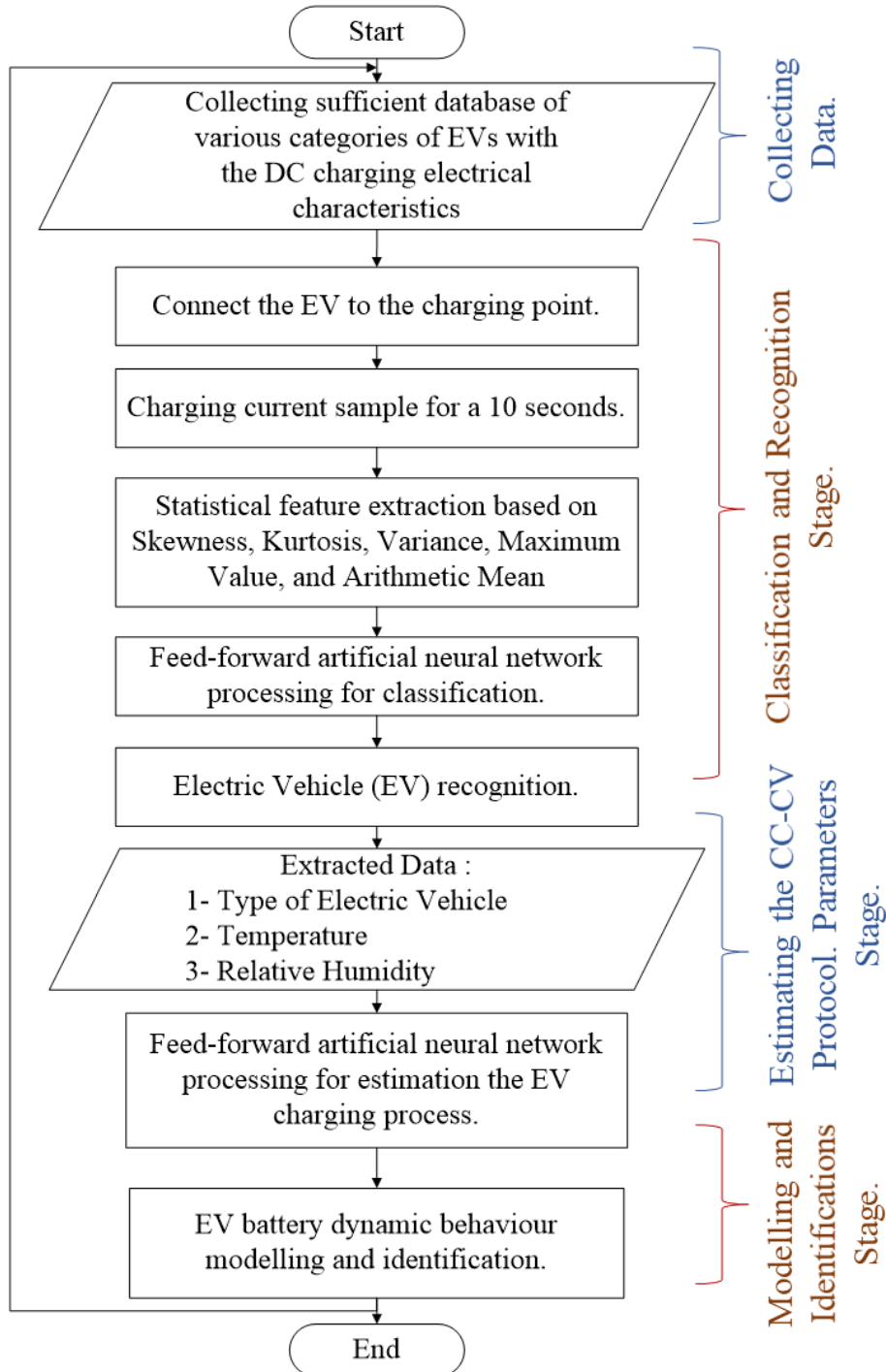


Figure 3-11 Flowchart of the overall proposed system starting from EV connected to the charging pile till the battery is fully charged.

Chapter 3

3.5 Chapter Summary

This chapter introduced novel fast charging algorithms for electric vehicles (EVs), which cover the process of entering the EV into the charging station and connecting to the charging pile until leaving the station fully charged. In the first stage, an investigation of the impact of temperature and/or relative humidity on the charging process of plug-in EVs (PEVs) is conducted using the constant current-constant voltage (CC-CV) protocol with lithium-polymer ion batteries of a single cell of 1000 mAh and a battery pack of 2200 mAh. It is observed that whenever the temperature is increased the total charging interval time increased by 3.73% and whenever the relative humidity is increased the total charging interval time is increased by 23.54%.

This was followed by a novel PEV classification and recognition model under the impacts of various ambient circumstances. The feedforward backpropagation neural network (FFBP-NN), a supervised classification algorithm supported by the statistical analysis of an instant charging current sample, was used. The proposed recognition model using the FFBP-NN ensured an accuracy of 83.2% despite the different EV capacities and battery surrounding temperature and relative humidity. This was followed by EV fast charging parameters estimation. The FFBP-NN perfectly estimated the charging current, terminal voltage, and charging interval time of the CC-CV protocol. The regression coefficient of the overall system reached 0.99952 and the maximum error between the simulated and experimental measured terminal voltage reached 1%. Then a sufficient identification model of the battery dynamic behaviour based on the Hammerstein-Wiener (HW) model was introduced. The model ensured a best fit of 89.62% and the maximum error between the simulated and measured data reached 1.19%.

Chapter 4

CAD, Design, and Development of EV Charging Protocol using AI for Fast Charging Under Dynamic Environment

4.1 Introduction

This chapter proposes novel fast charging techniques based on the multi-stage charging current (MSCC) to be compared with the conventional constant current-constant voltage (CC-CV) charging protocol to speed up the charging time, reduce the energy loss, and enhance the charging efficiency. Besides, a smart charger is proposed and implemented to improve the transient performance of the charging process while using renewable energy sources.

4.2 Multi-stage Charging Current (MSCC) Charging Protocol based on Cuckoo Optimization Algorithm (COA) at Constant Ambient Conditions

4.2.1 Estimation and calculation of the internal parameters of the proposed lithium-ion polymer battery model

Modelling of Lithium-ion batteries could be divided into two main categories: 1) the first category is the Electrochemical model that describes the electrochemical reaction occurring in the battery [71], and 2) the second category is its electronic equivalent circuit that is based on the characteristics of the lithium-ion battery and can be branched into Rint model, PNGV model, Thevenin model, RC first-order transient model and RC second-order transient that is also called Dual Polarization (DP) model [37, 264-267]. The RC second-order transient equivalent circuit model (DP model) in Figure 4-1 represents the transient behaviour of the lithium-ion polymer battery. The DP model has proved to be the closest circuit model that can be used to explain the performance and behaviour of lithium-ion batteries due to the dependency on the electrochemical and concentration polarization internal resistances and capacitances [68]. Hence, the target is modelling the lithium-ion battery while defining all its internal parameters.

The RC second-order transient model consists of three main sectors [268-271]: open circuit voltage OCV , which depends on the battery state of charge, internal resistances including the ohmic internal resistance (R_i), the electrochemical polarization internal resistance (R_α) and the concentration polarization internal resistance (R_β) and lastly, the internal capacitances such as the electrochemical polarization capacitance (C_α) and the concentration polarization capacitance (C_β).

Chapter 4

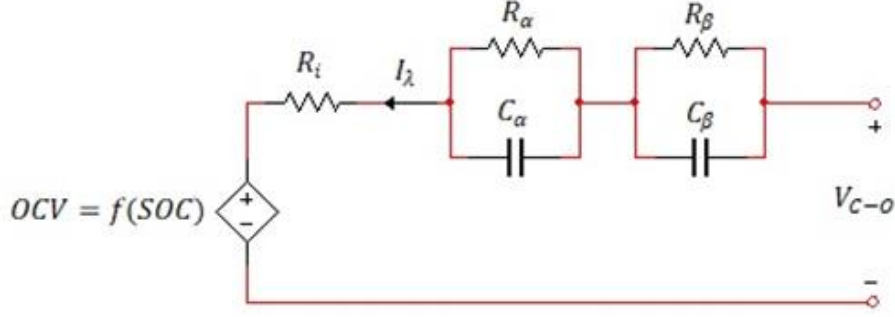


Figure 4-1 The proposed RC second-order transient equivalent model of a lithium-polymer battery.

The electrical behaviour and relationship between the circuit components can be expressed as follows.

$$I_{C_{\alpha\lambda}} = I_{\lambda} \left\{ 1 - \frac{1 - e^{\frac{-\Delta t}{R_{\alpha}C_{\alpha}}}}{\frac{\Delta t}{R_{\alpha}C_{\alpha}}} \right\} + I_{\lambda-1} \left\{ \frac{1 - e^{\frac{-\Delta t}{R_{\alpha}C_{\alpha}}}}{\frac{\Delta t}{R_{\alpha}C_{\alpha}}} - e^{\frac{-\Delta t}{R_{\alpha}C_{\alpha}}} \right\} + I_{C_{\alpha\lambda-1}} \left\{ e^{\frac{-\Delta t}{R_{\alpha}C_{\alpha}}} \right\} \quad 4-1$$

$$I_{C_{\beta\lambda}} = I_{\lambda} \left\{ 1 - \frac{1 - e^{\frac{-\Delta t}{R_{\beta}C_{\beta}}}}{\frac{\Delta t}{R_{\beta}C_{\beta}}} \right\} + I_{\lambda-1} \left\{ \frac{1 - e^{\frac{-\Delta t}{R_{\beta}C_{\beta}}}}{\frac{\Delta t}{R_{\beta}C_{\beta}}} - e^{\frac{-\Delta t}{R_{\beta}C_{\beta}}} \right\} + I_{C_{\beta\lambda-1}} \left\{ e^{\frac{-\Delta t}{R_{\beta}C_{\beta}}} \right\} \quad 4-2$$

Where, I_{λ} is the total current of the present stage λ , $I_{C_{\alpha\lambda}}$ is the stage current passes through the electrochemical polarization capacitance (C_{α}), $I_{C_{\beta\lambda}}$ is the current passes through the concentration polarization capacitance (C_{β}) and Δt is the change in interval time.

The detailed calculations and estimations of the OCV and the internal parameters of the proposed polymer lithium-ion battery are explained in the following sub-sections.

4.2.1.1 Open Circuit Voltage (OCV)-State of Charge (SOC) Method

There are various methods to estimate SOC. The first method is the Open Circuit Voltage (OCV) which is used to measure the voltage at the required SOC percentage, yet a precise relaxation time should be taken [272-274]. Secondly, the Coulombs Counting method relies on the current integration depending on a controlled sensor, however, regular calibration should be done to avoid any error [275-280]. The last one is the machine learning method, which is based on the reliability of the collected data and includes the following: artificial intelligent [259, 281, 282], the support vector machines algorithm (SVM) [283, 284] and Kalman filter family methods that rely on the state-space model, yet, the machine learning method has a poor performance in transients [285-291].

SOC with a low percentage of error is required to optimize the energy loss, the time interval required to charge the battery, safety usage, and battery management. The integration of the modified Coulomb Counting method with the OCV method has proved to cause no critical side effects during normal battery operation [278], and it can be expressed as

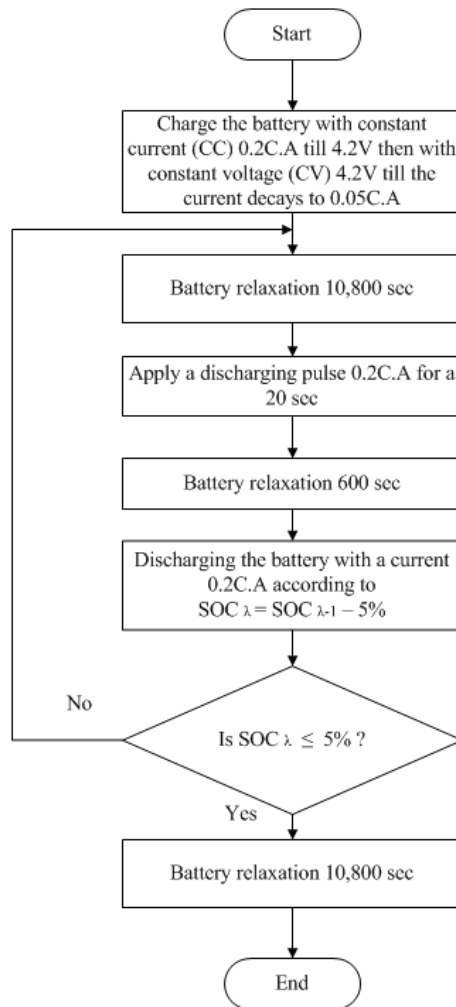
Chapter 4

$$SOC_{\lambda} = SOC_{\lambda-1} \pm \left(\eta \times \frac{\int_{t_0}^{\tau} I_{\lambda-1} \cdot d\tau}{C_{Rate}} \right) \times 100\% \quad 4-3$$

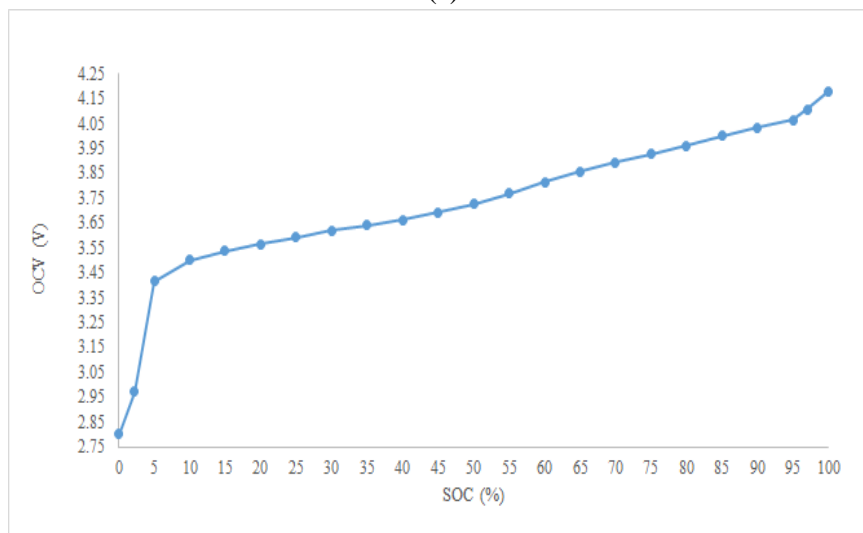
where \pm the positive sign for charging and the negative sign for discharging, SOC_{λ} is the state of the present charging stage λ , $I_{\lambda-1}$ is the current of the battery at stage $(\lambda - 1)$, η is the coulomb coefficient and it is constant =1 for discharging and =0.98 for charging and C_{Rate} is the rated capacity of the battery (Ah).

The procedures of SOC estimation are presented in the flow chart of Figure 4-2-a. The proposed procedures are implemented to draw the relationship between OCV compared to SOC at a room temperature of 25°C and relative humidity of 82% using NI myRIO-1900 as shown in Figure 4-2-b.

Chapter 4



(a)



(b)

Figure 4-2 Illustrates (a) the procedures of the OCV-SOC test method and (b) the relation between OCV-SOC of the lithium-polymer battery cell at room temperature 25°C.

Chapter 4

4.2.1.2 Internal Parameters of the Proposed Battery Model

The values of the proposed battery equivalent circuit model have been calculated based on the battery terminal potential difference during the discharging current pulses. The discharging current pulses have been implemented in a short interval time of 20 sec with a 600 sec relaxation period before and after the applied current pulse [268, 270]. Figure 4-3. shows specific voltages and times during the discharging pulses which are used to calculate the internal parameters of the lithium-polymer battery.

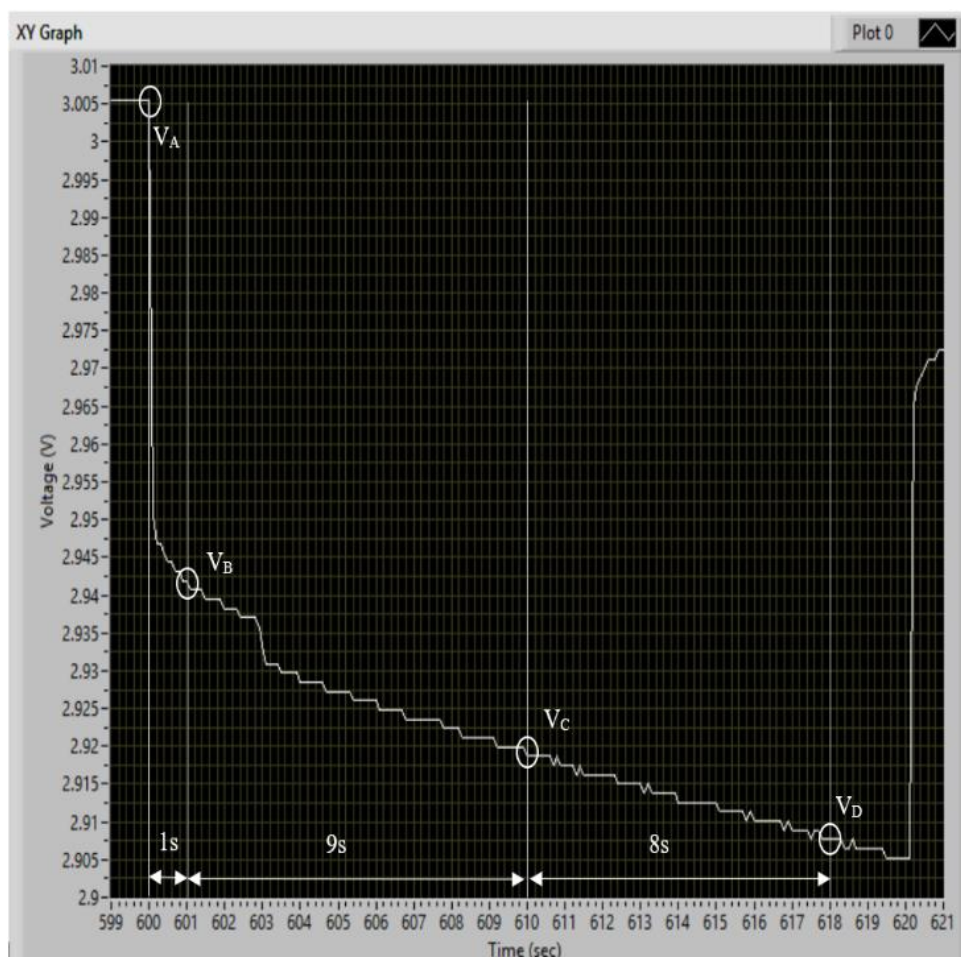


Figure 4-3 Discharging current pulse sample graph measured by NI myRIO during the interval time 20 s at room temperature 25°C.

By applying a discharging current pulse of 0.2A on the used polymer lithium-ion battery, the ohmic internal resistance R_i , the electrochemical polarization internal resistance R_α and the concentration polarization internal resistance R_β have been calculated after 1 sec, 10 sec, and 18 sec, respectively [268]. The equations given in [269] have been used to calculate the internal resistances and capacitances. The internal parameters of the proposed second-order transient equivalent circuit have been illustrated and calculated as follows:

(a) The ohmic internal resistance R_i calculated just after 1 sec of applying a discharging current pulse 0.2A. The values of ohmic internal resistance have been calculated by the immediate

Chapter 4

voltage and discharging current according to Equation 4-4 for each change in the state of charge (ΔSOC) = 5%

$$R_i = \frac{V_A - V_B}{I_{Discharging}} \quad 4-4$$

(b) The electrochemical polarization internal resistance R_α has been calculated after 10 sec of applying a discharging current pulse 0.2A. It depends mainly on the voltage difference within a short period of 9 sec. The electrochemical polarization internal resistance has been measured for each change in the state of charge (ΔSOC) = 5% by

$$R_\alpha = \frac{V_B - V_C}{I_{Discharging}} \quad 4-5$$

(c) The concentration polarization internal resistance R_β has been determined after 18 sec of applying a discharging current pulse 0.2A for each change in the state of charge (ΔSOC) = 5% by

$$R_\beta = \frac{V_C - V_D}{I_{Discharging}} \quad 4-6$$

(d) The electrochemical polarization capacitance C_α has been calculated by Equation 4-7 for each change of state of charge (ΔSOC) = 5%

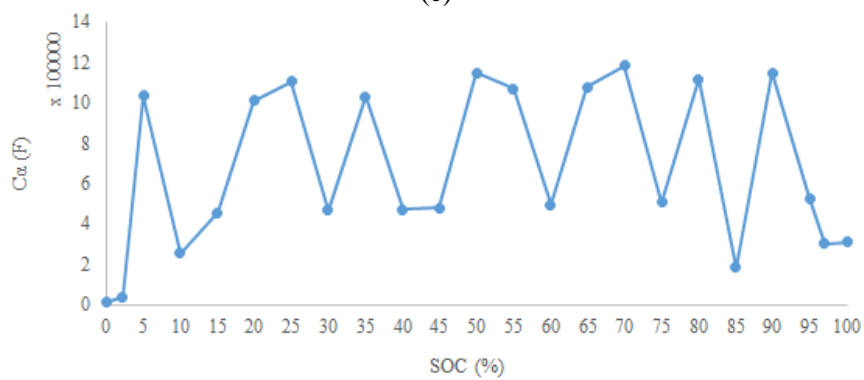
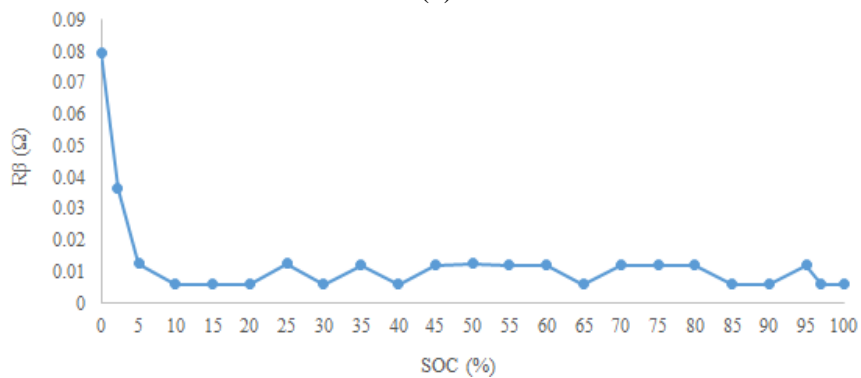
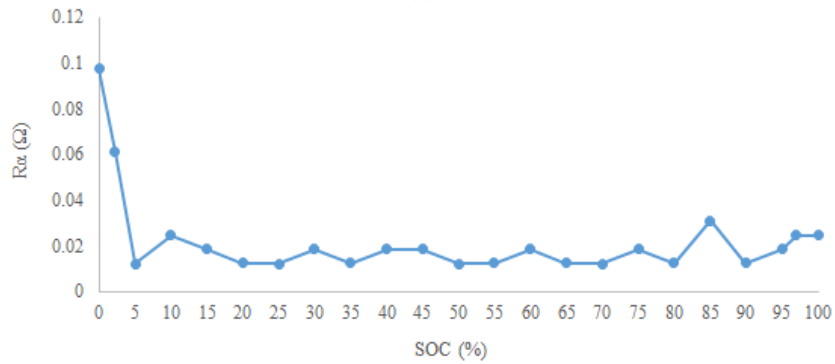
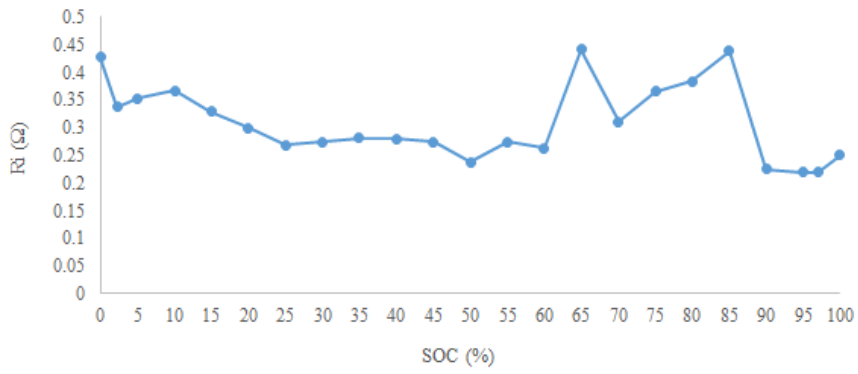
$$C_\alpha = \frac{9I}{(V_C - V_B) \ln\left(\frac{V_C}{V_B}\right)} \quad 4-7$$

(e) The concentration polarization capacitance C_β has been calculated by Equation 4-8 for each change of state of charge (ΔSOC) = 5%

$$C_\beta = \frac{8I}{(V_D - V_C) \ln\left(\frac{V_D}{V_C}\right)} \quad 4-8$$

The relationship between the internal parameters of the proposed battery model and SOC is presented in Figure 4-9.

Chapter 4



Chapter 4

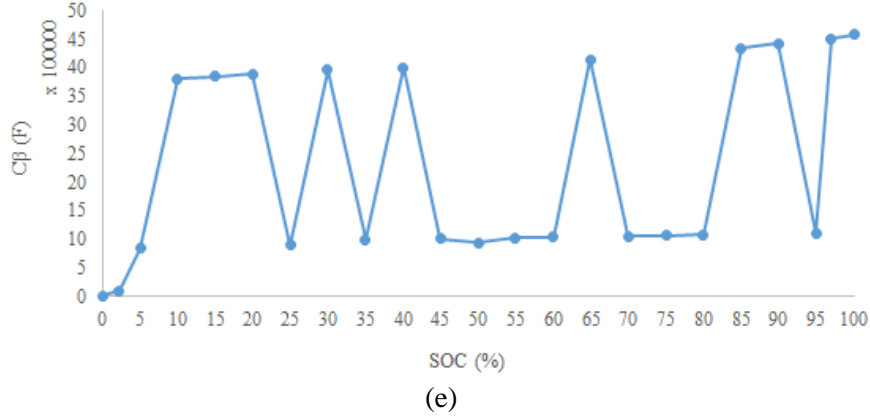


Figure 4-4 The relationship between the internal parameters of the proposed battery model (a) The ohmic internal resistance R_i , (b) The electrochemical polarization internal resistance R_{α} , (c) The concentration polarization internal resistance R_{β} , (d) The electrochemical polarization capacitance C_{α} and (e) The concentration polarization capacitance C_{β} corresponding to SOC during an interval discharging pulse 20s at room temperature 25°C.

4.2.2 Derivation of the Fast-Charging Fitness Function

To reach the battery's full capacity with a minimum charging interval time and energy consumption, an objective function (fitness function) should be minimized. The concept of the constructed objective function equation is based on the following equations which have been extracted from [74, 75, 78, 83]. The energy loss for the proposed RC second-order transient equivalent circuit can be expressed as follow.

$$E.L.(J) = \sum_{\lambda=1}^N \left[\{I_{\lambda}^2 R_i T_{\lambda}\} + \{(I_{\lambda} - I_{C_{\alpha\lambda}})^2 R_{\alpha} T_{\lambda}\} + \{(I_{\lambda} - I_{C_{\beta\lambda}})^2 R_{\beta} T_{\lambda}\} \right] \quad 4-9$$

Where N is the total number of constant current charging stages and T_{λ} is the total time of current charging at stage λ .

By considering the interval change in time of the system is $\Delta t = 1$ sec and the change of SOC is $\Delta SOC = 1\%$, the charging interval time for each stage will be expressed as $T_{\lambda}(sec) = (36/I_{\lambda})$ from Equation 4-3.

The objective function intended in this study stated in Equation 4-10 was obtained by using Equations 4-1, 4-2, 4-3, and 4-9.

Chapter 4

Objective Function

$$\begin{aligned}
&= \left[\omega_1 \chi \sum_{SOC_{\lambda-1}=1}^{SOC_{\lambda}} \sum_{\lambda=1}^N \left\{ I_{\lambda}^2 R_i \frac{36}{I_{\lambda}} \right\} \right. \\
&+ \left\{ \left(I_{\lambda} \left\{ \frac{1 - e^{-\frac{-\Delta t}{R_{\alpha} C_{\alpha}}}}{\frac{\Delta t}{R_{\alpha} C_{\alpha}}} \right\} - I_{\lambda-1} \left\{ \frac{1 - e^{-\frac{-\Delta t}{R_{\alpha} C_{\alpha}}}}{\frac{\Delta t}{R_{\alpha} C_{\alpha}}} - e^{-\frac{-\Delta t}{R_{\alpha} C_{\alpha}}} \right\} \right. \right. \\
&- \left. \left. I_{C_{\alpha\lambda-1}} \left\{ e^{-\frac{-\Delta t}{R_{\alpha} C_{\alpha}}} \right\} \right)^2 R_{\alpha} \frac{36}{I_{\lambda}} \right\} \\
&+ \left\{ \left(I_{\lambda} \left\{ \frac{1 - e^{-\frac{-\Delta t}{R_{\beta} C_{\beta}}}}{\frac{\Delta t}{R_{\beta} C_{\beta}}} \right\} - I_{\lambda-1} \left\{ \frac{1 - e^{-\frac{-\Delta t}{R_{\beta} C_{\beta}}}}{\frac{\Delta t}{R_{\beta} C_{\beta}}} - e^{-\frac{-\Delta t}{R_{\beta} C_{\beta}}} \right\} \right. \right. \\
&- \left. \left. I_{C_{\beta\lambda-1}} \left\{ e^{-\frac{-\Delta t}{R_{\beta} C_{\beta}}} \right\} \right)^2 R_{\beta} \frac{36}{I_{\lambda}} \right\} \left. \right] \\
&+ \left[\omega_2 \chi \sum_{\lambda=1}^N \left(\frac{(SOC_{\lambda} - SOC_{\lambda-1}) * 36}{I_{\lambda}} \right) \right]
\end{aligned} \tag{4-10}$$

Where ω_1 is the weighting factor of the total energy loss and it could be adjusted from 0 to 1 and ω_2 is the weighting factor of the total required charging interval time where $\omega_2 = 1 - \omega_1$.

4.2.3 Limitations of Fast Charging Algorithms

4.2.3.1 Cut Off Voltage of Each Stage ($V_{c-o_{\lambda}}$);

Every battery has a charging cut-off voltage which should not be exceeded to guarantee the battery from damage and overcharging. The proposed polymer lithium-ion battery should not exceed the maximum permitted voltage for each stage which can be expressed by $V_{c-o_{\lambda}} \leq 4.25V$

4.2.3.2 The Maximum Permitted Charging Current of Each Stage ($I_{\xi_{\lambda}}$)

The charging current should not exceed a security threshold value. The security threshold value can be presented as a relationship between the charging constant current (0.05C A – 1C A) and the charging interval time [292]. To avoid overcharging and damage to the battery, the maximum permitted charging current can be described as:

Chapter 4

$$I_{\xi_\lambda} = \begin{cases} 1 & T_\lambda \leq 2,480 \text{ sec} \\ \frac{-T_\lambda}{6000} + 1.413 & T_\lambda > 2,480 \text{ sec} \end{cases} \quad 4-11$$

where I_{ξ_λ} is the maximum permitted charging current for each stage and T_λ is the charging interval time of stage λ .

4.2.4 Fast Charging Implementation Algorithms

A lithium-ion polymer battery with a nominal capacity of 1000 mAh has been selected as a test case. The detailed specification of this battery is presented in Table 3-1.

Multi-stage fast charging methodologies have been implemented on the lithium-ion polymer battery to reach full capacity ($SOC_\lambda = 100\%$) as illustrated in Figure 4-5-a, which can be categorized into two main scenarios: the first scenario is the standard CC-CV method and the second scenario is the Multi-Stage Charging Current method (MSCC) based on Cuckoo Optimization Algorithm (COA). COA has been implemented on the proposed RC second-order transient equivalent circuit to determine the optimum charging interval time and the optimum energy loss during charging. COA is simulated using MATLAB (R2017a, The MathWorks Ltd, Natick, MA, USA). The MATLAB source code has been stated in detail in Appendix A. Furthermore, the steps performed to implement the proposed multi-stage charging current methodologies are presented in Figure 4-5-b.

Chapter 4

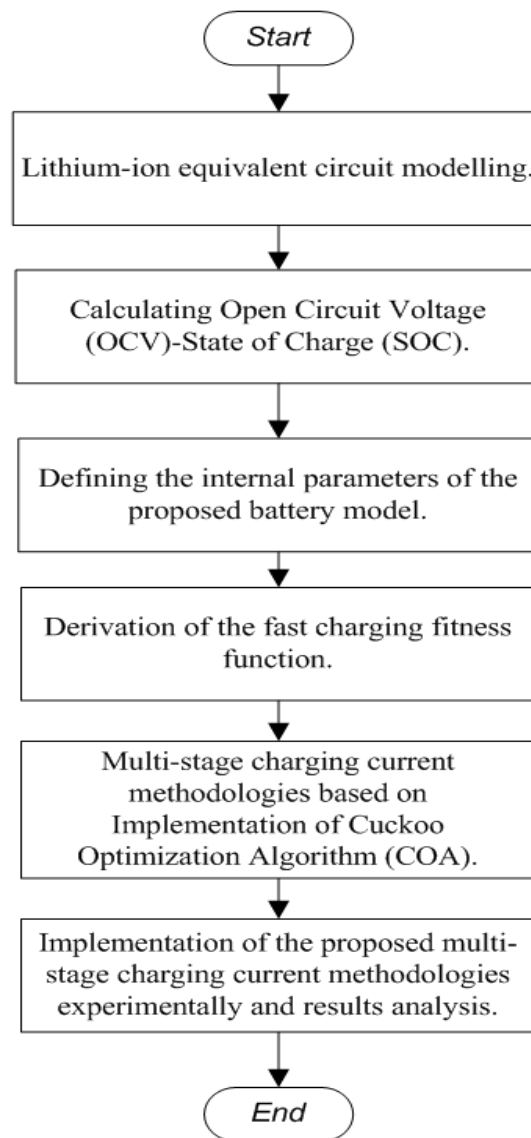
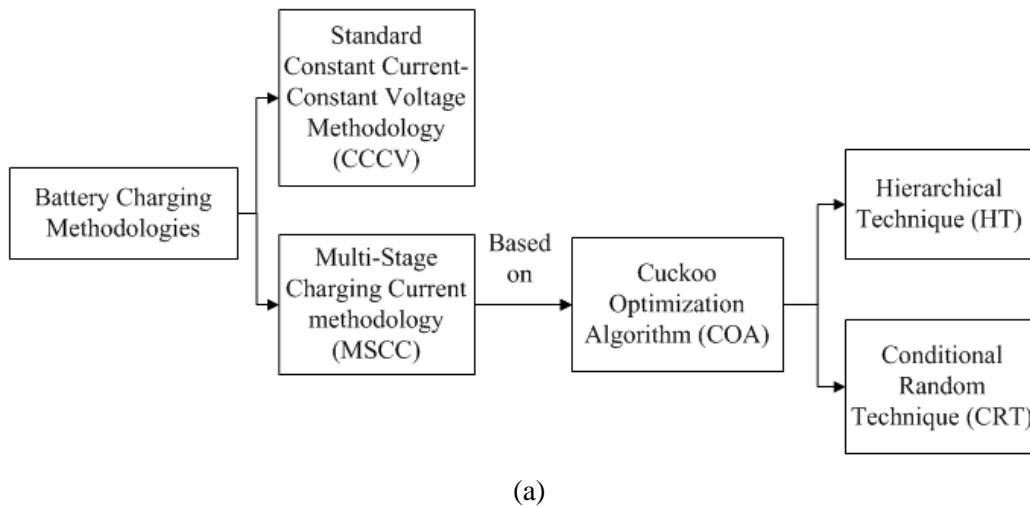


Figure 4-5 (a) The proposed scenarios of charging the lithium-polymer battery, and (b) The procedures performed to implement the proposed multi-stage charging current methodologies.

Chapter 4

4.2.4.1 Cuckoo Optimization Algorithm (COA)

COA is superior to various optimization algorithms (genetic algorithm, particle swarm, ant colony, ...etc) for multimodal objective functions due to its robustness to dynamic changes and broad applicability [293-295]. COA is inspired by the behaviour life of a species of bird called the Cuckoo. This technique is mainly the form of grown cuckoos and eggs. Grown cuckoos put their eggs in the nests of various birds as they have two probabilities: 1) the first is that the host bird kills the eggs, and 2) the second is that the eggs are not killed and recognized by the host bird and grow up and become a grown cuckoo [295, 296]. The cuckoo optimization algorithm is tending to find the best habitat for all cuckoos where there is a high opportunity for eggs to grow up. The best suitable habitat will be the target for cuckoos in other societies [295, 297]. The procedures of using the proposed COA are explained by the flowchart in Figure 4-6 illustrating each step including the initial population (Cuckoo's Habitat), Laying Eggs Style, Immigration of Cuckoo, Eliminating Cuckoos, and the convergence criteria.

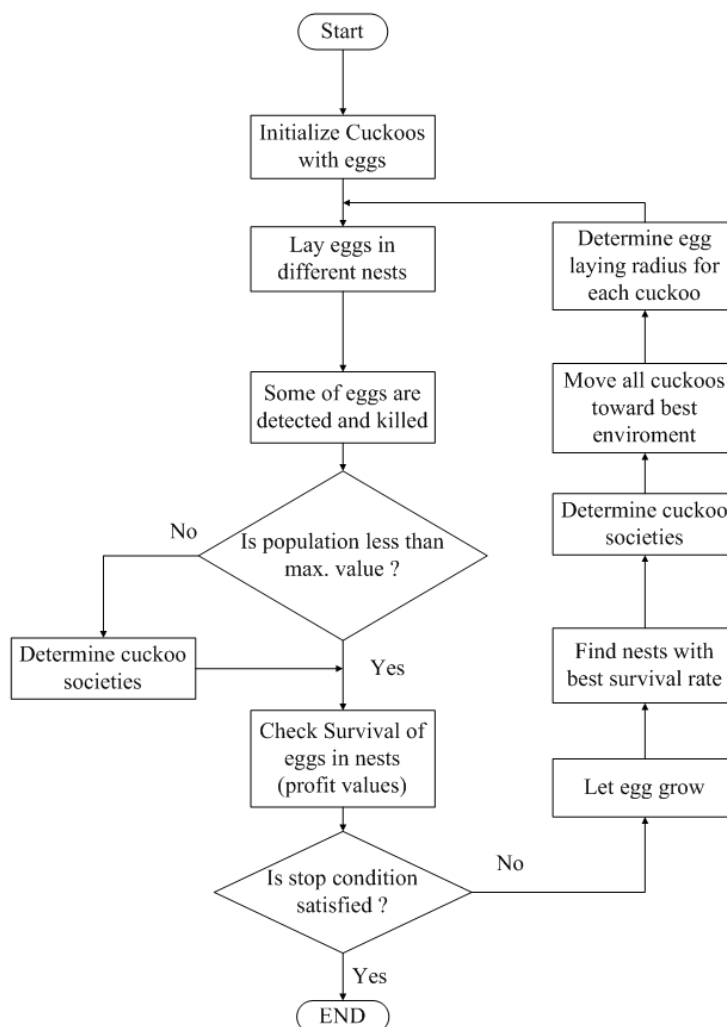


Figure 4-6 The flowchart of the Cuckoo Optimization Algorithm (COA).

Chapter 4

4.2.4.2 Constant Current-Constant Voltage (CC-CV) Protocol

The CC-CV charging protocol is the standard technique for any battery charging. It is performed on the polymer lithium-ion battery by applying a constant current of 1 A until the voltage reaches the cut-off value (4.25V) and then the voltage is held constant while the current decays to the minimum value of 0.05A. This method took 7,100 sec till the battery reached its full capacity (0 to 100% SOC) of 4.1785V after a relaxation time of 10,800s as shown in Figure 4-7-a.

4.2.4.3 Multi-stage Charging Current Based Cuckoo Optimization Algorithm (COA)

Multi-stage charging current methodologies have been applied to the lithium-ion polymer battery, and it is divided into two main scenarios based on the conditional boundaries of the currents as follows:

4.2.4.3.1 Hierarchical Technique (HT)

The first scenario is called Hierarchical Technique (HT) and it has been obtained by applying a hierarchical stepping-down variable constant currents during the charging process $I_\lambda \leq I_{\lambda-1}$ and presented in Figure 4-7-b.

Based on the Hierarchical Technique (HT), the battery reached full capacity (0 to 100% SOC) in 5,815 sec and based on the dynamic behaviour and relaxation theory of batteries, the capacity of the battery reached 97% (4.107 V) after a relaxation time 10,800 sec.

By applying HT based on COA, the total energy consumed during the charging process was reduced by 7.783%, the total charging interval time was reduced by 18.1% and the efficiency improved by 8% based on Equations 4-12, 4-13, and 4-14, respectively compared to CC-CV protocol test [298].

$$E_{Saved} = \frac{E.L_{CCCV} - E.L_{Proposed}}{E.L_{CCCV}} \times 100 \quad 4-12$$

$$T_{reduced} = \frac{T_{CCCV} - T_{Proposed}}{T_{CCCV}} \times 100 \quad 4-13$$

$$\eta_{charging} = \left(\frac{C_{disproposed}}{C_{chproposed}} - \frac{C_{disCCCV}}{C_{chCCCV}} \right) * 100 \quad 4-14$$

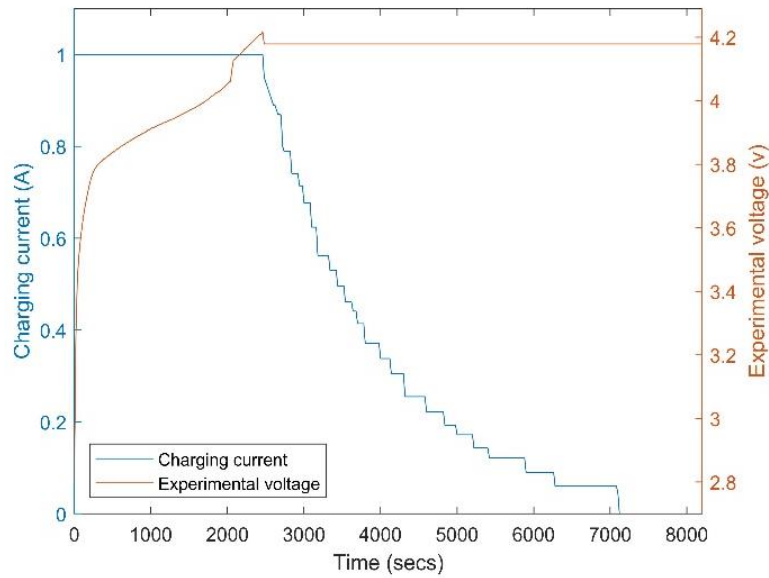
Where E_{Saved} is the energy saved, $T_{reduced}$ is the reduced charging interval time, $C_{disproposed}$ is the discharging capacity of the proposed technique, $C_{chproposed}$ is the charging capacity of the proposed technique and $\eta_{charging}$ is the improved efficiency of the proposed technique.

4.2.4.3.2 Conditional Random Technique (CRT)

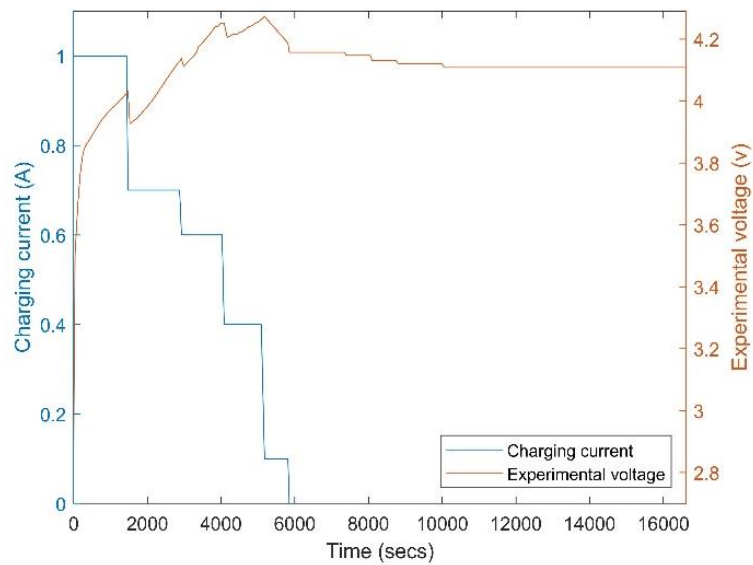
The second scenario was based on the conditional randomness of the cuckoo optimization algorithm which chooses the values of the stage current lying within the boundaries declared previously and presented in Figure 4-7-c. The battery reached its full capacity (0 to 100% SOC)

Chapter 4

in 5,506 sec, but based on the dynamic behaviour and relaxation theory of batteries, the capacity of the battery reached 97% after a relaxation time of 10,800 sec. The energy consumption saved by the Conditional Random Technique (CRT) is 10.408%, the time was reduced by 22.45%, and the efficiency improved by 14.1%.

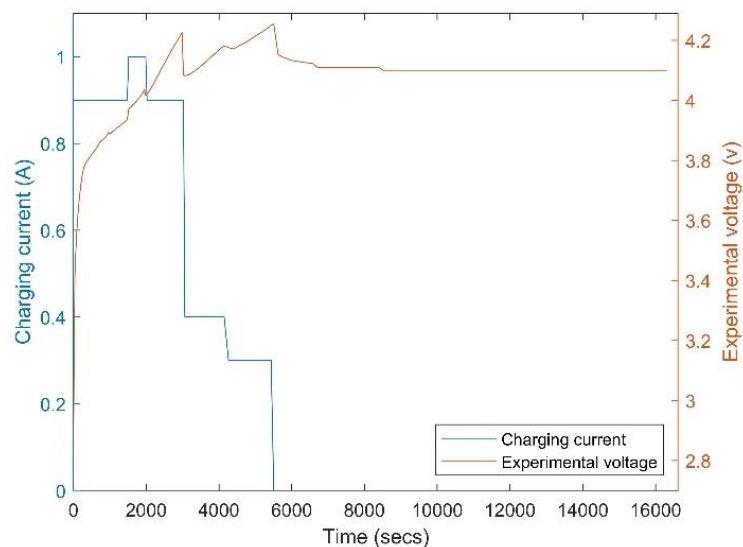


(a)



(b)

Chapter 4



(c)

Figure 4-7 Relationship between different charging methodologies for polymer lithium-ion battery at room temperature 25°C (a) The standard CC-CV protocol, (b) Multi-stage charging current method based on HT and (c) Multi-stage charging current method based on CRT.

The proposed previous two techniques improved the efficiency of the fast charging of the lithium-ion polymer battery with minimum energy loss and less interval time with respect to the previous data presented in the literature. The maximum error between the experimental and simulated voltage results of the two scenarios (HT and CRT) is presented in Figure 4-8. The maximum error of the proposed RC second-order equivalent circuit model reached 2.3%. The maximum error between the experimental and simulated charging voltages has been calculated by:

$$\varepsilon (\%) = \frac{\eta_{Experiment} - \eta_{Simulation}}{\eta_{Experiment}} * 100 \quad 4-15$$

where ε is the percentage of error and $\eta_{Experiment} - \eta_{Simulation}$ is the difference between the maximum experimental and simulated voltage points, respectively.

Chapter 4

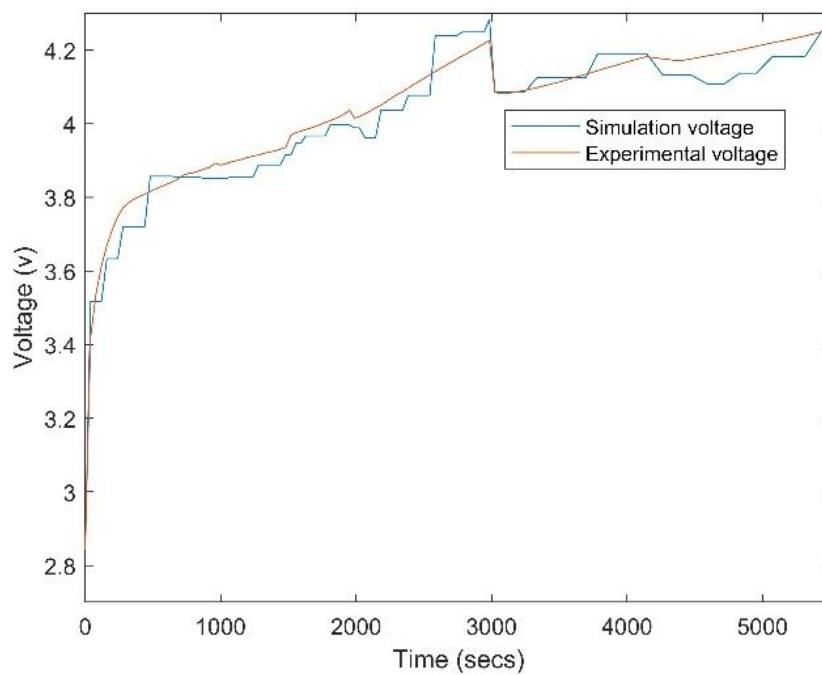
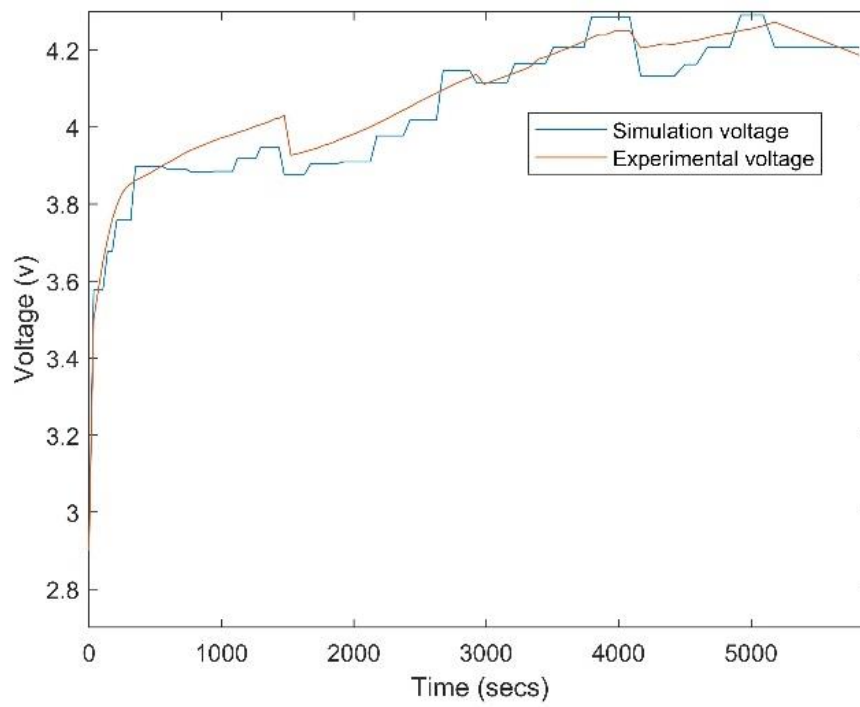


Figure 4-8 The maximum error declaration between experimental and simulated voltage results for both HT and CRT at room temperature 25°C, respectively.

Detailed results obtained from the previous techniques include charging stage current, charging interval time for each stage, total charging time for all the process, and total energy loss presented in Table 4-1. As shown, the proposed techniques based on COA and the simulation based on the RC second-order transient circuit have a good impact on the time required for charging and the energy consumed during the charging.

Chapter 4

Table 4-1 A detailed comparison between the CC-CV method and the proposed scenarios based on COA at room temperature 25°C.

	Standard CC-CV method	Cuckoo Optimization Algorithm (COA)	
		Hierarchical Technique (HT)	Conditional Random Technique (CRT)
I_1 (A)		1	0.9
I_2 (A)		0.7	1
I_3 (A)	1	0.6	0.9
I_4 (A)		0.4	0.4
I_5 (A)		0.1	0.3
T_1 (s)		1,474	1,493
T_2 (s)		1,451	484
T_3 (s)	7,100	1,157	1,018
T_4 (s)		1,096	1,264
T_5 (s)		637	1,247
Total charging Time (s)	7,100	5,815	5,506
Energy Loss (J)	1,127.667	1,039.9	1,010.3

4.2.5 Analysis of the Weighting Factors

In furtherance of the foregoing, each weight of the energy loss and charging interval time changed in Equation 4-10 to vary from 0 to 1 where $\omega_1 + \omega_2 = 1$. Any change in energy loss weight ω_1 or the charging interval time weight ω_2 will result in a different combination of five constant currents with different charging interval times based on COA as shown in Table 4-2.

Chapter 4

Table 4-2 The results of changing the weights of energy loss and charging interval time.

ω_1	0	0.1	0.2	0.3	0.4	0.5	0.6	0.7	0.8	0.9	1
ω_2	1	0.9	0.8	0.7	0.6	0.5	0.4	0.3	0.2	0.1	0
$I_1(A)$	0.9	1	1	1	0.8	0.9	0.4	1	1	0.8	1
$I_2(A)$	1	0.7	0.7	0.8	1	1	0.9	0.9	0.7	1	0.8
$I_3(A)$	0.9	0.5	1	0.9	0.7	0.9	1	0.7	0.8	0.9	0.8
$I_4(A)$	0.6	1	0.7	0.6	0.4	0.4	0.8	0.6	0.7	0.6	0.3
$I_5(A)$	0.3	0.3	0.6	0.4	0.4	0.3	0.5	0.6	0.6	0.4	0.2
$T_1(s)$	602	1,500	420	1,255	915	1,493	333	1,479	574	1,500	1,500
$T_2(s)$	1,445	1,468	1,145	1,076	1,435	484	874	474	1,392	590	1,438
$T_3(s)$	491	1,470	882	300	1,234	1,018	881	893	348	492	410
$T_4(s)$	1,219	893	1,500	1,254	704	1,264	1,356	1,299	1,421	1,217	1,474
$T_5(s)$	1,443	440	803	1,231	619	1,247	1,404	490	1,378	1,486	1,500
Time (s)	5,200	5,771	4,750	5,116	4,907	5,506	4,848	4,635	5,113	5,285	6,322
Energy Loss (J)	1,032.	994.50	1,066.1	1,023.7	964.904	1,010.3	984.381	1,053	995.922	921.47	1,073.1

Based on the relationship between the current of each stage, the interval time of each stage and the conditional constraints/boundaries, any change in the weight of energy loss or in the charging interval time will not affect the charging capacity based on COA.

COA rearranges the data and searches for the optimum solution to minimize energy loss and charging interval time based on the objective function regardless of the weighting factor as explained in Table 4-2.

4.3 Off-Board Charging Implementation using the Neural Network Predictive Controller (NNPC)

This section is presenting the implementation of the mentioned CC-CV and MSCC fast-charging protocols theoretically and the results are compared experimentally to prove the efficiency of the proposed controller.

4.3.1 Parasitic Buck Converter Model

The backbone of EV charging process systems and electric vehicle charging stations is the DC-DC converters. In this thesis, the basic parasitic DC-DC buck converter is utilized to step down the output voltage of the RESs represented in the PV system as shown in Figure 4-9. The modelling of the lithium-ion battery used is the RC second-order transient equivalent circuit

Chapter 4

model. This model represents the transient behaviour of the lithium-ion polymer battery as shown in Figure 4-9-a. This model has proved to be the closest circuit model that can be used to explain the performance and behaviour of lithium-ion batteries [268]. The values of the internal parameters corresponding to the battery state of charge (SOC) during an interval discharging pulse of 20s at room temperature of 25°C and relative humidity of 82% are presented and illustrated in Figure 4-4.

To describe the dynamic performance of the converter, The second-order differential equation of the parasitic DC-DC converter in terms of the duty cycle has been introduced by the average model mentioned in [147] and expressed in the following equations and the graphical model in Figure 4-9-b.

$$V_A = R_L i_L + L \frac{di_L}{dt} + V_m \quad 4-16$$

$$C \cdot \frac{dV_C}{dt} = i_L - \frac{V_m}{R_m} \quad 4-17$$

$$V_m = R_C \left(i_L - \frac{V_m}{R_m} \right) + V_C \quad 4-18$$

$$\frac{V_m(s)}{V_{RES}(s)} = \frac{V_m(s)}{D \cdot V_{RES}} = \frac{1}{s^2 LC + s \left(R_L C + \frac{L}{R_m} \right) + \left(\frac{R_L}{R_m} + 1 \right)} \quad 4-19$$

Where, V_A is the average voltage on the diode, R_L and R_C are the inductor and capacitor internal resistances, respectively, V_m is the measured voltage on the resistance R_m , and V_{RES} is the renewable energy sources voltage.

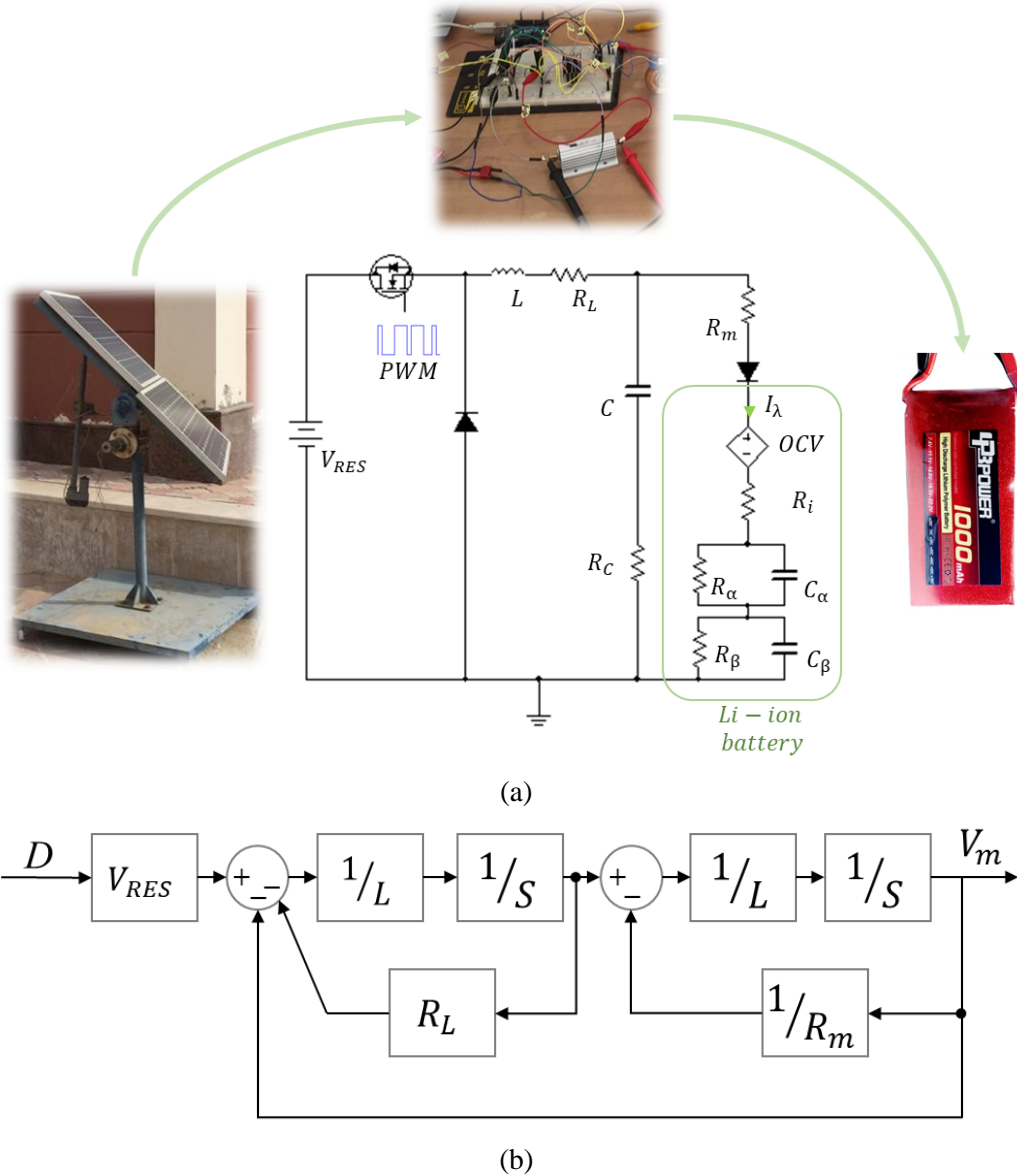


Figure 4-9 (a) The proposed construction of the charging control system, and (b) Graphical s-plane model of the DC-DC buck converter.

4.3.2 Charging Controllers Under Study

This section is proposing an advanced dynamic charge controller for the lithium-ion battery throughout implementing the constant current-constant voltage (CC-CV) and multi-stage charging current (MSCC) protocols. The charging currents of the MSCC protocol have been predetermined from the COA mentioned above. The controllers that have been utilized in this section can be split into the proportional, integral, and derivative (PID) controller, fuzzy logic controller (FLC), and the artificial neural network predictive controller supported by the long-short-term memory model (NNPC-LSTM). Due to the intermittency of the renewable energy sources (RES), the LSTM model is used as the input trained forecasted data to the NNPC controller as shown in Figure 4-10.

Chapter 4

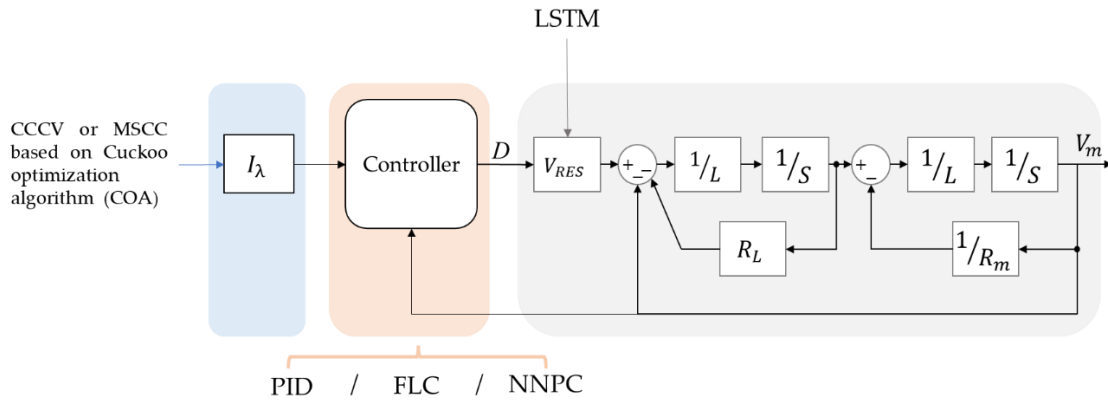


Figure 4-10 A schematic diagram of the proposed charging process using different controllers.

4.3.2.1 PID controller

PID controller is one of the conventional design controller techniques used for Dc-Dc converters [188, 299]. The proposed system has been investigated in discrete time with a sampling period of 1 ms. The process of selecting the controller parameters to ensure good performance is obtained by the automated tuning of the PID controller in MATLAB/Simulink. Where the proportional parameter (P) is 0.007667, the Integral parameter (I) is 3.667, and the derivative parameter (D) is -4.9×10^{-5} . The proposed charging process by the PID controller is expressed as a graphical model in Figure 4-11-a.

4.3.2.2 Fuzzy Logic Controller

The concept of FLC is proposed from the fuzzy set theory stated in [300]. FLC is a non-linear technique used in highly complex and non-linear systems as it is not requiring any mathematical model to control the system. It depends on the operator's experience to ensure sufficient rules to design the fuzzy controller [301]. FLC has been used widely to control the dc-dc converters as stated in [302-304]. FLC consists of three main stages fuzzification, rule base, and defuzzification as in Figure 4-11-b. The base rule of the dc-dc buck converter has been proposed in [304, 305]. The rule table of the proposed buck converter is shown in Table 4-3 where NB, NS, ZE, PS, and PB mean negative big, negative small, zero, positive small, and positive big, respectively.

Table 4-3 The rule table of the fuzzy logic controller (FLC).

Error (E) / Change in Error (CE)	NB	NS	ZE	PS	PB
NB	PB	PB	PS	PS	PS
NS	PB	PS	PS	PS	ZE
ZE	PS	PS	ZE	NS	NS
PS	ZE	NS	NS	NS	NB
PB	NS	NS	NS	NB	NB

Chapter 4

4.3.2.3 Neural Network Predictive Controller (NNPC)

On the other hand, NNPC is optimizing the plant performance over a specific time horizon by calculating the control input. The first stage is determining the forward dynamic behaviour of the plant model and it can be called system identification. The plant model identification represented in Figure 4-21-c is used by the controller to predict the future performance of the system. The training signal is predicted through the error between the plant output and the NN output. The NN plant uses the previous inputs and outputs to predict the future output values of the plant through backpropagation training as declared in Figure 4-11-c.

The controller output charging currents have been prevented to exceed the maximum constraints, as the input duty cycle was limited to the range from 0 to 1. In addition, the charging current is prevented to go beyond the 1A where the network has been trained offline in batch mode using the data collected from the proposed plant. The NNPC is developed based on the complete state-space represented model as mentioned in Equation 4-20.

$$\frac{d}{dt} \begin{bmatrix} i_L \\ V_m \end{bmatrix} = \begin{bmatrix} \frac{-R_L}{L} & \frac{-1}{L} \\ \frac{(L - CR_L R_C)R}{(R_m + R_C)CL} & -\frac{(L + CR_m R_C)}{(R_m + R_C)CL} \end{bmatrix} \begin{bmatrix} i_L \\ V_m \end{bmatrix} + \begin{bmatrix} \frac{1}{L} \\ \frac{R_m R_C}{(R_m + R_C)L} \end{bmatrix} V_{RES} \quad 4-20$$

Chapter 4

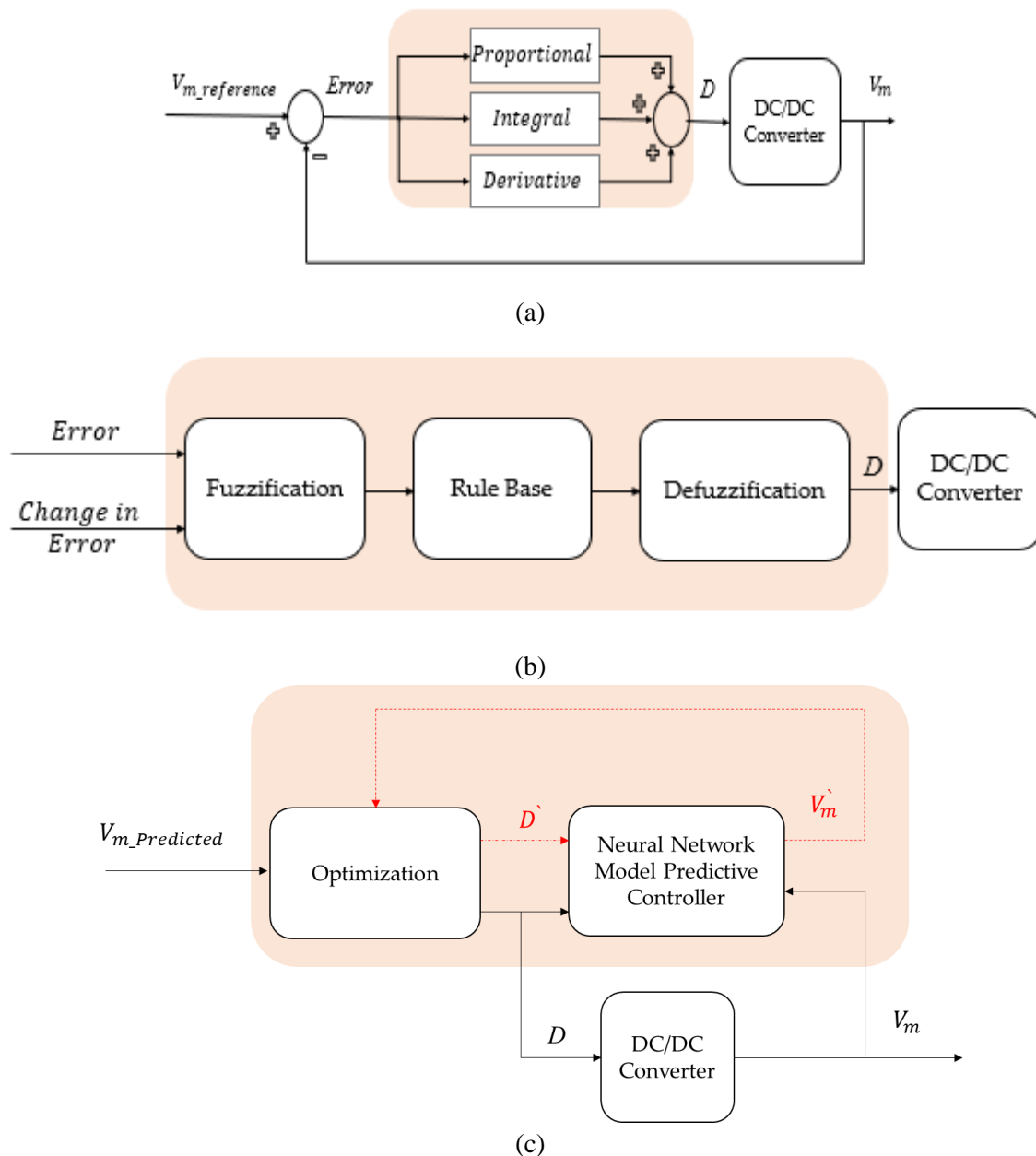


Figure 4-11 Graphical illustrative schematic of the PID, FLC, and NNPC controllers, respectively.

The NNPC is supported by the long-short-term memory model (LSTM) to forecast the PV panel output voltage offline and independent of the instantaneous climate change of the PV panel where all the data has been predicted and fed to the system to train the model.

4.3.2.4 Long-Short-Term Memory (LSTM) Model

Recently, researchers are forecasting PV power through several approaches categorized into statistical methods, physical methods, and artificial intelligent learning methods (AILMs) [306]. Statistical methods are dependent on historical data and exclude points that are not conducive to these models. Physical methods investigate the characteristics of PV power generation without a large amount of historical data. AILMs have utilized the mapping between input and output data and are used in power grids, energy consumption, pattern recognition, and power prediction [306]. To determine the power generated from the PV, solar radiation is

Chapter 4

estimated based on mathematical models supported by an artificial neural network (ANN). ANN is found to be more accurate compared to the regression model, empirical regression model, empirical coefficient model, angstrom model, and fuzzy logic [307-309]. AI methods especially neural networks (NNs) are used excessively to manage the power market operation based on precise load forecasting [310-312]. NNs are widely applied in forecasting, because of the dependency on multilayer perceptron, previous data, and the nonlinearity of the model [312]. Long-short-term memory (LSTM) is considered a variation of recurrent neural networks (RNN) and was originally developed by Hochreiter *et al.* [313]. LSTM has been applied in PV power prediction accurately by modelling the temporal changes in the PV data and forecasting the next step data [306]. However, the intermittency and randomness of solar power cause instability operation and control performance of the power grid. In addition, LSTM is typically implemented to capture the temporal patterns in monthly data and can estimate the power generation for any new site, in which weather information and terrain data are available as in South Korea [314]. In [315], the LSTM was combined with wavelet transform (WT) to decompose the solar energy time-series data into different frequency series for forecasting short-time output PV power.

LSTM is considered a state-of-the-art model of the recurrent neural system because of its impact on both the practical and theoretical fields. The LSTM architecture consists of a set of recurrently connected sub-networks, known as memory blocks. Figure 4-12 introduces the architecture which consists of the gates, the input signal, the output, the activation functions, and peephole connections [316]. The core equations of the LSTM are expressed in Equations 4-21 to 4-26 [317] and also are represented in Figure 4-12.

$$f_t = \sigma(W_f * [h_{t-1}, X_t] + b_f) \quad 4-21$$

$$i_t = \sigma(W_i * [h_{t-1}, X_t] + b_i) \quad 4-22$$

$$g_t = \tanh(W_g * [h_{t-1}, X_t] + b_g) \quad 4-23$$

$$c_t = f_t * c_{t-1} + i_t * g_t \quad 4-24$$

$$o_t = \sigma(W_o * [h_{t-1}, X_t] + b_o) \quad 4-25$$

$$h_t = o_t * \tanh(c_t) \quad 4-26$$

Where f_t , i_t , g_t , and o_t are the output value of the forget gate, input gate, update gate, and output gate, respectively, $W_{f,i,g,o}$ is the weight matrices, $b_{f,i,g,o}$ is the bias vectors, c_t is the memory cell, σ is the sigmoid activation function, h_{t-1} is the LSTM output value at time step $t - 1$, and X_t is the input data.

Chapter 4

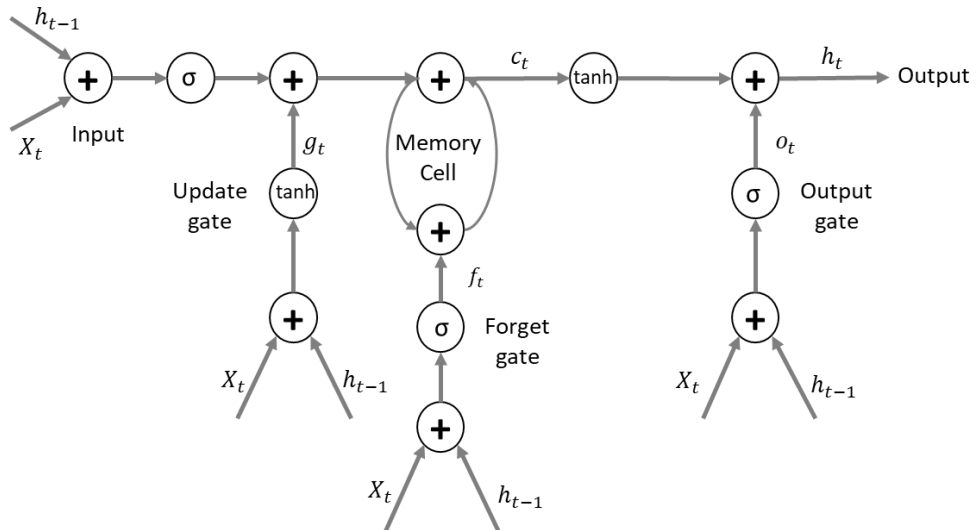


Figure 4-12 The LSTM-specific dissemination as illustrated in [317].

Due to the intermittency of the RESs, especially PV systems, that causes difficulties and reduction in the real-time control performance, LSTM is implemented to predict the PV output power, voltage, and current accurately and fed to the NNPC with sufficient data to be used in training the model offline with the minimum error.

4.3.3 Simulated Results and Experimental Analysis

The parameters of the DC-DC buck converter that has been used in the simulated and experimental investigation are $R_m = 10\Omega$, $L = 2.1\text{ mH}$, $R_L = 0.0071\Omega$, $C = 470\mu\text{F}$, $R_C = 0.117\Omega$, switching frequency of 31kHz, lithium-ion battery of 1000m.Ah with a nominal voltage of 3.7v and the nominal input voltage from RES is $V_{RES} = 25\text{V}$. The PV solar panel with rated maximum power 100W, rated voltage 18V and rated current of 5.56A.

To validate the proposed NNPC based on the LSTM method with respect to the PID, and FL controllers, the Arduino UNO microcontroller board is integrated with MATLAB/Simulink. The experimental setup implemented is expressed in Figure 4-13.

Chapter 4

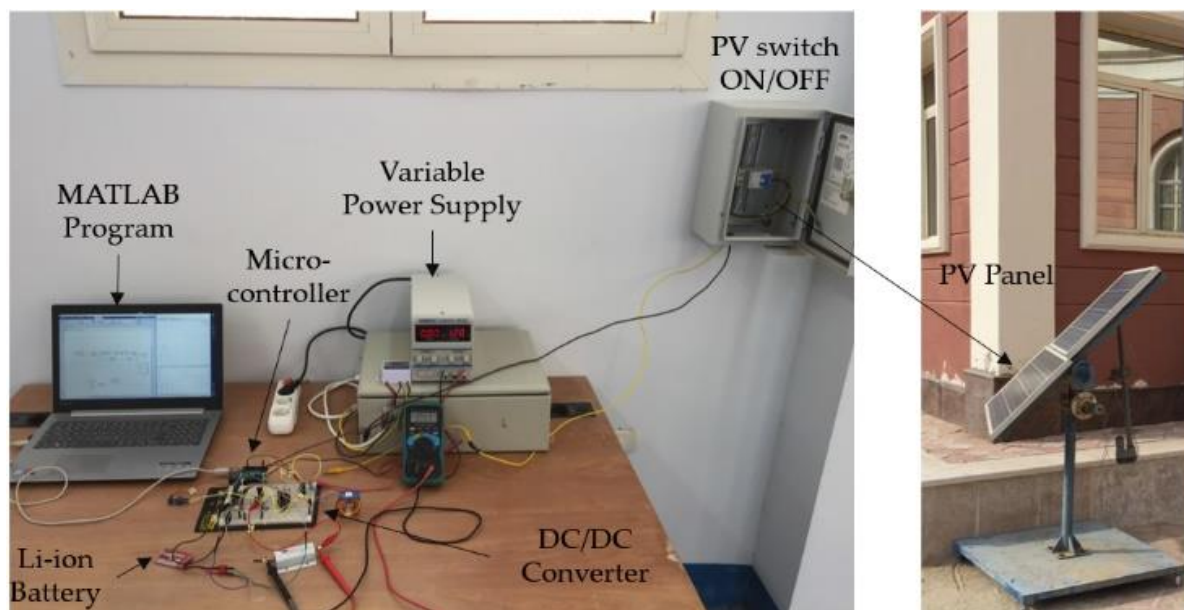


Figure 4-13 The experimental setup used in the charging process.

4.3.3.1 Simulated Results

The sampling time of each controller was set to be $T_s = 1 \text{ ms}$ and the reference voltage could be changed every 0.05sec. The results have been scrutinized theoretically through the MATLAB/Simulink simulator program where each training procedure took about 40 mins to be simulated on a laptop Intel(R) Core (TM) i7-8550U CPU 1.80GHz with 8GB RAM.

The output from MATLAB/Simulink program simulator is presented in Figure 4-14, where various scenarios have been implemented in the dynamic charging process. Figure 4-14-a presents the first scenario as the input voltage is maintained constant of 25V across the process and the multistage charging currents which are represented by V_m/R_m have been pronounced with a very low variation starting from 7.7V, 5.6V, and 8V. It is shown that NNPC-LSTM has a very high-speed response, enhanced settling time, and very low steady-state error with respect to the PID and FL controllers.

In Figure 4-14-b, the output charging current represented in V_m/R_m is maintained constant despite the variation in the input voltage of RES from 25V to 12V. It is observed that the NNPC-LSTM ensures the tracking of any change in the input voltage with the fastest response concerning the PID, and FL controllers.

Chapter 4

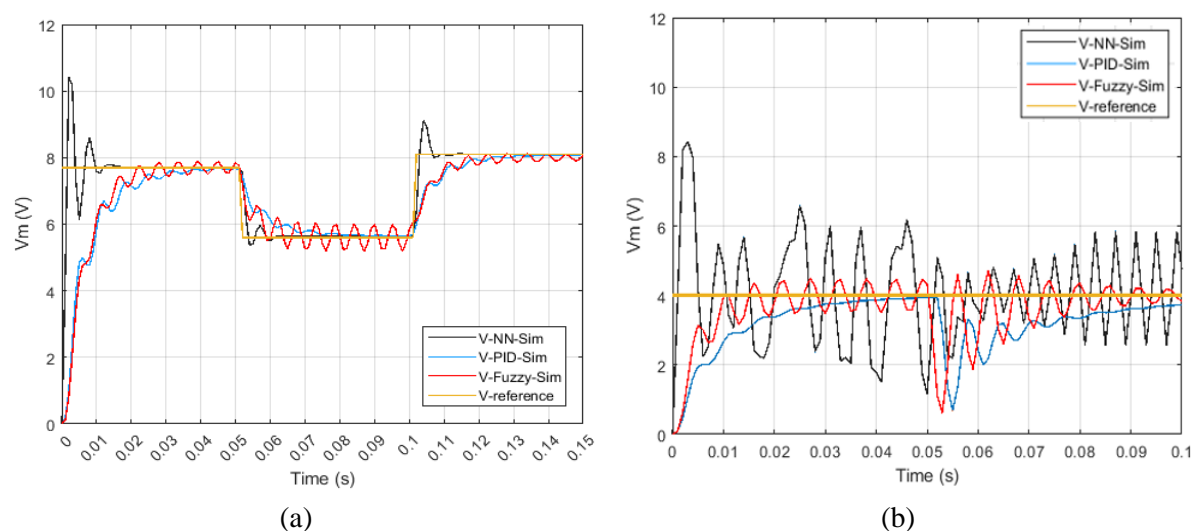


Figure 4-14 Simulated results for NNPC-LSTM and PID controllers where (a) reference voltage changes 7.7V, 5.6V, and 8V; (b) the input voltage changes from 25V to 12V.

4.3.3.2 Experimental Validation

Before the validation of the proposed experimental setup and implementation of the NNPC supported by the LSTM in the training stage of the system, we have to investigate the climate and its impact on the PV output power and the importance of the LSTM in predicting the output power of the PV system.

4.3.3.3 PV Output Power Based on the Solar Climate and Module Characteristics

The daily average amount of the total solar radiation incident to the horizontal surface at the surface in El-Sherouk City, Cairo, Egypt (latitude:30.1181 and Longitude:31.6089) during the year 2020 is implemented as shown in Figure 4-15-a. There is a significant variation in the insolation incident on the horizon surface during the year. To be more specific, a set of readings has been implemented on a mono-crystalline solar module at the British University in Egypt (BUE) with a rated maximum power of 100W, rated voltage of 18V, and rated current 5.56A and recorded by a PV system analyzer for 100 minutes on 17 December 2020 starting from at 12:20:00 pm GMT, time zone. As shown in Figures 4-15-b and 4-15-c, the output power of the PV panel varies from one minute to another that reflecting the output current and voltage.

The LSTM model in this research is responsible for two essential stages. The first stage is predicting the output power, voltage, and current of the PV panel to feed into the neural network predictive controller to train the model for accurate and robust dynamic performance. The second stage is giving the precision characteristics boundaries of the charging process. For example, in Figure 4-15-c the current reached 0.8A at the minute counter 20, this limit should be a limitation of the charging process, or if the required charging current is higher than 0.8A, the controller should complement the process by an alternative resource at this predetermined time.

The LSTM model is used to predict the PV output power throughout a training dataset of 34% of the data and tested with 66% as shown in Figure 4-15-d. The training dataset is considered as 1/3 of the overall data which reveals the effectiveness of the proposed network in predicting

Chapter 4

the PV output power however limited data is used in the training process. The root mean square error (RMSE) is used as a precision indicator of the PV output power estimation which reached in this research 5.0495 which is a good acceptable range according to the literature survey [306, 318].

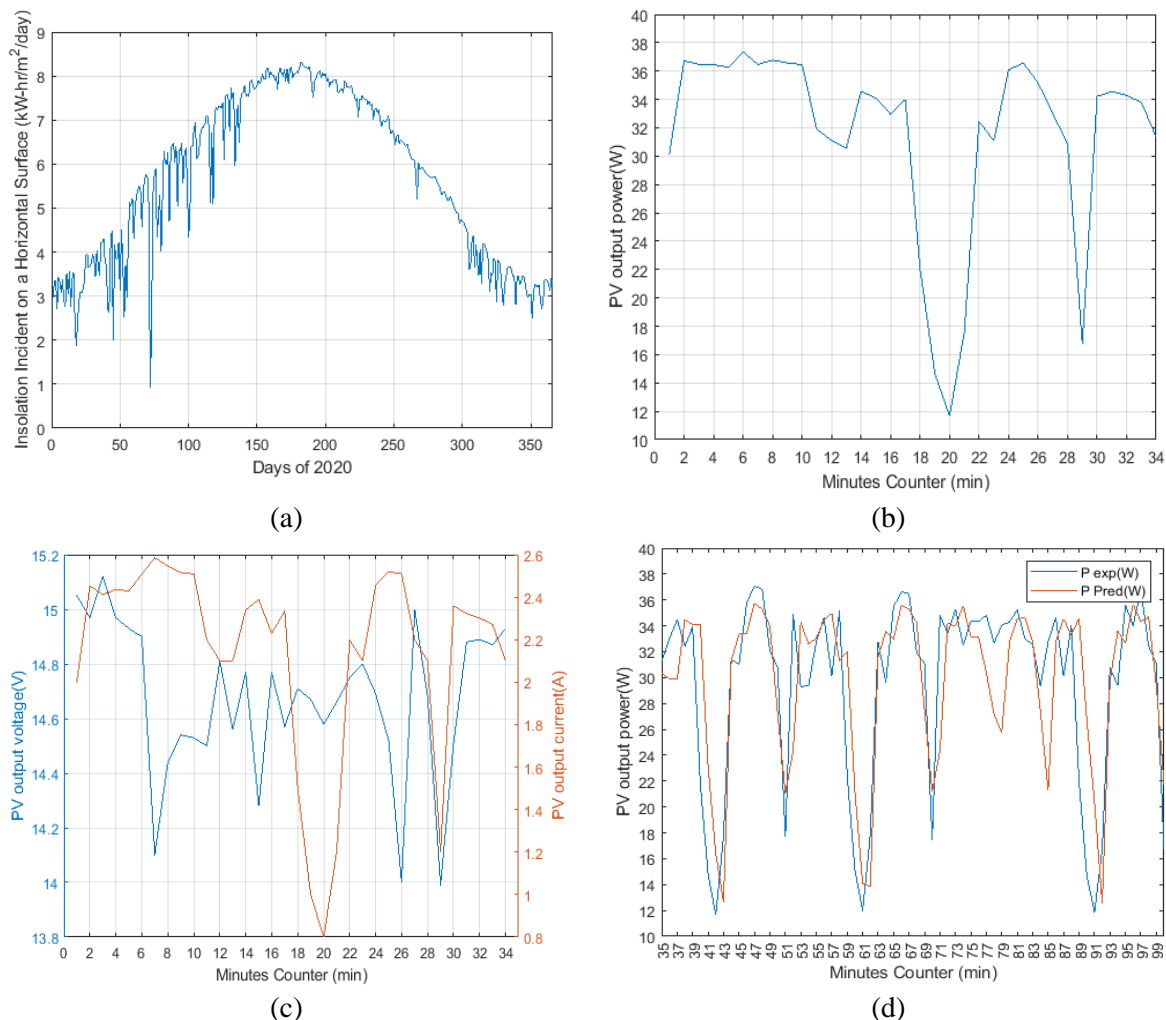


Figure 4-15 (a) The daily average amount of the total solar radiation incident the horizontal surface at the surface at El-Sherouk City, Cairo, Egypt; (b) the PV output power readings for 34 minutes; (c) the relation between the PV output voltage and current of the solar panel under study; and (d) Predicted and measured PV output voltage from the LSTM method.

4.3.3.4 Experimental analysis

In this subsection, a full experimental comparative study is investigated and proposed. Figure 4-16-a reveals the performance of the charging process for various output charging currents represented by the relation V_m/R_m . The NNPC-LSTM ensured a quiet speed response reached 1 m.sec concerning the PID controller which takes 0.03s and the FLC controller which takes 0.02s to reach the desired charging required current during a constant input voltage of 25V. Figure 4-16-b presents the effectiveness of the NNPC-LSTM to maintain the stability of the charging process with a minimum steady-state error concerning the PID controller and FLC during the change in the input voltage from 25V to 12V. Finally, Figure 4-16-c exposes the robustness and effectiveness of the proposed NNPC integrated based on the LSTM method

Chapter 4

which is used as training data for the NNPC and as a precise indicator of the boundaries of the charging process of the lithium-ion battery for different charging currents of 0.8A and 0.5A. In addition, during the charging process for any stage of charging, it is observed that the change in the OCV of the battery reached 1mV voltage ripple and 1 ms settling time as shown in Figure 4-16-c.

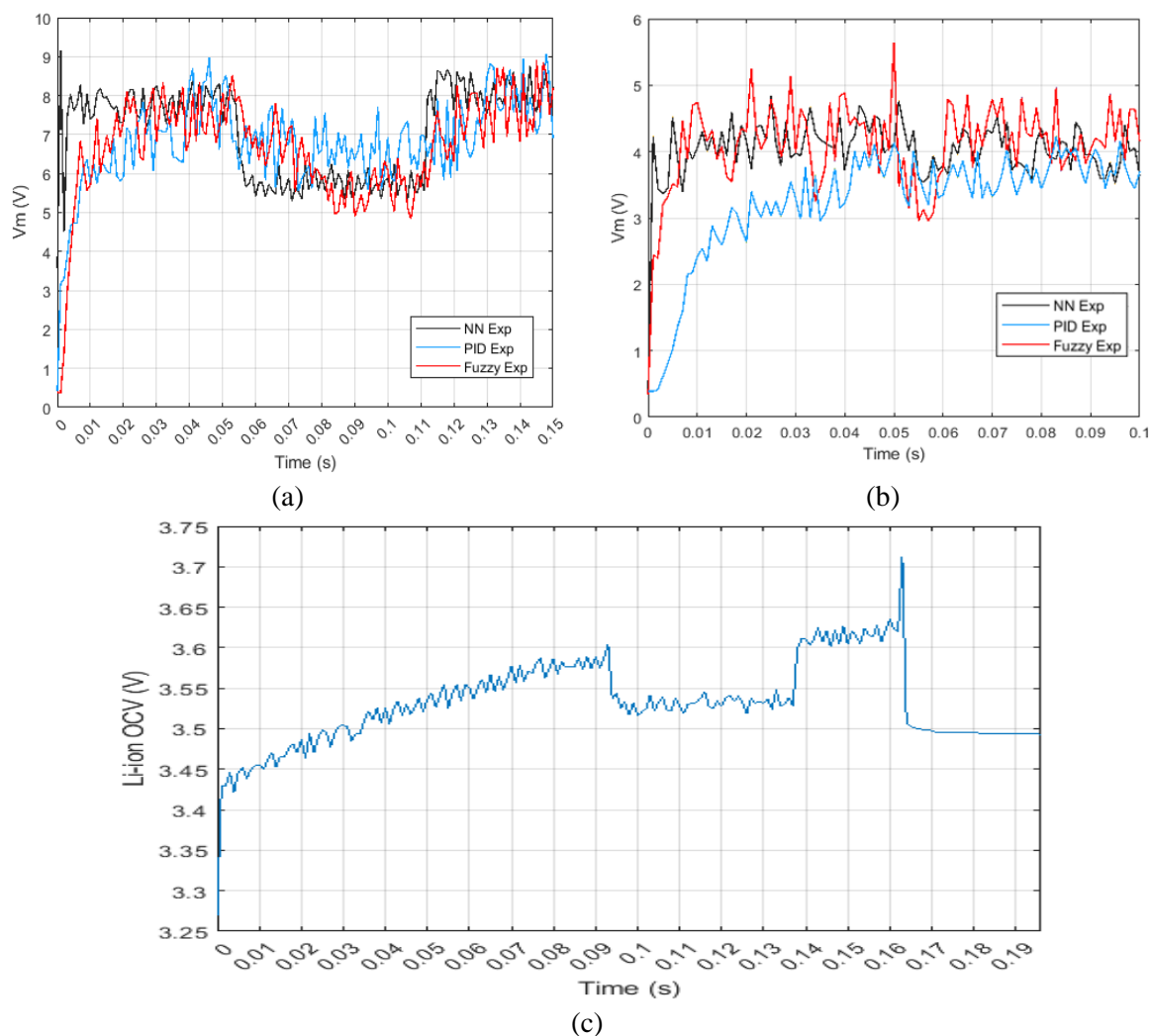


Figure 4-16 (a) Experimental results of the NNPC-LSTM, FL, and PID controllers with the reference voltage changes 7.7V, 5.6V, and 8V; (b) Experimental results for NNPC-LSTM, FL, and PID controllers with an input voltage change from 25V to 12V, and (c) The Dynamic behaviour of the lithium-ion battery during the charging process.

4.4 Chapter Summary

This chapter proposed new intelligent techniques based on the multi-stage charging current (MSCC) charging protocol. The proposed techniques are compared with the conventional CC-CV charging protocol and used to speed up the charging process whilst reducing energy consumption without degradation in light of the outrageous demand for lithium-polymer ion batteries in EVs. Two fitness functions are combined as the targeted objective function: energy losses (EL) and charging interval time (CIT). An intelligent optimization procedure based on the cuckoo optimization algorithm (COA) is implemented for the objective function of

Chapter 4

improving the charging performance of the lithium-polymer ion battery of 1000 mAh. These techniques are investigated, simulated, and experimentally validated. The CIT is reduced by 22.45% and 18.1% and the EL is reduced by 10.408% and 7.783% using the Conditional Random Technique (CRT) and the Hierarchical Technique (HT), respectively. Besides, the charging efficiency improved by 14.1% and 8% using the CRT and HT techniques, respectively.

Furthermore, a PV standalone smart charger is presented for off-board plug-in electric vehicles, represented by a small-scale lithium-ion polymer battery of 1000 mAh. The charger is utilized to implement the mentioned charging protocols while improving the transient performance. It comprised a DC-DC buck converter controlled by an artificial neural network predictive controller (NNPC), trained, and supported by the long short-term memory recurrent neural network (LSTM). The LSTM network model was utilized in the offline forecasting of the PV output power, which was fed to the NNPC as the training data. Additionally, it was used as an alarm flag for any possible PV output shortage during the charging process in the long- and short-term prediction to be supported by any other electricity source. The NNPC-LSTM controller was compared with the fuzzy logic (FL) and the conventional PID controllers while varying the input voltage and implementing the charging protocol. The controllers are simulated and experimentally validated where the NNPC-LSTM ensured the optimum transient performance concerning the FL and PID controllers where the ripples of the battery's terminal voltage reached 1mV and settling time of 1ms.

Chapter 5

System Integration, Testing, Validation, and Verification

5.1 Introduction

This chapter investigates the impact of the DC fast charging protocols that are discussed in the previous chapters on the utility grid. Several integration scenarios and case studies between the EVs represented by the electric vehicle charging station (EVCS) or/and any parking lot with the utility grid are proposed. The charging/discharging operations using the Vehicle-to-Grid (V2G) and Grid-to-Vehicle (G2V) technologies are securitized throughout the entire operation. The mentioned case studies are conducted in Egypt, which is a developing country that has recently started implementing fast-charging protocols for EVs and utilizing discharging operations to alleviate the peak load demand of the utility grid using the V2G technology. Therefore, the G2V technology in the EVCS is introduced and the ability of EVs to be charged and discharged during stochastic parking operations is explored.

5.2 Electric Vehicle Charging Station (EVCS) based on the Grid-to-Vehicle (G2V) Technology

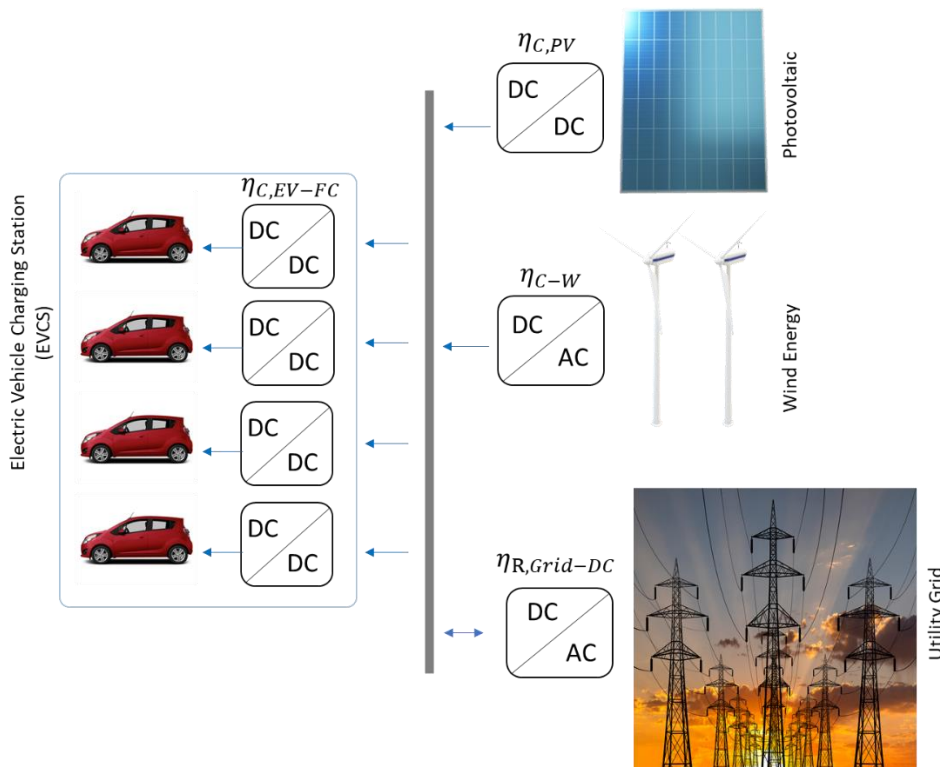
Egypt is considered a prime strategic location for renewable energy projects due to the sunny weather and high wind speed. Egypt aims to increase the generated electricity from RESs to 20% by 2022 and 42% by 2035 with the corresponding providing ratio; of 14% wind energy, 2% hydro, 22% PV, and 3% concentrating solar power (CSP) [319]. Part of Egypt's vision for 2030 is to increase the local content in all fields. The Ministry of Electricity and Renewable Energy (MOERE) ensured 30% local content for wind farms in 2018 and is expected to increase the remaining share to 70% by the end of 2022. In addition, the ministry is expected to reach 50% of the CSP by the end of 2022.

Due to the impact of the different local conditions such as weather, and structure on the economic results across the country, various scenarios based on the geographic locations are necessary to be implemented. In this thesis, the electric vehicle charging station under study is located in Egypt at the Cairo-Alexandria desert highway road (30°23.8'N, 30°23.1'E) as shown in Figure 5-1. This area has been chosen as it is considered the main road to the coastal sea area of Alexandria, reflecting the station's high EV density across the year. In this study, no electrical battery energy storage systems (BESS) have been used, due to the high investment cost, and the number of charges and discharges is limited [320]. In addition, the state of health constraints is considered a problem extending the lifetime of these facilities [320].

The availability of the renewable energy sources with their characteristics and EVs flow density and datasheet specifications will be represented in the following subsections.



(a)



(b)

Figure 5-1 The system under study is (a) a real place at the Cairo-Alexandria desert road, Egypt, and (b) Implemented schematic diagram of the proposed system.

5.2.1 Elements of the System Under Study

5.2.1.1 Photovoltaic system

In this study, an On-Grid solar system is utilized with 8.2 kW output power. The input data for the Homer simulation model is 25 years lifetime and the derating factor of 96% which minimized the output of the PV system by 4%. The PV output power can be expressed by the following equation [321-323]

Chapter 5

$$P_{pv} = G_i A_{pv} \eta_{pv} (1 - c_T (T_{PV} - T_{STC})) \quad 5-1$$

Where, G_i is the global solar irradiance (W/m^2), A_{pv} is the installed PV module surface (m^2), η_{pv} is the reference module efficiency (%), c_T is the temperature coefficient of the PV module and it is suggested to be $0.0048 \text{ }^\circ\text{C}^{-1}$ for silicon, T_{PV} is the PV cell temperature, which depends on the surrounding ambient conditions ($^\circ\text{C}$), and T_{STC} is the standard test condition (STC) temperature ($^\circ\text{C}$).

The scaled data of the global radiation of the EVCS area all over the year 2017 is displayed in Figure 5-2-a., and the PV output power for one day in May is expressed in Figure 5-2-b. The PV system capital, replacement, and operation and maintenance costs (O&M) are estimated to be 296,000 LE, 121,000 LE, and 185 LE, respectively where the LE is the official currency in Egypt and called the Egyptian Pound. The prices used in the model have been stated according to [324, 325]. The revenue from selling the PV energy to the grid in Egypt is 1.0858 LE/kWh [326, 327] and it is assumed that the charging by PV is 2.1716 LE/kWh, including all the controllers and protection facilities. However, the tariff for using electrical energy from the grid is 3.75 LE/kWh [326, 327].

5.2.1.2 Wind Energy System

In this study, a 20-kW wind turbine is used with a rotor diameter of 15.81 m, class III, cut-in wind speed of 2.75 m/s, cut-out speed of 20 m/s, and 20 years lifetime. The output power from the wind turbine could be approximately computed through the parametric technique as expressed in [328, 329]

$$P_a(u) = \begin{cases} P(u), & V_{c-i} \leq V \leq V_r \\ P_r, & V_r \leq V \leq V_{c-o} \\ 0, & V_{c-o} \leq V \text{ or } V \leq V_{c-i} \end{cases} \quad 5-2$$

Where, $P_a(u)$ is the wind turbine generator output power (kW), $P(u)$ is the linear variable region between the cut-in and cut-out speed (kW), P_r is the rated output power of the wind turbine (kW), V is the wind speed (m/s), V_r is the rated wind speed (m/s), V_{c-o} is the cut-out wind speed (m/s), and V_{c-i} is the cut-in wind speed (m/s).

The wind speed information for the year 2017 of the EVCS area is displayed in Figure 5-2-c., and the wind turbine generator output power for one day in May is expressed in Figure 5-2-d. The wind turbine capital, replacement, and operation and maintenance costs (O&M) are estimated to be 760,000 LE, 500,000 LE, and 1,850 LE, respectively. The prices used in the model have been stated according to the reference. The revenue for selling wind energy to the grid in Egypt is 1.4646 LE/kWh [326, 327] and it is assumed that the charging by the wind energy is 2.9292 LE/kWh, including all the controllers and protection facilities.

5.2.1.3 Electric Vehicles (EVs) charging demand and density in the station.

The total number of EVs that enter the EVCS during the day is estimated by Monte Carlo with a maximum of 12 EVs at 5:00 pm in [60]. However, in our study, the maximum number of

Chapter 5

EVs that enter the station is assumed to be 4 vehicles to be a moderate station size with high intensity. It is assumed that this station consists of 4 ports for DC fast charging based on the DC charging pros mentioned in the literature survey chapter. The distribution of EVs all over the day is expressed in Figure 5-2-e, where a maximum of 4 EVs enter the station hourly from 6:00 am to 10:00 pm.

It is considered that all the EVs are in the same category 2015 Chevrolet Spark EV with the same technical statistics expressed in Table 5-1. The required charging power for DC fast charging is represented in Figure 5-2-f and the data is quoted from the vehicle battery testing datasheet of the EV [251] where the maximum state of charge (SOC) is 94%.

Table 5-1 Statistics of 2015 Chevrolet Spark EV battery

Battery Nominal Cell Voltage	3.7 V
Nominal System Voltage	355.2 V
Rated Pack Capacity	52 Ah
Rated Pack Energy	19 kWh
Rated DC Charge Power	50 kW

Chapter 5

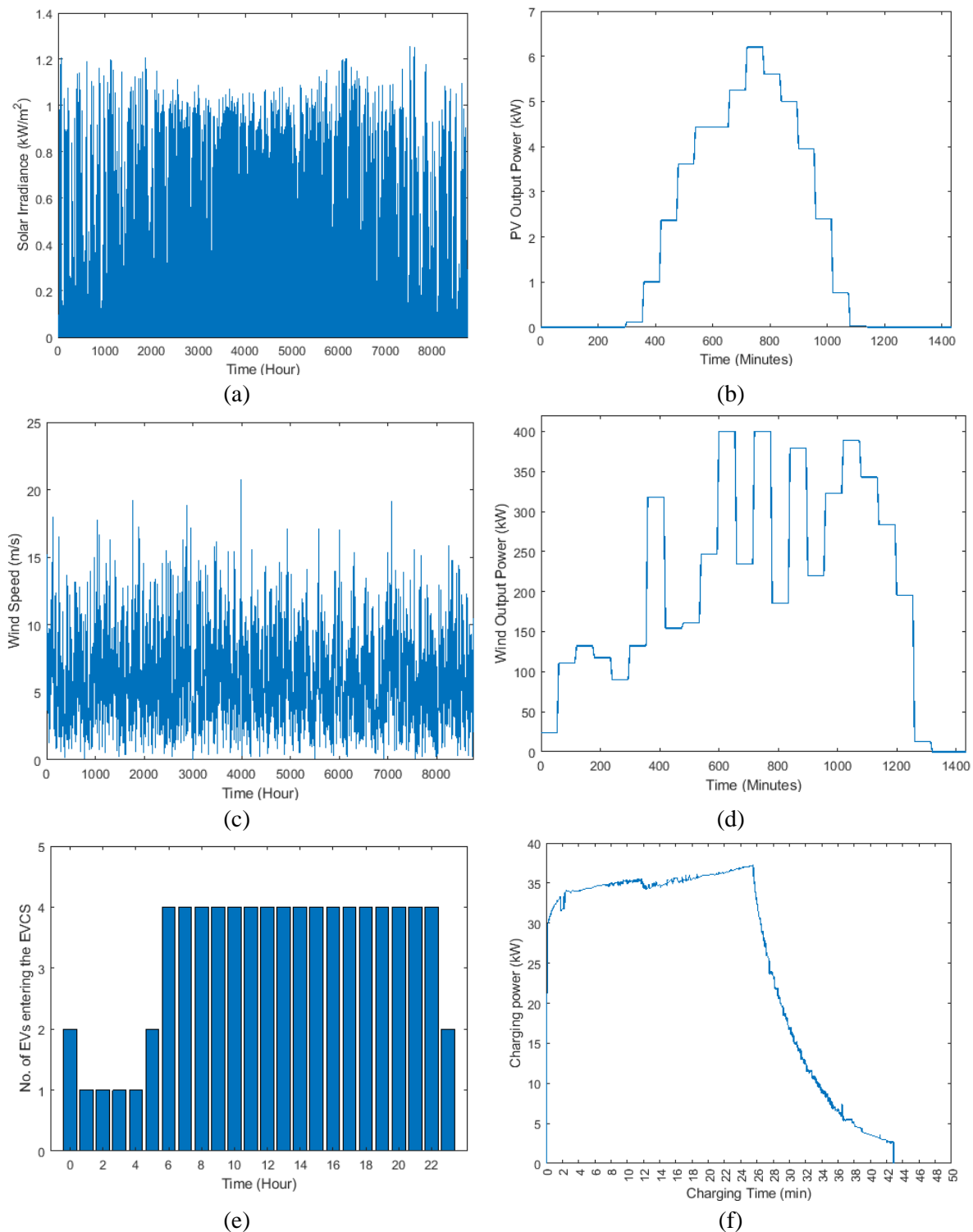


Figure 5-2 Overall RES and EVCS characteristics (a) Solar irradiance all over the year (W/m^2), (b) PV output power on the 15th of May 2017, (c) Wind speed over the year (m/s), (d) wind energy system output power on the 15th of May 2017, (e) Distribution of the EVs entering the EVCS daily, and (f) DC fast charging curve of the 2015 Chevrolet Spark EV battery.

5.2.2 Proposed hierarchal roles of the aggregator (operator)

5.2.2.1 EVs Charging Redistribution in the Station (Upper Stage) using Mixed Integer Linear Programming (MILP)

In this thesis, the system operator has a substantial upper role in the reliable matching of the electric generation and demand at the lowest possible operation cost during the day; however, the intermittency of RESs. This role is implemented by the smart scheduling of the EVs inside the EVCS. All the EVs will be charged by DC fast charging methodology to reach 94% SOC based on the datasheet and charging reports stated before. In addition, the load factor (LF) indicator has been used to measure the variability of consumption where it is the ratio between average real power demand and peak real power demand. A higher load factor is preferable and results in low energy costs [206]. It is assumed that the aggregator will select the charging point plugging-in time at a specific time in HH: MM for each EV based on its corresponding entering time. The allowable waiting time varies from 6 to 18 minutes in steps of 6 minutes to ensure the electric vehicle is parked and connected to its corresponding charging point. However, it is stated in the literature survey that the maximum waiting time of the suburban station with 4 ports maybe reaches 30 minutes [21]. The proposed system in this part calculates the standard deviation of all available alternatives (probabilities) as expressed in Equation 5-3. This equation has been solved as a mixed-integer linear programming (MILP) problem. The main advantage of the MILP is that the linear programming sub-problems can be solved quickly, and the linear constraints result in a convex feasible region to obtain the global optimum [330].

$$\sigma_i = \sqrt{\frac{1}{N-1} \sum_{m=0}^{M=60} \left[(P_{W_{m,h}} + P_{PV_{m,h}} - P_{EV_{m,h}}) - \left(\frac{\sum_{m=0}^{M=60} (P_{W_{m,h}} + P_{PV_{m,h}} - P_{EV_{m,h}})}{N} \right) \right]^2} \quad 5-3$$

Where, $P_{PV_{m,h}}$, $P_{W_{m,h}}$, $P_{EV_{m,h}}$ are the active power of the PV system, wind energy system, and the power required for EV charging, respectively in (kW) at the corresponding charging minute and hour.

In order to make the methodology clear, an example with 2 EVs entering the charging station at 05:00 am, based on Figure 5-2 and the illustration in Figure 5-3 is presented. The system has ten alternatives presented from time 05:06 to 05:24 where 1 or 2 EVs may be connected simultaneously or with a maximum delayed interval time of 18 minutes in steps of 6 minutes to ensure the required time for the EV to be parked and connected to its corresponding charging point. All the allowable probabilities are expressed by the green colour box in Figure 5-3. The hierarchal model based on MILP will choose the most flatted curve according to the standard deviation concept according to the starting time of charging. In the presented example, the optimum solution is the 7th alternative (σ_7) based on Equation 5-3 where EV_1 will be connected at 05:06 am and EV_2 will be connected at 05:24 am.

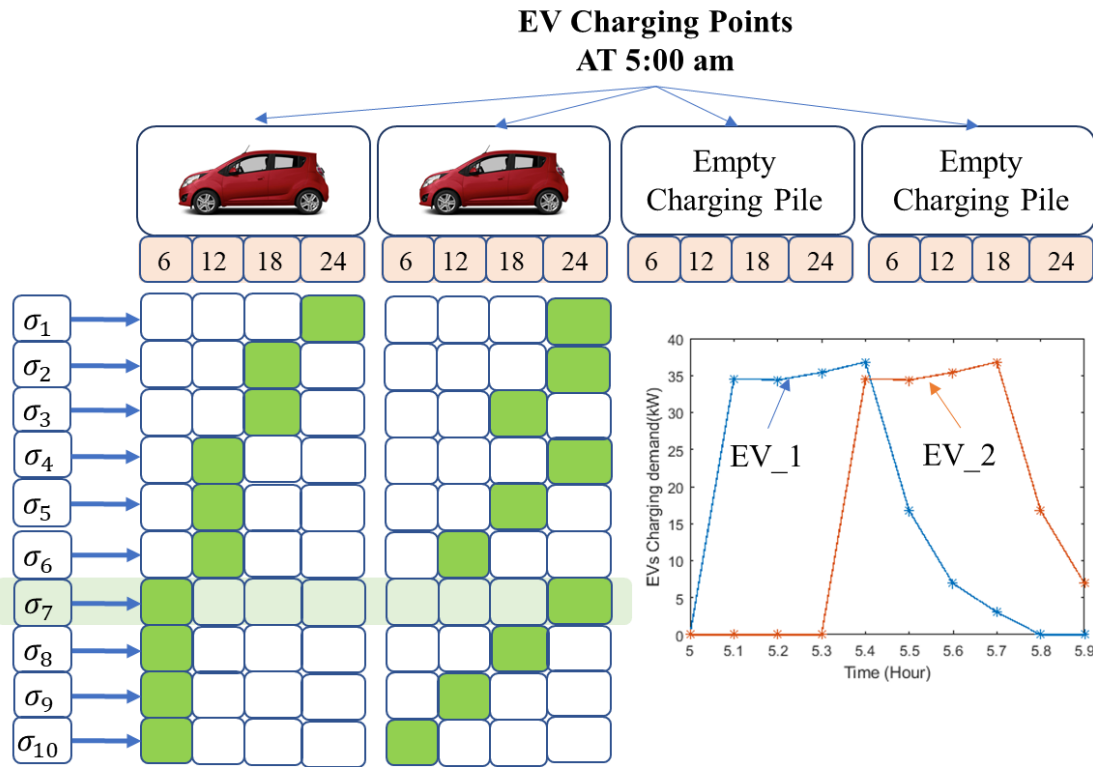


Figure 5-3 Schematic diagram of the probability of the upper stage hierarchical model.

5.2.2.2 Maximizing the EVCS Revenue and Minimizing the EVs Charging tariff (Second Stage) using Markov Decision Process Reinforcement Learning (MDP-RL)

One of the prevalent techniques due to the integration between RESs in the distribution networks is distribution feeder recognition (DFR). DFR is used to maximize certain objective functions subject to all operational constraints [331, 332]. It is noteworthy that the DFR has ignored the daily load variation and has been solved during a predetermined time interval. The DFR is carried out by managing the on/off states of tie switches and sectionalizing switches in a distribution feeder without islanding any buses [332]. Reconfiguration has been used in [333] to change the topology of the network by repositioning switches. In [334], the authors emphasized that system reconfiguration using sectionalizing and tie switches ensures the optimal and efficient operation of the microgrid.

In this subsection, the second stage of the proposed modelling is implemented based on multiple equations, each equation describes a specific available scenario. The equations have been extracted from [226]. This stage is applied using the data obtained from the PV system, wind energy system, and EV charging curve. The data is collected at the start of each hour and the decision has been taken to be implemented in steps of 6 minutes for manoeuvring the switches. The system can choose between the different scenarios based on restricted constraints corresponding to the available power in each step. The corresponding scenarios can be expressed as follows:

Chapter 5

5.2.2.2.1 Scenario 1

In the 1st scenario, the PV system can charge the EVs at the corresponding interval time based on the constraint in Equation 5-4 where the PV output power must be more than the EV charging demand. The objective function of this scenario can be represented in Equation 5-5, where the target is minimizing the EVs' tariff and maximizing the total revenue of the EVCS.

$$P_{PV_{m,h}} \geq P_{EV_{m,h}} \quad 5-4$$

$$\Psi_{PV} = \rho_{S,PV} \left(P_{PV_{m,h}} \cdot \eta_{C,PV} - \frac{P_{EV_{m,h}}}{\eta_{C,EV-FC}} \right) + \rho_{S,W} \cdot P_{W_{m,h}} \cdot \eta_{C-W} - \rho_{B,EV-PV} \frac{P_{EV_{m,h}}}{\eta_{C,EV-FC}} \quad 5-5$$

Where, $\rho_{S,PV}$, $\rho_{S,W}$ are the prices of selling the power to the utility grid from the PV system and wind energy turbine generator in (LE), respectively, $\rho_{B,EV-PV}$ is the EV charging tariff using the PV system in (LE), and $\eta_{C,PV}$, η_{C-W} , $\eta_{C,EV-FC}$ are the efficiencies of the DC/DC PV converter, AC/DC wind converter, and DC/DC EV fast-charging converter, respectively. In this section, all converters' efficiency is considered as 90%.

5.2.2.2.2 Scenario 2

In the 2nd scenario, EVs' demand will be supplied from the utility grid based on the constraint in Equation 5-6 and the objective function in Equation 5-7 where the surplus power of the grid must cover the charging demand of the EV.

$$P_{G_{m,h}} \geq P_{EV_{m,h}} \quad 5-6$$

$$\Psi_G = \rho_{S,PV} \cdot P_{PV_{m,h}} \cdot \eta_{C,PV} + \rho_{S,W} \cdot P_{W_{m,h}} \cdot \eta_{C-W} - \rho_{B,EV-G} \cdot \frac{P_{EV_{m,h}}}{\eta_{R,Grid-DC} \cdot \eta_{C,EV-FC}} \quad 5-7$$

Where, $\eta_{R,Grid-DC}$ is the efficiency of the grid rectifier and assumed to be 90% efficiency, and $\rho_{B,EV-G}$ is the EV charging tariff using the utility grid in (LE).

5.2.2.2.3 Scenario 3

In the 3rd scenario, the wind turbine generator can supply the EVs without any integration with the other suppliers based on the constraint in Equation 5-8 and the objective function in Equation 5-9 where the wind generator turbines must be greater than the EVs' charging load.

$$P_{W_{m,h}} \geq P_{EV_{m,h}} \quad 5-8$$

$$\Psi_W = \rho_{S,W} \left(P_{W_{m,h}} \cdot \eta_{C,W} - \frac{P_{EV_{m,h}}}{\eta_{C,EV-FC}} \right) + \rho_{S,PV} \cdot P_{PV_{m,h}} \cdot \eta_{C,PV} - \rho_{B,EV-W} \frac{P_{EV_{m,h}}}{\eta_{C,EV-FC}} \quad 5-9$$

Where, $\rho_{B,EV-W}$ is the EV charging tariff using the wind turbine generator in (LE).

Chapter 5

5.2.2.2.4 Scenario 4

In the 4th scenario, the generated power from the PV is not sufficient to charge the EVs, and also the power generated from the wind turbine is not sufficient to charge the EVs on its own, so both the RESs are integrated to fully charge the EVs in the station based on the constraint in Equation 5-10 and the objective function in Equation 5-11.

$$\begin{aligned} P_{PV_{m,h}} &< P_{EV_{m,h}}, \\ P_{W_{m,h}} &< P_{EV_{m,h}}, \\ P_{W_{m,h}} + P_{PV_{m,h}} &\geq P_{EV_{m,h}} \end{aligned} \quad 5-10$$

$$\begin{aligned} \Psi_{PV+W} = \rho_{S,W} &\left(P_{W_{m,h}} \cdot \eta_{C,W} + P_{PV_{m,h}} \cdot \eta_{C,PV} - \frac{P_{EV_{m,h}}}{\eta_{C,EV-FC}} \right) \\ &- \left(\rho_{B,EV-PV} \cdot P_{PV_{m,h}} \cdot \eta_{C,PV} \right. \\ &\left. + \rho_{B,EV-W} \cdot \eta_{C,W} \left(\frac{P_{EV_{m,h}}}{\eta_{C,EV-FC}} - P_{PV} \cdot \eta_{C,PV} \right) \right) \end{aligned} \quad 5-11$$

5.2.2.2.5 Scenario 5

In the 5th scenario, EVs could be charged through the integration between the PV system and utility grid where PV can't charge the EV on its own based on Equations 5-12, and 5-13.

$$\begin{aligned} P_{PV_{m,h}} &< P_{EV_{m,h}}, \\ P_{PV_{m,h}} + P_{G_{m,h}} &\geq P_{EV_{m,h}} \end{aligned} \quad 5-12$$

$$\begin{aligned} \Psi_{PV+G} = \rho_{S,W} \cdot P_{W_{m,h}} \cdot \eta_{C,W} \\ - \left(\frac{\rho_{B,EV-G}}{\eta_{R,Grid-DC}} \cdot \left(\frac{P_{EV_{m,h}}}{\eta_{C,EV-FC}} - P_{PV_{m,h}} \cdot \eta_{C,PV} \right) \right. \\ \left. + \rho_{B,EV-PV} \cdot \frac{P_{PV_{m,h}} \cdot \eta_{C,PV}}{\eta_{C,EV-FC}} \right) \end{aligned} \quad 5-13$$

5.2.2.2.6 Scenario 6

In the 6th scenario, EVs could be charged based on the integration between the wind energy and utility grid where the output power from the wind energy cannot charge the EVs on its own based on Equations 5-14, and 5-15.

$$\begin{aligned} P_{W_{m,h}} &< P_{EV_{m,h}}, \\ P_{W_{m,h}} + P_{G_{m,h}} &\geq P_{EV_{m,h}} \end{aligned} \quad 5-14$$

$$\begin{aligned} \Psi_{W+G} = \rho_{S,PV} \cdot P_{PV_{m,h}} \cdot \eta_{C,PV} \\ - \left(\frac{\rho_{B,EV-G}}{\eta_{R,Grid-DC}} \cdot \left(\frac{P_{EV_{m,h}}}{\eta_{C,EV-FC}} - P_{W_{m,h}} \cdot \eta_{C,W} \right) + \rho_{B,EV-W} \cdot \frac{P_{W_{m,h}} \cdot \eta_{C,W}}{\eta_{C,EV-FC}} \right) \end{aligned} \quad 5-15$$

Chapter 5

5.2.2.2.7 Scenario 7

In the 7th scenario, both the RESs could not supply the station even by the integration Therefore the grid must support the system as a third supplier, based on Equations 5-16 and 5-17.

$$\begin{aligned}
 P_{PV_{m,h}} &< P_{EV_{m,h}} \\
 P_{W_{m,h}} &< P_{EV_{m,h}} \\
 P_{PV_{m,h}} + P_{W_{m,h}} &< P_{EV_{m,h}} \\
 P_{W_{m,h}} + P_{PV_{m,h}} + P_{G_{m,h}} &\geq P_{EV_{m,h}}
 \end{aligned} \tag{5-16}$$

$$\begin{aligned}
 \Psi_{PV+W+G} = 0 - &\left(\frac{\rho_{B,EV-G}}{\eta_{R,Grid-DC}} \cdot \left(\frac{P_{EV_{m,h}}}{\eta_{C,EV-FC}} - P_{PV_{m,h}} \cdot \eta_{C,PV} - P_{W_{m,h}} \cdot \eta_{C,W} \right) \right. \\
 &\left. + \rho_{B,EV-PV} \cdot \frac{P_{PV_{m,h}} \cdot \eta_{C,PV}}{\eta_{C,EV-FC}} + \rho_{B,EV-W} \cdot \frac{P_{W_{m,h}} \cdot \eta_{C,W}}{\eta_{C,EV-FC}} \right)
 \end{aligned} \tag{5-17}$$

5.2.3 The implemented programming methodologies

5.2.3.1 Mixed Integer Linear Programming (MILP)

Mixed-integer linear programming (MILP) has been used widely in EV optimization problems as in [335] the operation of a fleet of E-mobile assets has been introduced based on the MILP to minimize the charging cost. In [336], bidirectional EV property represented in vehicle-to-home (V2H) and vehicle-to-grid (V2G) has been used to maximize revenues for the user using linear programming (LP) and MILP. MILP ensured a revenue reached 30% higher than LP. In [337], the spatially granular electricity systems optimisation model which is called ESONE based on the MILP is used to optimize the operational schedule and optimal power flow hourly in power system generation and transmission infrastructure in the presence of transport electrification. The scheduling issue in the centralized EVCS is designed as a MILP issue in [60, 338]. In addition, the MILP has been used in the charging coordination in unbalanced electrical distribution systems in [339]. The maximum amount of renewable energy sources and optimal operation time for EVs and appliances have been developed by MILP [340]. Hence, MILP has been used widely in EV optimization problems, as mentioned in the literature review. The integer variables are obtained using the branch and bound algorithm.

The objective function that describes the proposed model can be stated in Equation 5-18 which is concluded from Equation 5-4 to Equation 5-17

$$\begin{aligned}
 \delta = \sum_{h=0}^H \sum_{m=0}^M &\alpha_1 \Psi_{PV} + \alpha_2 \Psi_G + \alpha_3 \Psi_W + \alpha_4 \Psi_{PV+W} + \alpha_5 \Psi_{PV+G} + \alpha_6 \Psi_{W+G} \\
 &+ \alpha_7 \Psi_{PV+W+G}
 \end{aligned} \tag{5-18}$$

In the previous equation, α is the status of the switching scenario, where $\alpha = 1$ or 0 . $\alpha = 1$ means that this scenario will be implemented in its corresponding minute m and time h which will reflect on the concerning switches between the RES, EVs, and grid in Figure 5-1.

Chapter 5

5.2.3.2 Markov Decision Process Reinforcement Learning (MDP-RL)

Sequential decision problems evolve probabilistically based on a finite and discrete set of states and are solved using MDP-RL which is considered a mathematical method for modelling sequential decision processes [341]. RL has been utilized in many scopes such as game theory, swarm intelligence, operations research, learning robot control, and statistics [342]. RL proved its effectiveness to reformulate and solve optimization problems as in [343]. At each time slot of MDP-RL, the agent observes the state of the process, then selects and executes an action that is optional at this state; then, the agent receives a reward according to the action. The next time, the process moves to a new state and the probability of the process from the current state to a new state is affected by the chosen action. The decision is made based on the state, action, transition function, and reward function of the MDP-RL introduced in [219].

At the beginning of each time slot represented by an hour and minute h and m , the aggregator determines the charging demand, the RESs generated power, charging prices using the different alternative sources, the revenue from selling the power to the utility grid, and the time that the EV will be connected to the charging point. The EVs charging schedule system can be expressed as an agent which completes the DC fast charging of all EVs by making a sequence of the decision on the selection of supplying source PV, wind energy, grid, or any combination of the various available power. As shown in Figure 5-4, the EVCS can choose between seven scenarios as discussed in Equations 5-4 to 5-17 and the optimum track could be represented by the shaded path, which reflects the status of each source, as will be discussed in the results section. Each step is 6 mins long, where it is considered that all EVs enter the station with 5% SOC and leave the station with 94% SOC.

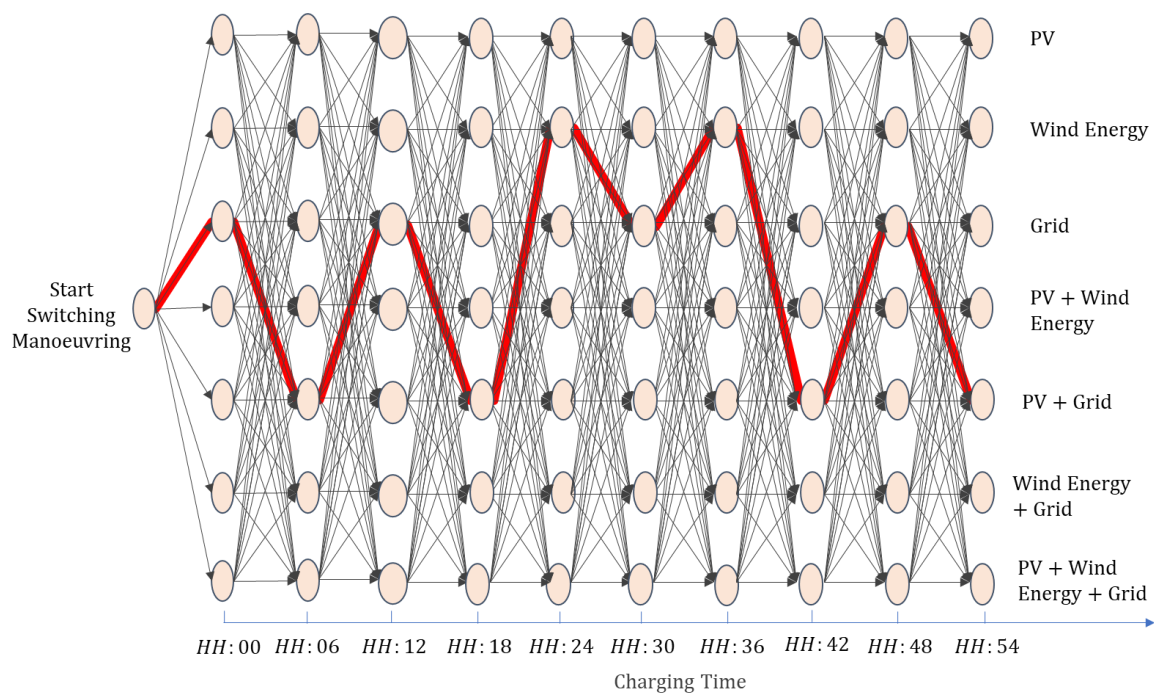


Figure 5-4 Schematic diagram of EVs fast charging optimum track based on a sequence of the decision on the selection of supplying source to reach full capacity 94% using the Markov Decision Process Reinforcement Learning (MDP-RL).

5.2.4 The Proposed Operation of the EVCS

Homer Pro simulated program has been used in this study as the first stage for our modelling, where all the data stated in section 2 of the PV system, Wind energy system, and EVs’ charging demand has been used as a data entry to the program. The simulated program selects the optimum feasible system architecture to supply the corresponding load. In our case study, the optimum solution is obtained by integrating the PV system, wind energy system, and utility grid. The capacity of the selected systems is a 7.05 kW PV system and a 400-kW wind energy system. In addition, the system indicates that the simple payback is 3.9 years, with a return of investment (ROI) of 21%, and an internal rate of return (IRR) of 25%. In addition, the energy to be purchased by this system is 85,184 kWh and the energy to be sold to the grid is 1,500,669 kWh. The output results from the Homer Pro simulated program represented in the rated capacity power, energy production, hours of penetration, penetration percentage, and Levelized cost for each renewable energy source are summarized in Table 5-2. Thus, the framework has been checked and perfectly evaluated using the Homer Pro program, so the next level reveals the first role of the aggregator, which redistributes the EVs’ charging demand to flatten the resultant active power without using the V2G property or the ToU pricing method.

Table 5-2 Analysis summary of the proposed microgrid

PV system	
Total electrical production	13,056 kWh/yr (0.648%)
Rated capacity	7.05 kW
Mean output	1.49 kW (35.8kWh/d)
Capacity factor	21.2%
PV penetration	2.66%
Hours of operation	4,386 hrs/yr
Levelized cost	1.52 LE/kWh
Wind Energy	
Total electrical production	1,918,104 kWh/yr (95.1%)
Rated capacity	400 kW
Mean output	219 kW
Capacity factor	54.7%
Wind penetration	391%
Hours of operation	7,709 hrs/yr
Levelized cost	0.688 LE/kWh

5.2.4.1 Scheduling the EVs in the Charging Station (Upper stage)

The influence of EVs’ fast charging in the EVCS on the daily load curve of the utility grid distribution network is presented in Figure 5-4. Without a price scheme of charging, without using the BESS or the vehicle-to-grid (V2G) capability, a better load profile with a low peak-to-average, load factor and peak-to-peak ratios is obtained using the MILP model based on the standard deviation concept as expressed in Equation 5-3. This equation has been implemented on the different scheduling alternatives to flat the curve and hence minimize the peak points of fast charging.

Chapter 5

The net active power difference between the generated power from RESs and the consumed power from the EVCS is presented in Figure 5-5-a where MILP is compared with the traditional operation, which based on all the EVs will be charged at the same time after 6 minutes of each hour. To judge the performance of the proposed approach, the peak of MILP to the peak of traditional operation percentage of change value at the same hour has been measured as declared in Figure 5-5-b. The surplus power from charging the EVs from the RESs has been reduced by 48.17% equivalent to 4.5 kW using the standard operation with respect to the MILP, at 07:00 am as shown in Figure 5-5-c.

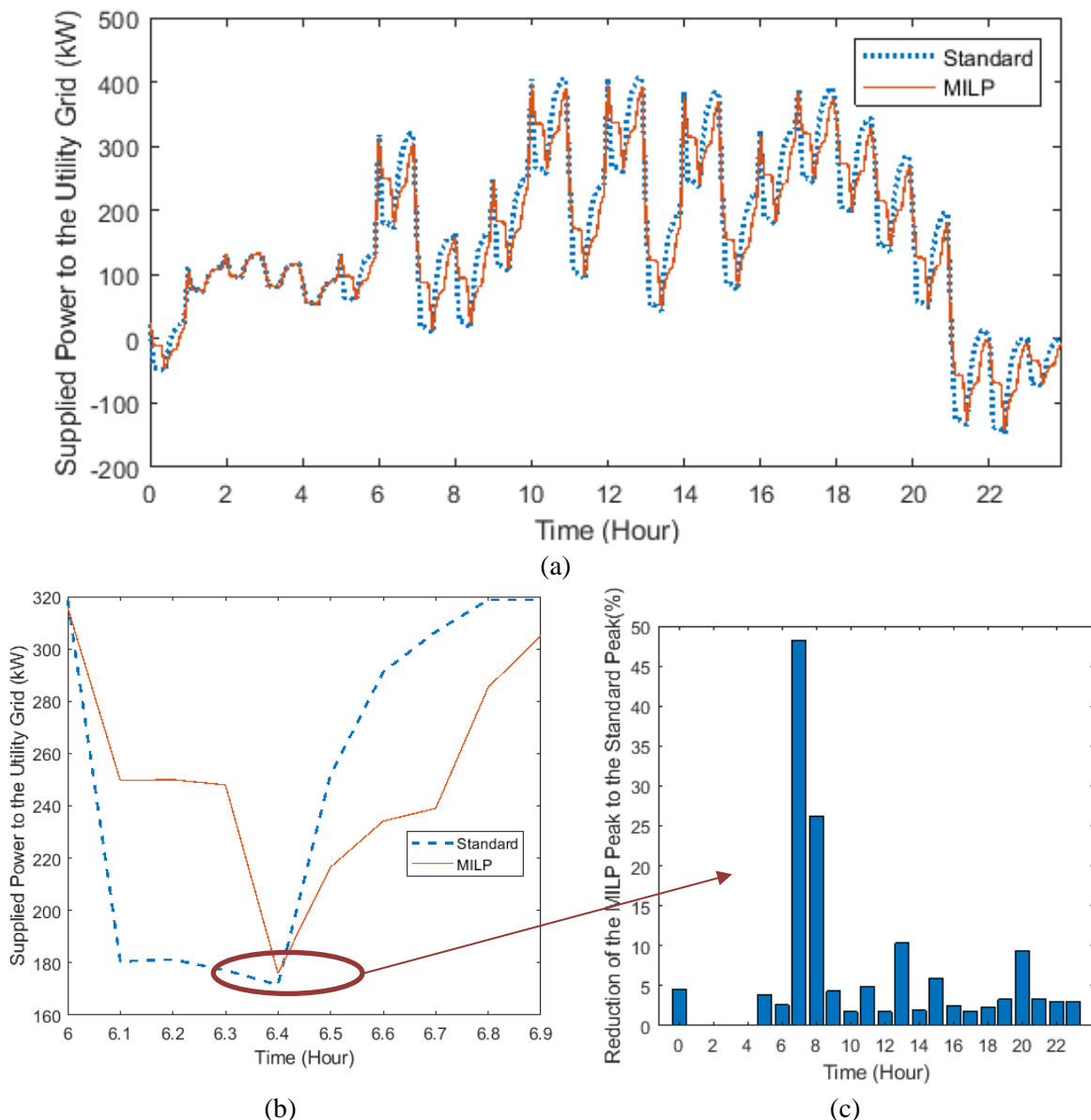


Figure 5-5 Results from the upper stage of the hierarchical model (a) EVCS active power difference between the generated power from RESs and the consumed power from the EVCS, (b) Declaration of the measurement method between the two peaks, and (c) peak to peak percentage of the surplus power from charging the EVs from the RESs between the MILP and traditional operation.

It is concluded that the proposed methodology based on MILP is minimizing the peak load hourly across the day by flattening the curve as in Figures 5-6-a and 5-6-b where a reduction

Chapter 5

reached 3.31% (4.5 kW) and 3.1% (2.25 kW) at 19:00 and 23:00, respectively. To illustrate the flexibility of the proposed model, the peak-to-average value has been calculated for each hour as shown in Figure 5-6-c. The peak-to-average was reduced by 4.5 kW which represents a reduction of 5.95% from 07:00 to 22:00 and it is noticed that from 02:00 to 04:00, no variation as only 1 EV enters the station. Finally, the load factor ratio is calculated to ensure the effectiveness of the proposed MILP model where the system ensured a load factor increase of 3.1276% where the LF of the traditional operation is 37.052% and the MILP model is 38.21% as shown in Figures 5-6-d.

In addition, by using the MILP, it is concluded that no variation will be obtained in the peak of MILP to the peak of traditional operation values while reducing the charging time to 30 minutes or/and the SOC to 88%. So, this stage based on the proposed methodology ensures satisfaction for both the EV's owner and the utility grid operator by balancing the generated and consumed power with only peak consumed power for 6 minutes.

Chapter 5

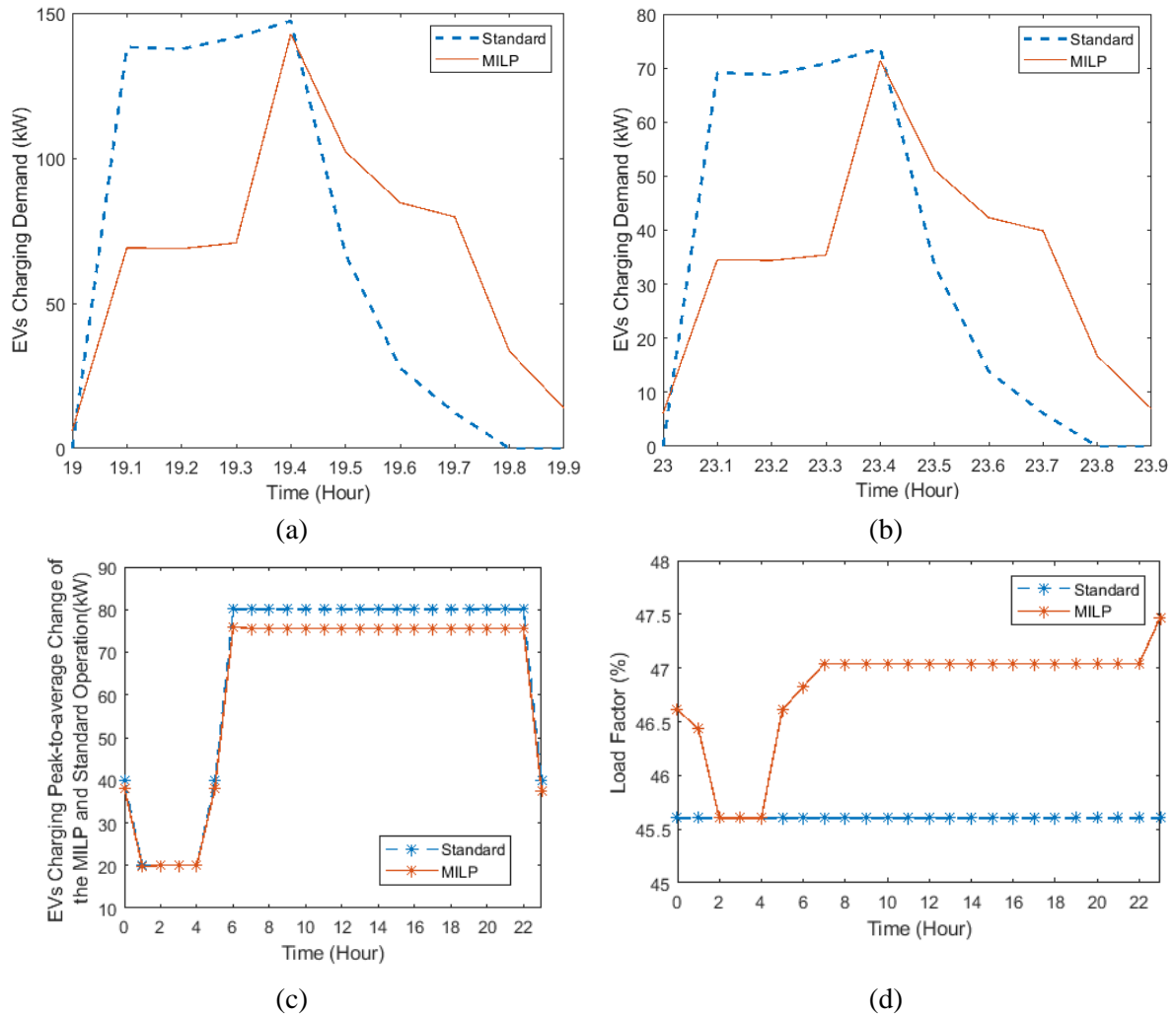


Figure 5-6 Results from the upper stage of the hierarchical model (a) EV charging demand using MILP and compared with traditional operation at 19:00, (b) EV charging demand using MILP and compared with traditional operation at 23:00, (c) EVs' charging demand peak-to-average change of the MILP and traditional operation, and (d) Load factor of the proposed model concerning the traditional operation.

5.2.4.2 Maximizing the EVCS Profit (Second stage)

The second role of the aggregator is to maximize the EVCS revenue and minimize the EVs tariff. In this role, two different methodologies have been implemented using MILP and MDP-RL methods and the results are compared with the traditional operation where the RESs will supply all the EVs and the surplus power will be supplied to the grid. As shown in Figures 5-7-a and 7-7-b, the EVs tariff percentage of change using MILP is bigger than using the MDP-RL with respect to the traditional operation, and also the EVCS revenue percentage of change using MILP is bigger than using MDP-RL with respect to the traditional operation.

EVs' charging tariff increased by 21.19 % (842.17977 LE/day) using MILP and 15.03% (597.442618 LE/day) using the MDP-RL. However, the increase in the EVCS revenue reached 28.88% (1,583.42205 LE/day) and 20.10% (1,101.92988 LE/day) using MILP and MDP-RL, respectively, as shown in Figure 5-7-c. It is concluded that using MDP-RL is more convenient to satisfy a moderate balance between the EV charging tariff and EVCS revenue which the

Chapter 5

revenue decreased by only 6.81% from the MILP and also the EV charging tariff decreased by 5.08%. By using the MDP-RL the station will ensure a revenue of 2,403,122.26 LE/year, with respect to the traditional operation of EVCS of 2,000,917.849 LE/year.

The switching manoeuvring status of electrical resources that resulted in these findings has been declared in detail in Appendix B.

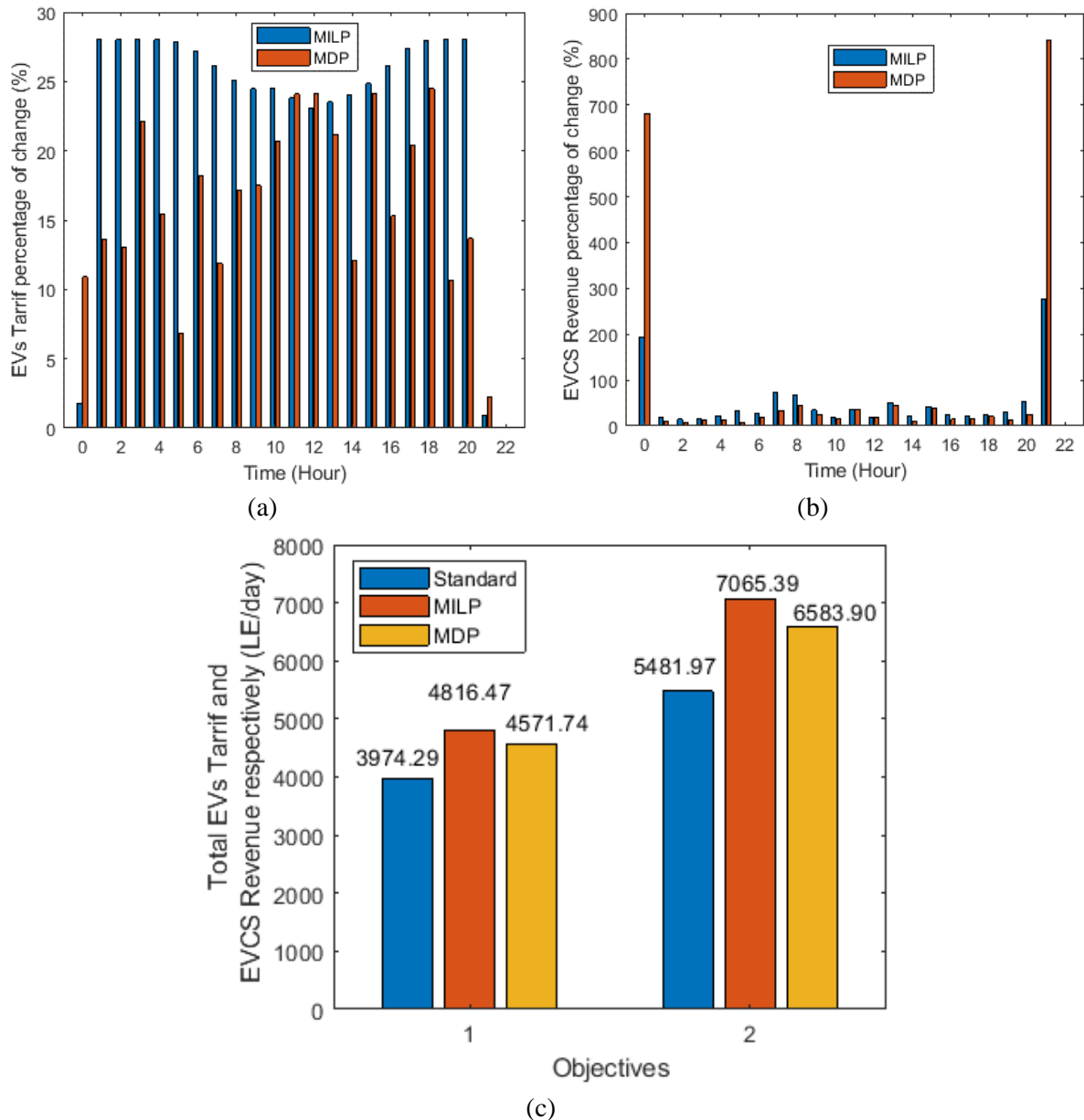


Figure 5-7 Results from the second stage of the hierarchal model compared to the standard operation (a) EVs charging tariff percentage of change, (b) EVCS revenue percentage of change, and (c) Total EVs charging tariff and EVCS revenue obtained by the main equation represented by the two objective functions.

5.3 Stochastic EVs Parking Operations based on the Vehicle-to-Grid (V2G) and Grid-to-Vehicle (G2V) Technologies

5.3.1 Operating Framework

This part proposed the vital development of a central aggregator which regulates the charging and discharging process of various EV categories while balancing the consumed and supplied power of the utility grid. The proposed framework depends on the arrival time, departure time, initial SOC, required final SOC, EV category and energy price for both the V2G and G2V technologies as shown in Figure 5-8. We assumed that the EVs had the information and communication devices installed and were in direct contact with the central aggregator. The specifications of the three random EV categories used for this study (Nissan Leaf (2020), Tesla Model S (p100d) and Mustang Mach-E) are stated in Table 5-3. It was assumed that the EVs had an initial SOC of 50%, the tariff for using the electrical energy from the grid was 3.75 LE/kWh [326, 327], and the revenue from using the V2G technology was 5.625 LE/kWh as an incentive for the EVs owners. All the stated specifications and assumptions were used for testing and proving the robust dynamic effectiveness of the proposed aggregator methodology based on the G2V and V2G technologies.

The hierarchical control of the proposed framework was to minimize the degradation cost of the EV energy storage capacity and maximize the EV owner’s profit while shaving the load power demand, as will be discussed in the following sections.

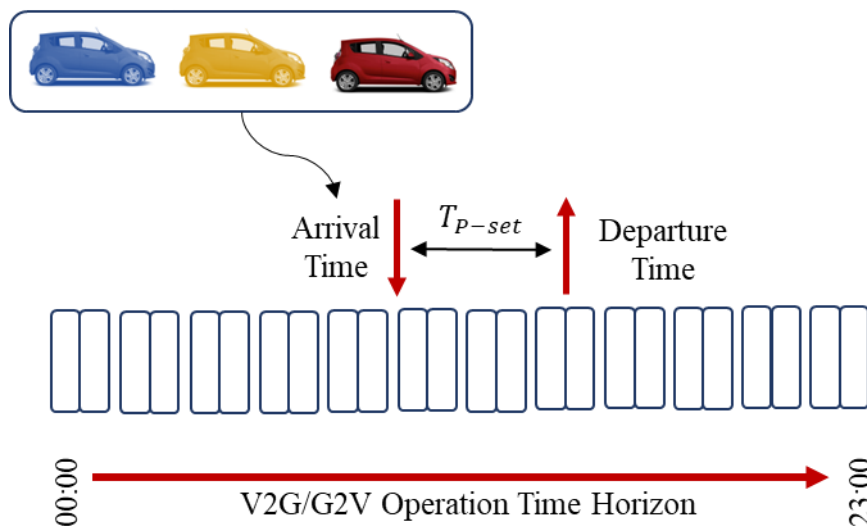


Figure 5-8 Operational V2G/G2V time across the day.

Chapter 5

Table 5-3 The utilized EVs' categories, rated battery capacity, and battery cost as extracted from the EV's model specification [244, 246]

EV	Category	Rated Battery Capacity (kWh)	Battery Cost Per kWh (LE/kWh)
EV_1	Nissan Leaf (2020)	40	4837.89
EV_2	Tesla Model S (p100d)	100	3677.58
EV_3	Mustang Mach-E	68	4051.24

5.3.2 Battery Degradation Cost Model

Battery degradation is considered the key factor for evaluating the performance and quality of EV batteries based on their capacity and efficiency [5]. The battery discharging depth (BDD) and lifecycle of the lithium-ion batteries are presented in Figure 5-9. These statistics were collected from an empirical datasheet of various lithium-ion batteries [246]. The analysis perfectly matches the outcomes of the following equation as in [244, 246].

$$N_{cl}(d) = \frac{\alpha}{d^\beta} \quad 5-19$$

where, N_{cl} is the life span charging/discharging cycles of an EV battery with an overall depth of discharge d and α , β are the coefficients of battery specifications.

As shown in Figure 5-9, the relation between the BDD and lifecycle is a non-linear function. However, in [244, 245], the battery degradation function is considered a linear function at every time step and the corresponding scenario and can be represented by Equation 5-20

$$\Psi_{tc}^{BDC} = \sum_{c=1}^{C_{EV}} \sum_{t=1}^{T_{P-set}} \frac{2.03 \cdot a_0 \cdot \Psi_c^{BC} \cdot DOD \cdot P_{tc}^{V2G}}{E_c^{max} \cdot \eta_D} \quad 5-20$$

Where c is the category of EV, t is the parking interval time, Ψ_c^{BC} is the price of the battery (LE), E_c^{max} is the maximum battery capacity (kWh), η_D is the discharging efficiency (assumed to be 95%), DOD is the maximum depth of the discharge in each segment and can be represented by the state of charge $1 - SOC_c^f(t + T_{set})$, a_0 is the polynomial coefficient of the cycle depth degradation function (5.24×10^{-4}) and P_{tc}^{V2G} is the discharging of power from the EV to the utility grid (kW).

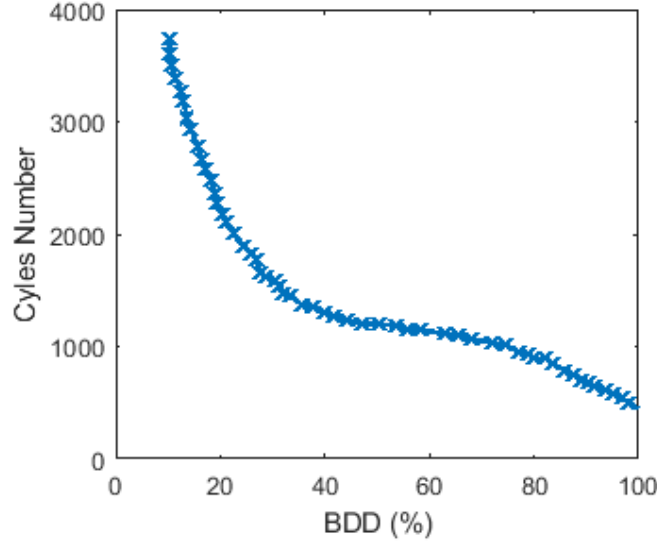


Figure 5-9 Relationship between the charging/discharging cycles and the battery degradation depths (BDDs) during their life span [246].

5.3.3 Proposed V2G Scheduling Modelling and Constraints

The objective function of the proposed model targets the minimization of the degradation cost and maximization of the EV owner’s revenue after using the V2G technology while parking. It can be represented by the Equations from 5-21 to 5-23 which have been extracted from [244-246]. This formulation is considered a complex constraint comprised of two objective functions.

$$\text{Minimize } (K_1 - K_2) \tag{5-21}$$

$$K_1 = \sum_{t=1}^{T_{P-set}} \sum_{c=1}^{C_{EV}} \psi_{tc}^{BDC} \cdot T_{set} \tag{5-22}$$

$$K_2 = \sum_{t=1}^{T_{P-set}} \sum_{c=1}^{C_{EV}} \left((\varepsilon \cdot P_{tc}^{V2G} \cdot \psi_{tc}^{RC-V2G}) - ((1 - \varepsilon) \cdot P_{tc}^{G2V} \cdot \psi_{tc}^{TC-G2V}) \right) \cdot T_{set} \tag{5-23}$$

Where, P_{tc}^{G2V} is the EV charging power from the utility grid (kW), ψ_{tc}^{TC-G2V} is the EV charging tariff cost while using the G2V technology (LE/kWh), ψ_{tc}^{RC-V2G} is the EV owner discharging revenue cost while using the V2G technology (LE/kWh) and ε is a switching binary number (1 or 0) to ensure using either the V2G or G2V technology at the corresponding interval time.

The constraints used in this chapter were represented by the Equations from 5-24 to 5-27 where the SOC at the beginning and end of each interval time were less than 95% and more than 20%, and the average power demand of the utility grid was equal to the average required power throughout the day.

$$0.2 \leq SOC_{tc}^f(t + T_{set}) \leq 0.95 \quad 5-24$$

$$0.2 \leq SOC_{tc}^i(t) \leq 0.95 \quad 5-25$$

$$SOC_c^f(t + T_{set}) = SOC_c^i(t) + \sum_{t=1}^{T_{P-set}} \left(\frac{\varepsilon \cdot P_{ij}^{G2V} \cdot \eta_{ij}^{G2V} - \frac{(1 - \varepsilon) \cdot P_{ij}^{V2G}}{\eta_{ij}^{V2G}}}{E_c^{max}} \right) \cdot T_{set} \quad 5-26$$

$$P_{tc}^{Average} = \sum_{t=1}^{T_{P-set}} \sum_{c=1}^{C_{EV}} (P_{tc}^{V2G} - P_{tc}^{G2V}) \quad 5-27$$

where, $SOC_c^f(t + T_{set})$ is the final SOC for each EV category, $SOC_c^i(t)$ is the initial SOC for the interval time segment and T_{P-set} is the set of parking time slots with a similar charge/discharge power.

5.3.4 Solving Based on the Genetic Algorithm (GA)

The proposed fitness function accompanied by the previous constraints was solved using the genetic algorithm (GA). The topology of the genetic algorithm is based on the biological evolution process of the computational data and the mechanism of natural genetics selection. The GA is composed of three main significant operators, namely reproduction, crossover, and mutation. These operators result in an optimum solution using a fitness function that maps the natural objective function [344]. The GA is a heuristic algorithm that can easily choose satisfactory solutions using its own characteristics stemming from its good global search performance and low complexity [345]. The GA can find the near-optimal solution faster than the MILP method as stated in [346]. The topology of the GA is inspired by the biological evolution process of computational data and the mechanism of natural genetics selection [347, 348]. GA is composed of three main significant operators, which are reproduction, crossover and mutation. These operators result in an optimum solution using a fitness function, as it maps the natural objective function. The genetic Algorithm's population is represented by a set of chromosome strings. In each generation, a new organ of the population (chromosome) is generated using the data from the fittest chromosome from the past population. Each chromosome gets a value of fitness through a fitness function which represents the ability of the chromosome to produce offspring. When the fitness value is high, it represents the better solution for maximization and when the fitness value is low represents the better solution for minimization problems. All parts of the GA (Initial population, fitness evaluation function, reproduction approach, crossover operator and mutation operator) are illustrated by a flowchart in Figure 5-10 [349].

Chapter 5

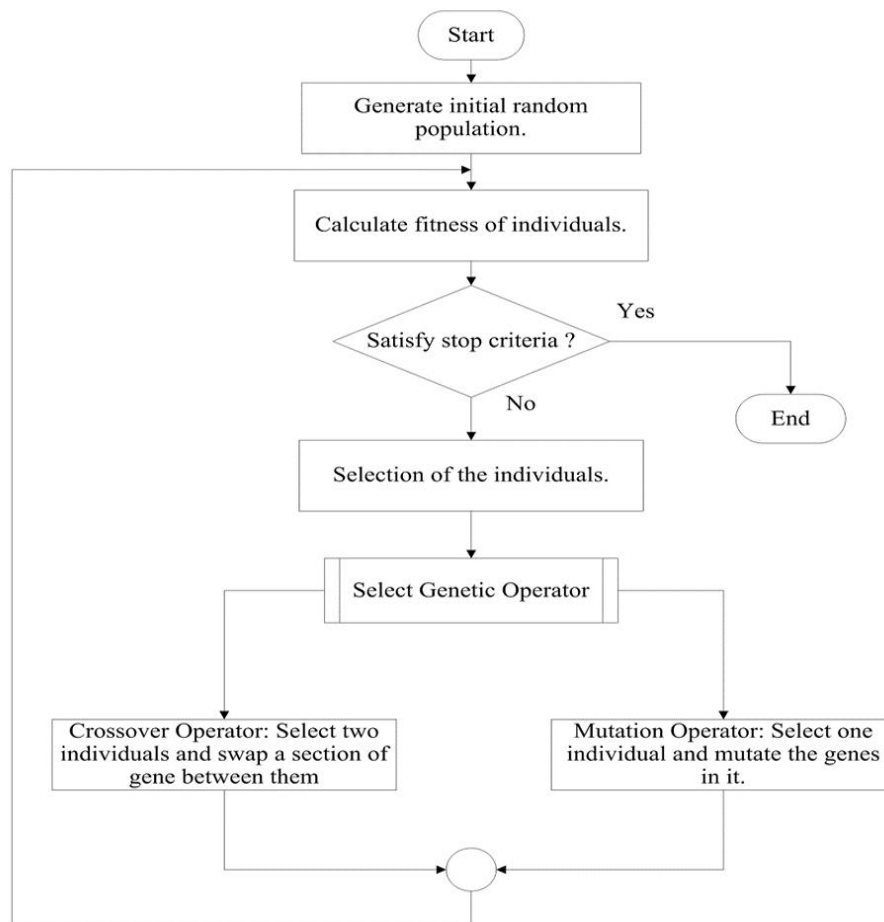


Figure 5-10 Flowchart for Genetic Algorithm (GA).

In this section, we utilized the GA to minimize the degradation cost while maximizing the profit of the EV owner by using the V2G technology. The obtained results had a strong impact with respect to the literature survey, as summarized in the literature survey chapter. A complete flow chart of the proposed electric vehicle utility grid aggregator methodology based on the G2V and V2G technologies is expressed in Figure 5-11.

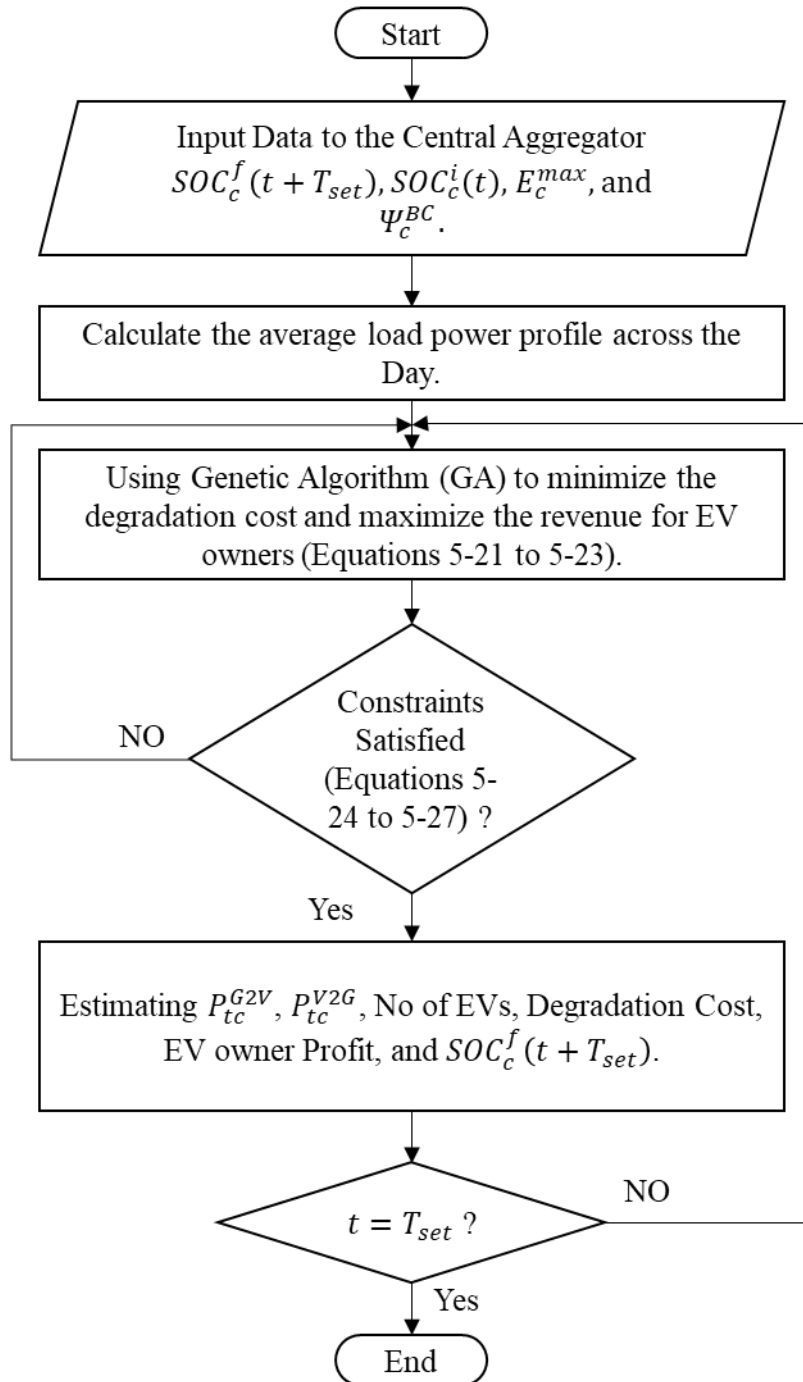


Figure 5-11 Complete flowchart architecture of the proposed aggregator methodology.

5.3.5 Charging/Discharging System Understudy

The Egyptian Electrical Unified Network (EEUN) consists of six geographical regions: Cairo, Canal, Delta, Alexandria/West Delta, Middle Egypt and Upper Egypt [350, 351]. The transmission system of the utility grid electricity was designed at 500 kV, 400 kV, 220 kV, 132 kV and 66 kV levels, the distribution networks at 11 kV and the loads at 400 V. The power quality was measured on the primary substation (11 kV) as active power load within 24 h, as shown in Figure 5-12. The stated power demand represented the deficiency of the utility grid in the presence of fast-charging electric vehicle charging stations and normal grid loads as

Chapter 5

discussed in our previous section and in Figure 5-5-a. The target was utilizing smart charging and discharging schedules to reduce the peak load and shape the load profile in the power grid to reach an average load profile throughout the day, as shown in Figure 5-12.

In this section, two scenarios were investigated and compared to each other at different hours throughout the day. The first scenario is implemented using the fitness function with the battery degradation impact function and the second scenario was implemented while ignoring the battery degradation cost. Both scenarios were investigated in various case studies throughout the day as represented in Figure 5-12.

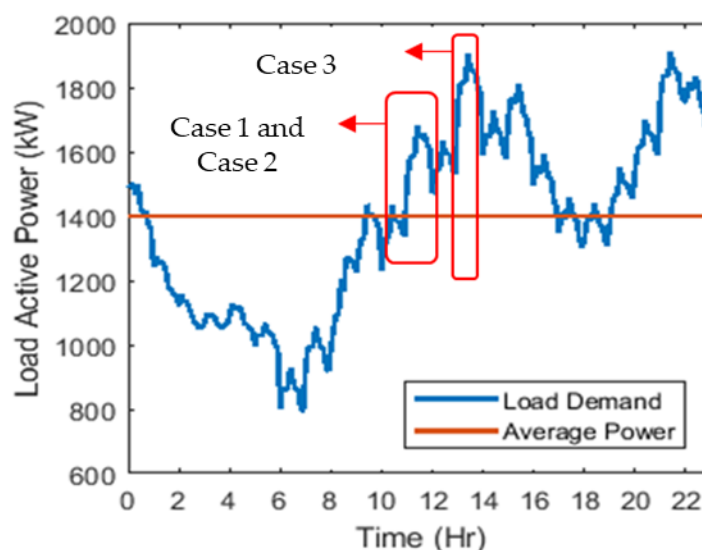


Figure 5-12 Load active power demand across the day without EV penetration.

5.3.5.1 Case Study 1: Continuous Parking for a 2 h Interval Time

In Case 1, we assumed that all the EVs would remain continuously parked for 2 hours from 10:00 to 12:00. The target was to shave the peak load demand of the utility grid using the G2V/V2G technologies to reach the required average power.

The aggregator's role was to select the number of EVs for each category to participate in the V2G/G2V technology trade and determine the required charging/discharging power while maximizing the SOC and revenue of the EV owner and minimizing the battery degradation cost. The number of EVs, final SOC, degradation cost and EV owner profit for the interval time are expressed in Table 5-4 and represented in Figure 5-13.

The simulation interval time was 6 min to ensure the accuracy of the model. The EV SOC levels are expressed in Figure 5-13-a where the EVs of the first and third categories were charged with various capacities for both scenarios while minimizing the degradation cost and maximizing the profit. However, the second EV category was discharged by 0.85% and 1.16%, respectively for both scenarios to compensate for the deficiency in the utility grid. The battery degradation cost was investigated for each EV category, as shown in Figure 5-13-b. The degradation cost using the GA was decreased by 40.9256%, 44.1757% and 42.544% for EV categories 1, 2, and 3, respectively, with respect to the objective function without considering the degradation cost. It was observed that the revenue for each EV owner in Scenario 2 was

Chapter 5

higher than in Scenario 1, as shown in Figure 5-13-c. The load demand of the utility grid was reduced by 17.125% at 11:30 am and maintained almost equal to the calculated average required power across the parking interval time as shown in Figure 5-13-d.

Table 5-4 The V2G/G2V output summary of the 1st case study.

	Scenario 1 Time: 10:00 to 12:00	Scenario 2 Time: 10:00 to 12:00
Number of EVs (EVs)		
EV-1	8	14
EV-2	362	272
EV-3	1	11
Final SOC (%)		
EV-1	77.77%	61.31%
EV-2	49.15%	48.84%
EV-3	58.01%	52.36%
Degradation Cost (LE)		
EV-1	0.9765 LE	1.6530 LE
EV-2	0.0877 LE	0.1571 LE
EV-3	0.6658 LE	1.1588 LE
EV owner Profit (LE)		
EV-1	-34.2 LE	-8.8 LE
EV-2	4.589 LE	6.79 LE
EV-3	-14.9 LE	4.429 LE

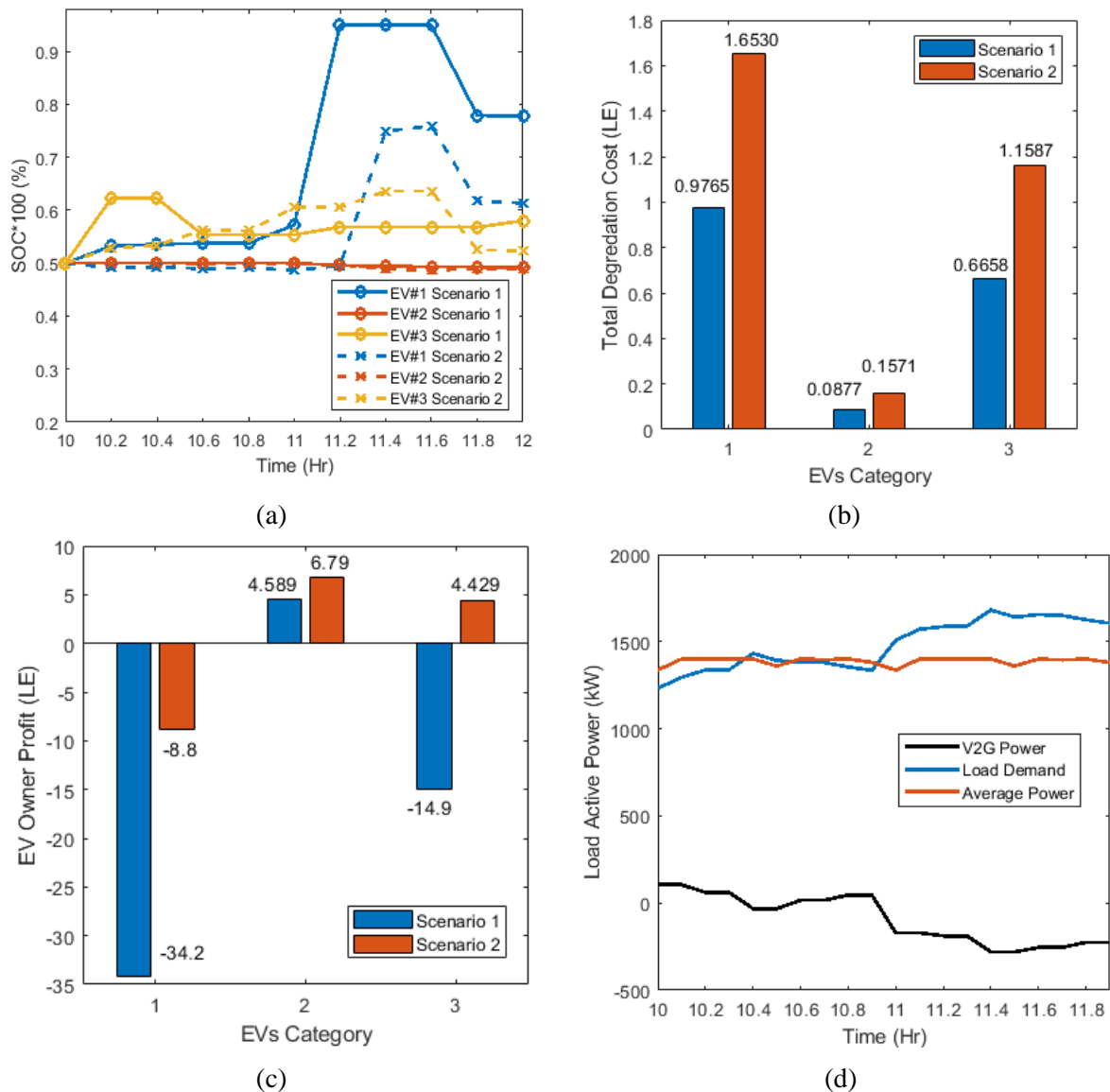


Figure 5-13 Framework outputs while continuously parking for a 2 h interval time for both scenarios (a) state of charge levels of all EV categories, (b) total degradation cost, (c) EV owner revenue from the V2G technology and (d) resultant load profile.

5.3.5.2 Case Study 2: Stochastic Parking for a 2 h Interval Time

In Case 2, we assumed that various numbers of EVs would be stochastically parked for 2 hrs. from 10:00 to 12:00. The model ensured the effectiveness of selecting the appropriate number of EVs and the charging/discharging power for each hour. The target was to shave the peak load demand of the utility grid using the G2V/V2G technologies and the variance of the parked EVs. The aggregator's role was to select the number of EVs for each category to participate in the V2G/G2V technologies while maximizing the SOC and revenue of the EV owner and minimizing the battery degradation cost. The number of EVs, final SOC for each hour, degradation cost and EV owner profit for each hour are expressed in Table 5-5 and introduced in Figure 5-14.

Chapter 5

A detailed schematic for the EV SOC levels after every 6 min is expressed in Figure 5-14-a. Almost all the EVs reached a capacity of more than 60% for both scenarios while minimizing the degradation cost and maximizing the profit. The battery degradation cost was investigated for each EV category, as shown in Figure 5-14-b. The degradation cost decreased by 11.18%, 20.29% and 15.42% for EV categories 1, 2, and 3, respectively. However, the revenue for each EV category owner in Scenario 2 was higher than in Scenario 1, as shown in Figure 5-14-c. The load demand of the utility grid was reduced to almost 16.7718% at 11:24 and remained equal to the calculated average required power throughout the day, as shown in Figure 5-14-d.

Table 5-5 The V2G/G2V output summary of the 2nd case study.

	Scenario 1		Scenario 2	
	Time: 10:00 to 11:00	Time: 11:00 to 12:00	Time: 10:00 to 11:00	Time: 11:00 to 12:00
Number of EVs (EVs)				
EV-1	3	3	2	3
EV-2	1	510	1	42
EV-3	2	186	2	148
Final SOC (%)				
EV-1	59.99%	61.92%	61.02%	63.6%
EV-2	60.01%	59.85%	59.99%	59.09%
EV-3	59.99%	58.81%	59.99%	58.06%
Degradation Cost (LE)				
EV-1	8.5 LE	0.0158 LE	9.4623 LE	0.1258 LE
EV-2	3.3875 LE	0.0359 LE	4.0179 LE	0.277 LE
EV-3	5.4939 LE	0.2498 LE	6.4311 LE	0.3598 LE
EV owner Profit (LE)				
EV-1	0	-2.9891 LE	4.8152 LE	-3.708 LE
EV-2	0	0.9611 LE	0.0528 LE	5.9294 LE
EV-3	0	4.5313 LE	0.0235 LE	7.1238 LE

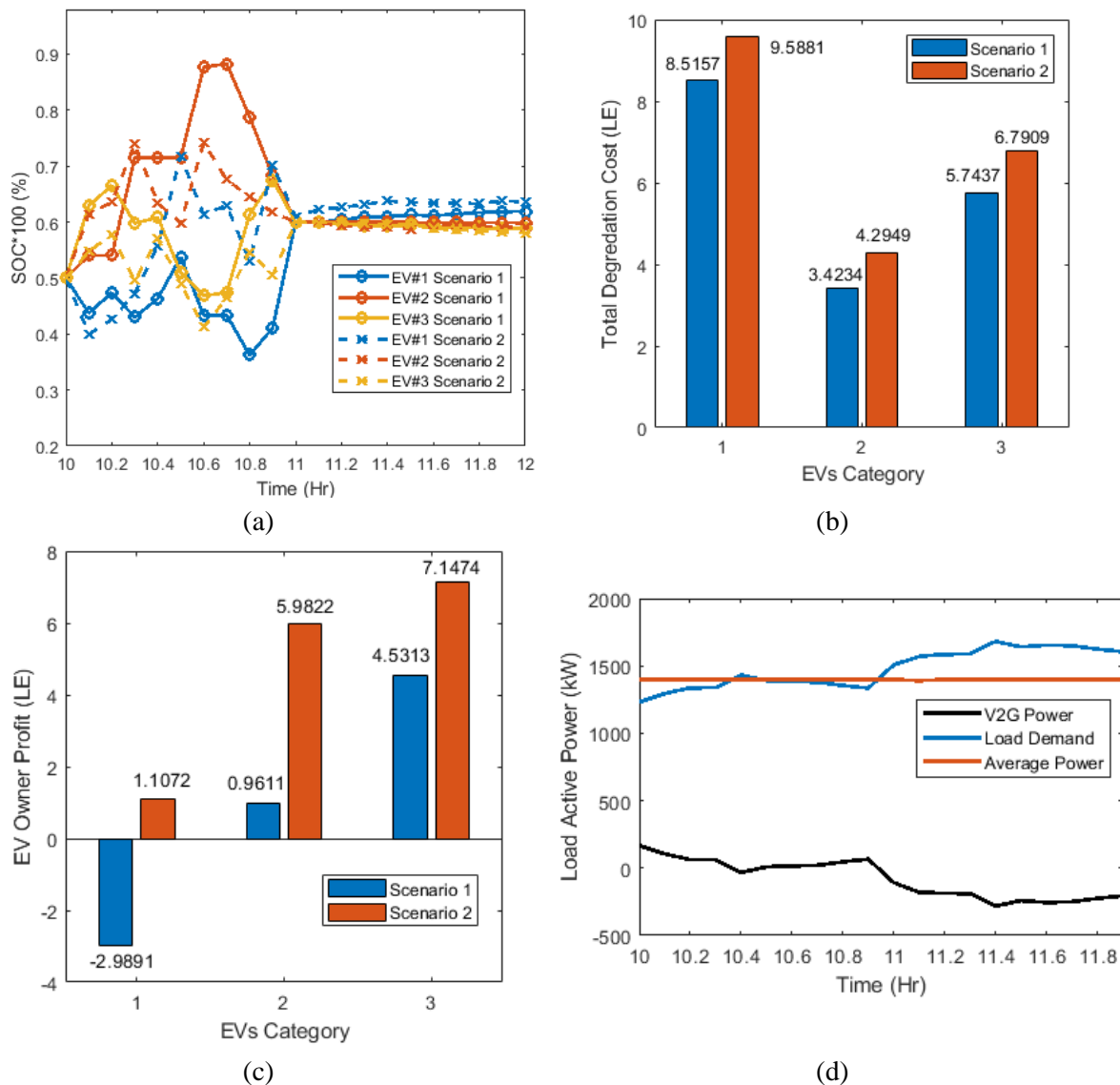


Figure 5-14 Framework outputs while stochastic parking for a 2 h interval time for both scenarios (a) state of charge levels of all EV categories, (b) total degradation cost, (c) EV owner revenue from the V2G technology and (d) resultant load profile.

5.3.5.3 Case Study 3: Parking for a 1-h Interval Time

In Case 3, we assumed that all EVs would only park for 1 hr across the day from 13:00 to 14:00. The required EVs for each category to participate are stated in Table 5-6.

The SOC level is introduced in Figure 5-15-a where EV categories 1 and 3 reached 60% of the SOC. However, EV category 2 reached 48% of the SOC in Scenario 1 and 41% of the SOC in Scenario 2. The battery degradation cost was investigated for each EV category, as shown in Figure 5-15-b, where the degradation cost decreased by 28.05%, 82.04% and 36.41% for EV categories 1, 2, and 3, respectively. The profit for each EV category owner is expressed in Figure 5-15-c. It concluded that the EVs would be charged with an incentive revenue from the grid. EV category 2 discharged by approx. 2% and 9% for Scenario 1 and Scenario 2, respectively, while showing a profit of 9.3029 LE and 48.0133 LE, respectively, to compensate

Chapter 5

for the power deficiency in the utility grid. Figure 5-15-d reveals the effectiveness of the GA in tracing the aggregator's constrained objective function to minimize the load demand to 1400 kW where the power reduction reached approx. 26.5%.

Table 5-6 The V2G/G2V output summary of the 3rd case study.

	Scenario 1 Time: 13:00 to 14:00	Scenario 2 Time: 13:00 to 14:00
Number of EVs (EVs)		
EV-1	1	1
EV-2	277	52
EV-3	3	1
Final SOC (%)		
EV-1	60.23%	60.33%
EV-2	48.26%	41.01%
EV-3	60.39%	63.78%
Degradation Cost (LE)		
EV-1	4.6919 LE	6.5213 LE
EV-2	0.3471 LE	1.9322 LE
EV-3	4.9929 LE	7.8514 LE
EV owner Profit (LE)		
EV-1	0.0006 LE	0.0036 LE
EV-2	9.3029 LE	48.0133 LE
EV-3	0.0011 LE	2.8661 LE

Chapter 5

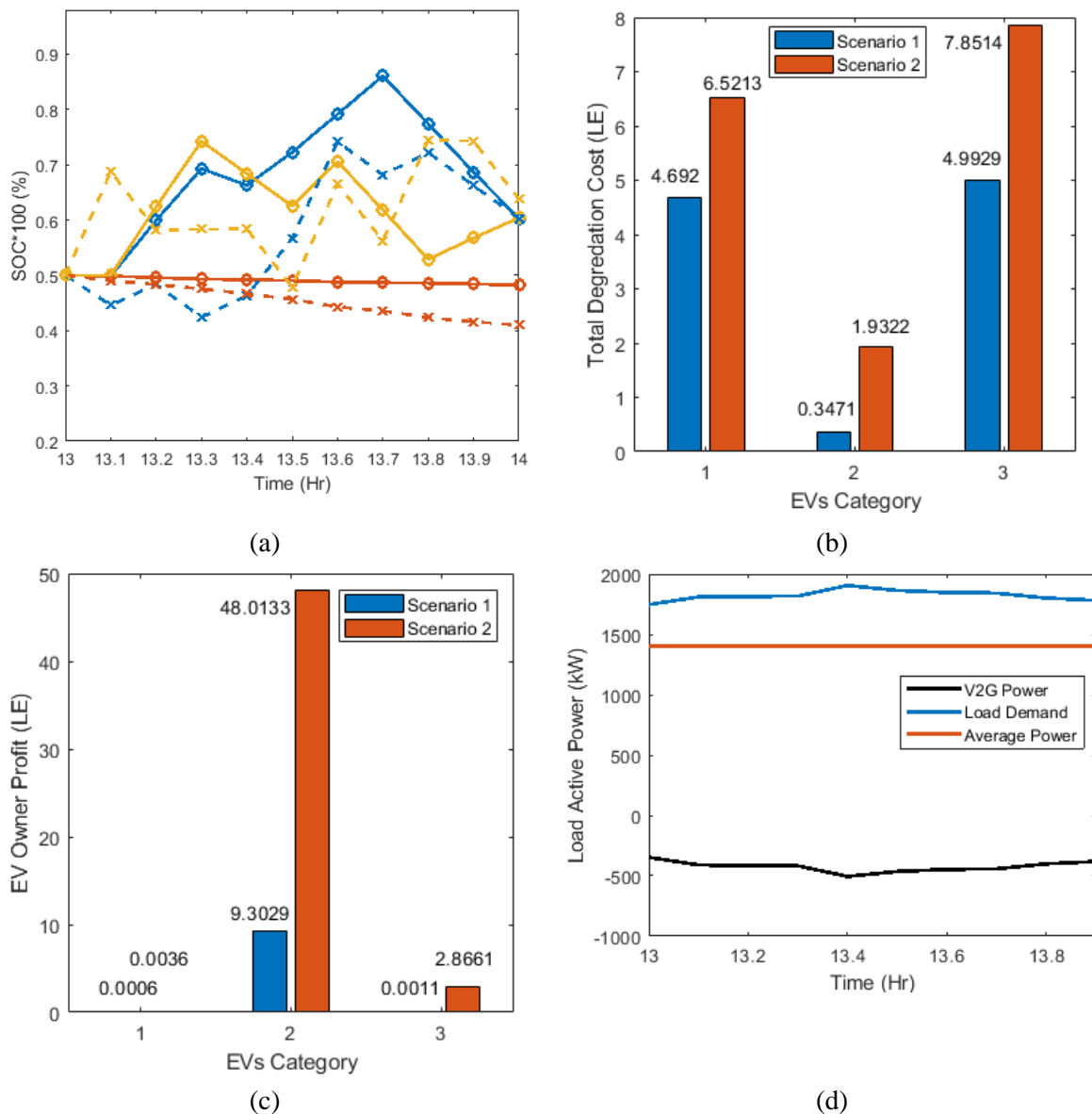


Figure 5-15 Framework outputs while parking for 1 h interval time for both scenarios (a) state of charge levels of all EV categories, (b) total degradation cost, (c) EV owner revenue from the V2G technology and (d) resultant load profile.

The investigated cases charged the EVs with minimum battery degradation cost and maximum EV owner revenue and minimized the peak load profile to reach the required average power of the utility grid throughout the day. In addition, the results obtained in this thesis ensured the applicability of utilizing the proposed methodology for any EV model with different specifications and brands.

5.4 Chapter Summary

This chapter proposed a novel role for the aggregators by utilizing the Grid-to-Vehicle (G2V) and Vehicle-to-Grid (V2G) technologies. Firstly, a novel hierarchical framework model for electric vehicle charging station (EVCS) aggregators has been introduced. The model is responsible for achieving a high EVCS revenue and minimum charging tariff while balancing

Chapter 5

the generated and consumed powers during the fast-charging process. The balancing issue has been solved without using any electrical energy storage system (ESS) or extra batteries or using the discharging capability of the EV itself (V2G) or demand side management (DSM) which is considered a suitable solution for automobile electrification in developing countries. In addition, the maximum profit of the station is obtained without using the ToU pricing method or any BESS. The main contributions of this chapter are represented by the hierarchical roles of the aggregators, which could be summarized in the following points.

- a) The upper stage is organizing and scheduling the EVs while entering the station during the day using mixed integer linear programming (MILP) to satisfy the balance between the generated and consumed powers. The proposed methodology is based on selecting an appropriate and accurate time to plug in the electric vehicle to be fully charged (94% SOC) according to the specification of the battery to ensure the satisfaction of the driver.
- b) Minimizing the peak load demand occurred due to the DC fast charging and consequently flattening the difference between the power generated from the RESs and power consumed by the EVCS. As the peak demand is reduced, the generation capacity of the RESs and utility grid will not be overstretched, and system stability would be improved. The MILP has been implemented and effectively reduced the peak load demand by 3.31% (4.5 kW) and increased the load factor (LF) by 3.1276% with respect to the standard operation.
- c) The second stage is maximizing the profit of the DC fast-charging electric vehicle station while minimizing the EVs' charging tariff which is considered a conflicting objective function using the manoeuvring capability of the switches between the renewable energy sources and the utility grid. The status of each switch is perfectly predetermined using the Markov decision process reinforcement learning technique (MDP-RL) and compared with MILP and traditional operation. The EVCS revenue has increased by 28.88% and 20.1% and the EV charging tariff increased by 21.19% and 15.03% using the MILP and MDP-RL, respectively with respect to the standard operation.

To increase the controllability of load shaving, the V2G technology has been investigated throughout the stochastic EVs parking operations. Three main EV categories were used in the charging and discharging process. The integration between the EVs and the utility grid achieved the balance of energy production and consumption to charge the EVs while shaving the load demand to reduce the pressure on the utility grid. The proposed approaches could be used throughout the day including for commercial and residential hours. The main challenge was designing a framework based on the Genetic Algorithm (GA) that dealt with the initial SOC, arrival and departure time, charging and discharging required power, degradation effect, and G2V/V2G technology impact. The battery degradation cost for each EV category was minimized by 40.93%, 44.18% and 42.544% in the 1st case study, 11.18%, 20.29% and 15.42% in the 2nd case study and 28.05%, 82.04% and 36.41% in the 3rd case study compared with the standard operation. In addition, the model effectively minimized the load demand by 17.125%,

Chapter 5

16.7718%, and 26.5% (371 kW) for the three case studies, respectively to reach the average power of the utility grid throughout the day.

Chapter 6

Conclusions, Major Findings, Recommendations, and Future Work

5.1. Conclusion

This thesis presented the development of an EV charging protocol using AI for fast charging in a dynamic environment, with a focus on vehicle-to-grid integration. A smart and effective charging framework is proposed, starting from connecting the plug-in EV (PEV) to the charging pile in the charging stations, or any parking lot equipped with EV chargers until the PEV is fully charged at different ambient conditions (temperature and relative humidity). PEV is represented by small-scale lithium-polymer ion batteries of a single cell 1000 mAh and a battery pack of 2200 mAh. In the first stage, the temperature or/and relative humidity impact on the charging process has been investigated experimentally. It is concluded that temperature accompanied by the relative humidity has a huge impact on the charging process. It is observed that whenever the relative humidity increased while fixing the temperature the total charging time increased by almost 23.54%. Besides, whenever the temperature is increased while fixing the relative humidity the total charging interval time is increased by almost 3.73%. Hence, any variance in the ambient conditions results in a change in the electrical charging parameters. The classification, recognition, estimation, and identification stages are considered mandatory fast-charging processes. In this thesis, the feedforward back-propagation neural networks (FFBP-NN) algorithm is implemented to classify and recognise the EV capacity, temperature, and relative humidity where the accuracy for the overall network reached 83.2%. This was followed by an accurate estimation of the charging parameters using the constant current-constant voltage (CC-CV) protocol at the corresponding temperature and relative humidity based on the FFBP-NN. The percentage of error at this stage between the simulated and the experimental results reached 1%, which is acceptable to the battery specifications. Then, an efficient identification model of the battery dynamic behaviour is obtained using the Hammerstein-Wiener (HW) nonlinear black box model with an error of 1.19%.

Novel optimization techniques based on the multi-stage charging current (MSCC) charging protocol using the Cuckoo Optimization Algorithm (COA) are proposed and compared with the constant current-constant voltage (CC-CV) charging protocol. COA was implemented on an objective function that is used for the fast charging of the lithium-ion polymer battery of 1000 mAh to minimize the charging interval time and energy loss while maximizing the charging efficiency. The proposed algorithm was applied to a dynamic mathematical model based on the RC second-order transient equivalent circuit. A comparison between the two implemented techniques based on the MSCC protocol and CC-CV protocol was performed yielding the following results: 1) Hierarchical Technique (HT) reached its full capacity (0 to 100% SOC), causing a reduction in both the charging interval time and energy loss by 18.1% and 7.783%, respectively and improved the efficiency by 8 %, 2) Conditional Random Technique (CRT) reached its full capacity (0 to 100% SOC), caused a reduction in both the charging interval time and energy loss by 22.45% and 10.408%, respectively and improved the

Chapter 6

efficiency by 14.1%. The maximum error between the proposed simulation model and the experimental work is 2.3%. The proposed techniques proved that whenever the weight of energy loss or charging interval time is changed, new currents and interval times will be regenerated to optimize the fitness function. The CRT ensured optimum charging interval time, efficiency, and minimum energy loss concerning the conventional CC-CV charging protocol.

To implement the CC-CV and MSCC protocols, a new artificial intelligence charging controller for the PV standalone off-board plug-in EVs is proposed. The charging point was controlled by the neural network predictive controller (NNPC) integrated with the long short-term memory network model (LSTM), which was applied to the DC-DC buck converters. In comparison to the conventional PID control and fuzzy logic controller (FLC), the NNPC-LSTM revealed better dynamic performance and robustness in various aspects. The NNPC-LSTM ensured high stability and a high-speed charging response while charging the small-scale lithium-polymer ion battery of 1000 mAh using the CC-CV and MSCC protocols under variable input voltages. The battery terminal voltage ripple and charging current ripple were minimized to reach 1mV and 1mA, respectively. Due to the stochastic behaviour of the PV system, the LSTM method was used with two main roles. The first role was training the NNPC with the predicted PV output power based on a set of offline data. The second role was estimating the characteristics of the charging process to make sure that the PV output power fulfilled the requirement of the process; otherwise, the system must be supplied from another source during a shortage of PV power. The root mean square error (RMSE) obtained from using the LSTM reached 5.0495. The simulated and experimental investigation confirmed that the NNPC integrated with the LSTM model could track the predetermined reference and maintain the stability of the process under any condition. The proposed controller could be extended and implemented on any DC-DC converter since the state-space model of the converter exists. In addition, the NNPC-LSTM could be scaled up and used for charging large-capacity lithium-ion batteries.

The impact of the EVs charging schemes on the utility grid is investigated and novel techno-economic scenarios and case studies are implemented. This thesis emphasized the vital role of the aggregator which is considered the direct interface between EVs and the utility grid. A novel smart techno-economic operation of the electric vehicle charging station (EVCS) in Egypt is implemented and controlled by the aggregator based on a hierarchal model. Egypt is considered a prime strategic location for renewable energy projects due to the sunny weather and high wind speed. The upper stage of the model is ensuring the balance between the generated power from the renewable energy sources (RESs) and the consumed power from the EVCS due to the fast DC charging of EVs. It has been implemented throughout organizing and scheduling the EVs while entering the station during the day. The second stage is maximizing the EVCS profit and minimizing the EVs tariff however, it is challenging as both objectives conflict with each other. The mixed integer linear programming (MILP) is used in the upper model and reduced the consumed power by 4.5 kW. As the peak demand is reduced, the generation capacity of the RESs and grid will not be overstretched, and system stability would be improved. In the second model, the MILP and Markov decision process reinforcement learning (MDP-RL) have maximized the profit by 28.88% and 20.10.54%, respectively.

Chapter 6

However, an increase in the EVs charging tariff is obtained of 21.19.739%, and 15.03%, respectively. Hence, the MDP-RL is considered more convenient to satisfy a moderate balance between the EV charging tariff and EVCS revenue.

In addition, a novel and robust central aggregator hierarchical optimization algorithm based on the genetic algorithm (GA) was investigated to alleviate the utility grid load demand using the V2G technology. The proposed algorithm has been implemented throughout the stochastic EV parking operation. The model minimized the battery degradation cost and maximized the EV owner profit by selecting the number of EVs that would participate in the V2G and G2V technologies to shave the load demand of the utility grid. Two scenarios were stated and compared to each other. The first scenario combined the degradation effect while the second scenario ignored the degradation cost of the battery. Three types of EV categories were assumed to penetrate the grid based on three case studies depending on the parking period. The model based on the GA effectively minimized the load demand by 26.5% (371 kW) to reach the average power of the utility grid throughout the day while minimizing the battery degradation cost by 82.04% compared with the standard operation. Hence, it is recommended to utilize the integration between the EVs stochastic parking with the utility grid.

5.2. Recommendations and future work

This research could be further extended through the following main bullets:

- Investigating and implementing the neural network recognition and classification algorithms using different scaled-up lithium-ion battery modules which are in the automobile market (such as Nissan, Tesla, Mustang, BYD, SAIC, BMW, and Porsche) at various operating ambient conditions (temperature and relative humidity).
- Virtual representation of the EV dynamic behaviour using the Digital Twins model throughout utilizing electrical and electro-mechanical sensors to identify and model the EV under different ambient circumstances.
- Fast charging the EV using the wireless charging methodology not only at the charging piles or stations but across all the roads to improve the charging time while minimizing the energy loss and eliminating eddy current. This could be complemented by controlling the alignment of the sending and receiving coils while moving. In addition, the cycle life of wireless charging should be compared with the conventional conductive charging protocols.
- Investigating the impact of the temperature and relative humidity conditions on the EV wireless charging and the EV powertrain where the charging operating ambient conditions change from country to country even across the day in the same place.
- Investigating the EVs' ability to stabilize the deficiency of the utility grid voltage, power and frequency using the V2G and G2V technologies by controlling the EVs' reactive power. This could be implemented using a smart bidirectional charging inverter in the electric vehicle charging station or private homes.

References

- [1] J. A. Sanguesa, V. Torres-Sanz, P. Garrido, F. J. Martinez, and J. M. Marquez-Barja, "A review on electric vehicles: Technologies and challenges," *Smart Cities*, vol. 4, no. 1, pp. 372-404, 2021. <https://doi.org/10.3390/smartcities4010022>
- [2] Y. Motoaki, W. Yi, and S. Salisbury, "Empirical analysis of electric vehicle fast charging under cold temperatures," *Energy Policy*, vol. 122, pp. 162-168, 2018. <https://doi.org/10.1016/j.enpol.2018.07.036>
- [3] F. Leng, C. M. Tan, and M. Pecht, "Effect of temperature on the aging rate of Li ion battery operating above room temperature," *Scientific reports*, vol. 5, no. 1, pp. 1-12, 2015. <https://doi.org/10.1038/srep12967>
- [4] M. Bayati, M. Abedi, M. Farahmandrad, G. B. Gharehpetian, and K. Tehrani, "Important Technical Considerations in Design of Battery Chargers of Electric Vehicles," *Energies*, vol. 14, no. 18, p. 5878, 2021. <https://doi.org/10.3390/en14185878>
- [5] B. Bibak and H. Tekiner-Moğulkoç, "A comprehensive analysis of Vehicle to Grid (V2G) systems and scholarly literature on the application of such systems," *Renewable Energy Focus*, vol. 36, pp. 1-20, 2021. <https://doi.org/10.1016/j.ref.2020.10.001>
- [6] Y. Zhou and X. Li, "Vehicle to grid technology: A review," in *2015 34th Chinese Control Conference (CCC)*, 2015: IEEE, pp. 9031-9036. <https://doi.org/10.1109/ChiCC.2015.7261068>
- [7] A. Khaksari, G. Tsaousoglou, P. Makris, K. Steriotis, N. Efthymiopoulos, and E. Varvarigos, "Sizing of electric vehicle charging stations with smart charging capabilities and quality of service requirements," *Sustainable Cities and Society*, vol. 70, p. 102872, 2021. <https://doi.org/10.1016/j.scs.2021.102872>
- [8] International Energy Agency (IEA), "Global EV Outlook 2021", <https://www.iea.org/reports/global-ev-outlook-2021>, May 2021.
- [9] M. Yilmaz and P. T. Krein, "Review of battery charger topologies, charging power levels, and infrastructure for plug-in electric and hybrid vehicles," *IEEE transactions on Power Electronics*, vol. 28, no. 5, pp. 2151-2169, 2012. <https://doi.org/10.1109/TPEL.2012.2212917>
- [10] C. Z. El-Bayeh, K. Alzaareer, A.-M. I. Aldaoudeyeh, B. Brahmi, and M. Zellagui, "Charging and discharging strategies of electric vehicles: A survey," *World Electric Vehicle Journal*, vol. 12, no. 1, p. 11, 2021. <https://doi.org/10.3390/wevj12010011>
- [11] M. R. Khalid, M. S. Alam, A. Sarwar, and M. J. Asghar, "A Comprehensive review on electric vehicles charging infrastructures and their impacts on power-quality of the utility grid," *ETransportation*, vol. 1, p. 100006, 2019. <https://doi.org/10.1016/j.etrans.2019.100006>
- [12] M. Muthukumar, N. Rengarajan, B. Velliyangiri, M. Omprakas, C. Rohit, and U. K. Raja, "The development of fuel cell electric vehicles—A review," *Materials Today: Proceedings*, vol. 45, pp. 1181-1187, 2021. <https://doi.org/10.1016/j.matpr.2020.03.679>

References

- [13] M. Nour, J. P. Chaves-Ávila, G. Magdy, and Á. Sánchez-Miralles, "Review of positive and negative impacts of electric vehicles charging on electric power systems," *Energies*, vol. 13, no. 18, p. 4675, 2020. <https://doi.org/10.3390/en13184675>
- [14] T. Chen, XP. Zhang, J. Wang, J. Li, C. Wu, M. Hu, H. Bian, "A review on electric vehicle charging infrastructure development in the UK," *Journal of Modern Power Systems and Clean Energy*, vol. 8, no. 2, pp. 193-205, 2020. <https://doi.org/10.35833/MPCE.2018.000374>
- [15] M. Guarnieri, "Looking back to electric cars," in *2012 Third IEEE HISTory of ELection-technology CONference (HISTELCON)*, 2012: IEEE, pp. 1-6. <https://doi.org/10.1109/HISTELCON.2012.6487583>
- [16] S. General Requirements; Standard; IEC: Geneva, 2014., "Plugs, Socket-Outlets, Vehicle Couplers and Vehicle Inlets—Conductive Charging of Electric Vehicles—Part 1," *International Electrotechnical Commission.*, 2014.
- [17] P. SAE International: Warrendale, USA, 2009., " Vehicle Architecture for Data Communications Standards—Class B Data Communications Network Interface; Standard," *SAE International*, 2009.
- [18] H. Shareef, M. M. Islam, and A. Mohamed, "A review of the stage-of-the-art charging technologies, placement methodologies, and impacts of electric vehicles," *Renewable and Sustainable Energy Reviews*, vol. 64, pp. 403-420, 2016. <https://doi.org/10.1016/j.rser.2016.06.033>
- [19] H. Das, M. Rahman, S. Li, and C. Tan, "Electric vehicles standards, charging infrastructure, and impact on grid integration: A technological review," *Renewable and Sustainable Energy Reviews*, vol. 120, p. 109618, 2020. <https://doi.org/10.1016/j.rser.2019.109618>
- [20] K. K. Duru, C. Karra, P. Venkatachalam, S. A. Betha, A. A. Madhavan, and S. Kalluri, "Critical Insights Into Fast Charging Techniques for Lithium-Ion Batteries in Electric Vehicles," *IEEE Transactions on Device and Materials Reliability*, vol. 21, no. 1, pp. 137-152, 2021. <https://doi.org/10.1109/TDMR.2021.3051840>
- [21] E. Ucer, I. Koyuncu, M. C. Kisacikoglu, M. Yavuz, A. Meintz, and C. Rames, "Modeling and analysis of a fast charging station and evaluation of service quality for electric vehicles," *IEEE Transactions on Transportation Electrification*, vol. 5, no. 1, pp. 215-225, 2019. <https://doi.org/10.1109/TTE.2019.2897088>
- [22] H. Tu, H. Feng, S. Srdic, and S. Lukic, "Extreme fast charging of electric vehicles: A technology overview," *IEEE Transactions on Transportation Electrification*, vol. 5, no. 4, pp. 861-878, 2019. <https://doi.org/10.1109/TTE.2019.2958709>
- [23] Y. Yang, M. El Baghdadi, Y. Lan, Y. Benomar, J. Van Mierlo, and O. Hegazy, "Design methodology, modeling, and comparative study of wireless power transfer systems for electric vehicles," *Energies*, vol. 11, no. 7, p. 1716, 2018. <https://doi.org/10.3390/en11071716>
- [24] N. Mohamed, F. Aymen, M. Alqarni, R.A. Turky, B. Alamri, ZM. Ali, SH. Aleem, "A new wireless charging system for electric vehicles using two receiver coils," *Ain Shams Engineering Journal*, 2021. <https://doi.org/10.1016/j.asej.2021.08.012>

References

- [25] H. Wu, "A Survey of Battery Swapping Stations for Electric Vehicles: Operation Modes and Decision Scenarios," *IEEE Transactions on Intelligent Transportation Systems*, 2021. <https://doi.org/10.1109/TITS.2021.3125861>
- [26] M. R. Sarker, H. Pandžić, and M. A. Ortega-Vazquez, "Optimal operation and services scheduling for an electric vehicle battery swapping station," *IEEE transactions on power systems*, vol. 30, no. 2, pp. 901-910, 2014. <https://doi.org/10.1109/TPWRS.2014.2331560>
- [27] T. M. D. o. E. Resources, "INSTALLATION GUIDE FOR ELECTRIC VEHICLE SUPPLY EQUIPMENT (EVSE)," June, 2014. <https://www.mass.gov/doc/electric-vehicle-charging-infrastructure-manual/download>
- [28] M. Knez, G. K. Zevnik, and M. Obrecht, "A review of available chargers for electric vehicles: United States of America, European Union, and Asia," *Renewable and Sustainable Energy Reviews*, vol. 109, pp. 284-293, 2019. <https://doi.org/10.1016/j.rser.2019.04.013>
- [29] S. Manzetti and F. Mariasiu, "Electric vehicle battery technologies: From present state to future systems," *Renewable and Sustainable Energy Reviews*, vol. 51, pp. 1004-1012, 2015. <https://doi.org/10.1016/j.rser.2015.07.010>
- [30] M. A. Hannan, M. M. Hoque, A. Hussain, Y. Yusof, and P. J. Ker, "State-of-the-art and energy management system of lithium-ion batteries in electric vehicle applications: Issues and recommendations," *Ieee Access*, vol. 6, pp. 19362-19378, 2018. <https://doi.org/10.1109/ACCESS.2018.2817655>
- [31] T. Waldmann, M. Wilka, M. Kasper, M. Fleischhammer, and M. Wohlfahrt-Mehrens, "Temperature dependent ageing mechanisms in Lithium-ion batteries—A Post-Mortem study," *Journal of Power Sources*, vol. 262, pp. 129-135, 2014. <https://doi.org/10.1016/j.jpowsour.2014.03.112>
- [32] H. Wu, X. Zhang, R. Cao, and C. Yang, "An investigation on electrical and thermal characteristics of cylindrical lithium-ion batteries at low temperatures," *Energy*, vol. 225, p. 120223, 2021. <https://doi.org/10.1016/j.energy.2021.120223>
- [33] J. Jagemont, L. Boulon, and Y. Dubé, "Characterization and modeling of a hybrid-electric-vehicle lithium-ion battery pack at low temperatures," *IEEE Transactions on Vehicular Technology*, vol. 65, no. 1, pp. 1-14, 2015. <https://doi.org/10.1109/TVT.2015.2391053>
- [34] C. Wu, C. Zhu, Y. Ge, and Y. Zhao, "A review on fault mechanism and diagnosis approach for Li-ion batteries," *Journal of Nanomaterials*, vol. 2015, 2015. <https://doi.org/10.1155/2015/631263>
- [35] D. Belov and M.-H. Yang, "Failure mechanism of Li-ion battery at overcharge conditions," *Journal of Solid State Electrochemistry*, vol. 12, no. 7-8, pp. 885-894, 2008. <https://doi.org/10.1007/s10008-007-0449-3>
- [36] N. Wassiliadis, J. Schneider, A. Frank, L. Wildfeuer, X. Liu, A. Jossen, M. Lienkamp, "Review of fast charging strategies for lithium-ion battery systems and their applicability for battery electric vehicles," *Journal of Energy Storage*, vol. 44, p. 103306, 2021. <https://doi.org/10.1016/j.est.2021.103306>

References

- [37] Y. Gao, X. Zhang, Q. Cheng, B. Guo, and J. Yang, "Classification and review of the charging strategies for commercial lithium-ion batteries," *IEEE Access*, vol. 7, pp. 43511-43524, 2019. <https://doi.org/10.1109/ACCESS.2019.2906117>
- [38] C. Chen, Z. Wei, and A. C. Knoll, "Charging Optimization for Li-ion Battery in Electric Vehicles: A Review," *IEEE Transactions on Transportation Electrification*, 2021. <https://doi.org/10.1109/TTE.2021.3135525>
- [39] Y. Miao, P. Hynan, A. Von Jouanne, and A. Yokochi, "Current Li-ion battery technologies in electric vehicles and opportunities for advancements," *Energies*, vol. 12, no. 6, p. 1074, 2019. <https://doi.org/10.3390/en12061074>
- [40] S. Chen, N. Bao, A. Garg, X. Peng, and L. Gao, "A fast charging-cooling coupled scheduling method for a liquid cooling-based thermal management system for Lithium-ion batteries," *Engineering*, vol. 7, no. 8, pp. 1165-1176, 2021. <https://doi.org/10.1016/j.eng.2020.06.016>
- [41] Y. Ding, Z. P. Cano, A. Yu, J. Lu, and Z. Chen, "Automotive Li-ion batteries: current status and future perspectives," *Electrochemical Energy Reviews*, vol. 2, no. 1, pp. 1-28, 2019. <https://doi.org/10.1007/s41918-018-0022-z>
- [42] Z. Guo, B. Y. Liaw, X. Qiu, L. Gao, and C. Zhang, "Optimal charging method for lithium ion batteries using a universal voltage protocol accommodating aging," *Journal of Power Sources*, vol. 274, pp. 957-964, 2015. <https://doi.org/10.1016/j.jpowsour.2014.10.185>
- [43] P. Keil and A. Jossen, "Charging protocols for lithium-ion batteries and their impact on cycle life—An experimental study with different 18650 high-power cells," *Journal of Energy Storage*, vol. 6, pp. 125-141, 2016. <https://doi.org/10.1016/j.est.2016.02.005>
- [44] S. Sachan, S. Deb, and S. N. Singh, "Different charging infrastructures along with smart charging strategies for electric vehicles," *Sustainable Cities and Society*, vol. 60, p. 102238, 2020. <https://doi.org/10.1016/j.scs.2020.102238>
- [45] S. Tamilselvi, S. Gunasundari, N. Karuppiyah, RK. Razak, S. Madhusudan, VM. Nagarajan, T. Sathish, MZ. Shamim, CA. Saleel, A. Afzal, "A Review on Battery Modelling Techniques," *Sustainability*, vol. 13, no. 18, p. 10042, 2021. <https://doi.org/10.3390/su131810042>
- [46] J. Khalfi, N. Boumaaz, A. Soulmani, and E. M. Laadissi, "Nonlinear Modeling of Lithium-Ion Battery Cells for Electric Vehicles using a Hammerstein–Wiener Model," *Journal of Electrical Engineering & Technology*, vol. 16, no. 2, pp. 659-669, 2021. <https://doi.org/10.1007/s42835-020-00607-2>
- [47] A. Seaman, T.-S. Dao, and J. McPhee, "A survey of mathematics-based equivalent-circuit and electrochemical battery models for hybrid and electric vehicle simulation," *Journal of Power Sources*, vol. 256, pp. 410-423, 2014. <https://doi.org/10.1016/j.jpowsour.2014.01.057>
- [48] S. Li, J. Li, H. He, and H. Wang, "Lithium-ion battery modeling based on Big Data," *Energy Procedia*, vol. 159, pp. 168-173, 2019. <https://doi.org/10.1016/j.egypro.2018.12.046>

References

- [49] R. Mehta and A. Gupta, "An improved single-particle model with electrolyte dynamics for high current applications of lithium-ion cells," *Electrochimica Acta*, vol. 389, p. 138623, 2021. <https://doi.org/10.1016/j.electacta.2021.138623>
- [50] J. Tian, Y. Wang, and Z. Chen, "An improved single particle model for lithium-ion batteries based on main stress factor compensation," *Journal of Cleaner Production*, vol. 278, p. 123456, 2021. <https://doi.org/10.1016/j.jclepro.2020.123456>
- [51] F. An, W. Zhou, and P. Li, "A comparison of model prediction from P2D and particle packing with experiment," *Electrochimica Acta*, vol. 370, p. 137775, 2021. <https://doi.org/10.1016/j.electacta.2021.137775>
- [52] R. Bermejo, "Numerical analysis of a finite element formulation of the P2D model for Lithium-ion cells," *Numerische Mathematik*, pp. 1-43, 2021. <https://doi.org/10.1007/s00211-021-01235-2>
- [53] F. Zhou and C. Bao, "Analysis of the lithium-ion battery capacity degradation behavior with a comprehensive mathematical model," *Journal of Power Sources*, vol. 515, p. 230630, 2021. <https://doi.org/10.1016/j.jpowsour.2021.230630>
- [54] W. Shuai, E. Li, and H. Wang, "An equivalent circuit model of a deformed Li-ion battery with parameter identification," *International Journal of Energy Research*, vol. 44, no. 11, pp. 8372-8387, 2020. <https://doi.org/10.1002/er.5500>
- [55] X. Zhang, W. Zhang, and G. Lei, "A review of li-ion battery equivalent circuit models," *Trans. Electr. Electron. Mater.*, vol. 17, no. 6, pp. 311-316, 2016. <https://doi.org/10.4313/TEEM.2016.17.6.311>
- [56] T. Grandjean, A. McGordon, and P. Jennings, "Structural identifiability of equivalent circuit models for Li-ion batteries," *Energies*, vol. 10, no. 1, p. 90, 2017. <https://doi.org/10.3390/en10010090>
- [57] J. Vetter, P. Novák, MR. Wagner, C. Veit, KC. Möller, JO. Besenhard, M. Winter, M. Wohlfahrt-Mehrens, C. Vogler, A. Hammouche, "Ageing mechanisms in lithium-ion batteries," *Journal of power sources*, vol. 147, no. 1-2, pp. 269-281, 2005. <https://doi.org/10.1016/j.jpowsour.2005.01.006>
- [58] J. H. Lee, H. M. Lee, and S. Ahn, "Battery dimensional changes occurring during charge/discharge cycles—thin rectangular lithium ion and polymer cells," *Journal of power sources*, vol. 119, pp. 833-837, 2003. [https://doi.org/10.1016/S0378-7753\(03\)00281-7](https://doi.org/10.1016/S0378-7753(03)00281-7)
- [59] I.-H. Cho, P.-Y. Lee, and J.-H. Kim, "Analysis of the effect of the variable charging current control method on cycle life of Li-ion batteries," *Energies*, vol. 12, no. 15, p. 3023, 2019. <https://doi.org/10.3390/en12153023>
- [60] P. Makeen, S. Memon, M. Elkasrawy, S. O. Abdullatif, and H. A. Ghali, "Smart green charging scheme of centralized electric vehicle stations," *International Journal of Green Energy*, pp. 1-9, 2021. <https://doi.org/10.1080/15435075.2021.1947822>
- [61] S. Zhu, C. Hu, Y. Xu, Y. Jin, and J. Shui, "Performance improvement of lithium-ion battery by pulse current," *Journal of Energy Chemistry*, vol. 46, pp. 208-214, 2020. <https://doi.org/10.1016/j.jechem.2019.11.007>

References

- [62] J. M. Amanor-Boadu and A. Guiseppi-Elie, "Improved performance of li-ion polymer batteries through improved pulse charging algorithm," *Applied Sciences*, vol. 10, no. 3, p. 895, 2020. <https://doi.org/10.3390/app10030895>
- [63] Z. Chu, X. Feng, L. Lu, J. Li, X. Han, and M. Ouyang, "Non-destructive fast charging algorithm of lithium-ion batteries based on the control-oriented electrochemical model," *Applied energy*, vol. 204, pp. 1240-1250, 2017. <https://doi.org/10.1016/j.apenergy.2017.03.111>
- [64] P. H. Notten, J. O. het Veld, and J. Van Beek, "Boostcharging Li-ion batteries: A challenging new charging concept," *Journal of Power Sources*, vol. 145, no. 1, pp. 89-94, 2005. <https://doi.org/10.1016/j.jpowsour.2004.12.038>
- [65] A. B. Khan and W. Choi, "Optimal charge pattern for the high-performance multistage constant current charge method for the li-ion batteries," *IEEE transactions on energy conversion*, vol. 33, no. 3, pp. 1132-1140, 2018. <https://doi.org/10.1109/TEC.2018.2801381>
- [66] C.-L. Liu, S.-C. Wang, Y.-H. Liu, and M.-C. Tsai, "An optimum fast charging pattern search for Li-ion batteries using particle swarm optimization," in *The 6th International Conference on Soft Computing and Intelligent Systems, and The 13th International Symposium on Advanced Intelligence Systems*, 2012: IEEE, pp. 727-732. <https://doi.org/10.1109/SCIS-ISIS.2012.6505335>
- [67] H. Min, W. Sun, X. Li, D. Guo, Y. Yu, T. Zhu, Z. Zhao, "Research on the optimal charging strategy for Li-ion batteries based on multi-objective optimization," *Energies*, vol. 10, no. 5, p. 709, 2017. <https://doi.org/10.3390/en10050709>
- [68] L. Zhang, H. Peng, Z. Ning, Z. Mu, and C. Sun, "Comparative research on RC equivalent circuit models for lithium-ion batteries of electric vehicles," *Applied Sciences*, vol. 7, no. 10, p. 1002, 2017. <https://doi.org/10.3390/app7101002>
- [69] C. Zhang, K. Li, S. Mcloone, and Z. Yang, "Battery modelling methods for electric vehicles-A review," in *2014 European Control Conference (ECC)*, 2014: IEEE, pp. 2673-2678. <https://doi.org/10.1109/ECC.2014.6862541>
- [70] F. M. González-Longatt, "Circuit based battery models: A review," in *Proceedings of 2nd Congreso Iberoamericano De Estudiantes de Ingenieria Electrica, Puerto la Cruz, Venezuela*, 2006.
- [71] Z. Haizhou, "Modeling of Lithium-ion Battery for Charging/Discharging Characteristics Based on Circuit Model," *International Journal of Online Engineering*, vol. 13, no. 6, 2017.
- [72] S. Lin, H. Zhao, and A. Burke, "A first-order transient response model for lithium-ion batteries of various chemistries: Test data and model validation," *UC Davis: Institute of Transportation Studies*. 2012. <https://escholarship.org/uc/item/8z95w488>.
- [73] R. Mathieu, O. Briat, P. Gyan, and J.-M. Vinassa, "Fast charging for electric vehicles applications: Numerical optimization of a multi-stage charging protocol for lithium-ion battery and impact on cycle life," *Journal of Energy Storage*, vol. 40, p. 102756, 2021. <https://doi.org/10.1016/j.est.2021.102756>

References

- [74] G.-J. Chen, Y.-H. Liu, S.-C. Wang, Y.-F. Luo, and Z.-Z. Yang, "Searching for the optimal current pattern based on grey wolf optimizer and equivalent circuit model of Li-ion batteries," *Journal of Energy Storage*, vol. 33, p. 101933, 2021. <https://doi.org/10.1016/j.est.2020.101933>
- [75] Y. Li, K. Li, Y. Xie, J. Liu, C. Fu, and B. Liu, "Optimized charging of lithium-ion battery for electric vehicles: Adaptive multistage constant current–constant voltage charging strategy," *Renewable Energy*, vol. 146, pp. 2688-2699, 2020. <https://doi.org/10.1016/j.renene.2019.08.077>
- [76] X. Hu, Y. Zheng, X. Lin, and Y. Xie, "Optimal multistage charging of NCA/graphite lithium-ion batteries based on electrothermal-aging dynamics," *IEEE Transactions on Transportation Electrification*, vol. 6, no. 2, pp. 427-438, 2020. <https://doi.org/10.1109/TTE.2020.2977092>
- [77] L. Jiang, Y. Li, Y. Huang, J. Yu, X. Qiao, Y. Wang, C. Huang, Y. Cao, "Optimization of multi-stage constant current charging pattern based on Taguchi method for Li-Ion battery," *Applied Energy*, vol. 259, p. 114148, 2020.
- [78] C.-H. Lee, T.-W. Chang, S.-H. Hsu, and J.-A. Jiang, "Taguchi-based PSO for searching an optimal four-stage charge pattern of Li-ion batteries," *Journal of Energy Storage*, vol. 21, pp. 301-309, 2019. <https://doi.org/10.1016/j.est.2018.11.031>
- [79] J. Sun, Q. Ma, R. Liu, T. Wang, and C. Tang, "A novel multiobjective charging optimization method of power lithium-ion batteries based on charging time and temperature rise," *International Journal of Energy Research*, vol. 43, no. 13, pp. 7672-7681, 2019. <https://doi.org/10.1002/er.4727>
- [80] S.-S. Yun and S.-C. Kee, "Improved Multilevel Multistage Constant-Current Constant-Voltage Superfast Charging of Multiple Cells," *Journal of Electrical Engineering & Technology*, pp. 1-11, 2021. <https://doi.org/10.1007/s42835-021-00896-1>
- [81] S. U. Jeon, J.-W. Park, B.-K. Kang, and H.-J. Lee, "Study on Battery Charging Strategy of Electric Vehicles Considering Battery Capacity," *IEEE Access*, 2021. <https://doi.org/10.1109/ACCESS.2021.3090763>
- [82] A. Tomaszewska, Z. Chu, X. Feng, S. O'kane, X. Liu, J. Chen, C. Ji, E. Endler, R. Li, L. Liu, Y. Li, "Lithium-ion battery fast charging: A review," *ETransportation*, vol. 1, p. 100011, 2019. <https://doi.org/10.1016/j.etrans.2019.100011>
- [83] L. Patnaik, A. Praneeth, and S. S. Williamson, "A closed-loop constant-temperature constant-voltage charging technique to reduce charge time of lithium-ion batteries," *IEEE Transactions on Industrial Electronics*, vol. 66, no. 2, pp. 1059-1067, 2018. <https://doi.org/10.1109/TIE.2018.2833038>
- [84] P. Nambisan, P. Saha, and M. Khanra, "Real-time optimal fast charging of Li-ion batteries with varying temperature and charging behaviour constraints," *Journal of Energy Storage*, vol. 41, p. 102918, 2021. <https://doi.org/10.1016/j.est.2021.102918>
- [85] Z. Chen, X. Shu, R. Xiao, W. Yan, Y. Liu, and J. Shen, "Optimal charging strategy design for lithium-ion batteries considering minimization of temperature rise and

References

- energy loss," *International Journal of Energy Research*, vol. 43, no. 9, pp. 4344-4358, 2019. <https://doi.org/10.1002/er.4560>
- [86] M. Xu, R. Wang, B. Reichman, and X. Wang, "Modeling the effect of two-stage fast charging protocol on thermal behavior and charging energy efficiency of lithium-ion batteries," *Journal of Energy Storage*, vol. 20, pp. 298-309, 2018. <https://doi.org/10.1016/j.est.2018.09.004>
- [87] D. Ouyang, J. Weng, M. Chen, and J. Wang, "Impact of high-temperature environment on the optimal cycle rate of lithium-ion battery," *Journal of Energy Storage*, vol. 28, p. 101242, 2020. <https://doi.org/10.1016/j.est.2020.101242>
- [88] D. C. Robertson, L. Flores, AR. Dunlop, SE. Trask, FL. Usseglio-Viretta, AM. Colclasure, Z. Yang, I. Bloom, "Effect of Anode Porosity and Temperature on the Performance and Lithium Plating During Fast-Charging of Lithium-Ion Cells," *Energy Technology*, vol. 9, no. 1, p. 2000666, 2021. <https://doi.org/10.1002/ente.202000666>
- [89] D. Ouyang, J. Weng, J. Hu, J. Liu, M. Chen, Q. Huang, J. Wang, "Effect of high temperature circumstance on lithium-ion battery and the application of phase change material," *Journal of The Electrochemical Society*, vol. 166, no. 4, p. A559, 2019. <https://doi.org/10.1149/2.0441904jes>
- [90] C. Zhao, B. Zhang, Y. Zheng, S. Huang, T. Yan, and X. Liu, "Hybrid Battery Thermal Management System in Electrical Vehicles: A Review," *Energies*, vol. 13, no. 23, p. 6257, 2020. <https://doi.org/10.3390/en13236257>
- [91] Y. Yin and S.-Y. Choe, "Actively temperature controlled health-aware fast charging method for lithium-ion battery using nonlinear model predictive control," *Applied Energy*, vol. 271, p. 115232, 2020. <https://doi.org/10.1016/j.apenergy.2020.115232>
- [92] T. Liu, X.-G. Yang, S. Ge, Y. Leng, and C.-Y. Wang, "Ultrafast charging of energy-dense lithium-ion batteries for urban air mobility," *ETransportation*, vol. 7, p. 100103, 2021. <https://doi.org/10.1016/j.etrans.2021.100103>
- [93] M.-T. F. Rodrigues, G. Babu, H. Gullapalli, K. Kalaga, FN. Sayed, K. Kato, J. Joyner, PM. Ajayan, "A materials perspective on Li-ion batteries at extreme temperatures," *nature energy*, vol. 2, no. 8, pp. 1-14, 2017. <https://doi.org/10.1038/nenergy.2017.108>
- [94] Y. Liu, Y. Zhu, and Y. Cui, "Challenges and opportunities towards fast-charging battery materials," *Nature Energy*, vol. 4, no. 7, pp. 540-550, 2019. <https://doi.org/10.1038/s41560-019-0405-3>
- [95] X.-G. Yang, G. Zhang, S. Ge, and C.-Y. Wang, "Fast charging of lithium-ion batteries at all temperatures," *Proceedings of the National Academy of Sciences*, vol. 115, no. 28, pp. 7266-7271, 2018. <https://doi.org/10.1073/pnas.1807115115>
- [96] Z. Li, J. Huang, B. Y. Liaw, V. Metzler, and J. Zhang, "A review of lithium deposition in lithium-ion and lithium metal secondary batteries," *Journal of power sources*, vol. 254, pp. 168-182, 2014. <https://doi.org/10.1016/j.jpowsour.2013.12.099>

References

- [97] T. M. Bandhauer, S. Garimella, and T. F. Fuller, "A critical review of thermal issues in lithium-ion batteries," *Journal of the Electrochemical Society*, vol. 158, no. 3, p. R1, 2011. <https://doi.org/10.1149/1.3515880>
- [98] K. Liu, Y. Liu, D. Lin, A. Pei, and Y. Cui, "Materials for lithium-ion battery safety," *Science advances*, vol. 4, no. 6, p. eaas9820, 2018. <https://doi.org/10.1126/sciadv.aas9820>
- [99] Z. Guo, X. Dong, S. Yuan, Y. Wang, and Y. Xia, "Humidity effect on electrochemical performance of Li–O₂ batteries," *Journal of Power Sources*, vol. 264, pp. 1-7, 2014. <https://doi.org/10.1016/j.jpowsour.2014.04.079>
- [100] Z. Chen, J. Wang, J. Huang, T. Fu, G. Sun, S. Lai, R. Zhou, K. Li, J. Zhao, "The high-temperature and high-humidity storage behaviors and electrochemical degradation mechanism of LiNi_{0.6}Co_{0.2}Mn_{0.2}O₂ cathode material for lithium ion batteries," *Journal of Power Sources*, vol. 363, pp. 168-176, 2017. <https://doi.org/10.1016/j.jpowsour.2017.07.087>
- [101] J. Li, E. Murphy, J. Winnick, and P. A. Kohl, "The effects of pulse charging on cycling characteristics of commercial lithium-ion batteries," *Journal of Power Sources*, vol. 102, no. 1-2, pp. 302-309, 2001. [https://doi.org/10.1016/S0378-7753\(01\)00820-5](https://doi.org/10.1016/S0378-7753(01)00820-5)
- [102] B. Purushothaman and U. Landau, "Rapid charging of lithium-ion batteries using pulsed currents: A theoretical analysis," *Journal of The Electrochemical Society*, vol. 153, no. 3, p. A533, 2006. <https://doi.org/10.1149/1.2161580>
- [103] S. Li, Q. Wu, D. Zhang, Z. Liu, Y. He, ZL Wang, C. Sun, "Effects of pulse charging on the performances of lithium-ion batteries," *Nano Energy*, vol. 56, pp. 555-562, 2019. <https://doi.org/10.1016/j.nanoen.2018.11.070>
- [104] H. Lv, X. Huang, and Y. Liu, "Analysis on pulse charging–discharging strategies for improving capacity retention rates of lithium-ion batteries," *Ionics*, pp. 1-22, 2020. <https://doi.org/10.1007/s11581-019-03404-8>
- [105] S. Bhilai, "Comparative study of P, PI and PID controller for speed control of VSI-fed induction motor". *Int J Eng Dev Res.* 2014;2:2740-4.
- [106] Y. Qin, J. Du, L. Lu, M. Gao, F. Haase, J. Li, M. Ouyang, "A rapid lithium-ion battery heating method based on bidirectional pulsed current: heating effect and impact on battery life," *Applied Energy*, vol. 280, p. 115957, 2020. <https://doi.org/10.1016/j.apenergy.2020.115957>
- [107] C. Qiu, G. He, W. Shi, M. Zou, and C. Liu, "The polarization characteristics of lithium-ion batteries under cyclic charge and discharge," *Journal of Solid State Electrochemistry*, vol. 23, no. 6, pp. 1887-1902, 2019. <https://doi.org/10.1007/s10008-019-04282-w>
- [108] M. Song and S.-Y. Choe, "Fast and safe charging method suppressing side reaction and lithium deposition reaction in lithium ion battery," *Journal of Power Sources*, vol. 436, p. 226835, 2019. <https://doi.org/10.1016/j.jpowsour.2019.226835>
- [109] Y. Zhao, B. Lu, Y. Song, and J. Zhang, "A modified pulse charging method for lithium-ion batteries by considering stress evolution, charging time and capacity

References

- utilization," *Frontiers of Structural and Civil Engineering*, vol. 13, no. 2, pp. 294-302, 2019. <https://doi.org/10.1007/s11709-018-0460-z>
- [110] M. Li, M. Feng, D. Luo, and Z. Chen, "Fast charging Li-ion batteries for a new era of electric vehicles," *Cell Reports Physical Science*, p. 100212, 2020. <https://doi.org/10.1016/j.xcrp.2020.100212>
- [111] M. Weiss, R. Ruess, J. Kasnatscheew, Y. Levartovsky, NR. Levy, P. Minnmann, L. Stolz, T. Waldmann, M. Wohlfahrt-Mehrens, D. Aurbach, M. Winter, "Fast Charging of Lithium-Ion Batteries: A Review of Materials Aspects," *Advanced Energy Materials*, vol. 11, no. 33, p. 2101126, 2021. <https://doi.org/10.1002/aenm.202101126>
- [112] J.-G. Han, MY. Jeong, K. Kim, C. Park, CH. Sung, DW. Bak, KH. Kim, KM. Jeong, NS. Choi, "An electrolyte additive capable of scavenging HF and PF5 enables fast charging of lithium-ion batteries in LiPF6-based electrolytes," *Journal of Power Sources*, vol. 446, p. 227366, 2020. <https://doi.org/10.1016/j.jpowsour.2019.227366>
- [113] A. M. Colclasure, TR. Tanim, AN. Jansen, SE. Trask, AR. Dunlop, BJ. Polzin, I. Bloom, D. Robertson, L. Flores, M. Evans, EJ. Dufek, "Electrode scale and electrolyte transport effects on extreme fast charging of lithium-ion cells," *Electrochimica Acta*, vol. 337, p. 135854, 2020. <https://doi.org/10.1016/j.electacta.2020.135854>
- [114] Z. Du, D. L. Wood III, and I. Belharouak, "Enabling fast charging of high energy density Li-ion cells with high lithium ion transport electrolytes," *Electrochemistry Communications*, vol. 103, pp. 109-113, 2019. <https://doi.org/10.1016/j.elecom.2019.04.013>
- [115] J. B. Habedank, L. Kraft, A. Rheinfeld, C. Krezdorn, A. Jossen, and M. F. Zaeh, "Increasing the discharge rate capability of lithium-ion cells with laser-structured graphite anodes: Modeling and simulation," *Journal of The Electrochemical Society*, vol. 165, no. 7, p. A1563, 2018. <https://doi.org/10.1149/2.1181807jes>
- [116] Y. Zeng, D. Chalise, S. D. Lubner, S. Kaur, and R. S. Prasher, "A review of thermal physics and management inside lithium-ion batteries for high energy density and fast charging," *Energy Storage Materials*, 2021. <https://doi.org/10.1016/j.ensm.2021.06.008>
- [117] W. Cai, YX. Yao, GL. Zhu, C. Yan, LL. Jiang, C. He, JQ. Huang, Q. Zhang, "A review on energy chemistry of fast-charging anodes," *Chemical Society Reviews*, vol. 49, no. 12, pp. 3806-3833, 2020. <https://doi.org/10.1039/C9CS00728H>
- [118] M. Pan, C. Sun, J. Liu, and Y. Wang, "Automatic recognition and location system for electric vehicle charging port in complex environment," *IET Image Processing*, vol. 14, no. 10, pp. 2263-2272, 2020. <https://doi.org/10.1049/iet-ipr.2019.1138>
- [119] X. Peng, S. Chen, A. Garg, N. Bao, and B. Panda, "A review of the estimation and heating methods for lithium-ion batteries pack at the cold environment," *Energy Science & Engineering*, vol. 7, no. 3, pp. 645-662, 2019. <https://doi.org/10.1002/ese3.279>

References

- [120] G. Rajendran, C. A. Vaithilingam, N. Misron, K. Naidu, and M. R. Ahmed, "A comprehensive review on system architecture and international standards for electric vehicle charging stations," *Journal of Energy Storage*, vol. 42, p. 103099, 2021. <https://doi.org/10.1016/j.est.2021.103099>
- [121] P. Barnes, A. Savva, K. Dixon, H. Bull, L. Rill, D. Karsann, S. Croft, J. Schimpf, H. Xiong, "Electropolishing valve metals with a sulfuric acid-methanol electrolyte at low temperature," *Surface and Coatings Technology*, vol. 347, pp. 150-156, 2018. <https://doi.org/10.1016/j.surfcoat.2018.04.082>
- [122] M. Saccoccio, J. Yu, Z. Lu, SC. Kwok, J. Wang, KK. Yeung, MM. Yuen, F. Ciucci, "Low temperature pulsed laser deposition of garnet $\text{Li}_6\text{.4La}_3\text{Zr}_1\text{.4Ta}_0\text{.6O}_{12}$ films as all solid-state lithium battery electrolytes," *Journal of Power Sources*, vol. 365, pp. 43-52, 2017. <https://doi.org/10.1016/j.jpowsour.2017.08.020>
- [123] L. Wang, T. Mei, W. Liu, J. Sun, Q. Zhou, and Y. Qian, "Low temperature chemical synthesis of silicon nanoparticles as anode materials for lithium-ion batteries," *Materials Chemistry and Physics*, vol. 220, pp. 308-312, 2018. <https://doi.org/10.1016/j.matchemphys.2018.08.075>
- [124] G. Xia, L. Cao, and G. Bi, "A review on battery thermal management in electric vehicle application," *Journal of power sources*, vol. 367, pp. 90-105, 2017. <https://doi.org/10.1016/j.jpowsour.2017.09.046>
- [125] M. Ye, H. Gong, R. Xiong, and H. Mu, "Research on the battery charging strategy with charging and temperature rising control awareness," *IEEE Access*, vol. 6, pp. 64193-64201, 2018. <https://doi.org/10.1109/ACCESS.2018.2876359>
- [126] Y. Bao, W. Dong, and D. Wang, "Online internal resistance measurement application in lithium ion battery capacity and state of charge estimation," *Energies*, vol. 11, no. 5, p. 1073, 2018. <https://doi.org/10.3390/en11051073>
- [127] Q. Navid and A. Hassan, "An accurate and precise grey box model of a low-power lithium-ion battery and capacitor/supercapacitor for accurate estimation of state-of-charge," *Batteries*, vol. 5, no. 3, p. 50, 2019. <https://doi.org/10.3390/batteries5030050>
- [128] M. Luzi, F. M. F. Mascioli, M. Paschero, and A. Rizzi, "A white-box equivalent neural network circuit model for SoC estimation of electrochemical cells," *IEEE Transactions on Neural Networks and Learning Systems*, vol. 31, no. 2, pp. 371-382, 2019. <https://doi.org/10.1109/TNNLS.2019.2901062>
- [129] J. Khalfi, N. Boumaaz, A. Soulmani, and E. M. Laadissi, "Box–Jenkins Black-Box Modeling of a Lithium-Ion Battery Cell Based on Automotive Drive Cycle Data," *World Electric Vehicle Journal*, vol. 12, no. 3, p. 102, 2021. <https://doi.org/10.3390/wevj12030102>
- [130] M. B. Jamshidi, M. Jamshidi, and S. Rostami, "An intelligent approach for nonlinear system identification of a li-ion battery," in *2017 IEEE 2nd International Conference on Automatic Control and Intelligent Systems (I2CACIS)*, 2017: IEEE, pp. 98-103. <https://doi.org/10.1109/I2CACIS.2017.8239040>
- [131] B. Xia, X. Zhao, R. De Callafon, H. Garnier, T. Nguyen, and C. Mi, "Accurate Lithium-ion battery parameter estimation with continuous-time system

References

- identification methods," *Applied energy*, vol. 179, pp. 426-436, 2016. <https://doi.org/10.1016/j.apenergy.2016.07.005>
- [132] K. Tsang, L. Sun, and W. L. Chan, "Identification and modelling of Lithium ion battery," *Energy Conversion and Management*, vol. 51, no. 12, pp. 2857-2862, 2010. <https://doi.org/10.1016/j.enconman.2010.06.024>
- [133] A. W. Danté, K. Agbossou, S. Kelouwani, A. Cardenas, and J. Bouchard, "Online modeling and identification of plug-in electric vehicles sharing a residential station," *International Journal of Electrical Power & Energy Systems*, vol. 108, pp. 162-176, 2019. <https://doi.org/10.1016/j.ijepes.2018.12.024>
- [134] X. Hu, D. Cao, and B. Egardt, "Condition monitoring in advanced battery management systems: Moving horizon estimation using a reduced electrochemical model," *IEEE/ASME Transactions on Mechatronics*, vol. 23, no. 1, pp. 167-178, 2017. <https://doi.org/10.1109/TMECH.2017.2675920>
- [135] X. Lin, "Theoretical analysis of battery SOC estimation errors under sensor bias and variance," *IEEE Transactions on Industrial Electronics*, vol. 65, no. 9, pp. 7138-7148, 2018. <https://doi.org/10.1109/TIE.2018.2795521>
- [136] H. E. Perez, X. Hu, S. Dey, and S. J. Moura, "Optimal charging of Li-ion batteries with coupled electro-thermal-aging dynamics," *IEEE Transactions on Vehicular Technology*, vol. 66, no. 9, pp. 7761-7770, 2017. <https://doi.org/10.1109/TVT.2017.2676044>
- [137] A. Ito, A. Kawashima, T. Suzuki, S. Inagaki, T. Yamaguchi, and Z. Zhou, "Model predictive charging control of in-vehicle batteries for home energy management based on vehicle state prediction," *IEEE Transactions on Control Systems Technology*, vol. 26, no. 1, pp. 51-64, 2017. <https://doi.org/10.1109/TCST.2017.2664727>
- [138] F. Rassaei, W.-S. Soh, and K.-C. Chua, "A statistical modelling and analysis of residential electric vehicles' charging demand in smart grids," in *2015 IEEE Power & Energy Society Innovative Smart Grid Technologies Conference (ISGT)*, 2015: IEEE, pp. 1-5. <https://doi.org/10.1109/ISGT.2015.7131894>
- [139] Z. Darabi and M. Ferdowsi, "Extracting probability distribution functions applicable for PHEVs charging load profile," in *PES T&D 2012*, 2012: IEEE, pp. 1-6. <https://doi.org/10.1109/TDC.2012.6281435>
- [140] A. Ashtari, E. Bibeau, S. Shahidinejad, and T. Molinski, "PEV charging profile prediction and analysis based on vehicle usage data," *IEEE Transactions on Smart Grid*, vol. 3, no. 1, pp. 341-350, 2011. <https://doi.org/10.1109/TSG.2011.2162009>
- [141] I. S. Bayram and I. Papapanagiotou, "A survey on communication technologies and requirements for internet of electric vehicles," *EURASIP Journal on Wireless Communications and Networking*, vol. 2014, no. 1, pp. 1-18, 2014. <https://doi.org/10.1186/1687-1499-2014-223>
- [142] H. Guo, D. Hou, S. Du, L. Zhao, J. Wu, and N. Yan, "A driving pattern recognition-based energy management for plug-in hybrid electric bus to counter the noise of stochastic vehicle mass," *Energy*, vol. 198, p. 117289, 2020. <https://doi.org/10.1016/j.energy.2020.117289>

References

- [143] P. Quan, H. Lin, Z. Liang, and S. Di, "Research on fast identification and location of contour features of electric vehicle charging port in complex scenes," *IEEE Access*, 2021. <https://doi.org/10.1109/ACCESS.2021.3092210>
- [144] L. Ma and Y. Zhang, "Research on vehicle license plate recognition technology based on deep convolutional neural networks," *Microprocessors and Microsystems*, vol. 82, p. 103932, 2021. <https://doi.org/10.1016/j.micpro.2021.103932>
- [145] M. İnci, M. Büyük, M. H. Demir, and G. İlbey, "A review and research on fuel cell electric vehicles: Topologies, power electronic converters, energy management methods, technical challenges, marketing and future aspects," *Renewable and Sustainable Energy Reviews*, vol. 137, p. 110648, 2021. <https://doi.org/10.1016/j.rser.2020.110648>
- [146] M. Ahrabi, M. Abedi, H. Nafisi, M. A. Mirzaei, B. Mohammadi-Ivatloo, and M. Marzband, "Evaluating the effect of electric vehicle parking lots in transmission-constrained AC unit commitment under a hybrid IGDT-stochastic approach," *International Journal of Electrical Power & Energy Systems*, vol. 125, p. 106546, 2021. <https://doi.org/10.1016/j.ijepes.2020.106546>
- [147] W. Dong, S. Li, X. Fu, Z. Li, M. Fairbank, and Y. Gao, "Control of a buck DC/DC converter using approximate dynamic programming and artificial neural networks," *IEEE Transactions on Circuits and Systems I: Regular Papers*, vol. 68, no. 4, pp. 1760-1768, 2021. <https://doi.org/10.1109/TCSI.2021.3053468>
- [148] Z. Xia and J. A. A. Qahouq, "State-of-charge balancing of lithium-ion batteries with state-of-health awareness capability," *IEEE Transactions on Industry Applications*, vol. 57, no. 1, pp. 673-684, 2020. <https://doi.org/10.1109/TIA.2020.3029755>
- [149] K. Uddin, A. D. Moore, A. Barai, and J. Marco, "The effects of high frequency current ripple on electric vehicle battery performance," *Applied energy*, vol. 178, pp. 142-154, 2016. <https://doi.org/10.1016/j.apenergy.2016.06.033>
- [150] S. De Breucker, K. Engelen, R. D'hulst, and J. Driesen, "Impact of current ripple on Li-ion battery ageing," *World Electric Vehicle Journal*, vol. 6, no. 3, pp. 532-540, 2013. <https://doi.org/10.3390/wevj6030532>
- [151] N. Sujitha and S. Krithiga, "RES based EV battery charging system: A review," *Renewable and Sustainable Energy Reviews*, vol. 75, pp. 978-988, 2017. <https://doi.org/10.1016/j.rser.2016.11.078>
- [152] Y. Xiao, C. Liu, and F. Yu, "An integrated on-board EV charger with safe charging operation for three-phase IPM motor," *IEEE Transactions on Industrial Electronics*, vol. 66, no. 10, pp. 7551-7560, 2018. <https://doi.org/10.1109/TIE.2018.2880712>
- [153] C.-H. Lee, M.-Y. Chen, S.-H. Hsu, and J.-A. Jiang, "Implementation of an SOC-based four-stage constant current charger for Li-ion batteries," *Journal of Energy Storage*, vol. 18, pp. 528-537, 2018. <https://doi.org/10.1016/j.est.2018.06.010>
- [154] G.-C. Hsieh, L.-R. Chen, and K.-S. Huang, "Fuzzy-controlled Li-ion battery charge system with active state-of-charge controller," *IEEE Transactions on industrial electronics*, vol. 48, no. 3, pp. 585-593, 2001. <https://doi.org/10.1109/41.925585>

References

- [155] L.-R. Chen, R. C. Hsu, and C.-S. Liu, "A design of a grey-predicted Li-ion battery charge system," *IEEE Transactions on Industrial Electronics*, vol. 55, no. 10, pp. 3692-3701, 2008. <https://doi.org/10.1109/TIE.2008.928106>
- [156] M. Bayati, M. Abedi, M. Farahmandrad, and G. B. Gharehpetian, "Delivering smooth power to pulse-current battery chargers: Electric vehicles as a case in point," *IEEE Transactions on Power Electronics*, vol. 36, no. 2, pp. 1295-1302, 2020. <https://doi.org/10.1109/TPEL.2020.3005929>
- [157] T. Chen, P. Fu, X. Chen, S. Dou, L. Huang, S. He, Z. Wang, "An Optimal Control Algorithm with Reduced DC-Bus Current Fluctuation for Multiple Charging Modes of Electric Vehicle Charging Station," *World Electric Vehicle Journal*, vol. 12, no. 3, p. 107, 2021. <https://doi.org/10.3390/wevj12030107>
- [158] N. A. Kelly and T. L. Gibson, "Solar photovoltaic charging of high voltage nickel metal hydride batteries using DC power conversion," *Journal of Power Sources*, vol. 196, no. 23, pp. 10430-10441, 2011. <https://doi.org/10.1016/j.jpowsour.2011.07.043>
- [159] A. R. Bhatti, Z. Salam, M. J. B. A. Aziz, and K. P. Yee, "A critical review of electric vehicle charging using solar photovoltaic," *International Journal of Energy Research*, vol. 40, no. 4, pp. 439-461, 2016. <https://doi.org/10.1002/er.3472>
- [160] S. Balci, A. Kayabasi, and B. Yildiz, "ANN-based estimation of the voltage ripple according to the load variation of battery chargers," *International Journal of Electronics*, vol. 107, no. 1, pp. 17-27, 2020. <https://doi.org/10.1080/00207217.2019.1591530>
- [161] W. W. A. Silva, T. R. Oliveira, and P. F. Donoso-Garcia, "An improved voltage-shifting strategy to attain concomitant accurate power sharing and voltage restoration in droop-controlled DC microgrids," *IEEE Transactions on Power Electronics*, vol. 36, no. 2, pp. 2396-2406, 2020. <https://doi.org/10.1109/TPEL.2020.3009619>
- [162] M. S. Sadabadi, "A distributed control strategy for parallel DC-DC converters," *IEEE Control Systems Letters*, vol. 5, no. 4, pp. 1231-1236, 2020. <https://doi.org/10.1109/LCSYS.2020.3025411>
- [163] H. Al-Baidhani, M. K. Kazimierczuk, and A. Reatti, "Nonlinear modeling and voltage-mode control of DC-DC boost converter for CCM," in *2018 IEEE International Symposium on Circuits and Systems (ISCAS)*, 2018: IEEE, pp. 1-5. <https://doi.org/10.1109/ISCAS.2018.8351078>
- [164] H. Al-Baidhani, T. Salvatierra, R. Ordonez, and M. K. Kazimierczuk, "Simplified Nonlinear Voltage-Mode Control of PWM DC-DC Buck Converter," *IEEE Transactions on Energy Conversion*, 2020. <https://doi.org/10.1109/TEC.2020.3007739>
- [165] P. Roy, K. Banerjee, and S. Saha, "Comparison study on the basis of transient response between Voltage Mode Control (VMC) & Current Mode Control (CMC) of buck converter," in *2018 International Symposium on Devices, Circuits and Systems (ISDCS)*, 2018: IEEE, pp. 1-4. <https://doi.org/10.1109/ISDCS.2018.8379636>

References

- [166] Z. Liu, L. Xie, A. Bemporad, and S. Lu, "Fast linear parameter varying model predictive control of buck DC-DC converters based on FPGA," *IEEE Access*, vol. 6, pp. 52434-52446, 2018. <https://doi.org/10.1109/ACCESS.2018.2869043>
- [167] B. Wang, V. R. K. Kanamarlapudi, L. Xian, X. Peng, K. T. Tan, and P. L. So, "Model predictive voltage control for single-inductor multiple-output DC-DC converter with reduced cross regulation," *IEEE transactions on industrial electronics*, vol. 63, no. 7, pp. 4187-4197, 2016. <https://doi.org/10.1109/TIE.2016.2532846>
- [168] U. Yilmaz, A. Kircay, and S. Borekci, "PV system fuzzy logic MPPT method and PI control as a charge controller," *Renewable and Sustainable Energy Reviews*, vol. 81, pp. 994-1001, 2018. <https://doi.org/10.1016/j.rser.2017.08.048>
- [169] W. S. Levine, L. Grüne, R. Goebel, SV. Rakovic, A. Mesbah, I. Kolmanovsky, S. Di Cairano, DA. Allan, JB. Rawlings, MA. Sehr, RR. Bitmead, "Handbook of model predictive control," 2018. <https://doi.org/10.1007/978-3-319-77489-3>
- [170] Y. Danaiyen, I. Altas, and E. Sahin, "Model Predictive Control of a DC-DC Buck Converter," *Sigma J Eng & Nat Sci*, vol. 8, no. 2, pp. 91-97, 2017.
- [171] Q. Xu, Y. Yan, C. Zhang, T. Dragicevic, and F. Blaabjerg, "An offset-free composite model predictive control strategy for DC/DC buck converter feeding constant power loads," *IEEE Transactions on Power Electronics*, vol. 35, no. 5, pp. 5331-5342, 2019. <https://doi.org/10.1109/TPEL.2019.2941714>
- [172] L. Liang, H. Ye, and G. Y. Li, "Toward intelligent vehicular networks: A machine learning framework," *IEEE Internet of Things Journal*, vol. 6, no. 1, pp. 124-135, 2018. <https://doi.org/10.1109/JIOT.2018.2872122>
- [173] W. Tong, A. Hussain, W. X. Bo, and S. Maharjan, "Artificial intelligence for vehicle-to-everything: A survey," *IEEE Access*, vol. 7, pp. 10823-10843, 2019. <https://doi.org/10.1109/ACCESS.2019.2891073>
- [174] M. Shibl, L. Ismail, and A. Massoud, "Machine learning-based management of electric vehicles charging: Towards highly-dispersed fast chargers," *Energies*, vol. 13, no. 20, p. 5429, 2020. <https://doi.org/10.3390/en13205429>
- [175] S. Shahriar, A. Al-Ali, A. H. Osman, S. Dhou, and M. Nijim, "Machine learning approaches for EV charging behavior: A review," *IEEE Access*, vol. 8, pp. 168980-168993, 2020. <https://doi.org/10.1109/ACCESS.2020.3023388>
- [176] M. Dabbaghjamanesh, A. Moeini, and A. Kavousi-Fard, "Reinforcement learning-based load forecasting of electric vehicle charging station using Q-learning technique," *IEEE Transactions on Industrial Informatics*, vol. 17, no. 6, pp. 4229-4237, 2020. <https://doi.org/10.1109/TII.2020.2990397>
- [177] Q. Dang, D. Wu, and B. Boulet, "A Q-learning based charging scheduling scheme for electric vehicles," in *2019 IEEE Transportation Electrification Conference and Expo (ITEC)*, 2019: IEEE, pp. 1-5. <https://doi.org/10.1109/ITEC.2019.8790603>
- [178] P. M. Attia, A. Grover, N. Jin, KA. Severson, TM. Markov, YH. Liao, MH. Chen, B. Cheong, N. Perkins, Z. Yang, PK. Herring, "Closed-loop optimization of fast-charging protocols for batteries with machine learning," *Nature*, vol. 578, no. 7795, pp. 397-402, 2020. <https://doi.org/10.1038/s41586-020-1994-5>

References

- [179] A. Ahmadian, B. Mohammadi-Ivatloo, and A. Elkamel, "A review on plug-in electric vehicles: Introduction, current status, and load modeling techniques," *Journal of Modern Power Systems and Clean Energy*, vol. 8, no. 3, pp. 412-425, 2020. <https://doi.org/10.35833/MPCE.2018.000802>
- [180] C. Alaoui, "Hybrid vehicle energy management using deep learning," in *2019 International Conference on Intelligent Systems and Advanced Computing Sciences (ISACS)*, 2019: IEEE, pp. 1-5. <https://doi.org/10.1109/ISACS48493.2019.9068880>
- [181] M. Vosoogh, M. Rashidinejad, A. Abdollahi, and M. Ghaseminezhad, "An Intelligent Day Ahead Energy Management Framework for Networked Microgrids Considering High Penetration of Electric Vehicles," *IEEE Transactions on Industrial Informatics*, 2020. <https://doi.org/10.1109/TII.2020.2977989>
- [182] S. Saadatmand, P. Shamsi, and M. Ferdowsi, "The Voltage Regulation of a Buck Converter Using a Neural Network Predictive Controller," in *2020 IEEE Texas Power and Energy Conference (TPEC)*, 2020: IEEE, pp. 1-6. <https://doi.org/10.1109/TPEC48276.2020.9042588>
- [183] C. Cui, N. Yan, and C. Zhang, "An Intelligent Control Strategy for buck DC-DC Converter via Deep Reinforcement Learning," *arXiv preprint arXiv:2008.04542*, 2020. <https://doi.org/10.48550/arXiv.2008.04542>
- [184] H. Maruta, D. Mitsutake, and F. Kurokawa, "A neural network based reference modified PID control with simple duration design for digitally controlled dc-dc converters," *International Journal of Renewable Energy Research (IJRER)*, vol. 6, no. 2, pp. 550-560, 2016. <https://doi.org/10.20508/ijrer.v6i2.4402.g6842>
- [185] G. Abbas, U. Farooq, and M. U. Asad, "Application of neural network based model predictive controller to power switching converters," in *The 2011 International Conference and Workshop on Current Trends in Information Technology (CTIT 11)*, 2011: IEEE, pp. 132-136. <https://doi.org/10.1109/CTIT.2011.6107948>
- [186] G. Rojas-Dueñas, J.-R. Riba, K. Kahalerras, M. Moreno-Eguilaz, A. Kadechkar, and A. Gomez-Pau, "Black-Box Modelling of a DC-DC Buck Converter Based on a Recurrent Neural Network," in *2020 IEEE International Conference on Industrial Technology (ICIT)*, 2020: IEEE, pp. 456-461. <https://doi.org/10.1109/ICIT45562.2020.9067098>
- [187] N. HINOV, T. HRANOV, and B. GILEV, "Comparision of Different Methods for Controlling DC-DC Converters in Constant Current Mode," in *2020 21st International Symposium on Electrical Apparatus & Technologies (SIELA)*, 2020: IEEE, pp. 1-5. <https://doi.org/10.1109/SIELA49118.2020.9167050>
- [188] M. Rajamani, R. Rajesh, and M. Willjuice Iruthayarajan, "Design and experimental validation of PID controller for buck converter: A multi-objective evolutionary algorithms based approach," *IETE Journal of Research*, pp. 1-12, 2021. <https://doi.org/10.1080/03772063.2021.1905564>
- [189] A. Dehghanzadeh, G. Farahani, H. Vahedi, and K. Al-Haddad, "Model predictive control design for DC-DC converters applied to a photovoltaic system," *International Journal of Electrical Power & Energy Systems*, vol. 103, pp. 537-544, 2018. <https://doi.org/10.1016/j.ijepes.2018.05.004>

References

- [190] S. Ding, W. X. Zheng, J. Sun, and J. Wang, "Second-order sliding-mode controller design and its implementation for buck converters," *IEEE Transactions on Industrial Informatics*, vol. 14, no. 5, pp. 1990-2000, 2017. <https://doi.org/10.1109/TII.2017.2758263>
- [191] E. Vidal-Idiarte, A. Marcos-Pastor, R. Giral, J. Calvente, and L. Martinez-Salamero, "Direct digital design of a sliding mode-based control of a PWM synchronous buck converter," *IET Power Electronics*, vol. 10, no. 13, pp. 1714-1720, 2017. <https://doi.org/10.1049/iet-pel.2016.0975>
- [192] C. Sain, A. Banerjee, P. K. Biswas, T. S. Babu, and T. Dragicevic, "Updated PSO optimised fuzzy-PI controlled buck type multi-phase inverter-based PMSM drive with an over-current protection scheme," *IET Electric Power Applications*, vol. 14, no. 12, pp. 2331-2339, 2020. <https://doi.org/10.1049/iet-epa.2020.0165>
- [193] M. Saoudi, A. El-Sayed, and H. Metwally, "Design and implementation of closed-loop control system for buck converter using different techniques," *IEEE Aerospace and Electronic Systems Magazine*, vol. 32, no. 3, pp. 30-39, 2017. <https://doi.org/10.1109/MAES.2017.150261>
- [194] A. G. Soriano-Sánchez, M. A. Rodríguez-Licea, F. J. Pérez-Pinal, and J. A. Vázquez-López, "Fractional-order approximation and synthesis of a PID controller for a buck converter," *Energies*, vol. 13, no. 3, p. 629, 2020. <https://doi.org/10.3390/en13030629>
- [195] M. Hemphill, "Electricity distribution system planning for an increasing penetration of plug-in electric vehicles in new south wales," in *2012 22nd Australasian Universities Power Engineering Conference (AUPEC)*, 2012: IEEE, pp. 1-6.
- [196] Z. Liu and Q. Wu, "EV charging analysis based on the National Travel Surveys of the Nordic Area," in *2014 IEEE PES General Meeting| Conference & Exposition*, 2014: IEEE, pp. 1-6. <https://doi.org/10.1109/PESGM.2014.6939315>
- [197] C.-T. Ma, "System planning of grid-connected electric vehicle charging stations and key technologies: A review," *Energies*, vol. 12, no. 21, p. 4201, 2019. <https://doi.org/10.3390/en12214201>
- [198] J. Quiros-Tortos, L. Ochoa, and T. Butler, "How electric vehicles and the grid work together: Lessons learned from one of the largest electric vehicle trials in the world," *IEEE Power and Energy Magazine*, vol. 16, no. 6, pp. 64-76, 2018. <https://doi.org/10.1109/MPE.2018.2863060>
- [199] H. Ren, A. Zhang, F. Wang, X. Yan, Y. Li, N. Duić, M. Shafie-khah, JP. Catalão, "Optimal scheduling of an EV aggregator for demand response considering triple level benefits of three-parties," *International Journal of Electrical Power & Energy Systems*, vol. 125, p. 106447, 2021. <https://doi.org/10.1016/j.ijepes.2020.106447>
- [200] J. Michaelis, T. Gnann, and A.-L. Klingler, "Load Shifting Potentials of Plug-In Electric Vehicles—A Case Study for Germany," *World Electric Vehicle Journal*, vol. 9, no. 2, p. 21, 2018. <https://doi.org/10.3390/wevj9020021>
- [201] S. Pirouzi, J. Aghaei, V. Vahidinasab, T. Niknam, and A. Khodaei, "Robust linear architecture for active/reactive power scheduling of EV integrated smart

References

- distribution networks," *Electric Power Systems Research*, vol. 155, pp. 8-20, 2018. <https://doi.org/10.1016/j.epsr.2017.09.021>
- [202] M. Muratori, "Impact of uncoordinated plug-in electric vehicle charging on residential power demand," *Nature Energy*, vol. 3, no. 3, pp. 193-201, 2018. <https://doi.org/10.1038/s41560-017-0074-z>
- [203] S. Cai and R. Matsushashi, "Model Predictive Control for EV Aggregators Participating in System Frequency Regulation Market," *IEEE Access*, vol. 9, pp. 80763-80771, 2021. <https://doi.org/10.1109/ACCESS.2021.3085345>
- [204] J. C. Mukherjee and A. Gupta, "Distributed charge scheduling of plug-in electric vehicles using inter-aggregator collaboration," *IEEE Transactions on Smart Grid*, vol. 8, no. 1, pp. 331-341, 2016. <https://doi.org/10.1109/TSG.2016.2515849>
- [205] B. Geng, J. K. Mills, and D. Sun, "Coordinated charging control of plug-in electric vehicles at a distribution transformer level using the vTOU-DP approach," in *2012 IEEE Vehicle Power and Propulsion Conference*, 2012: IEEE, pp. 1469-1474. <https://doi.org/10.1109/VPPC.2012.6422681>
- [206] M. Uddin, M. F. Romlie, M. F. Abdullah, S. Abd Halim, and T. C. Kwang, "A review on peak load shaving strategies," *Renewable and Sustainable Energy Reviews*, vol. 82, pp. 3323-3332, 2018. <https://doi.org/10.1016/j.rser.2017.10.056>
- [207] A. Mishra, D. Irwin, P. Shenoy, and T. Zhu, "Scaling distributed energy storage for grid peak reduction," in *Proceedings of the fourth international conference on Future energy systems*, 2013, pp. 3-14. <https://doi.org/10.1145/2487166.2487168>
- [208] L. Kütt, E. Saarijärvi, M. Lehtonen, A. Rosin, and H. Mölder, "Load shifting in the existing distribution network and perspectives for EV charging-case study," in *IEEE PES Innovative Smart Grid Technologies, Europe*, 2014: IEEE, pp. 1-6. <https://doi.org/10.1109/ISGTEurope.2014.7028938>
- [209] H. Onda, S. Yamamoto, H. Takeshit, S. Okamoto, and N. Yamanaka, "Peak load shifting and electricity charges reduction realized by electric vehicle storage virtualization," *AASRI Procedia*, vol. 7, pp. 101-106, 2014. <https://doi.org/10.1016/j.aasri.2014.05.036>
- [210] M. Aziz, T. Oda, T. Mitani, Y. Watanabe, and T. Kashiwagi, "Utilization of electric vehicles and their used batteries for peak-load shifting," *Energies*, vol. 8, no. 5, pp. 3720-3738, 2015. <https://doi.org/10.3390/en8053720>
- [211] W. Wu and B. Lin, "Benefits of electric vehicles integrating into power grid," *Energy*, vol. 224, p. 120108, 2021. <https://doi.org/10.1016/j.energy.2021.120108>
- [212] L. Yu, Y. Li, G. Huang, and C. An, "A robust flexible-probabilistic programming method for planning municipal energy system with considering peak-electricity price and electric vehicle," *Energy Conversion and Management*, vol. 137, pp. 97-112, 2017. <https://doi.org/10.1016/j.enconman.2017.01.028>
- [213] O. Elma, "A dynamic charging strategy with hybrid fast charging station for electric vehicles," *Energy*, vol. 202, p. 117680, 2020. <https://doi.org/10.1016/j.energy.2020.117680>
- [214] A. Dogan, M. Kuzlu, M. Pipattanasomporn, S. Rahman, and T. Yalcinoz, "Impact of EV charging strategies on peak demand reduction and load factor improvement,"

References

- in *2015 9th International Conference on Electrical and Electronics Engineering (ELECO)*, 2015: IEEE, pp. 374-378. <https://doi.org/10.1109/ELECO.2015.7394559>
- [215] M. W. Khan and J. Wang, "Multi-agents based optimal energy scheduling technique for electric vehicles aggregator in microgrids," *International Journal of Electrical Power & Energy Systems*, vol. 134, p. 107346, 2022. <https://doi.org/10.1016/j.ijepes.2021.107346>
- [216] H. Rashidizadeh-Kermani, H. R. Najafi, A. Anvari-Moghaddam, and J. M. Guerrero, "Optimal decision-making strategy of an electric vehicle aggregator in short-term electricity markets," *Energies*, vol. 11, no. 9, p. 2413, 2018. <https://doi.org/10.3390/en11092413>
- [217] K. Li, Q. Mu, F. Wang, Y. Gao, G. Li, M. Shafie-Khah, JP. Catalão, Y. Yang, J. Ren, "A business model incorporating harmonic control as a value-added service for utility-owned electricity retailers," *IEEE Transactions on Industry Applications*, vol. 55, no. 5, pp. 4441-4450, 2019. <https://doi.org/10.1109/TIA.2019.2922927>
- [218] K. G. Firouzjah, "Profit-based electric vehicle charging scheduling: Comparison with different strategies and impact assessment on distribution networks," *International Journal of Electrical Power & Energy Systems*, vol. 138, p. 107977, 2022. <https://doi.org/10.1016/j.ijepes.2022.107977>
- [219] S. Wang, S. Bi, and Y. A. Zhang, "Reinforcement learning for real-time pricing and scheduling control in EV charging stations," *IEEE Transactions on Industrial Informatics*, vol. 17, no. 2, pp. 849-859, 2019. <https://doi.org/10.1109/TII.2019.2950809>
- [220] T. G. Alghamdi, D. Said, and H. T. Mouftah, "Profit Maximization for EVSEs-Based Renewable Energy Sources in Smart Cities With Different Arrival Rate Scenarios," *IEEE Access*, vol. 9, pp. 58740-58754, 2021. <https://doi.org/10.1109/ACCESS.2021.3070485>
- [221] A. Thangaraj, S. A. E. Xavier, and R. Pandian, "Optimal coordinated operation scheduling for electric vehicle aggregator and charging stations in integrated electricity transportation system using hybrid technique," *Sustainable Cities and Society*, vol. 80, p. 103768, 2022. <https://doi.org/10.1016/j.scs.2022.103768>
- [222] Z. Yang, K. Li, and A. Foley, "Computational scheduling methods for integrating plug-in electric vehicles with power systems: A review," *Renewable and Sustainable Energy Reviews*, vol. 51, pp. 396-416, 2015. <https://doi.org/10.1016/j.rser.2015.06.007>
- [223] M. Hijjo and G. Frey, "Multi-objective optimization for scheduling isolated microgrids," in *2018 IEEE International Conference on Industrial Technology (ICIT)*, 2018: IEEE, pp. 1037-1042. <https://doi.org/10.1109/ICIT.2018.8352321>
- [224] S. Wang, S. Bi, Y.-J. A. Zhang, and J. Huang, "Electrical vehicle charging station profit maximization: Admission, pricing, and online scheduling," *IEEE Transactions on Sustainable Energy*, vol. 9, no. 4, pp. 1722-1731, 2018. <https://doi.org/10.1109/TSTE.2018.2810274>

References

- [225] R. A. Biroon, Z. Abdollahi, and R. Hadidi, "Fast and regular electric vehicle charging impacts on the distribution feeders," in *2019 IEEE Industry Applications Society Annual Meeting*, 2019: IEEE, pp. 1-7. <https://doi.org/10.1109/IAS.2019.8912036>
- [226] L. Yang and H. Ribberink, "Investigation of the potential to improve DC fast charging station economics by integrating photovoltaic power generation and/or local battery energy storage system," *Energy*, vol. 167, pp. 246-259, 2019. <https://doi.org/10.1016/j.energy.2018.10.147>
- [227] T. Ding, Z. Zeng, J. Bai, B. Qin, Y. Yang, and M. Shahidehpour, "Optimal electric vehicle charging strategy with Markov decision process and reinforcement learning technique," *IEEE Transactions on Industry Applications*, vol. 56, no. 5, pp. 5811-5823, 2020. <https://doi.org/10.1109/TIA.2020.2990096>
- [228] J. A. P. Lopes, F. J. Soares, and P. M. R. Almeida, "Integration of electric vehicles in the electric power system," *Proceedings of the IEEE*, vol. 99, no. 1, pp. 168-183, 2010. <https://doi.org/10.1109/JPROC.2010.2066250>
- [229] H. Yu, S. Niu, Y. Shang, Z. Shao, Y. Jia, and L. Jian, "Electric vehicles integration and vehicle-to-grid operation in active distribution grids: A comprehensive review on power architectures, grid connection standards and typical applications," *Renewable and Sustainable Energy Reviews*, vol. 168, p. 112812, 2022. <https://doi.org/10.1016/j.rser.2022.112812>
- [230] R. Zhang, X. Cheng, and L. Yang, "Flexible energy management protocol for cooperative EV-to-EV charging," *IEEE Transactions on Intelligent Transportation Systems*, vol. 20, no. 1, pp. 172-184, 2018. <https://doi.org/10.1109/TITS.2018.2807184>
- [231] B. K. Sovacool and R. F. Hirsh, "Beyond batteries: An examination of the benefits and barriers to plug-in hybrid electric vehicles (PHEVs) and a vehicle-to-grid (V2G) transition," *Energy Policy*, vol. 37, no. 3, pp. 1095-1103, 2009. <https://doi.org/10.1016/j.enpol.2008.10.005>
- [232] P. Rezaei, J. Frolik, and P. D. Hines, "Packetized plug-in electric vehicle charge management," *IEEE Transactions on Smart Grid*, vol. 5, no. 2, pp. 642-650, 2014. <https://doi.org/10.1109/TSG.2013.2291384>
- [233] J. Hu, S. You, M. Lind, and J. Østergaard, "Coordinated charging of electric vehicles for congestion prevention in the distribution grid," *IEEE Transactions on Smart Grid*, vol. 5, no. 2, pp. 703-711, 2013. <https://doi.org/10.1109/TSG.2013.2279007>
- [234] S. Liu and A. H. Etemadi, "A dynamic stochastic optimization for recharging plug-in electric vehicles," *IEEE Transactions on Smart Grid*, vol. 9, no. 5, pp. 4154-4161, 2017. <https://doi.org/10.1109/TSG.2017.2652329>
- [235] T. Castillo-Calzadilla, A. Alonso-Vicario, C. E. Borges, and C. Martin, "E-Mobility in Positive Energy Districts," *Buildings*, vol. 12, no. 3, p. 264, 2022. <https://doi.org/10.3390/buildings12030264>
- [236] H. Saber, H. Ranjbar, S. Fattaheian-Dehkordi, M. Moeini-Aghtaie, M. Ehsan, and M. Shahidehpour, "Transactive Energy Management of V2G-Capable Electric

References

- Vehicles in Residential Buildings: An MILP Approach," *IEEE Transactions on Sustainable Energy*, 2022. <https://doi.org/10.1109/TSTE.2022.3173943>
- [237] R. Vignali, A. Falsone, F. Ruiz, and G. Grusso, "Towards a comprehensive framework for V2G optimal operation in presence of uncertainty," *Sustainable Energy, Grids and Networks*, vol. 31, p. 100740, 2022. <https://doi.org/10.1016/j.segan.2022.100740>
- [238] H. Wei, Y. Zhang, Y. Wang, W. Hua, R. Jing, and Y. Zhou, "Planning integrated energy systems coupling V2G as a flexible storage," *Energy*, vol. 239, p. 122215, 2022. <https://doi.org/10.1016/j.energy.2021.122215>
- [239] M. O. Badawy and Y. Sozer, "Power flow management of a grid tied PV-battery system for electric vehicles charging," *IEEE Transactions on Industry Applications*, vol. 53, no. 2, pp. 1347-1357, 2016. <https://doi.org/10.1109/TIA.2016.2633526>
- [240] Z. Wang, P. Jochem, and W. Fichtner, "A scenario-based stochastic optimization model for charging scheduling of electric vehicles under uncertainties of vehicle availability and charging demand," *Journal of Cleaner Production*, vol. 254, p. 119886, 2020. <https://doi.org/10.1016/j.jclepro.2019.119886>
- [241] K. Ginigeme and Z. Wang, "Distributed optimal vehicle-to-grid approaches with consideration of battery degradation cost under real-time pricing," *IEEE Access*, vol. 8, pp. 5225-5235, 2020. <https://doi.org/10.1109/ACCESS.2019.2963692>
- [242] B. Xu, J. Zhao, T. Zheng, E. Litvinov, and D. S. Kirschen, "Factoring the cycle aging cost of batteries participating in electricity markets," *IEEE Transactions on Power Systems*, vol. 33, no. 2, pp. 2248-2259, 2017. <https://doi.org/10.1109/TPWRS.2017.2733339>
- [243] H. Farzin, M. Fotuhi-Firuzabad, and M. Moeini-Aghtaie, "A practical scheme to involve degradation cost of lithium-ion batteries in vehicle-to-grid applications," *IEEE Transactions on Sustainable Energy*, vol. 7, no. 4, pp. 1730-1738, 2016. <https://doi.org/10.1109/TSTE.2016.2558500>
- [244] U. ur Rehman, "A robust vehicle to grid aggregation framework for electric vehicles charging cost minimization and for smart grid regulation," *International Journal of Electrical Power & Energy Systems*, vol. 140, p. 108090, 2022. <https://doi.org/10.1016/j.ijepes.2022.108090>
- [245] S. Zeynali, N. Rostami, A. Ahmadian, and A. Elkamel, "Stochastic energy management of an electricity retailer with a novel plug-in electric vehicle-based demand response program and energy storage system: A linearized battery degradation cost model," *Sustainable Cities and Society*, vol. 74, p. 103154, 2021. <https://doi.org/10.1016/j.scs.2021.103154>
- [246] S.-A. Amamra and J. Marco, "Vehicle-to-grid aggregator to support power grid and reduce electric vehicle charging cost," *IEEE Access*, vol. 7, pp. 178528-178538, 2019. <https://doi.org/10.1109/ACCESS.2019.2958664>
- [247] Y. Zheng, Z. Shao, X. Lei, Y. Shi, and L. Jian, "The economic analysis of electric vehicle aggregators participating in energy and regulation markets considering battery degradation," *Journal of Energy Storage*, vol. 45, p. 103770, 2022. <https://doi.org/10.1016/j.est.2021.103770>

References

- [248] D. Castelvechi, "Electric cars and batteries: how will the world produce enough?," *Nature*, vol. 596, no. 7872, pp. 336-339, 2021. <https://doi.org/10.1038/d41586-021-02222-1>
- [249] W. Chen, J. Liang, Z. Yang, and G. Li, "A review of lithium-ion battery for electric vehicle applications and beyond," *Energy Procedia*, vol. 158, pp. 4363-4368, 2019. <https://doi.org/10.1016/j.egypro.2019.01.783>
- [250] E. Blasius and Z. Wang, "Effects of charging battery electric vehicles on local grid regarding standardized load profile in administration sector," *Applied energy*, vol. 224, pp. 330-339, 2018. <https://doi.org/10.1016/j.apenergy.2018.04.073>
- [251] I. N. Laboratory, "2015 Chevrolet Volt Charging Power Profiles," 2022, doi: <https://inl.gov/>.
- [252] "063450, LI-POLYMER BATTERY PACKS Specification," MAR 16, 2006, <https://www.sparkfun.com/datasheets/Batteries/UnionBattery-1000mAh.pdf>.
- [253] F. Richardson, D. Reynolds, and N. Dehak, "Deep neural network approaches to speaker and language recognition," *IEEE signal processing letters*, vol. 22, no. 10, pp. 1671-1675, 2015. <https://doi.org/10.1109/LSP.2015.2420092>
- [254] A. Vaswani, N. Shazeer, N. Parmar, J. Uszkoreit, L. Jones, AN. Gomez, L. Kaiser, I. Polosukhin, "Attention is all you need," *Advances in neural information processing systems*, vol. 30, 2017.
- [255] B. Attallah, A. Serir, and Y. Chahir, "Feature extraction in palmprint recognition using spiral of moment skewness and kurtosis algorithm," *Pattern Analysis and Applications*, vol. 22, no. 3, pp. 1197-1205, 2019. <https://doi.org/10.1007/s10044-018-0712-5>
- [256] P. Li, Y. Benezeth, R. Macwan, K. Nakamura, R. Gomez, C. Li, F. Yang, "Video-based pulse rate variability measurement using periodic variance maximization and adaptive Two-window peak detection," *Sensors*, vol. 20, no. 10, p. 2752, 2020. <https://doi.org/10.3390/s20102752>
- [257] A. K. Jain, R. P. W. Duin, and J. Mao, "Statistical pattern recognition: A review," *IEEE Transactions on pattern analysis and machine intelligence*, vol. 22, no. 1, pp. 4-37, 2000. <https://doi.org/10.1109/34.824819>
- [258] E. Chemali, P. J. Kollmeyer, M. Preindl, and A. Emadi, "State-of-charge estimation of Li-ion batteries using deep neural networks: A machine learning approach," *Journal of Power Sources*, vol. 400, pp. 242-255, 2018. <https://doi.org/10.1016/j.jpowsour.2018.06.104>
- [259] M. A. Hannan, M. S. H. Lipu, A. Hussain, M. H. Saad, and A. Ayob, "Neural network approach for estimating state of charge of lithium-ion battery using backtracking search algorithm," *Ieee Access*, vol. 6, pp. 10069-10079, 2018. <https://doi.org/10.1109/ACCESS.2018.2797976>
- [260] S. Asante-Okyere, Q. Xu, R. A. Mensah, C. Jin, and Y. Y. Ziggah, "Generalized regression and feed forward back propagation neural networks in modelling flammability characteristics of polymethyl methacrylate (PMMA)," *Thermochimica Acta*, vol. 667, pp. 79-92, 2018. <https://doi.org/10.1016/j.tca.2018.07.008>

References

- [261] K.-K. Xu, H.-D. Yang, and C.-J. Zhu, "A novel extreme learning machine-based Hammerstein-Wiener model for complex nonlinear industrial processes," *Neurocomputing*, vol. 358, pp. 246-254, 2019. <https://doi.org/10.1016/j.neucom.2019.05.049>
- [262] A. Wills, T. B. Schön, L. Ljung, and B. Ninness, "Identification of hammerstein-wiener models," *Automatica*, vol. 49, no. 1, pp. 70-81, 2013. <https://doi.org/10.1016/j.automatica.2012.09.018>
- [263] E. S. Nadimi, O. Green, V. Blanes-Vidal, J. J. Larsen, and L. P. Christensen, "Hammerstein-Wiener model for the prediction of temperature variations inside silage stack-bales using wireless sensor networks," *Biosystems engineering*, vol. 112, no. 3, pp. 236-247, 2012. <https://doi.org/10.1016/j.biosystemseng.2012.04.007>
- [264] X. Zhang, W. Zhang, and G. Lei, "A review of li-ion battery equivalent circuit models," *Transactions on Electrical and Electronic Materials*, vol. 17, no. 6, pp. 311-316, 2016. <https://doi.org/10.4313/TEEM.2016.17.6.311>
- [265] B. Chen, H. Ma, H. Fang, H. Fan, K. Luo, and B. Fan, "An approach for state of charge estimation of Li-ion battery based on Thevenin equivalent circuit model," in *2014 Prognostics and System Health Management Conference (PHM-2014 Hunan)*, 2014: IEEE, pp. 647-652. <https://doi.org/10.1109/PHM.2014.6988253>
- [266] T. R. Grandjean, A. McGordon, and P. A. Jennings, "Structural identifiability of equivalent circuit models for Li-ion batteries," *Energies*, vol. 10, no. 1, p. 90, 2017. <https://doi.org/10.3390/en10010090>
- [267] V. Johnson, "Battery performance models in ADVISOR," *Journal of power sources*, vol. 110, no. 2, pp. 321-329, 2002. [https://doi.org/10.1016/S0378-7753\(02\)00194-5](https://doi.org/10.1016/S0378-7753(02)00194-5)
- [268] S. S. Madani, E. Schaltz, and S. Knudsen Kær, "An electrical equivalent circuit model of a lithium titanate oxide battery," *Batteries*, vol. 5, no. 1, p. 31, 2019. <https://doi.org/10.3390/batteries5010031>
- [269] H. He, R. Xiong, and J. Fan, "Evaluation of lithium-ion battery equivalent circuit models for state of charge estimation by an experimental approach," *energies*, vol. 4, no. 4, pp. 582-598, 2011. <https://doi.org/10.3390/en4040582>
- [270] A.-I. Stroe, D.-I. Stroe, M. Swierczynski, R. Teodorescu, and S. K. Kær, "Lithium-ion battery dynamic model for wide range of operating conditions," in *2017 International Conference on Optimization of Electrical and Electronic Equipment (OPTIM) & 2017 Intl Aegean Conference on Electrical Machines and Power Electronics (ACEMP)*, 2017: IEEE, pp. 660-666. <https://doi.org/10.1109/OPTIM.2017.7975044>
- [271] Y. Yu, N. Narayan, V. Vega-Garita, J. Popovic-Gerber, Z. Qin, M. Wagemaker, P. Bauer, M. Zeman, "Constructing accurate equivalent electrical circuit models of lithium iron phosphate and lead-acid battery cells for solar home system applications," *Energies*, vol. 11, no. 9, p. 2305, 2018. <https://doi.org/10.3390/en11092305>
- [272] H. Hemi, N. M'Sirdi, A. Naamane, and B. Ikken, "Open Circuit Voltage of a Lithium ion Battery Model adjusted by data fitting," in *2018 6th International*

References

- Renewable and Sustainable Energy Conference (IRSEC)*, 2018: IEEE, pp. 1-5. <https://doi.org/10.1109/IRSEC.2018.8702860>
- [273] R. Xiong and Q. Yu, "Open circuit voltage and state of charge online estimation for lithium ion batteries," *Energy Procedia*, vol. 142, pp. 1902-1907, 2017. <https://doi.org/10.1016/j.egypro.2017.12.388>
- [274] W.-Y. Chang, "The state of charge estimating methods for battery: A review," *International Scholarly Research Notices*, vol. 2013, 2013. <http://dx.doi.org/10.1155/2013/953792>
- [275] I. Baccouche, A. Mlayah, S. Jemmali, B. Manai, and N. E. B. Amara, "\$ Implementation of a Coulomb counting algorithm for SOC estimation of Li-Ion battery for multimedia applications," in *2015 IEEE 12th International Multi-Conference on Systems, Signals & Devices (SSD15)*, 2015: IEEE, pp. 1-6. <https://doi.org/10.1109/SSD.2015.7348255>
- [276] J. Xie, J. Ma, and K. Bai, "Enhanced coulomb counting method for state-of-charge estimation of lithium-ion batteries based on peukert's law and coulombic efficiency," *Journal of Power Electronics*, vol. 18, no. 3, pp. 910-922, 2018. <https://doi.org/10.6113/JPE.2018.18.3.910>
- [277] K. S. Ng, C.-S. Moo, Y.-P. Chen, and Y.-C. Hsieh, "Enhanced coulomb counting method for estimating state-of-charge and state-of-health of lithium-ion batteries," *Applied energy*, vol. 86, no. 9, pp. 1506-1511, 2009. <https://doi.org/10.1016/j.apenergy.2008.11.021>
- [278] I. Baccouche, S. Jemmali, A. Mlayah, B. Manai, and N. E. B. Amara, "Implementation of an improved Coulomb-counting algorithm based on a piecewise SOC-OCV relationship for SOC estimation of li-IonBattery," *arXiv preprint arXiv:1803.10654*, 2018. <https://doi.org/10.48550/arXiv.1803.10654>
- [279] R. Xiong, J. Cao, Q. Yu, H. He, and F. Sun, "Critical review on the battery state of charge estimation methods for electric vehicles," *IEEE Access*, vol. 6, pp. 1832-1843, 2017. <https://doi.org/10.1109/ACCESS.2017.2780258>
- [280] S. Sindhuja and K. Vasanth, "Modified coulomb counting method of SOC estimation for uninterruptible power supply system's battery management system," in *2015 International Conference on Control, Instrumentation, Communication and Computational Technologies (ICCICCT)*, 2015: IEEE, pp. 197-203. <https://doi.org/10.1109/ICCICCT.2015.7475275>
- [281] L. Kang, X. Zhao, and J. Ma, "A new neural network model for the state-of-charge estimation in the battery degradation process," *Applied Energy*, vol. 121, pp. 20-27, 2014. <https://doi.org/10.1016/j.apenergy.2014.01.066>
- [282] M. Sheikhan, R. Pardis, and D. Gharavian, "State of charge neural computational models for high energy density batteries in electric vehicles," *Neural Computing and Applications*, vol. 22, no. 6, pp. 1171-1180, 2013. <https://doi.org/10.1007/s00521-012-0883-8>
- [283] D. Andre, C. Appel, T. Soczka-Guth, and D. U. Sauer, "Advanced mathematical methods of SOC and SOH estimation for lithium-ion batteries," *Journal of power sources*, vol. 224, pp. 20-27, 2013. <https://doi.org/10.1016/j.jpowsour.2012.10.001>

References

- [284] J. C. A. Anton, P. J. G. Nieto, C. B. Viejo, and J. A. V. Vilán, "Support vector machines used to estimate the battery state of charge," *IEEE Transactions on power electronics*, vol. 28, no. 12, pp. 5919-5926, 2013. <https://doi.org/10.1109/TPEL.2013.2243918>
- [285] P. Spagnol, S. Rossi, and S. M. Savaresi, "Kalman filter SoC estimation for Li-ion batteries," in *2011 IEEE International Conference on Control Applications (CCA)*, 2011: IEEE, pp. 587-592. <https://doi.org/10.1109/CCA.2011.6044480>
- [286] J. Zhang and C. Xia, "State-of-charge estimation of valve regulated lead acid battery based on multi-state Unscented Kalman Filter," *International Journal of Electrical Power & Energy Systems*, vol. 33, no. 3, pp. 472-476, 2011. <https://doi.org/10.1016/j.ijepes.2010.10.010>
- [287] R.-E. Tudoroiu, M. Zaheeruddin, S.-M. Radu, and N. Tudoroiu, "Real-time implementation of an extended Kalman filter and a PI observer for state estimation of rechargeable Li-Ion batteries in hybrid electric vehicle applications—A case study," *Batteries*, vol. 4, no. 2, p. 19, 2018. <https://doi.org/10.3390/batteries4020019>
- [288] M. Lagraoui, S. Doubabi, and A. Rachid, "SOC estimation of Lithium-ion battery using Kalman filter and Luenberger observer: A comparative study," in *2014 International renewable and sustainable energy conference (IRSEC)*, 2014: IEEE, pp. 636-641. <https://doi.org/10.1109/IRSEC.2014.7059849>
- [289] Z. Yu, R. Huai, and L. Xiao, "State-of-charge estimation for lithium-ion batteries using a kalman filter based on local linearization," *Energies*, vol. 8, no. 8, pp. 7854-7873, 2015. <https://doi.org/10.3390/en8087854>
- [290] S. Yang, C. Deng, Y. Zhang, and Y. He, "State of charge estimation for lithium-ion battery with a temperature-compensated model," *Energies*, vol. 10, no. 10, p. 1560, 2017. <https://doi.org/10.3390/en10101560>
- [291] P. Shi and Y. Zhao, "Application of unscented Kalman filter in the SOC estimation of Li-ion battery for Autonomous Mobile Robot," in *2006 IEEE International Conference on Information Acquisition*, 2006: IEEE, pp. 1279-1283. <https://doi.org/10.1109/ICIA.2006.305934>
- [292] X. Wu, W. Shi, and J. Du, "Multi-objective optimal charging method for lithium-ion batteries," *Energies*, vol. 10, no. 9, p. 1271, 2017. <https://doi.org/10.3390/en10091271>
- [293] X.-S. Yang and S. Deb, "Cuckoo search via Lévy flights," in *2009 World congress on nature & biologically inspired computing (NaBIC)*, 2009: Ieee, pp. 210-214. <https://doi.org/10.1109/NABIC.2009.5393690>
- [294] P. Makeen, R. Swief, T. Abdel-Salam, and N. H. El-Amary, "Smart hybrid micro-grid integration for optimal power sharing-based water cycle optimization technique," *Energies*, vol. 11, no. 5, p. 1083, 2018. <https://doi.org/10.3390/en11051083>
- [295] R. Rajabioun, "Cuckoo optimization algorithm," *Applied soft computing*, vol. 11, no. 8, pp. 5508-5518, 2011. <https://doi.org/10.1016/j.asoc.2011.05.008>

References

- [296] V. V. G. Pentapalli and R. K. Varma, "Cuckoo search optimization and its applications: A review," *Int. J. Adv. Res. Comput. Commun. Eng*, vol. 5, no. 11, pp. 2319-5940, 2016.
- [297] M. Ameryan, M. R. A. Totonchi, and S. J. S. Mahdavi, "Clustering based on cuckoo optimization algorithm," in *2014 Iranian conference on intelligent systems (ICIS)*, 2014: IEEE, pp. 1-6. <https://doi.org/10.1109/IranianCIS.2014.6802605>
- [298] S.-C. Wang and Y.-H. Liu, "A PSO-based fuzzy-controlled searching for the optimal charge pattern of Li-ion batteries," *IEEE Transactions on Industrial Electronics*, vol. 62, no. 5, pp. 2983-2993, 2014. <https://doi.org/10.1109/TIE.2014.2363049>
- [299] M. M. Nishat, F. Faisal, A. J. Evan, M. M. Rahaman, M. S. Sifat, and H. F. Rabbi, "Development of genetic algorithm (ga) based optimized PID controller for stability analysis of DC-DC buck converter," *Journal of Power and Energy Engineering*, vol. 8, no. 09, p. 8, 2020.
- [300] L. A. Zadeh, "Fuzzy sets," in *Fuzzy sets, fuzzy logic, and fuzzy systems: selected papers by Lotfi A Zadeh*: World Scientific, 1996, pp. 394-432.
- [301] A. Ilyas, M. R. Khan, and M. Ayyub, "FPGA based real-time implementation of fuzzy logic controller for maximum power point tracking of solar photovoltaic system," *Optik*, vol. 213, p. 164668, 2020. <https://doi.org/10.1016/j.ijleo.2020.164668>
- [302] C.-M. Lin, V.-H. La, and T.-L. Le, "DC–DC converters design using a type-2 wavelet fuzzy cerebellar model articulation controller," *Neural Computing and Applications*, vol. 32, no. 7, pp. 2217-2229, 2020. <https://doi.org/10.1007/s00521-018-3755-z>
- [303] C.-H. Cheng, P.-J. Cheng, and M.-T. Wu, "Fuzzy logic design of self-tuning switching power supply," *Expert Systems with Applications*, vol. 37, no. 4, pp. 2929-2936, 2010. <https://doi.org/10.1016/j.eswa.2009.09.043>
- [304] S. K. Gadari, P. Kumar, K. Mishra, A. R. Bhowmik, and A. K. Chakraborty, "Detailed analysis of Fuzzy Logic Controller for Second order DC-DC Converters," in *2019 8th International Conference on Power Systems (ICPS)*, 2019: IEEE, pp. 1-6. <https://doi.org/10.1109/ICPS48983.2019.9067607>
- [305] S. Kumar, "Fuzzy Logic Controller on Buck Converter " *MATLAB Central File Exchange*, 2022. [Online]. <https://www.mathworks.com/matlabcentral/fileexchange/86257-fuzzy-logic-controller-on-buck-converter>.
- [306] G. Li, S. Xie, B. Wang, J. Xin, Y. Li, and S. Du, "Photovoltaic Power Forecasting With a Hybrid Deep Learning Approach," *IEEE Access*, vol. 8, pp. 175871-175880, 2020. <https://doi.org/10.1109/ACCESS.2020.3025860>
- [307] A. K. Yadav and S. Chandel, "Solar radiation prediction using Artificial Neural Network techniques: A review," *Renewable and sustainable energy reviews*, vol. 33, pp. 772-781, 2014. <https://doi.org/10.1016/j.rser.2013.08.055>

References

- [308] T. Kim, W. Ko, and J. Kim, "Analysis and impact evaluation of missing data imputation in day-ahead PV generation forecasting," *Applied Sciences*, vol. 9, no. 1, p. 204, 2019. <https://doi.org/10.3390/app9010204>
- [309] T. Khatib, A. Ghareeb, M. Tamimi, M. Jaber, and S. Jaradat, "A new offline method for extracting IV characteristic curve for photovoltaic modules using artificial neural networks," *Solar Energy*, vol. 173, pp. 462-469, 2018. <https://doi.org/10.1016/j.solener.2018.07.092>
- [310] K.-B. Song, Y.-S. Baek, D. H. Hong, and G. Jang, "Short-term load forecasting for the holidays using fuzzy linear regression method," *IEEE transactions on power systems*, vol. 20, no. 1, pp. 96-101, 2005. <https://doi.org/10.1109/TPWRS.2004.835632>
- [311] L. Hernandez, C. Baladron, JM. Aguiar, B. Carro, AJ. Sanchez-Esguevillas, J. Lloret, J. Massana, "A survey on electric power demand forecasting: future trends in smart grids, microgrids and smart buildings," *IEEE Communications Surveys & Tutorials*, vol. 16, no. 3, pp. 1460-1495, 2014. <https://doi.org/10.1109/SURV.2014.032014.00094>
- [312] K. Yan, H. Shen, L. Wang, H. Zhou, M. Xu, and Y. Mo, "Short-term solar irradiance forecasting based on a hybrid deep learning methodology," *Information*, vol. 11, no. 1, p. 32, 2020. <https://doi.org/10.3390/info11010032>
- [313] S. Hochreiter and J. Schmidhuber, "LSTM can solve hard long time lag problems," *Advances in neural information processing systems*, pp. 473-479, 1997.
- [314] Y. Jung, J. Jung, B. Kim, and S. Han, "Long short-term memory recurrent neural network for modeling temporal patterns in long-term power forecasting for solar PV facilities: Case study of South Korea," *Journal of Cleaner Production*, vol. 250, p. 119476, 2020. <https://doi.org/10.1016/j.jclepro.2019.119476>
- [315] M. Mishra, P. B. Dash, J. Nayak, B. Naik, and S. K. Swain, "Deep learning and wavelet transform integrated approach for short-term solar PV power prediction," *Measurement*, vol. 166, p. 108250, 2020. <https://doi.org/10.1016/j.measurement.2020.108250>
- [316] G. Van Houdt, C. Mosquera, and G. Nápoles, "A review on the long short-term memory model," *Artificial Intelligence Review*, vol. 53, pp. 5929-5955, 2020.
- [317] K. Wang, X. Qi, and H. Liu, "Photovoltaic power forecasting based LSTM-Convolutional Network," *Energy*, vol. 189, p. 116225, 2019. <https://doi.org/10.1016/j.energy.2019.116225>
- [318] H. Zhou, Y. Zhang, L. Yang, Q. Liu, K. Yan, and Y. Du, "Short-term photovoltaic power forecasting based on long short term memory neural network and attention mechanism," *Ieee Access*, vol. 7, pp. 78063-78074, 2019. <https://doi.org/10.1109/ACCESS.2019.2923006>
- [319] I. T. Administration, "Egypt - Country Commercial Guide," Online Reference 2020-09-15 2020, Available: [https://www.trade.gov/country-commercial-guides/egypt-renewable-energy#:~:text=Egypt%20intends%20to%20increase%20the,CSP\)%203%20percent%20by%202035](https://www.trade.gov/country-commercial-guides/egypt-renewable-energy#:~:text=Egypt%20intends%20to%20increase%20the,CSP)%203%20percent%20by%202035).

References

- [320] A. Azizivahed, A. Arefi, S. Ghavidel, M. Shafie-Khah, L. Li, J. Zhang, JP. Catalão, "Energy management strategy in dynamic distribution network reconfiguration considering renewable energy resources and storage," *IEEE transactions on sustainable energy*, vol. 11, no. 2, pp. 662-673, 2019. <https://doi.org/10.1109/TSTE.2019.2901429>
- [321] F. Fazelpour, M. Vafaiepour, O. Rahbari, and R. Shirmohammadi, "Considerable parameters of using PV cells for solar-powered aircrafts," *Renewable and Sustainable Energy Reviews*, vol. 22, pp. 81-91, 2013. <https://doi.org/10.1016/j.rser.2013.01.016>
- [322] M. Mattei, G. Notton, C. Cristofari, M. Muselli, and P. Poggi, "Calculation of the polycrystalline PV module temperature using a simple method of energy balance," *Renewable energy*, vol. 31, no. 4, pp. 553-567, 2006. <https://doi.org/10.1016/j.renene.2005.03.010>
- [323] D. Yan and C. Ma, "Stochastic planning of electric vehicle charging station integrated with photovoltaic and battery systems," *IET Generation, Transmission & Distribution*, vol. 14, no. 19, pp. 4217-4224, 2020. <https://doi.org/10.1049/iet-gtd.2019.1737>
- [324] M. Samy, S. Barakat, and H. Ramadan, "Techno-economic analysis for rustic electrification in Egypt using multi-source renewable energy based on PV/wind/FC," *International Journal of Hydrogen Energy*, vol. 45, no. 20, pp. 11471-11483, 2020. <https://doi.org/10.1016/j.ijhydene.2019.04.038>
- [325] S. Reviews, "Solar panel cost Egypt: Prices & data 2022," 2022. [Online]. Available: <https://www.solarreviews.com/solar-panel-cost/arkansas/egypt>.
- [326] M. o. E. a. E. C. i. Egypt, "Ministry of Electricity and Energy Company in Egypt," Online Reference, 2022. [Online]. Available: http://www.moee.gov.eg/test_new/Home.aspx.
- [327] N. a. R. E. A. (NERA), "Electric Feeding Tariff," Ministry of Electricity and Renewable Energy, 2022. [Online]. Available: <http://nrea.gov.eg/test/en/Home>.
- [328] R. Kot, M. Rolak, and M. Malinowski, "Comparison of maximum peak power tracking algorithms for a small wind turbine," *Mathematics and Computers in Simulation*, vol. 91, pp. 29-40, 2013. <https://doi.org/10.1016/j.matcom.2013.03.010>
- [329] M. Lydia, S. S. Kumar, A. I. Selvakumar, and G. E. P. Kumar, "A comprehensive review on wind turbine power curve modeling techniques," *Renewable and Sustainable Energy Reviews*, vol. 30, pp. 452-460, 2014. <https://doi.org/10.1016/j.rser.2013.10.030>
- [330] S. Samsatli and N. J. Samsatli, "A general mixed integer linear programming model for the design and operation of integrated urban energy systems," *Journal of Cleaner Production*, vol. 191, pp. 458-479, 2018. <https://doi.org/10.1016/j.jclepro.2018.04.198>
- [331] M. R. Narimani, A. A. Vahed, R. Azizipanah-Abarghooee, and M. Javidsharifi, "Enhanced gravitational search algorithm for multi-objective distribution feeder reconfiguration considering reliability, loss and operational cost," *IET Generation,*

References

- Transmission & Distribution*, vol. 8, no. 1, pp. 55-69, 2014. <https://doi.org/10.1049/iet-gtd.2013.0117>
- [332] Z. Wu and X. Xia, "Optimal switching renewable energy system for demand side management," *Solar Energy*, vol. 114, pp. 278-288, 2015. <https://doi.org/10.1016/j.solener.2015.02.001>
- [333] M. Dabbaghjamanesh, A. Kavousi-Fard, S. Mehraeen, J. Zhang, and Z. Y. Dong, "Sensitivity analysis of renewable energy integration on stochastic energy management of automated reconfigurable hybrid AC–DC microgrid considering DLR security constraint," *IEEE Transactions on Industrial Informatics*, vol. 16, no. 1, pp. 120-131, 2019. <https://doi.org/10.1109/TII.2019.2915089>
- [334] S. Thakar, A. Vijay, and S. Doolla, "System reconfiguration in microgrids," *Sustainable energy, grids and networks*, vol. 17, p. 100191, 2019. <https://doi.org/10.1016/j.segan.2019.100191>
- [335] P. Akaber, T. Hughes, and S. Sobolev, "MILP-based customer-oriented E-Fleet charging scheduling platform," *IET Smart Grid*, vol. 4, no. 2, pp. 215-223, 2021. <https://doi.org/10.1049/stg2.12034>
- [336] T. Kern, P. Dossow, and E. Morlock, "Revenue opportunities by integrating combined vehicle-to-home and vehicle-to-grid applications in smart homes," *Applied Energy*, vol. 307, p. 118187, 2022. <https://doi.org/10.1016/j.apenergy.2021.118187>
- [337] C. F. Heuberger, P. K. Bains, and N. Mac Dowell, "The EV-olution of the power system: A spatio-temporal optimisation model to investigate the impact of electric vehicle deployment," *Applied Energy*, vol. 257, p. 113715, 2020. <https://doi.org/10.1016/j.apenergy.2019.113715>
- [338] M. T. Hussain, N. B. Sulaiman, M. S. Hussain, and M. Jabir, "Optimal Management strategies to solve issues of grid having Electric Vehicles (EV): A review," *Journal of Energy Storage*, vol. 33, p. 102114, 2021. <https://doi.org/10.1016/j.est.2020.102114>
- [339] J. F. Franco, M. J. Rider, and R. Romero, "A mixed-integer linear programming model for the electric vehicle charging coordination problem in unbalanced electrical distribution systems," *IEEE Transactions on Smart Grid*, vol. 6, no. 5, pp. 2200-2210, 2015. <https://doi.org/10.1109/TSG.2015.2394489>
- [340] P. Mesarić and S. Krajcar, "Home demand side management integrated with electric vehicles and renewable energy sources," *Energy and Buildings*, vol. 108, pp. 1-9, 2015. <https://doi.org/10.1016/j.enbuild.2015.09.001>
- [341] C. Zhang, Y. Liu, F. Wu, B. Tang, and W. Fan, "Effective charging planning based on deep reinforcement learning for electric vehicles," *IEEE Transactions on Intelligent Transportation Systems*, vol. 22, no. 1, pp. 542-554, 2020. <https://doi.org/10.1109/TITS.2020.3002271>
- [342] A. Mani, S. A. Bakar, P. Krishnan, and S. Yaacob, "Comparison of optimized Markov Decision Process using Dynamic Programming and Temporal Differencing—A reinforcement learning approach," in *Journal of Physics:*

References

- Conference Series*, 2021, vol. 2107, no. 1: IOP Publishing, p. 012026. <https://doi.org/10.1088/1742-6596/2107/1/012026>
- [343] N. Mazyavkina, S. Sviridov, S. Ivanov, and E. Burnaev, "Reinforcement learning for combinatorial optimization: A survey," *Computers & Operations Research*, vol. 134, p. 105400, 2021. <https://doi.org/10.1016/j.cor.2021.105400>
- [344] Z. Michalewicz and M. Schoenauer, "Evolutionary algorithms for constrained parameter optimization problems," *Evolutionary computation*, vol. 4, no. 1, pp. 1-32, 1996. <https://doi.org/10.1162/evco.1996.4.1.1>
- [345] X. Lü, Y. Wu, J. Lian, Y. Zhang, C. Chen, P. Wang, L. Meng, "Energy management of hybrid electric vehicles: A review of energy optimization of fuel cell hybrid power system based on genetic algorithm," *Energy Conversion and Management*, vol. 205, p. 112474, 2020. <https://doi.org/10.1016/j.enconman.2020.112474>
- [346] P. Kuendee and U. Janjarassuk, "A comparative study of mixed-integer linear programming and genetic algorithms for solving binary problems," in *2018 5th International Conference on Industrial Engineering and Applications (ICIEA)*, 2018: IEEE, pp. 284-288. <https://doi.org/10.1109/IEA.2018.8387111>
- [347] Z. Michalewicz and M. Schoenauer, "Evolutionary Algorithms," *Encyclopedia of Information Systems*, vol. 2, pp. 259-267, 2002.
- [348] A.-a. H. Mantawy, "Genetic Algorithms Application to Electric Power Systems," *Genetic Algorithms in Applications; Rustem, P., Ed.; InTech: London, UK*, 2012.
- [349] M. N. Ab Wahab, S. Nefti-Meziani, and A. Atyabi, "A comprehensive review of swarm optimization algorithms," *PloS one*, vol. 10, no. 5, p. e0122827, 2015. <https://doi.org/10.1371/journal.pone.0122827>
- [350] A. A. Radwan, A. A. Zaki Diab, A.-H. M. Elsayed, H. Haes Alhelou, and P. Siano, "Active distribution network modeling for enhancing sustainable power system performance; a case study in Egypt," *Sustainability*, vol. 12, no. 21, p. 8991, 2020. <https://doi.org/10.3390/su12218991>
- [351] M. A. Tolba, H. Rezk, V. Tulsy, A. A. Z. Diab, A. Y. Abdelaziz, and A. Vanin, "Impact of optimum allocation of renewable distributed generations on distribution networks based on different optimization algorithms," *Energies*, vol. 11, no. 1, p. 245, 2018. <https://doi.org/10.3390/en11010245>

Appendix A

Source Code Listings

The MATLAB source code that has been utilised in both the hierarchical technique (HT) and the conditional random technique (CRT) using the multi-stage charging current (MSCC) based on the cuckoo optimisation algorithm (COA) is stated as follows.

```
a= [4.1785 0.2505 0.0245 0.006 309317 4581000 100;...
    4.1077 0.22 0.0245 0.006 304467 4509111 97;...
    4.0625 0.2195 0.0185 0.012 528134 1114917 95;...
    4.0344 0.2255 0.0125 0.006 1148558 4429111 90;...
    4.0002 0.439 0.031 0.006 183058 4339556 85;...
    3.9612 0.3845 0.0125 0.012 1118318 1077944 80;...
    3.927 0.366 0.0185 0.012 506465 1069139 75;...
    3.85 0.311 0.12 0.012 1183312 1051167 70;...
    3.825 0.442 0.0125 0.006 1075781 4148333 65;...
    3.81348 0.2624 0.0185 0.012 494264 1043361 60;...
    3.7683 0.2745 0.0125 0.012 1069099 1030472 55;...
    3.72681 0.23805 0.012 0.012 1149375 940941 50;...
    3.69141 0.27455 0.0185 0.012 477894 1008778 45;...
    3.6621 0.2805 0.0185 0.006 473884 4001889 40;...
    3.64041 0.28205 0.0125 0.012 1031832 994528 35;...
    3.6194 0.2745 0.0185 0.006 468427 3955778 30;...
    3.59253 0.26865 0.012 0.012 1105500 904998 25;...
    3.5657 0.299 0.0125 0.006 1009339 3892000 20;...
    3.5364 0.3295 0.0185 0.006 456068 3851333 15;...
    3.4998 0.3665 0.0245 0.006 256697 3801111 10;...
    3.38 0.3535 0.012 0.013 1033781 846246 5;...
    3.24143 0.33815 0.061 0.036 38309 94815 2.25;...
    2.9736 0.427 0.0975 0.08 13626 18105 0 ];

% Input the starting voltage of the battery
V1=2.9

if (V1<=2.9724) && (V1>=2.75)
SOC_1=0
elseif (V1<=3.24143) && (V1>2.9724)
SOC_1=2.25
elseif (V1<=3.41431) && (V1>3.24143)
SOC_1=5
elseif (V1<=3.4998) && (V1>3.41431)
SOC_1=10
elseif (V1<=3.5364) && (V1>3.4998)
SOC_1=15
elseif (V1<=3.5657) && (V1>3.5364)
SOC_1=20
elseif (V1<=3.59253) && (V1>3.5657)
SOC_1=25
elseif (V1<=3.6194) && (V1>3.59253)
```

Appendix A

```
SOC_1=30
elseif (V1<=3.64041) && (V1>3.6194)
SOC_1=35
elseif (V1<=3.6621) && (V1>3.64041)
SOC_1=40
elseif (V1<=3.69141) && (V1>3.6621)
SOC_1=45
elseif (V1<=3.72681) && (V1>3.69141)
SOC_1=50
elseif (V1<=3.7683) && (V1>3.72681)
SOC_1=55
elseif (V1<=3.81348) && (V1>3.7683)
SOC_1=60
elseif (V1<=3.8562) && (V1>3.81348)
SOC_1=65
elseif (V1<=3.89404) && (V1>3.8562)
SOC_1=70
elseif (V1<=3.927) && (V1>3.89404)
SOC_1=75
elseif (V1<=3.9612) && (V1>3.927)
SOC_1=80
elseif (V1<=4.0002) && (V1>3.9612)
SOC_1=85
elseif (V1<=4.0344) && (V1>4.0002)
SOC_1=90
elseif (V1<=4.0637) && (V1>4.0344)
SOC_1=95
elseif (V1<=4.1077) && (V1>4.0637)
SOC_1=97
else
SOC_1=100
end

%% The First Stage
%T_1=I(6)
Ec1_2=0;
SOC_2_2=SOC_1+(100*((I(1)*I(6))/3600));
SOC_2_2=ceil(SOC_2_2)
for SOC_2=SOC_1:1:SOC_2_2
if (SOC_2<=2.25) && (SOC_2>=0)
R0_2=a(23,2);
R1_2=a(23,3);
R2_2=a(23,4);
C1_2=a(23,5);
C2_2=a(23,6);
V2=a(23,1);
elseif (SOC_2<=5) && (SOC_2>2.25)
R0_2=a(22,2);
R1_2=a(22,3);
R2_2=a(22,4);
C1_2=a(22,5);
```

Appendix A

```
C2_2=a(22,6);
V2=a(22,1);
elseif (SOC_2<=10) && (SOC_2>5)
R0_2=a(21,2);
R1_2=a(21,3);
R2_2=a(21,4);
C1_2=a(21,5);
C2_2=a(21,6);
V2=a(21,1);
elseif (SOC_2<=15) && (SOC_2>10)
R0_2=a(20,2);
R1_2=a(20,3);
R2_2=a(20,4);
C1_2=a(20,5);
C2_2=a(20,6);
V2=a(20,1);
elseif (SOC_2<=20) && (SOC_2>15)
R0_2=a(19,2);
R1_2=a(19,3);
R2_2=a(19,4);
C1_2=a(19,5);
C2_2=a(19,6);
V2=a(19,1);
elseif (SOC_2<=25) && (SOC_2>20)
R0_2=a(18,2);
R1_2=a(18,3);
R2_2=a(18,4);
C1_2=a(18,5);
C2_2=a(18,6);
V2=a(18,1);
elseif (SOC_2<=30) && (SOC_2>25)
R0_2=a(17,2);
R1_2=a(17,3);
R2_2=a(17,4);
C1_2=a(17,5);
C2_2=a(17,6);
V2=a(17,1);
elseif (SOC_2<=35) && (SOC_2>30)
R0_2=a(16,2);
R1_2=a(16,3);
R2_2=a(16,4);
C1_2=a(16,5);
C2_2=a(16,6);
V2=a(16,1);
elseif (SOC_2<=40) && (SOC_2>35)
R0_2=a(15,2);
R1_2=a(15,3);
R2_2=a(15,4);
C1_2=a(15,5);
C2_2=a(15,6);
V2=a(15,1);
```

Appendix A

```
elseif (SOC_2<=45) && (SOC_2>40)
R0_2=a(14,2);
R1_2=a(14,3);
R2_2=a(14,4);
C1_2=a(14,5);
C2_2=a(14,6);
V2=a(14,1);
elseif (SOC_2<=50) && (SOC_2>45)
R0_2=a(13,2);
R1_2=a(13,3);
R2_2=a(13,4);
C1_2=a(13,5);
C2_2=a(13,6);
V2=a(13,1);
elseif (SOC_2<=55) && (SOC_2>50)
R0_2=a(12,2);
R1_2=a(12,3);
R2_2=a(12,4);
C1_2=a(12,5);
C2_2=a(12,6);
V2=a(12,1);
elseif (SOC_2<=60) && (SOC_2>55)
R0_2=a(11,2);
R1_2=a(11,3);
R2_2=a(11,4);
C1_2=a(11,5);
C2_2=a(11,6);
V2=a(11,1);
elseif (SOC_2<=65) && (SOC_2>60)
R0_2=a(10,2);
R1_2=a(10,3);
R2_2=a(10,4);
C1_2=a(10,5);
C2_2=a(10,6);
V2=a(10,1);
elseif (SOC_2<=70) && (SOC_2>65)
R0_2=a(9,2);
R1_2=a(9,3);
R2_2=a(9,4);
C1_2=a(9,5);
C2_2=a(9,6);
V2=a(9,1);
elseif (SOC_2<=75) && (SOC_2>70)
R0_2=a(8,2);
R1_2=a(8,3);
R2_2=a(8,4);
C1_2=a(8,5);
C2_2=a(8,6);
V2=a(8,1);
elseif (SOC_2<=80) && (SOC_2>75)
R0_2=a(7,2);
```

Appendix A

```
R1_2=a(7,3);
R2_2=a(7,4);
C1_2=a(7,5);
C2_2=a(7,6);
V2=a(7,1);
elseif (SOC_2<=85) && (SOC_2>80)
R0_2=a(6,2);
R1_2=a(6,3);
R2_2=a(6,4);
C1_2=a(6,5);
C2_2=a(6,6);
V2=a(6,1);
elseif (SOC_2<=90) && (SOC_2>85)
R0_2=a(5,2);;
R1_2=a(5,3);
R2_2=a(5,4);
C1_2=a(5,5);
C2_2=a(5,6);
V2=a(5,1);
elseif (SOC_2<=95) && (SOC_2>90)
R0_2=a(4,2);
R1_2=a(4,3);
R2_2=a(4,4);
C1_2=a(4,5);
C2_2=a(4,6);
V2=a(4,1);
elseif (SOC_2<=97) && (SOC_2>95)
R0_2=a(3,2);
R1_2=a(3,3);
R2_2=a(3,4);
C1_2=a(3,5);
C2_2=a(3,6);
V2=a(3,1);
elseif (SOC_2<=100) && (SOC_2>97)
R0_2=a(2,2);
R1_2=a(2,3);
R2_2=a(2,4);
C1_2=a(2,5);
C2_2=a(2,6);
V2=a(2,1);
else
R0_2=a(1,2);
R1_2=a(1,3);
R2_2=a(1,4);
C1_2=a(1,5);
C2_2=a(1,6);
V2=a(1,1);
end
SOC_2
Vt_2=V2+(R0_2*I(1))+...
```

Appendix A

```
(R1_2*((I(1)*(1-exp(-
1/(R1_2*C1_2))))/(1/(R1_2*C1_2))))+...
(R2_2*((I(1)*(1-exp(-1/(R2_2*C2_2))))/(1/(R2_2*C2_2))))

Ec1_2=Ec1_2...
+((36/I(1))*R0_2*power(I(1),2))...
+(36/I(1))*R1_2*power(((I(1)*(1-exp(-
1/(R1_2*C1_2))))/(1/(R1_2*C1_2))),2)...
+(36/I(1))*R2_2*power(((I(1)*(1-exp(-
1/(R2_2*C2_2))))/(1/(R2_2*C2_2))),2);
end
Ec1_2;

%% The Second Stage
%T_2=I(7)
Ec1_3=0;
SOC_3_3=SOC_2_2+(((I(2)*I(7))/3600)*100);
SOC_3_3=ceil(SOC_3_3)
for SOC_3=(SOC_2_2+1):1:SOC_3_3
    if (SOC_3<=2.25) && (SOC_3>=0)
        R0_3=a(23,2);
        R1_3=a(23,3);
        R2_3=a(23,4);
        C1_3=a(23,5);
        C2_3=a(23,6);
        V3=a(23,1);
    elseif (SOC_3<=5) && (SOC_3>2.25)
        R0_3=a(22,2);
        R1_3=a(22,3);
        R2_3=a(22,4);
        C1_3=a(22,5);
        C2_3=a(22,6);
        V3=a(22,1);
    elseif (SOC_3<=10) && (SOC_3>5)
        R0_3=a(21,2);
        R1_3=a(21,3);
        R2_3=a(21,4);
        C1_3=a(21,5);
        C2_3=a(21,6);
        V3=a(21,1);
    elseif (SOC_3<=15) && (SOC_3>10)
        R0_3=a(20,2);
        R1_3=a(20,3);
        R2_3=a(20,4);
        C1_3=a(20,5);
        C2_3=a(20,6);
        V3=a(20,1);
    elseif (SOC_3<=20) && (SOC_3>15)
        R0_3=a(19,2);
        R1_3=a(19,3);
        R2_3=a(19,4);
```

Appendix A

```
C1_3=a(19,5);
C2_3=a(19,6);
V3=a(19,1);
elseif (SOC_3<=25) && (SOC_3>20)
R0_3=a(18,2);
R1_3=a(18,3);
R2_3=a(18,4);
C1_3=a(18,5);
C2_3=a(18,6);
V3=a(18,1);
elseif (SOC_3<=30) && (SOC_3>25)
R0_3=a(17,2);
R1_3=a(17,3);
R2_3=a(17,4);
C1_3=a(17,5);
C2_3=a(17,6);
V3=a(17,1);
elseif (SOC_3<=35) && (SOC_3>30)
R0_3=a(16,2);
R1_3=a(16,3);
R2_3=a(16,4);
C1_3=a(16,5);
C2_3=a(16,6);
V3=a(16,1);
elseif (SOC_3<=40) && (SOC_3>35)
R0_3=a(15,2);
R1_3=a(15,3);
R2_3=a(15,4);
C1_3=a(15,5);
C2_3=a(15,6);
V3=a(15,1);
elseif (SOC_3<=45) && (SOC_3>40)
R0_3=a(14,2);
R1_3=a(14,3);
R2_3=a(14,4);
C1_3=a(14,5);
C2_3=a(14,6);
V3=a(14,1);
elseif (SOC_3<=50) && (SOC_3>45)
R0_3=a(13,2);
R1_3=a(13,3);
R2_3=a(13,4);
C1_3=a(13,5);
C2_3=a(13,6);
V3=a(13,1);
elseif (SOC_3<=55) && (SOC_3>50)
R0_3=a(12,2);
R1_3=a(12,3);
R2_3=a(12,4);
C1_3=a(12,5);
C2_3=a(12,6);
```

Appendix A

```
V3=a(12,1);
elseif (SOC_3<=60) && (SOC_3>55)
R0_3=a(11,2);
R1_3=a(11,3);
R2_3=a(11,4);
C1_3=a(11,5);
C2_3=a(11,6);
V3=a(11,1);
elseif (SOC_3<=65) && (SOC_3>60)
R0_3=a(10,2);
R1_3=a(10,3);
R2_3=a(10,4);
C1_3=a(10,5);
C2_3=a(10,6);
V3=a(10,1);
elseif (SOC_3<=70) && (SOC_3>65)
R0_3=a(9,2);
R1_3=a(9,3);
R2_3=a(9,4);
C1_3=a(9,5);
C2_3=a(9,6);
V3=a(9,1);
elseif (SOC_3<=75) && (SOC_3>70)
R0_3=a(8,2);
R1_3=a(8,3);
R2_3=a(8,4);
C1_3=a(8,5);
C2_3=a(8,6);
V3=a(8,1);
elseif (SOC_3<=80) && (SOC_3>75)
R0_3=a(7,2);
R1_3=a(7,3);
R2_3=a(7,4);
C1_3=a(7,5);
C2_3=a(7,6);
V3=a(7,1);
elseif (SOC_3<=85) && (SOC_3>80)
R0_3=a(6,2);
R1_3=a(6,3);
R2_3=a(6,4);
C1_3=a(6,5);
C2_3=a(6,6);
V3=a(6,1);
elseif (SOC_3<=90) && (SOC_3>85)
R0_3=a(5,2);;
R1_3=a(5,3);
R2_3=a(5,4);
C1_3=a(5,5);
C2_3=a(5,6);
V3=a(5,1);
elseif (SOC_3<=95) && (SOC_3>90)
```

Appendix A

```

R0_3=a(4,2);
R1_3=a(4,3);
R2_3=a(4,4);
C1_3=a(4,5);
C2_3=a(4,6);
V3=a(4,1);
elseif (SOC_3<=97) && (SOC_3>95)
R0_3=a(3,2);
R1_3=a(3,3);
R2_3=a(3,4);
C1_3=a(3,5);
C2_3=a(3,6);
V3=a(3,1);
elseif (SOC_3<=100) && (SOC_3>97)
R0_3=a(2,2);
R1_3=a(2,3);
R2_3=a(2,4);
C1_3=a(2,5);
C2_3=a(2,6);
V3=a(2,1);
else
R0_3=a(1,2);
R1_3=a(1,3);
R2_3=a(1,4);
C1_3=a(1,5);
C2_3=a(1,6);
V3=a(1,1);
end
SOC_3
Vt_3=V3+(R0_3*I(2))+...
(R1_3*((I(2)*(1-exp(-1/(R1_3*C1_3))))/(1/(R1_3*C1_3)))-
(I(1)*((1-exp(-1/(R1_3*C1_3)))/(1/(R1_3*C1_3)))-exp(-
1/(R1_3*C1_3))))))+...
(R2_3*((I(2)*(1-exp(-1/(R2_3*C2_3))))/(1/(R2_3*C2_3)))-
(I(1)*((1-exp(-1/(R2_3*C2_3)))/(1/(R2_3*C2_3)))-exp(-
1/(R2_3*C2_3))))))

Ec1_3=Ec1_3...
+((36/I(2))*R0_3*power(I(2),2))...
+(36/I(2))*R1_3*power(((I(2)*(1-exp(-
1/(R1_3*C1_3)))/(1/(R1_3*C1_3)))-I(1)*((1-exp(-
1/(R1_3*C1_3)))/(1/(R1_3*C1_3)))-exp(-1/(R1_3*C1_3)))))-
((I(1)+((I(1)*(1-exp(-
1/(R1_3*C1_3)))/(1/(R1_3*C1_3))))*(exp(-
1/(R1_3*C1_3))),2))...
+(36/I(2))*R2_3*power(((I(2)*(1-exp(-
1/(R2_3*C2_3)))/(1/(R2_3*C2_3)))-I(1)*((1-exp(-
1/(R2_3*C2_3)))/(1/(R2_3*C2_3)))-exp(-1/(R2_3*C2_3)))))-
((I(1)+((I(1)*(1-exp(-
1/(R1_3*C1_3)))/(1/(R1_3*C1_3))))*(exp(-1/(R1_3*C1_3))),2));
end

```

Appendix A

```
Ec1_3;

%% The Third Stage
%T_3=I(8)
Ec1_4=0;
SOC_4_4=SOC_3_3+(((I(8)*I(3))/3600)*100);
SOC_4_4=ceil(SOC_4_4)
for SOC_4=(SOC_3_3+1):1:SOC_4_4
    if (SOC_4<=2.25) && (SOC_4>=0)
        R0_4=a(23,2);
        R1_4=a(23,3);
        R2_4=a(23,4);
        C1_4=a(23,5);
        C2_4=a(23,6);
        V4=a(23,1);
    elseif (SOC_4<=5) && (SOC_4>2.25)
        R0_4=a(22,2);
        R1_4=a(22,3);
        R2_4=a(22,4);
        C1_4=a(22,5);
        C2_4=a(22,6);
        V4=a(22,1);
    elseif (SOC_4<=10) && (SOC_4>5)
        R0_4=a(21,2);
        R1_4=a(21,3);
        R2_4=a(21,4);
        C1_4=a(21,5);
        C2_4=a(21,6);
        V4=a(21,1);
    elseif (SOC_4<=15) && (SOC_4>10)
        R0_4=a(20,2);
        R1_4=a(20,3);
        R2_4=a(20,4);
        C1_4=a(20,5);
        C2_4=a(20,6);
        V4=a(20,1);
    elseif (SOC_4<=20) && (SOC_4>15)
        R0_4=a(19,2);
        R1_4=a(19,3);
        R2_4=a(19,4);
        C1_4=a(19,5);
        C2_4=a(19,6);
        V4=a(19,1);
    elseif (SOC_4<=25) && (SOC_4>20)
        R0_4=a(18,2);
        R1_4=a(18,3);
        R2_4=a(18,4);
        C1_4=a(18,5);
        C2_4=a(18,6);
        V4=a(18,1);
    elseif (SOC_4<=30) && (SOC_4>25)
```

Appendix A

```
R0_4=a(17,2);
R1_4=a(17,3);
R2_4=a(17,4);
C1_4=a(17,5);
C2_4=a(17,6);
V4=a(17,1);
elseif (SOC_4<=35) && (SOC_4>30)
R0_4=a(16,2);
R1_4=a(16,3);
R2_4=a(16,4);
C1_4=a(16,5);
C2_4=a(16,6);
V4=a(16,1);
elseif (SOC_4<=40) && (SOC_4>35)
R0_4=a(15,2);
R1_4=a(15,3);
R2_4=a(15,4);
C1_4=a(15,5);
C2_4=a(15,6);
V4=a(15,1);
elseif (SOC_4<=45) && (SOC_4>40)
R0_4=a(14,2);
R1_4=a(14,3);
R2_4=a(14,4);
C1_4=a(14,5);
C2_4=a(14,6);
V4=a(14,1);
elseif (SOC_4<=50) && (SOC_4>45)
R0_4=a(13,2);
R1_4=a(13,3);
R2_4=a(13,4);
C1_4=a(13,5);
C2_4=a(13,6);
V4=a(13,1);
elseif (SOC_4<=55) && (SOC_4>50)
R0_4=a(12,2);
R1_4=a(12,3);
R2_4=a(12,4);
C1_4=a(12,5);
C2_4=a(12,6);
V4=a(12,1);
elseif (SOC_4<=60) && (SOC_4>55)
R0_4=a(11,2);
R1_4=a(11,3);
R2_4=a(11,4);
C1_4=a(11,5);
C2_4=a(11,6);
V4=a(11,1);
elseif (SOC_4<=65) && (SOC_4>60)
R0_4=a(10,2);
R1_4=a(10,3);
```

Appendix A

```
R2_4=a(10,4);
C1_4=a(10,5);
C2_4=a(10,6);
V4=a(10,1);
elseif (SOC_4<=70) && (SOC_4>65)
R0_4=a(9,2);
R1_4=a(9,3);
R2_4=a(9,4);
C1_4=a(9,5);
C2_4=a(9,6);
V4=a(9,1);
elseif (SOC_4<=75) && (SOC_4>70)
R0_4=a(8,2);
R1_4=a(8,3);
R2_4=a(8,4);
C1_4=a(8,5);
C2_4=a(8,6);
V4=a(8,1);
elseif (SOC_4<=80) && (SOC_4>75)
R0_4=a(7,2);
R1_4=a(7,3);
R2_4=a(7,4);
C1_4=a(7,5);
C2_4=a(7,6);
V4=a(7,1);
elseif (SOC_4<=85) && (SOC_4>80)
R0_4=a(6,2);
R1_4=a(6,3);
R2_4=a(6,4);
C1_4=a(6,5);
C2_4=a(6,6);
V4=a(6,1);
elseif (SOC_4<=90) && (SOC_4>85)
R0_4=a(5,2);
R1_4=a(5,3);
R2_4=a(5,4);
C1_4=a(5,5);
C2_4=a(5,6);
V4=a(5,1);
elseif (SOC_4<=95) && (SOC_4>90)
R0_4=a(4,2);
R1_4=a(4,3);
R2_4=a(4,4);
C1_4=a(4,5);
C2_4=a(4,6);
V4=a(4,1);
elseif (SOC_4<=97) && (SOC_4>95)
R0_4=a(3,2);
R1_4=a(3,3);
R2_4=a(3,4);
C1_4=a(3,5);
```

Appendix A

```

C2_4=a(3,6);
V4=a(3,1);
elseif (SOC_4<=100) && (SOC_4>97)
R0_4=a(2,2);
R1_4=a(2,3);
R2_4=a(2,4);
C1_4=a(2,5);
C2_4=a(2,6);
V4=a(2,1);
else
R0_4=a(1,2);
R1_4=a(1,3);
R2_4=a(1,4);
C1_4=a(1,5);
C2_4=a(1,6);
V4=a(1,1);
end
Vt_4=V4+(R0_4*I(3))+...
(R1_4*((I(3)*(1-exp(-1/(R1_4*C1_4))))/(1/(R1_4*C1_4)))-
(I(2)*((1-exp(-1/(R1_4*C1_4)))/(1/(R1_4*C1_4)))-exp(-
1/(R1_4*C1_4))))))+...
(R2_4*((I(3)*(1-exp(-1/(R2_4*C2_4))))/(1/(R2_4*C2_4)))-
(I(2)*((1-exp(-1/(R2_4*C2_4)))/(1/(R2_4*C2_4)))-exp(-
1/(R2_4*C2_4))))))
Ec1_4=Ec1_4...
+((36/I(3))*R0_4*power(I(3),2))...
+(36/I(3))*R1_4*power(((I(3)*(1-exp(-
1/(R1_4*C1_4)))/(1/(R1_4*C1_4)))-I(2)*((1-exp(-
1/(R1_4*C1_4)))/(1/(R1_4*C1_4)))-exp(-
1/(R1_4*C1_4))))),2))...
+(36/I(3))*R2_4*power(((I(3)*(1-exp(-
1/(R2_4*C2_4)))/(1/(R2_4*C2_4)))-I(2)*((1-exp(-
1/(R2_4*C2_4)))/(1/(R2_4*C2_4)))-exp(-1/(R2_4*C2_4))))),2));
end
Ec1_4;

%% The Fourth Stage
%T_4=I(9)
Ec1_5=0;
SOC_5_5=SOC_4_4+(((I(9)*I(4))/3600)*100);
SOC_5_5=ceil(SOC_5_5)
for SOC_5=(SOC_4_4+1):1:SOC_5_5
if (SOC_5<=2.25) && (SOC_5>=0)
R0_5=a(23,2);
R1_5=a(23,3);
R2_5=a(23,4);
C1_5=a(23,5);
C2_5=a(23,6);
V5=a(23,1);
elseif (SOC_5<=5) && (SOC_5>2.25)
R0_5=a(22,2);

```

Appendix A

```
R1_5=a(22,3);
R2_5=a(22,4);
C1_5=a(22,5);
C2_5=a(22,6);
V5=a(22,1);
elseif (SOC_5<=10) && (SOC_5>5)
R0_5=a(21,2);
R1_5=a(21,3);
R2_5=a(21,4);
C1_5=a(21,5);
C2_5=a(21,6);
V5=a(21,1);
elseif (SOC_5<=15) && (SOC_5>10)
R0_5=a(20,2);
R1_5=a(20,3);
R2_5=a(20,4);
C1_5=a(20,5);
C2_5=a(20,6);
V5=a(20,1);
elseif (SOC_5<=20) && (SOC_5>15)
R0_5=a(19,2);
R1_5=a(19,3);
R2_5=a(19,4);
C1_5=a(19,5);
C2_5=a(19,6);
V5=a(19,1);
elseif (SOC_5<=25) && (SOC_5>20)
R0_5=a(18,2);
R1_5=a(18,3);
R2_5=a(18,4);
C1_5=a(18,5);
C2_5=a(18,6);
V5=a(18,1);
elseif (SOC_5<=30) && (SOC_5>25)
R0_5=a(17,2);
R1_5=a(17,3);
R2_5=a(17,4);
C1_5=a(17,5);
C2_5=a(17,6);
V5=a(17,1);
elseif (SOC_5<=35) && (SOC_5>30)
R0_5=a(16,2);
R1_5=a(16,3);
R2_5=a(16,4);
C1_5=a(16,5);
C2_5=a(16,6);
V5=a(16,1);
elseif (SOC_5<=40) && (SOC_5>35)
R0_5=a(15,2);
R1_5=a(15,3);
R2_5=a(15,4);
```

Appendix A

```
C1_5=a(15,5);
C2_5=a(15,6);
V5=a(15,1);
elseif (SOC_5<=45) && (SOC_5>40)
R0_5=a(14,2);
R1_5=a(14,3);
R2_5=a(14,4);
C1_5=a(14,5);
C2_5=a(14,6);
V5=a(14,1);
elseif (SOC_5<=50) && (SOC_5>45)
R0_5=a(13,2);
R1_5=a(13,3);
R2_5=a(13,4);
C1_5=a(13,5);
C2_5=a(13,6);
V5=a(13,1);
elseif (SOC_5<=55) && (SOC_5>50)
R0_5=a(12,2);
R1_5=a(12,3);
R2_5=a(12,4);
C1_5=a(12,5);
C2_5=a(12,6);
V5=a(12,1);
elseif (SOC_5<=60) && (SOC_5>55)
R0_5=a(11,2);
R1_5=a(11,3);
R2_5=a(11,4);
C1_5=a(11,5);
C2_5=a(11,6);
V5=a(11,1);
elseif (SOC_5<=65) && (SOC_5>60)
R0_5=a(10,2);
R1_5=a(10,3);
R2_5=a(10,4);
C1_5=a(10,5);
C2_5=a(10,6);
V5=a(10,1);
elseif (SOC_5<=70) && (SOC_5>65)
R0_5=a(9,2);
R1_5=a(9,3);
R2_5=a(9,4);
C1_5=a(9,5);
C2_5=a(9,6);
V5=a(9,1);
elseif (SOC_5<=75) && (SOC_5>70)
R0_5=a(8,2);
R1_5=a(8,3);
R2_5=a(8,4);
C1_5=a(8,5);
C2_5=a(8,6);
```

Appendix A

```
V5=a(8,1);
elseif (SOC_5<=80) && (SOC_5>75)
R0_5=a(7,2);
R1_5=a(7,3);
R2_5=a(7,4);
C1_5=a(7,5);
C2_5=a(7,6);
V5=a(7,1);
elseif (SOC_5<=85) && (SOC_5>80)
R0_5=a(6,2);
R1_5=a(6,3);
R2_5=a(6,4);
C1_5=a(6,5);
C2_5=a(6,6);
V5=a(6,1);
elseif (SOC_5<=90) && (SOC_5>85)
R0_5=a(5,2);;
R1_5=a(5,3);
R2_5=a(5,4);
C1_5=a(5,5);
C2_5=a(5,6);
V5=a(5,1);
elseif (SOC_5<=95) && (SOC_5>90)
R0_5=a(4,2);
R1_5=a(4,3);
R2_5=a(4,4);
C1_5=a(4,5);
C2_5=a(4,6);
V5=a(4,1);
elseif (SOC_5<=97) && (SOC_5>95)
R0_5=a(3,2);
R1_5=a(3,3);
R2_5=a(3,4);
C1_5=a(3,5);
C2_5=a(3,6);
V5=a(3,1);
elseif (SOC_5<=100) && (SOC_5>97)
R0_5=a(2,2);
R1_5=a(2,3);
R2_5=a(2,4);
C1_5=a(2,5);
C2_5=a(2,6);
V5=a(2,1);
else
R0_5=a(1,2);
R1_5=a(1,3);
R2_5=a(1,4);
C1_5=a(1,5);
C2_5=a(1,6);
V5=a(1,1);
end
```

Appendix A

```

Vt_5=V5+(R0_5*I(4))+...
    (R1_5*((I(4)*(1-exp(-1/(R1_5*C1_5))))/(1/(R1_5*C1_5)))-
(I(3)*((1-exp(-1/(R1_5*C1_5)))/(1/(R1_5*C1_5)))-(exp(-
1/(R1_5*C1_5))))))+...
    (R2_5*((I(4)*(1-exp(-1/(R2_5*C2_5))))/(1/(R2_5*C2_5)))-
(I(3)*((1-exp(-1/(R2_5*C2_5)))/(1/(R2_5*C2_5)))-(exp(-
1/(R2_5*C2_5))))))

Ec1_5=Ec1_5...
    +(36/I(4))*R0_5*power(I(4),2)...
    +(36/I(4))*(R1_5*power(((I(4)*(1-exp(-
1/(R1_5*C1_5)))/(1/(R1_5*C1_5)))-(I(3)*((1-exp(-
1/(R1_5*C1_5)))/(1/(R1_5*C1_5)))-(exp(-
1/(R1_5*C1_5))))),2))...
    +(36/I(4))*(R2_5*power(((I(4)*(1-exp(-
1/(R2_5*C2_5)))/(1/(R2_5*C2_5)))-(I(3)*((1-exp(-
1/(R2_5*C2_5)))/(1/(R2_5*C2_5)))-(exp(-1/(R2_5*C2_5))))),2));
end
Ec1_5;

%% The Fifth Stage
%T_5=I(10)
Ec1_6=0;
SOC_Final=SOC_5_5+(100*((I(5)*I(10))/3600))
for SOC_6=(SOC_5_5+1):1:SOC_Final
    if (SOC_6<=2.25)&&(SOC_6>=0)
        R0_6=a(23,2);
        R1_6=a(23,3);
        R2_6=a(23,4);
        C1_6=a(23,5);
        C2_6=a(23,6);
        V6=a(23,1);
    elseif (SOC_6<=5)&&(SOC_6>2.25)
        R0_6=a(22,2);
        R1_6=a(22,3);
        R2_6=a(22,4);
        C1_6=a(22,5);
        C2_6=a(22,6);
        V6=a(22,1);
    elseif (SOC_6<=10)&&(SOC_6>5)
        R0_6=a(21,2);
        R1_6=a(21,3);
        R2_6=a(21,4);
        C1_6=a(21,5);
        C2_6=a(21,6);
        V6=a(21,1);
    elseif (SOC_6<=15)&&(SOC_6>10)
        R0_6=a(20,2);
        R1_6=a(20,3);
        R2_6=a(20,4);
        C1_6=a(20,5);

```

Appendix A

```
C2_6=a(20,6);
V6=a(20,1);
elseif (SOC_6<=20) && (SOC_6>15)
R0_6=a(19,2);
R1_6=a(19,3);
R2_6=a(19,4);
C1_6=a(19,5);
C2_6=a(19,6);
V6=a(19,1);
elseif (SOC_6<=25) && (SOC_6>20)
R0_6=a(18,2);
R1_6=a(18,3);
R2_6=a(18,4);
C1_6=a(18,5);
C2_6=a(18,6);
V6=a(18,1);
elseif (SOC_6<=30) && (SOC_6>25)
R0_6=a(17,2);
R1_6=a(17,3);
R2_6=a(17,4);
C1_6=a(17,5);
C2_6=a(17,6);
V6=a(17,1);
elseif (SOC_6<=35) && (SOC_6>30)
R0_6=a(16,2);
R1_6=a(16,3);
R2_6=a(16,4);
C1_6=a(16,5);
C2_6=a(16,6) ;
V6=a(16,1);
elseif (SOC_6<=40) && (SOC_6>35)
R0_6=a(15,2);
R1_6=a(15,3);
R2_6=a(15,4);
C1_6=a(15,5);
C2_6=a(15,6) ;
V6=a(15,1);
elseif (SOC_6<=45) && (SOC_6>40)
R0_6=a(14,2);
R1_6=a(14,3);
R2_6=a(14,4);
C1_6=a(14,5);
C2_6=a(14,6);
V6=a(14,1);
elseif (SOC_6<=50) && (SOC_6>45)
R0_6=a(13,2);
R1_6=a(13,3);
R2_6=a(13,4);
C1_6=a(13,5);
C2_6=a(13,6);
V6=a(13,1);
```

Appendix A

```
elseif (SOC_6<=55) && (SOC_6>50)
R0_6=a(12,2);
R1_6=a(12,3);
R2_6=a(12,4);
C1_6=a(12,5);
C2_6=a(12,6);
V6=a(12,1);
elseif (SOC_6<=60) && (SOC_6>55)
R0_6=a(11,2);
R1_6=a(11,3);
R2_6=a(11,4);
C1_6=a(11,5);
C2_6=a(11,6);
V6=a(11,1);
elseif (SOC_6<=65) && (SOC_6>60)
R0_6=a(10,2);
R1_6=a(10,3);
R2_6=a(10,4);
C1_6=a(10,5);
C2_6=a(10,6);
V6=a(10,1);
elseif (SOC_6<=70) && (SOC_6>65)
R0_6=a(9,2);
R1_6=a(9,3);
R2_6=a(9,4);
C1_6=a(9,5);
C2_6=a(9,6);
V6=a(9,1);
elseif (SOC_6<=75) && (SOC_6>70)
R0_6=a(8,2);
R1_6=a(8,3);
R2_6=a(8,4);
C1_6=a(8,5);
C2_6=a(8,6);
V6=a(8,1);
elseif (SOC_6<=80) && (SOC_6>75)
R0_6=a(7,2);
R1_6=a(7,3);
R2_6=a(7,4);
C1_6=a(7,5);
C2_6=a(7,6);
V6=a(7,1);
elseif (SOC_6<=85) && (SOC_6>80)
R0_6=a(6,2);
R1_6=a(6,3);
R2_6=a(6,4);
C1_6=a(6,5);
C2_6=a(6,6);
V6=a(6,1);
elseif (SOC_6<=90) && (SOC_6>85)
R0_6=a(5,2);;
```

Appendix A

```

R1_6=a(5,3);
R2_6=a(5,4);
C1_6=a(5,5);
C2_6=a(5,6);
V6=a(5,1);
elseif (SOC_6<=95) && (SOC_6>90)
R0_6=a(4,2);
R1_6=a(4,3);
R2_6=a(4,4);
C1_6=a(4,5);
C2_6=a(4,6);
V6=a(4,1);
elseif (SOC_6<=97) && (SOC_6>95)
R0_6=a(3,2);
R1_6=a(3,3);
R2_6=a(3,4);
C1_6=a(3,5);
C2_6=a(3,6);
V6=a(3,1);
elseif (SOC_6<=100) && (SOC_6>97)
R0_6=a(2,2);
R1_6=a(2,3);
R2_6=a(2,4);
C1_6=a(2,5);
C2_6=a(2,6);
V6=a(2,1);
else
R0_6=a(1,2);
R1_6=a(1,3);
R2_6=a(1,4);
C1_6=a(1,5);
C2_6=a(1,6);
V6=a(1,1);
end
Vt_6=V6+(R0_6*I(5))+...
(R1_6*((I(5)*(1-exp(-1/(R1_6*C1_6))))/(1/(R1_6*C1_6)))-
(I(4)*((1-exp(-1/(R1_6*C1_6)))/(1/(R1_6*C1_6)))-exp(-
1/(R1_6*C1_6))))))+...
(R2_6*((I(5)*(1-exp(-1/(R2_6*C2_6))))/(1/(R2_6*C2_6)))-
(I(4)*((1-exp(-1/(R2_6*C2_6)))/(1/(R2_6*C2_6)))-exp(-
1/(R2_6*C2_6))))))
Ec1_6=Ec1_6...
+((36/I(5))*R0_6*power(I(5),2))+...
+(36/I(5))*R1_6*power(((I(5)*(1-exp(-
1/(R1_6*C1_6)))/(1/(R1_6*C1_6)))-I(4)*((1-exp(-
1/(R1_6*C1_6)))/(1/(R1_6*C1_6)))-exp(-
1/(R1_6*C1_6))))),2))+...
+(36/I(5))*R2_6*power(((I(5)*(1-exp(-
1/(R2_6*C2_6)))/(1/(R2_6*C2_6)))-I(4)*((1-exp(-
1/(R2_6*C2_6)))/(1/(R2_6*C2_6)))-exp(-1/(R2_6*C2_6))))),2));

```

Appendix A

```
end
```

```
Ec1_6;
```

```
%% The Fitness Function
```

```
Energy_Loss=(1*(Ec1_2+Ec1_3+Ec1_4+Ec1_5+Ec1_6))+(1*(I(6)+I(7)+  
I(8)+I(9)+I(10)))
```

Appendix B Complementary Data

The status of each switch for the MILP and MDP-RL methods is precisely declared in Table B-1, where P, W, and G are corresponding to the PV, wind energy, and grid switching status, respectively. The condition of each switch is considered as a binary number where 1 means the switch is closed and 0 means the switch is opened.

Table B-1 Switching manoeuvring status of sources

HH	0	1	2	3	4	5	6	7	8	9	10	11	12	13	14	15	16	17	18	19	20	21	22	23
MM	MILP																							
00	P	0	0	0	0	0	0	1	1	1	1	1	1	1	1	1	1	1	1	0	0	0	0	0
	W	1	0	1	1	1	1	0	0	0	0	0	0	0	0	0	0	0	0	0	0	0	0	0
	G	0	1	0	0	0	0	1	1	1	1	1	1	1	1	1	1	1	1	1	1	1	1	1
06	P	0	0	0	0	0	1	1	1	1	1	1	1	1	1	1	1	1	1	0	0	0	0	0
	W	1	0	0	0	0	0	0	0	0	0	0	0	0	0	0	0	0	0	0	0	1	0	0
	G	1	1	1	1	1	1	1	1	1	1	1	1	1	1	1	1	1	1	1	1	1	1	1
12	P	0	0	0	0	0	1	1	1	1	1	1	1	1	1	1	1	1	1	0	0	0	0	0
	W	1	0	0	0	0	0	0	0	0	0	0	0	0	0	0	0	0	0	0	0	1	0	0
	G	1	1	1	1	1	1	1	1	1	1	1	1	1	1	1	1	1	1	1	1	1	1	1
18	P	0	0	0	0	0	1	1	1	1	1	1	1	1	1	1	1	1	1	0	0	0	0	0
	W	1	0	0	0	0	0	0	0	0	0	0	0	0	0	0	0	0	0	0	0	1	0	0
	G	1	1	1	1	1	1	1	1	1	1	1	1	1	1	1	1	1	1	1	1	1	1	1
24	P	0	0	0	0	0	1	1	1	1	1	1	1	1	1	1	1	1	1	0	0	0	0	0
	W	1	0	0	0	0	0	0	0	0	0	0	0	0	0	0	0	0	0	0	0	1	0	0
	G	1	1	1	1	1	1	1	1	1	1	1	1	1	1	1	1	1	1	1	1	1	1	1
30	P	0	0	0	0	0	1	1	1	1	1	1	1	1	1	1	1	1	1	0	0	0	0	0
	W	1	0	0	0	0	0	0	0	0	0	0	0	0	0	0	0	0	0	0	0	1	0	0
	G	1	1	1	1	1	1	1	1	1	1	1	1	1	1	1	1	1	1	1	1	1	1	1
36	P	0	0	0	0	0	1	1	1	1	1	1	1	1	1	1	1	1	1	0	0	0	0	0
	W	1	0	0	0	0	0	0	0	0	0	0	0	0	0	0	0	0	0	0	0	1	0	0
	G	1	1	1	1	1	1	1	1	1	1	1	1	1	1	1	1	1	1	1	1	1	1	1
42	P	0	0	0	0	0	1	1	1	1	1	1	1	1	1	1	1	1	1	0	0	0	0	0
	W	1	0	0	0	0	0	0	0	0	0	0	0	0	0	0	0	0	0	0	0	1	0	0
	G	1	1	1	1	1	1	1	1	1	1	1	1	1	1	1	1	1	1	1	1	1	1	1
48	P	0	0	0	0	0	1	1	1	1	1	1	1	1	1	1	1	1	1	0	0	0	0	0
	W	0	1	1	1	1	0	0	0	0	0	0	0	0	0	0	0	0	0	0	0	1	0	0
	G	1	0	0	0	0	1	1	1	1	1	1	1	1	1	1	1	1	1	1	1	1	1	1
54	P	0	0	0	0	0	1	1	1	1	1	1	1	1	1	1	1	1	1	0	0	0	0	0
	W	0	1	1	1	1	0	0	0	0	0	0	0	0	0	0	0	0	0	0	0	0	0	0
	G	1	0	0	0	0	1	1	1	1	1	1	1	1	1	1	1	1	1	1	1	1	1	1
		MDP-RL																						
00	P	0	0	0	0	0	0	0	0	0	0	0	1	0	1	1	1	0	0	0	0	0	0	0
	W	0	0	0	0	0	0	0	1	0	1	0	0	1	0	0	0	1	0	1	1	0	0	0
	G	1	1	1	1	1	1	0	1	0	1	0	0	1	1	1	0	1	0	1	0	1	1	1
06	P	0	0	0	0	0	0	1	0	0	0	1	0	1	0	1	1	0	1	0	0	0	0	0
	W	0	1	1	0	0	1	0	1	0	1	0	0	1	0	0	0	0	0	0	0	0	0	0
	G	1	0	0	1	1	0	1	0	1	0	1	0	1	1	1	1	1	1	1	1	1	1	1
12	P	0	0	0	0	0	0	0	1	0	1	0	1	0	0	1	0	0	0	0	0	0	0	0
	W	0	0	0	0	0	0	0	1	0	0	0	0	1	0									

Appendix B

	W	0	1	1	0	0	1	0	0	0	0	0	0	0	0	0	1	1	0	0	1	1	0	0
	G	1	0	0	1	1	0	1	1	1	1	1	1	1	1	1	0	0	1	1	0	1	1	1
36	P	0	0	0	0	0	0	0	1	0	0	0	1	0	1	0	1	0	0	0	0	0	0	0
	W	0	0	0	0	0	1	1	0	1	0	0	0	0	0	0	1	0	0	0	1	0	0	0
	G	1	1	1	1	1	0	0	1	0	1	1	1	1	1	1	0	1	1	1	0	1	1	1
42	P	0	0	0	0	0	1	1	0	0	1	0	1	0	1	0	0	0	0	0	0	0	0	0
	W	1	0	1	0	1	0	0	1	1	0	1	0	0	0	1	0	0	0	0	1	1	1	0
	G	1	1	0	1	0	1	1	0	0	1	0	1	1	1	0	1	1	1	1	0	0	1	1
48	P	0	0	0	0	0	0	0	0	1	0	0	0	0	1	0	0	0	0	1	0	0	0	0
	W	0	0	1	1	1	1	0	0	0	0	0	1	0	0	0	1	1	0	0	1	0	1	0
	G	1	1	0	0	0	0	1	1	1	1	1	0	1	1	1	0	0	1	1	0	1	1	1
54	P	0	0	0	0	0	1	1	1	1	0	1	1	0	0	1	1	0	0	0	0	0	0	0
	W	0	0	1	1	1	0	0	0	0	0	0	0	0	1	0	0	0	0	1	1	0	0	0
	G	1	1	0	0	0	1	1	1	1	1	1	1	1	0	1	1	1	1	0	0	1	1	1